MIXTURE PREPARATION AND COMBUSTION IN SPARK IGNITION ENGINES

DHARI AWAD HASSON, B.Sc., M.Eng.

Doctor of Philosophy

The University of Aston in Birmingham

August, 1986

MIXTURE PREPARATION AND COMBUSTION

IN

SPARK IGNITION ENGINES

TO MY BROTHERS, THE BRAVE IRAQI SOLDIERS AT

THE

EASTERN FRONT OF OUR ARABIAN COUNTRY

THE UNIVERSITY OF ASTON IN BIRMINGHAM

MIXTURE PREPARATION AND COMBUSTION IN SPARK IGNITION ENGINES

BY
DHARI AWAD HASSON

A thesis submitted for the degree of
Doctor of Philosophy, 1986

SUMMARY

A 16-component fuel model of motor gasoline is used to study the evaporation of petrol entering the cylinder of a spark ignition engine in droplet form and the effects of the droplets on engine performance and the production of unburnt hydrocarbons. Predictions are compared with experimental data obtained from tests on a Ricardo E6 single cylinder engine equipped with an SU constant depression carburettor.

A preliminary study of mixture preparation in the carburettor and intake manifold, based on the analysis of Boam and Finlay (1979) and supported by extensive experimental investigation of the wall film of liquid petrol, is used to provide some indication of the droplet size, temperature and composition at inlet to the engine.

A step-wise mathematical model for the induction, compression, combustion, expansion and exhaust processes of a spark ignition engine has been developed. From the induction model it is possible to predict the spectrum of droplet sizes and their Sauter mean diameter (SMD) prior to compression. The concept of the SMD is used to study the droplet behavior during compression and combustion : droplets of less than 20 microns in diameter at entry to the engine are shown to have negligible effect on the combustion process.

A series of experimental investigations have been carried out to study the effects on wall film deposition and entrainment of the intake manifold design and other engine operating parameters. Results indicate that the presence of a mitre bend in the manifold destroys the effect of the throttle plate in distributing the liquid fuel in the system.

A new model of liquid wall film formation and destruction has been suggested. The model comprises a set of empirical equations to determine the liquid wall film quantity at the carburettor exit, the rates of droplet deposition and entrainment and a bend factor to account for the effect of a bend on the liquid film deposition. The validity of the model has been tested by comparing the predicted and measured liquid wall film flowrates at different flow and engine operating conditions. The results indicate that the model is reliable.

KEY WORDS

Multicomponent Fuel, Mixture Preparation, Wall Film Spark Ignition Engines, Cycle Simulation

ACKNOWLEDGEMENTS

The author wishes to make note of, and extend his most sincere thanks to all who have provided assistance and support during the duration of the project.

Mr. W.L. Flint is particularly acknowledged for his technical and moral support which he has so readily provided, especially so in the light of increasing workload.

Very special thanks are also due to my faithful wife Sanaa, and to my daughters Ghufran, Hinned and Sumaya for their encouragement and support to pursue the work I have enjoyed.

Technical assistance is indispensable to any research project. It is essential in order to complement the efforts of the researcher, and to enable the work to progress at a faster rate. To these roles, the efforts of Tom, Alan, Paul, Jim, Barry and many others, are acknowledged.

Very special thanks and respect to those researchers who publish their findings in order not only to gain the benefits of being famous, but to contribute to the field they work in.

The staff and fellow research students, in particular, Sidhu, Abderrezak, Shola, Mohammed, Meng, Vijay are formally acknowledged for their friendship and advice.

Finally, the author is indebted to the Iraqi Government for the scholarship which made it possible for him to undertake this research.

LIST OF CONTENTS

LIST OF FIGURES

LIST OF PLATES

LIST OF TABLES

NOMENCLATURE

The symbols used in the present work are defined directly following the equation they appear in. Therefore, a list of notations is not given here.

CHAPTER ONE

INTRODUCTION

1.1 General

1.2 Mixture Quality

1.3 Structure of the Thesis

1.1 General

The carburetted spark ignition engine and its problems have been the subject of investigations for many years. Although its basic operating principle was illustrated more than 100 years ago, little was known until recent years about the factors affecting the combustion process. Studies on the engine performance and the problem of air pollution have shown that the quality of the air-fuel mixture introduced to the cylinder is a major factor in determining the rate of combustion and has a considerable effect on engine performance and the associated exhaust emissions.

During the development of this type of engine, an enormous amount of theoretical research has been carried out on the subject of combustion assuming a homogeneous fuel vapour-air mixture. This assumption was based on the belief that the high volatility of the liquid fuel ensures that complete evaporation should occur during the intake process within both the intake system and inside the engine cylinder. Furthermore, for any droplets of liquid fuel which fail to achieve complete evaporation during the intake process, it was postulated that they should be totally vaporised during the compression stroke prior to ignition due to the increase in mixture temperature and the enhancement of the temperature-sensitive droplet evaporation.

There is no strong evidence in the literature that supports the assumption of complete liquid fuel evaporation prior to ignition in a conventional spark ignition engine under normal operating conditions. However, Peters[1], who measured fuel droplets sizes inside the cylinder of a spark ignition engine with axial stratification, concluded that complete evaporation of fuel droplets is attainable. Unfortunately, his experimental results should not be generalised since:

a. the liquid fuel was injected into the inlet port of the engine while the inlet valve was open. Thus, the liquid fuel had a relatively unobstructed path into the engine cylinder which, in turn, reduced the opportunity of liquid wall film formation. This method of fuel introduction produced relatively small droplet sizes which ranged from 17.6 μm to 40.1 μm.

b. liquid fuels used in the tests were single component fuels with a relatively low boiling temperatures. It is well known that the presence of another fuel component in the liquid fuel mixture will result in a lower evaporation rate from the component in proportion to its molar fraction. Additionally, the use of low boiling temperature fuel produces a higher evaporation rate, which is well illustrated in Peters results. The data indicates that complete

evaporation of isopentane droplets (B.T. = 27.8^{0}C) occurred at 160^0 CA before top centre, while that of methanol droplets (B.T. = 65^{0}C) was at 80^0 CA before top centre. The conventional spark ignition engine fuel may contain fuel components with boiling temperatures well above 145^{0}C[42].

c. the experimental conditions at which the data was obtained were far removed from the normal engine operating conditions (e.g. inlet air temperature ranged from 65^{0}C to 169^{0}C) with a corresponding increase in fuel evaporation.

d. finally, for the measured droplet sizes, the present work predictions indicate that, under the same experimental conditions, complete fuel evaporation is possible even if the fuel is a multi-component one.

On the other hand, the theoretical study of fuel evaporation inside the engine cylinder undertaken by Liu et al.[2] indicated that iso-octane droplets of diameters larger than 50 μm would fail to achieve complete evaporation prior to ignition under normal operating conditions.

Furthermore, there are other engine operating conditions at which complete fuel evaporation is virtually impossible. For example, it is reasonable to expect that at

cold start, especially when the ambient temperature is low, the overall evaporation rate can be significantly retarded and "large" droplets may survive until spark discharge[2]. Additionally, droplets generated due to wall film disintegration at the inlet valve are expected to have larger sizes because of the relatively weak aerodynamic stripping acting on the liquid film. These droplets are mainly composed of heavier fuel fractions and also have less time for evaporation compared with the initial droplets generated in the intake system.

Finally, Liu et al. recognised another factor which may retard evaporation rate, that is, the effect of cylinder pressure on droplet evaporation. They suggested that during the compression stroke, while the increasing gas temperature tends to enhance the evaporation, the simultaneously increasing cylinder pressure tends to retard it. Their predictions indicated that droplet evaporation can be substantially reduced from the value obtained by considering the influence due to temperature increase alone.

The work described in this thesis is primarily concerned with the mixture preparation and combustion processes in a carburetted spark ignition engine. A comprehensive experimental investigation was carried out to study the effects of inlet manifold design and different engine operating conditions on the liquid wall film formation and the effects of liquid wall film separation on engine performance and emissions. The engine was a single

cylinder Ricardo E6 equipped with a constant depression carburettor and fuelled with 4-star petrol. Experimental data was used to derive a set of empirical equations describing the initial wall film quantity (at carburettor exit), the rates of droplets deposition and entrainment and a bend factor to correlate the measured influence of 90^0 bends.

A complete theoretical study of fuel evaporation and transportation in the intake system and within the engine cylinder, based on the models proposed by Boam and Finlay[42] and Law[21] respectively, was also carried out using a 16-component model of motor gasolene (B.T. = - 42^0C to 183.3^0C). A new model of the intake stroke is proposed which takes into account not only the filling effect of the process but also fuel evaporation during the process. In this model the cylinder is divided into numerous numbers of segments each of which is characterised by its own mass, number of droplets, droplet size and temperature with common cylinder pressure, temperature and fuel vapour concentration. At the trapped point (inlet valve closure) a new droplet Sauter mean diameter and temperature is calculated to be used during the compression and combustion phases. During flame propogation, fuel droplets trapped in the flame zone are considered to vaporise with combustion. In such type of evaporation the volatility of the fuel is no longer important, instead, oxygen concentration and the rate of heat transfer to the droplets are the dominant factors[11,20].

A comparison is made between experimental and computer predicted results with regard to liquid wall film flowrate, pressure-time diagrams and exhaust emissions in order to test the reliability of the models. Detailed parametric studies on the effects of different flow and engine operating conditions on mixture preparation and engine performance are presented.

1.2 Mixture Quality

Mixture quality, mentioned earlier, is not only the degree of liquid fuel evaporation but also the way in which the remaining liquid fuel is present and distributed in the mixture. The liquid fuel introduced to the air stream through the carburettor is not required to vaporise completely in the intake system, since it is found that this may drastically affect the volumetric efficiency of the engine[4]. It is also found that this form of mixture quality (with complete evaporation) is not the best "diet" for lean engine operation[10], and it may result in poor fuel distribution if adequate means of mixing are not provided[8].

In the carburetted spark ignition engine the combustible mixture is prepared in both the intake system and inside the cylinder. The heavier fuel components remain as liquid and traverse the intake system in the form of

entrained droplets and as liquid wall film, moving much more slowly along the walls of the intake system. In general, air and fuel vapour negotiate the geometry of the system with reasonable ease to give uniformity of fuel distribution to individual cylinders if the fuel vapour is well mixed with air.

Both forms of liquid fuel transport, as droplets and in the liquid wall film, lead to poor fuel distribution since the momentum of the droplets causes their flow paths to differ from that of the intake system geometry, while the wall film is sluggish and can be over-influenced by the geometry[75].

The recently adopted lean mixture operation seems to be an attractive proposition because it has the advantages of lower exhaust emissions with better fuel economy. However, lean mixture operation of a carburetted engine can be critically dependent on mixture quality and the distribution of the fuel between the individual cylinders and within each cylinder. Many investigators[33,44] have therefore, concluded that to achieve better mixture quality and distribution, the liquid wall film should be reduced to the minimum possible quantity. The controlled addition of heat through the manifold wall was suggested to be the most effective method to achieve that. In the present work, however, it is found that heating the liquid film prior to entry to the cylinder and the disintegration of the liquid film at the inlet valve are the key factors to achieve

During a sudden opening of the throttle plate the mixture is temporarily weakened due to both the increase in air flowrate and the delay of the fuel flow. The latter is due to the time required to build up the liquid wall film in the inlet manifold.

better overall results, since small, high temperature droplets will burn completely in the flame zone with negligible effects on other combustion parameters.

It is clear that the presence of the liquid wall film is the major factor in controlling mixture quality and distribution. This is believed to be due to its high quantity, which may reach up to 50% of the total fuel flow, and to its low velocity and volatility. The effects of the liquid wall film exist not only at steady engine operation, but also at sudden opening and closing of the throttle plate. The latter produces an abrupt rise in manifold depression which, in turn, produces a sudden suction of the liquid film. The first stage of a decelaration or idling is therefore, accompanied by a much more greater enrichment of the mixture. Consequently, carbon monoxide and hydrocarbon emissions are much greater at this stage.

The mechanisms of the wall film generation and destruction in the intake system of a carburetted engine are not fully understood. No work has yet been reported on the rates of droplets deposition and entrainment, which are not only important in determining the wall film quantity, but also in controlling the rate of fuel evaporation. In the present work a model for wall film deposition and entrainment, based on empirical correlations of the data obtained from a series of experimental investigations using different inlet manifold designs and engine operating conditions, is suggested and incorporated into the Boam and

Finlay model. In these experiments the mean wall film flowrate was measured using the slit method.

1.3 Structure of the Thesis

The thesis is divided into eight chapters and six appendices. The present chapter serves to introduce the theme and subjects relating to the thesis. Various topics are discussed briefly and qualitatively, while details elaborated on in later chapters. In chapter two, a survey is presented of relevant literature by other researchers. Their work is summarized and the relevance to the present work is highlighted. In chapters three and four, the theories relating to the mixture preparation processes and spark ignition engine cycle are developed respectively. In chapter three, the general equations of fuel atomization, transportation and evaporation are first derived and further developed for use in a computer program. In addition to reviewing the reported work on the spark ignition engine cycle details, the fourth chapter discusses the models used to predict flame propogation, heat transfer, formation of unburnt hydrocarbons, dissociation of combustion products and the onset of knock. Details of the experimental work are discussed in chapter five together with the derivation of wall film empirical equations. The computer programs of the mixture preparation and cycle simulation models are detailed in chapter six. The main structures are discussed with the aid of flow charts.

Program testing and the parametric study are presented in chapter seven. The final chapter, summarises the overall work, and presents its conclusions.

In the appendices, listings are provided of the computer programs developed together with other details, which though necessary, were felt likely to provide a distraction from the main text of the thesis.

CHAPTER TWO

LITERATURE SURVEY

2.1 Introduction

To satisfy the objectives of the present research, it was necessary to deal with many research areas. Mixture preparation, on one hand, requires a full knowledge of the history of liquid fuel from the carburettor jet to the end of the combustion process. This means that a complete study of fuel behaviour should be performed, including the interaction of various flow parameters within the intake system, during the gas exchange process and inside the engine cylinder. On the other hand, a cycle simulation was required to study the combustion process and the effect of the prepared mixture on the engine performance and emissions. This wide area of research required an extensive literature survey on the work reported in these areas.

This chapter commences with a detailed review of the reported work on fuel evaporation and mixture preparation. Cycle simulation models, however, have been surveyed in a more general way to give a broad appreciation of the models. Work on flame propagation, auto-ignition, heat transfer and other cycle details will be discussed later when dealing with the modelling of the cycle processes.

2.2 Mixture Preparation Effects on Engine Performance and Emissions

Several investigations have shown that mixture quality affects the ability of the engine to run on lean mixtures. Unfortunately, there is conflicting evidence as to what the optimum mixture state should be. Many researchers[3-7] have shown that fully vaporised homogeneous fuel-air mixture provides good lean operating capability. However, these results are at variance with other studies[8-10] which have shown that inhomogeneties in the induced fuel-air charge are beneficial for lean operation in engines.

Hughes and Goulburn[3] found that complete evaporation of the fuel in the intake manifold can overcome the well known cylinder to cylinder maldistribution problem. They used a coolant heated evaporator to produce complete evaporation of the fuel and create a homogeneous inlet charge. They concluded that the engine can run on a lean mixture with reduced exhaust emissions. However, a power reduction of 25% to 30% was also reported.

The work reported by Trayser et al.[4] indicated that complete evaporation of the fuel in the intake system can almost eliminate fuel maldistribution, but this will drastically affect the volumetric efficiency by changing the negligible volume of liquid fuel to a significant volume of fuel vapour.

Lindsay et al.[5] investigated the importance of good mixture quality and homogeneity on engine performance and exhaust emissions. They described a system based on a heat pipe using exhaust heat as a means of evaporating the fuel. They found that using such a device gives the opportunity for significant fuel economy, reduction in exhaust emissions and drivability improvement with only a minor sacrifice in power.

Dodd and Wisdom[6] in their study of the effect of mixture quality on exhaust emissions found that the most noticeable effect was the extended weak limit obtained with fully vaporised fuel. They also found that the emitted unburnt hydrocarbons at full throttle and half load were lower. Beale and Hodgetts[7] confirmed the ability of the engine to run on weak mixture with fully evaporated fuel, leading to a significant reduction in carbon monoxide and hydrocarbons emission.

However, Yu[8] in his study of the geometrical and temporal variations of air/fuel ratio, concluded that complete evaporation of the fuel does not improve geometric fuel distribution. Infact, his work showed that very poor distribution may result if adequate means of mixing are not provided.

Matthes and McGill[9] found that leaner operation was possible with bad atomisation and wetting of the manifold wall than with good atomisation. Their good atomisation

tests used 10-20 μm droplets, their bad atomisation tests used 400-700 μm droplets and their wall-wetted case employed a dribble of 400-700 μm on to the inlet port. Hydrocarbons emission varied by 20% among the three cases with good atomisation being lowest. Fuel consumption and carbon monoxide levels were almost totally insensitive to mixture quality, and the wall-wetted tests gave the leanest operation. Matthes and McGill hypothesized that the poor atomisation and wall-wetting resulted in some form of stratification and hetrogeneous combustion, which in turn, extended the lean operation limit.

Peters and Quader[10] in an attempt to resolve this variance in the literature initiated a study on the effect of mixture quality on lean mixture combustion. They found that a homogeneous prevaporised mixture of fuel and air is not the best "diet" for lean engine operation. They concluded that the use of premixed charge resulted in a richer "lean misfire limit", lower maximum burning rate, higher hydrocarbons emission, and increased indicated specific fuel consumption. They suggested that some form of hetrogeneous charge wetted with fuel droplets may be beneficial for lean operation.

2.3 Evaporation and Combustion of Fuel Droplets

Single droplet evaporation and combustion has been subjected to investigations for many years. For example

Maxwell, Stefan and Morse[11] found theoretically and experimentally that the mass rate of evaporation of a droplet into still air is proportional to the first power of the droplet diameter, and when the vapour pressure is a small fraction of the total pressure, to the first power of the difference between the vapour pressure at the droplet surface and an infinite distance. For higher partial pressures of the vapour a logarithmic function of the vapour pressure must be used.

In a comprehensive theoretical and experimental study, Frössling[12] extended these results to the case of a droplet evaporating in a moving gas stream of similar temperature. He obtained the following semi-empirical equation:

$$\frac{dm}{dt} = \frac{2\pi d_d}{RT} D M_w (P_{v,s} - P_{v,\infty})(1 + .276\ Sc^{1/3}\ Re_d^{1/2}) \quad (2.1)$$

where

$\frac{dm}{dt}$ is the mass rate of evaporation

d_d is the droplet diameter

R is the universal gas constant

T is the temperature of the stagnent film around the droplet

D is the diffusion coefficient of vapour in air

M_w is the vapour molecular weight

$P_{v,s}$ is the vapour pressure at the droplet surface

$P_{v,\infty}$ is the ambient vapour pressure

Sc is the Schmidt number

Re_d is the droplet Reynolds number

Spalding [13,14] presented a practical method for the measurement of vaporisation rate from the surface of a solid sphere of one inch diameter. The surface of the sphere was wetted by a liquid which was supplied such that the surface remained wet at all times. He also proposed a theory for droplet evaporation to calculate the time required for complete disappearance of a spherical liquid droplet. The following formula was suggested:

$$t = \frac{d_d^4 \rho_f}{8D\rho_a} \ln (1+B) \qquad (2.2)$$

where

B is the transfer number = $\frac{Cp}{L} (T_a - T_f)$

ρ is the density

Cp is the specific heat of the liquid fuel

L is the latent heat of evaporation

T is the temperature

a is for air

f is for fuel

Law[15] investigated the motion of an ensemble of monosized droplets undergoing evaporation in an adiabatic or isothermal gas stream. His predictions show that fine atomisation is a key factor in achieving fast evaporation. Law's evaporation model was based on Spalding's theory for droplet vaporisation.

Kadota and Hiroyasu[16,17] investigated experimentally and theoretically the evaporation of a single droplet in a gaseous environment at elevated pressures and temperatures. Their model covers the unsteady and steady-states of droplet evaporation, considering the effect of natural convection. The range of experimental conditions were: gas pressures from 1 atm. to 50 atm., and gas temperatures from 100^0C to 500^0C, which correspond to the subcritical, critical and supercritical states of the droplets. The high pressure model was compared with experimental data and with a conventional low pressure model. The results showed that the low pressure model failed to give satisfactory results under high pressure conditions, while the results predicted by the high pressure model were in good agreement with the experimental measurements.

Law[18], Law and Sirignano[19] modelled the unsteady droplet combustion caused by droplet heating assuming a quasi-steady gas phase processes and that the droplet temperature is spatially uniform but temporally varying. They concluded that droplet heating is a significant cause of the unsteadiness of droplet combustion and hence should be accounted for in any realistic analysis of the unsteady droplet combustion phenomena.

The reported work on multicomponent fuel droplet evaporation and combustion is very limited. Infact, the only available work is that of Law et al.[20] on the

evaporation process and of Law[21] on the combustion process. The first model analyses the vaporisation of a droplet in a strong convective gas stream, with particular emphasis on the generation of internal circulation and its effect on the internal heat and mass transfer processes. The second model uses two approaches to describe the gas-phase,diffusion controlled, unsteady combustion of a droplet in a stagnant, unbounded atmosphere. The models considered are "the ideal mixture", which assumes that the mixture behaves as an ideal mixture in its phase change characteristics, and the "shell" model, in which the components are assumed to be distributed as shells such that quasi-steady, single component vaporisation prevails for each shell. Both models indicated that the components vaporise approximately sequentially in the order of their relative volatilities, and that evaporation rate is insensitive to the mixture composition during combustion as well as vaporisation in hot environments.

2.4 Experimental Studies on Fuel Evaporation and Transportation in the Intake System

Little experimental work has been reported on the development of different phases in which fuel is present in the intake system of a running engine. This is believed to be due to the complexity of the flow regime and the great number of variables involved.

However, the problem of annular two-phase flow systems has received considerable attention from many investigators in other engineering applications. Information on the characteristics of liquid wall film, droplet deposition and entrainment is important for planning and designing cooling systems in nuclear and fossil-fuel power stations and in steam generators.

Krasiakova[22] measured wall film thickness in a horizontal pipe using a resistance technique. His work showed that a considerable eccentricity of the wall film existed. The length on which the film was measured was great, therefore, an average rather point wise measurement was made. The first local values of wall film thickness appeared in Ref.(23) which confirmed the eccentricity of the wall film reported by Krasiakova.

McManus[24] studied local liquid distribution and pressure drop in a horizontal annular two-phase flow. He measured wall film thickness using a probe inserted into the tube and brought into contact with the liquid film on the opposite wall. An electrical circuit was completed when the probe came into contact with the liquid. The probe was attached to a micrometer barrel which permitted the determination of the probe position at time of contact. McManus presented an empirical relation for meam film thickness at various tube circumferential positions, this relation is of the form:

$$\frac{h_m}{D_m} = a \frac{Re_L^{\,b}}{Re_g^{\,c}} \left(\frac{\rho_g}{\rho_L}\right)^d \left(\frac{\mu_L}{\mu_g}\right)^e \qquad (2.3)$$

where

h_m is the mean film thickness

D_m is the tube diameter

ρ is the density

μ is the dynamic viscosity

L is for liquid

g is for gas

a,b,c,d and e are empirical constants.

Gill et al.[25,26] reported that the flow rate of entrained droplets increases in the direction of the flow, but the characteristics such as droplet entrainment and deposition rates which determine the axial change of the droplet flow rate have not been examined.

Alexander and Coldren[27] carried out experiments on the deposition of 27 μm water droplets on the walls of a horizontal pipe. The deposition rate was estimated by examining the change in the radial profile of the droplets mass flux and correlated by:

$$Q_d = K_d\, C \qquad (2.4)$$

where

K_d is the mass transfer coefficient

$= 8.34338 \times 10^{-4}\ V_g^{\,1.17}$

C is the concentration of the droplets within the gas stream, (Kg/m^3)

V_g is the main gas velocity, (m/s)

Akagawa et al.[28] investigated the behaviour of water droplets, which are entrained from the wall film, and the droplet entrainment rate in a horizontal annular two-phase flow. Liquid droplets flowrate was measured by an isokinetic sampling probe, while the wall film was measured using the scoop method (in this method, a scoop plate of 0.5 mm thickness is fixed in a fully-developed region and is located 2.5 mm apart from the bottom of the duct). They found that the entrainment rate under the condition of constant gas velocity in the duct is significantly affected by the average liquid film thickness. They suggested that the entrainment rate may be calculated using the formula:

$$Q_e = 4.57 \times 10^{-7} \; h_m^{3.5} \; Vg^9 \; \rho_L \; (Kg/m^2.s) \qquad (2.5)$$

The foregoing references on two-phase flow have considered steady flow in a straight horizontal duct. The complex geometry and unsteady flow conditions of the engine intake system are factors which increase the difficulty of experimental research and analysis still further. However, many investigators have managed to study some of the observed phenomena in the intake system. Collins[29] developed a technique to measure air/fuel-vapour and air/total-fuel ratios of the mixture entering each cylinder of a 4-cylinder engine. These two ratios were used to estimate how much of the fuel was vaporised. He concluded that the values of air/fuel-vapour ratio obtained by such

measurements depend on the design of the sampling probe. Collin's results may be summarised as follows:

(i) there was a considerable maldistribution of the fuel, the inner pair of cylinders receive more than their share and the wall film tended to gravitate towards the rear cylinders,

(ii) not all the fuel is vaporised in the manifold. At half throttle condition 69% of the fuel was vaporised, while 81% at full throttle, and

(iii) the cylinder to cylinder variation of air/total-fuel ratio was generally reduced by heating the mixture.

Pao[30] using calorimetry and sampling probe techniques measured the air/fuel-vapour and the air/atomised-fuel ratios in an engine during the warm up period. He found that mixture quality stabilised in eight minutes. During the initial five minutes the rate of increase in the percentage of vaporised fuel is approximately equal to the rate of decrease in the percentage of wall film and that the total percentage of large and small droplets did not change during that time. The results indicated that the effect of

manifold pressure, air velocity and mixture temperature on the amount of atomised fuel are more significant at transient than at stablised conditions. Results also showed that the level of vaporised fuel stabilised at 70% of the metered fuel with the remaining 30% shared by both the large and small fuel droplets.

Finlay and Welsh[31] photographed fuel condition at various locations downstream of an air-valve carburettor needle over a range of engine speeds and loads. The photographs showed clearly the remarkable change in the condition of the entrained fuel that occurs during one cylinder filling cycle. Finlay and Welsh hypothesized this to be due to the pulsating nature of the air flow past the needle. The photographs also showed that the more the air flow the better the fuel atomisation. The measured droplet size was ranging from 25 - 300 μm depending on flow condition.

Nightingale and Tsatsami[32] measured wall film quantity separated at the end of a 4-cylinder engine manifold during a cold start. Their results indicated that wall film quantity can reach as much as 50% of the total fuel supplied for 50 seconds cranking time at full choke and for 80 seconds cranking time at 2/3 choke condition.

Finlay et al.[33] measured fuel distribution in the region of the throttle plate of an air valve carburettor. They used an isokinetic probe for droplet flowrate

measurement and a knife edged sampler for wall film flow rate measurement. Generally, the results indicate that:

(i) the droplets are not evenly distributed in the flow, they are more at the core than near the wall,

(ii) the distribution of both droplets and wall film is better downstream from the throttle plate than between the piston and the throttle plate,

(iii) dropwise mass flowrate downstream is less than that upstream in all test conditions,

(iv) wall film quantity downstream from the throttle plate is less than that upstream at both 1500 and 3000 rpm road load power, while it is more at 3000 rpm full power,

(v) the wall film is eccentrically distributed in the manifold at almost all the tested conditions.

Finally, Finlay et al. concluded that to improve mixture quality the wall film quantity should be reduced to the smallest possible amount.

Hayashi and Sawa[34] studied the transient characteristics of a carburetted engine while a stepwise closing the throttle plate. They concluded that the mixture in the cylinder becomes leaner temporarily after the

stepwise closing and thereafter returns to the condition which would exist under steady-state operation. They believed that this behavoiur is primarily caused by the transient effect of the wall film. They also reported some observations on the wall film during steady-state operation. These are summarised below:

(i) The mean wall film thickness depends mainly on the intake air velocity and air/fuel ratio, it's value being about 0.05 - 0.2 mm,

(ii) wall film flowrate increases in direct proportion to air velocity but in inverse proportion to air/fuel ratio,

(iii) in small engines, mean wall film velocity is equal to about 1 to 6 m/sec, this value corresponds to between 1/100 and 1/200 of air velocity, and

(vi) the percentage of wall film decreases with an increase in engine speed, air velocity, air/fuel ratio and the intake pipe length.

Evaporation rate, wall film deposition and entrainment rates may be well understood when the size/distribution of the droplets in the mixture is known. Such data are difficult to obtain in the high velocity, turbulent and pulsating air stream usually found in the intake manifold of a carburetted engine. However, many attempts to measure

fuel droplet size and distribution have been made using both steady test rigs and engines. Finlay et al.[35] measured droplet size/distribution in an engine manifold at different operating conditions using a Malvern laser particle sizer. The engine was equipped with an SU type carburettor and a specially designed viewing section. Nightingale and Tsatsami [36] used the same technique to measure droplet size in a steady test rig. The droplets were produced by three types of atomisers, viz. a constant depression carburettor, a sonic throat atomiser and the Hartmann Whistle (see Ref.(36)).

In both works the measured droplet size showed the same trend, as manifold depression increases droplet size decreases. The results indicated that fuel atomisation is of two types, primary at the fuel jet and secondary at the throttle plate. At part throttle conditions air velocity at the throttle plate is high and so the fuel is re-atomised by the shearing effect of the flow.

Phillips and Rayner[37] measured the size and distribution of droplets produced by a constant depression carburettor in a steady test rig using the Malvern particle sizer. They found that the Sauter mean diameter increases with high air/fuel ratios and reduced simulated engine speeds. For a simulated 1000 rpm road load condition test, droplet diameter ranged from 33 μm at air/fuel ratio of 10 to 80 μm at air/fuel ratio of 19, while for the 2000 rpm road load condition these were 20 to 45 μm respectively.

In these tests the liquid wall film had been removed upstream of the measuring section.

2.5 Mathematical Modelling of Mixture Preparation in the Intake system

The flow in the intake system of a carburetted spark ignition engine is extremely complex involving turbulent, pulsating, two-phase, multicomponent, annular flow. The geometry of the system not only involves frequent changes of cross-section particularly in the carburettor and at the throttle plate, but also includes bends and branch points in the manifold[42]. The fuel itself is a complex combination of many components and it undergoes not only evaporation but frequent deposition and re-entrainment of droplets between the main-flow and liquid wall film as the stream passes through the intake system.

Few models to study the evaporation and transportation of liquid fuel in the intake manifold and the effect of different flow parameters on these processes have been reported. It is generally assumed that:

(a) Fuel droplets are spherical, have uniform size and are homogeneous in temperature and concentration.

(b) The flow is turbulence free and that there is no chemical reaction in the induction system.

(c) The intake manifold is a straight, constant cross-sectional area pipe.

In addition to the above assumptions, each reported model has its own assumptions, these will be discussed with each model.

Yun et al.[38] presented a model to study fuel evaporation and transportation in a carburettor venturi. In their steady-state, one-dimensional model the fuel has been assumed to be a single component substance, present in the flow in droplet form only. They predicted that total evaporation within the carburettor is approximately 4% of the total fuel supplied. However, the validity of this prediction is not representative of the actual behaviour of the system as the vapour pressure of their fuel, n-octane, is very different from that of petrol.

Lo and Lalas[39] in their parametric study of fuel droplet flow and evaporation in an idealised induction system have included droplet coalescence in a steady-state, one-dimensional, single component fuel model. A study of the effects on fuel evaporation of such parameters as initial droplet size, wall surface roughness, fuel type, air velocity, exhaust gas recirculation, air/fuel ratio and heating the manifold wall was performed. Their predictions showed that:

(i) droplets of radius 15 μm or less will follow the main stream and also maintain 30% or more evaporation, while droplets of radius 60 μm or more will have difficulty in following the main stream and their evaporation rate is insignificant,

(ii) fuel type influences the charge mixture quality: dodecane drops showed negligible evaporation, while the same size of hexane droplets evaporated by 45% at the same conditions,

(iii) air/fuel ratio and wall surface roughness have little effect on evaporation,

(iv) the improvment of mixture quality due to air speed is not significant. The lower air speed caused relatively higher evaporation due to the longer residence time in the manifold, and

(v) the injection of hot exhaust into the intake manifold resulted in higher evaporation.

Finally, Lo and Lalas concluded that the best method of improving mixture quality and fuel distribution is by heating the manifold wall. They found that heat transfer into the mixture equivalent to 50% of its original total energy can achieve the best overall results, since excessive amounts of heat will result in undesirably low engine volumetric efficiency and poor performance.

Picken et al.[40] in their simplified model of fuel evaporation in the intake manifold concluded that for normal operating conditions of a carburetted engine, liquid-fuel will not be completely vaporised in the intake manifold. Most of the evaporation takes place inside the cylinder during the intake and compression processes.

Finlay et al.[41] proposed a steady-state, one-dimensional model of fuel evaporation in an air valve carburettor. The fuel which was treated as a multicomponent substance was assumed to be present in droplet form only. They studied the effects on fuel evaporation of fuel composition, fuel and air temperatures, air/fuel ratio, barometric pressure and droplet size. Their results showed that:

(i) total evaporation within the carburettor is approximately 20% of the total fuel,

(ii) the fuel, which is vaporised in the carburettor is mainly composed of lighter fractions,

(iii) evaporation increases as droplet size decreases, and

(iv) evaporation rate is strongly dependent on fuel and air temperatures but heating the fuel is more effective than heating the air.

Boam and Finlay[42] extended the work of Ref.(41) to include fuel evaporation and transportation in the intake manifold. They assumed that in the manifold the fuel is present as entrained droplets and wall film with a maximum quantity of 20% of total fuel mass flowrate. They also studied the effect of secondary atomisation which might occur at small throttle plate openings, and found that:

(i) secondary atomisation at the throttle plate has a powerful influence on fuel evaporation,

(ii) pressure reduction at the throttle plate has little effect on fuel evaporation,

(iii) heating the manifold wall is the most effective method of achieving maximum evaporation for a given input of heat, and that

(iv) engine speed and load have little effect on the percentage of the fuel vaporised within the carburettor, beyond the throttle plate, however, load has more effect due to the secondary atomisation.

Low et al.[43] developed a model for the flow of fuel droplets entrained in a non-steady, one-dimensional air flow. The model which is based on the method of characteristics takes account of three effects on the droplet, viz. heat transfer, evaporation and drag. They

assumed the fuel to be a single component present in droplet form only. The results agreed very well with those of Yun et al. [38].

In their two-dimensional, steady-state model, Servati and Yuen[44] studied the behaviour of liquid fuel droplets and liquid fuel wall film in an intake manifold. They developed a wall film deposition model assuming the wall film to be a Couette flow at the lower half segment of the pipe. A time constant representing the delay of the fuel transport in the intake manifold was defined and determined for a single cylinder engine. They also found that:

(i) wall film flowrate increases with the increase of initial droplet size and manifold length, and

(ii) wall film flowrate decreases with the increase of air velocity.

Their predictions also showed that the percentage wall film can be more than 90% of the total fuel flow at a distance of two pipe diameters from the fuel jet with droplet diameter of 100 μm and air velocity of 100 m/s.

2.6 Combustion Studies on Droplet-Vapour Systems

A considerable amount of information has been reported on the burning characteristics of either fuel vapour or

droplet suspensions, while very little knowledge on the burning characteristics of systems where these two forms of fuel coexist has been obtained. The insufficiency of the literature on this subject is not surprising in view of the experimental difficulties involved. Among these are[50]:

1. The difficulty in creation of a uniform and reproducible multidroplet mixture.

2. The problem of accurate measurement of mean droplet size, droplet-size distribution and the concentration of fuel vapour in the mixture.

3. The difficulty in measuring the rate of flame propogation through the mixture, since it is found that the presence of droplets has a significant influence.

To date, most of the work in the literature involving droplet-vapour system combustion has been carried out on steady-state test rigs, where the conditions are completely different from those found in the conventional engine. These results, however, can provide a good foundation for a broad understanding of the combustion in such a system within the engine cylinder.

The earliest published work in this area is the study of Burgoyne and Cohen[45]. They studied the effect of drop size on the laminar combustion properties of tetralin-air

mixtures. They found that mixtures consisting of monosized droplets with diameters less than 10 μm burned as though they were completely vaporised. They also found that droplets larger that 40 μm burned individually in their own envelope. A transition region existed between these two regimes. Over the size range examined, Burgoyne and Cohen found that the flame could be communicated from one droplet to another so long as the droplets were not separated by more than 30 diameters. Their results also showed that flame speed in the mixture can be maximised by adjusting the droplet size to an optimum diameter of 30 μm. The flame speed decreases with droplets either smaller or larger than the optimum size.

Sundukov and Predvoditelev[46] reported an experimental work on the measurement of flame speed in a two-phase mixture produced by a special burner-atomiser. They also developed a device to measure the liquid phase proportion in the mixture. Their study was confined to smaller-sized droplets only, due to the separation of the bigger-sized droplets in the mixing chamber of the burner. The results showed that there is an optimum value of air/fuel ratio to produce a maximum flame speed. They also showed that flame speed increased as the percentage vapour in the mixture is increased for a given total air/fuel ratio.

Hayashi and Kumagai[47] measured the burning time, peak pressure, flame speed and burning velocity for mixtures

containing mono-sized droplets up to a maximum diameter of 7 μm and for homogeneous vapour-air mixtures using an expansion apparatus based on the principle of the Wilson cloud chamber. They also performed microphotographic studies of flame propogation in mixtures containing larger droplets of about 20 μm in diameter. They found that the effects of fuel droplets on the burning characteristics are more significant for fast burning mixtures than for slow burning mixtures which suggested that ethanol droplets of several microns in diameter are not completely evaporated in the pre-heating zone. Their microphotographs showed that the flame front in a mixture containing droplets about 20 μm in diameter is not smooth in structure, in contrast to that of a homogeneous vapour-air mixture.

In related work, Mizutani and Nakajima[48,49] studied the effect of adding Kerosene droplets to propane-air mixtures in a steady flow burner[48] and in a bomb[49]. Their burner work showed that the maximum burning velocities of propane-kerosene droplet systems were considerably higher than those of propane-air mixtures and even higher than those of drop clouds of kerosene. The bomb tests produced similar conclusions concerning the enhancement of the flame speed by the droplets. In both tests the effects of droplets were more prominent for lean mixtures and for mixtures with a low intensity of turbulence in the flame zone.

Ballal and Lefebvre[50] proposed a model of flame propogation in mixtures in which the fuel is present in the form of multidroplet mist, or vapour, or both. They also carried out flame speed measurements for three different fuels over a range of values of droplet size, vapour concentration, equivalence ratio and pressure to validate their model. The basic assumption of the model is that, under normal steady-state conditions, the rate of flame propogation through a fuel mist is always such that the quench time of the reaction zone is just equal to the sum of the evaporation and chemical reaction times. Their expression of flame speed is:

$$S_L = \alpha_g \left[\frac{C_3^3 (1 - \Omega) \rho_f d_{32}^2}{8 C_1 \rho_g \log_e (1 + B)} + \frac{\alpha_g^2}{S_{LV}^2} \right]^{-0.5} \qquad (2.6)$$

where

S_L is the laminar flame speed

S_{LV} is the laminar flame speed for gaseous or fully vaporised, premixed mixture

α_g is the thermal diffusivity

Ω is the fraction of total fuel in form of vapour

$C_1 = d_{20}/d_{32}$, $C_3 = d_{30}/d_{32}$ experimentally determined constants that define the drop size distribution

d_{20} is the mean surface area diameter

d_{30} is the mean volume diameter

d_{32} is the sauter mean diameter

ρ_f and ρ_g are the densities of liquid and gas phases respectively

The validity of the model has been supported by a close level of agreement between flame speed predictions based on the above expression and the corresponding values obtained for three different fuels when tested over a wide range of experimental conditions using a vertical tube.

In their studies on NO_x production in aerodynamically stabilised, 40-80 μm diameter, monodisperse isopropanol-air spray flames, Nizami and Cernansky[51,52] observed significant droplet size effects and an optimum droplet diameter with regard to lowest NO_x levels. In general, as the droplet size decreases, NO_x also decreases reaching a minimum value when the droplet size is approximately 50 μm. Further reduction in droplet diameter increases NO_x, ultimately reaching the value of the prevaporised/premixed mixture. Sarv et al.[53] studied the effects of using four different hydrocarbon fuels droplets on NO_x emissions in one-dimensional monodisperse spray combustion system. Their results confirmed the observations of Nizami and Cernansky about the optimum droplet size for minimum NO_x emissions. For all of the tested fuels the optimum droplet size was in the range 43-58 μm. Their theoretical analysis and experimental observations also indicated that the extent of prevaporisation is an important factor in determining the mimimum NO_x point.

Limited data in the literature indicates that droplets can also affect the ignitibility of a fuel-air mixture. For example, Rao and Lefebvre[54] have shown that for

kerosene droplets sprayed into a 19 m/s air flow at 25^0C inlet temperature, the ignition limit could be extended from air/fuel ratio of 17.25 with 76 μm droplets to air/fuel ratio of 26.33 with 59 μm droplets. They also found that atomisation quality is more important than ignition energy for lean mixtures. Ballal and Lefebvre[55] studied the ignition and flame quenching of steadily flowing heterogeneous fuel-air mixtures. They measured the minimum ignition energies over a wide range of fuels and mean drop sizes. Their results demonstrated that the optimum spark gap width (i.e. the gap width corresponding to minimum ignition energy) increases with the increase in mean droplet size. Unfortunately, they did not investigate droplets smaller than 40 μm. Thus if an optimum droplet size for ignition existed, as has been shown in the flame speed studies, they would not have observed it.

In engines however, the effect of droplet size on the combustion and related parameters has been studied in connection with the diesel engines only. For example, Mansouri et al.[56] in their engine simulation found that thermal efficiency, NO_x emissions, and pressure during the combustion and expansion processes are sensitive to changes in mean droplet size. Their results showed that as the droplet diameter increases, these parameters decrease slowly up to 20 μm and then rapidly for droplet diameters more than 20 μm.

2.7 Cycle Simulation Models

Prior to the appearance of high speed digital computers, attempts to predict the performance of spark ignition engines suffered from the difficulties of great arithmetic complexity and tedious repetitive calculations. The development of the thermodynamic charts eliminated many of these tedious calculations with regard to thermal dissociation of the burnt gases. Such charts have been widely used in the analysis of the Otto cycle from the time of their introduction in 1936 by Hershey et al.[57]. While these charts allow a considerable reduction in the mathematical difficulties of the Otto cycle analysis, however, they are not general as they are presented for a particular fuel and a selected number of air/fuel ratios. Also a constant volume combustion is considered so that the effect of engine design parameters cannot be effectively determined without great difficulty.

Rabezzana et al.[58] developed a method for the analysis of flame propogation during combustion which took into account combustion chamber geometry, spark timing and piston motion. Although, this analysis considered the thermodynamics of the working mixture in an incomplete manner, pressure-time diagrams could be calculated from measured flame propagation rates. These analyses were hindered because fundamental data about flame propogation was not available. However, even if such data had been available, the great magnitude of the calculations involved

would have precluded any extensive analysis.

The problem of considering the combined effects of mixture composition, variable specific heats, dissociation, flame propagation, heat transfer, piston motion and other combustion related phenomena simultaneously presented such a formidable mathematical obstacle that not until the widespread use of digital computers was such an alalysis contemplated. In this context, Edson[59] in 1960, proposed an analytical model for combustion in the spark ignition engines which was suitable for programming on a digital computer. His analysis included the effects of flame propagation, dissociation, and piston motion, but did not include heat transfer. Edson visualised three separate subsystems existing in the combustion chamber during combustion, viz. the burnt, the unburnt, and the small segment of mass being transferred from the unburnt to the burnt condition.

In 1964, Patterson and Wylen[60] suggested a model to simulate the spark iginition engine combustion. A spherical flame propagation was assumed and the position of the flame front relative to the ignition point was determined from the burnt gas volume and the length-volume distribution of the combustion chamber. The rate of flame travel was based on the laminar flame theory of Semenov[61]. Combustion was assumed to occur in numerous small increments each of which consisted of seven steps. Each increment included the burning of some of the charge, piston motion, and heat

transfer according to the expression of Eichelberge[62].

Strange[63] published some work on the analysis of an ideal Otto cycle which included the effects of heat transfer, finite combustion rates, chemical dissociation and mechanical losses. During combustion the system was assumed to comprise ten cells of equal mass. These cells were allowed to react one at a time to form equilibrium products. An iterative procedure was used to determine the correct system mass and energy balance. When these had been proved to be correct, heat transfer and system volume changes were considered.

Phillipps and Orman[64] in 1966, reported a completely new analytical model of a spark ignition engine combustion. They attempted to simulate the combustion in a Ricardo E6 engine and, in so doing, utilised the concept of spherical flame propagation. The flame propagation was assumed to follow that predicted by the thermal laminar theory of Mallard and Le Chatelier[65] with a modification to allow for the effects of turbulence. The model took into account heat transfer, dissociation and finite rates of heat release as dictated by flame propagation across the combution chamber.

Lucas and James[66] developed a mathematical model of the compression, combustion and expansion phases of the Renault IFP variable compression ratio engine. Finite rates of flame propagation and heat release were computed on the

basis of Semenov's theory[61]. To allow for the effects of turbulence, Semenov's estimate of laminar burning velocity was multiplied by a term derived from flame speed measurements in the engine. They performed a parametric study on the effects of some engine operating variables such as air/fuel ratio, spark timing, compression ratio, exhaust residuals and injected water as a means of controlling certain emissions.

Benson et al.[67] presented a complete spark ignition engine cycle simulation, including the intake and exhaust systems. The model combines a power cycle simulation with a gas dynamic model for the cylinder and ducts allowing for chemical reactions in the exhaust pipe. The power cycle simulation requires one empirical factor to correct for the turbulent speed of the spherically assumed flame front. In this model Kuehl's expression for laminar flame speed[68] was used on the basis that it is the only expression which takes into account the effect of pressure on flame speed.

Hiroyasu and Kadota[69] developed a new model to study the combustion and exhaust emissions in spark ignition engines. Their model consists of two major parts, a flame propagation model and an emission formation model. The model overcomes the shortcoming of the previously reported models in that it does not require any measured pressures for calibration. In this model, the flame was assumed to propagate across the combustion chamber as a spherical front emanating from a spark plug; a heterogeneous temperature

field and uniform pressure in the cylinder were also assumed. The cylinder was assumed to consist of unburnt gas and numerous elements of burnt gas which burned during successive small increments of the crank angle. A study on the effects of chamber geometry, air/fuel ratio, turbulence intensity and other parameters on the pressure and temperature history, burnt mass fraction and exhaust emissions was carried out.

All simulation models surveyed above have assumed that the working mixture to consist mainly of air, exhaust residuals and single component fuel in the vapour form only. Soliman[70], however, in his study on the effect of methane/kerosene mixture as spark ignition engine fuel has diverged from the commonly assumed vapour-air-residuals working mixture. He assumed it to consist of liquid fuel droplets in addition to the usual three components. Soliman, using Spalding's equation for single droplet evaporation[13], calculated the evaporation rate during the compression and combustion phases before the droplets were traversed by the flame front. He did not consider the evaporation and combustion of the droplets when they are in the flame zone and assumed the flame propagated in a vapour-air mixture only. Any liquid fuel left behind the flame front was assumed to continue to evaporate in an oxygen free atmosphere to form part of the emitted unburnt hydrocarbons. Soliman reported that cylinder pressure increases as the assumed vapour content of the mixture increases. The two-zone combustion model takes into account heat transfer,

flame quenching and auto-ignition phenomena.

In a recently published spark ignition engine model, Yuen and Servati[71] included an intake manifold model which accounts for not only the manifold filling effect (which was included in Benson's model Ref.(67)), but also fuel evaporation, deposition and entrainment. The model has been designed to study engine performance in terms of its drivability and emissions during a rapid transient. No attempts have been made to simulate the cycle phases and other in-cylinder phenomena, instead a general correlation for mean effective pressure was used to predict power generation. The emissions model was based entirely on the correlation of existing data tabulated as a function of inlet air flowrate and air/fuel ratio within the cylinder.

2.8 Closing Remarks

This literature survey clearly indicates that a lot of work has been done to understand and solve some of the problems associated with the spark ignition engine operation. A significant physical insight into the evaporation and transportation of air-fuel mixture can be gained through the model of Boam and Finlay. Although this model does not appear to deal with the wall film quantitively, it nevertheless gives a good representation of the whole flow in the intake manifold: by treating the fuel as a multicomponent substance present in the manifold as

droplets and wall film, the model becomes more representative than simpler single component, single form models. The model is supported by good agreement between the predicted overall evaporation and the measurements of Collins[29] and Pao[30] under steady engine operation.

The reported cycle simulations show that great efforts have been made in this area of research. Very advanced theoretical modelling has been applied especially in the combustion phase of the cycle. However, the survey also indicates that some work is still needed for better understanding of this type of engine. Many conclusions have been withdrawn in both areas of interest. These are summarised below:

(1) The effects of mixture preparation on engine performance and emissions are still not clearly defined.

(2) No satisfactory work has yet been reported which clarifies the behaviour of the wall film; its deposition, entrainment and the manner in which it really affects engine performance and emissions.

(3) Fuel evaporation during the gas exchange process has never been dealt with.

(4) The evaporation and combustion of multicomponent fuels within the cylinder during the compression and combustion phases of the cycle need more attention.

(5) The combustion of two-phase mixture, and the effect of droplet size have not been modelled in any spark ignition cycle simulation.

(6) The effect of the multicomponent fuel on different combustion parameters such as flame propgation and auto-ignition has not been studied.

(7) Cycle simulations should be more detailed. They should include flame quenching, auto-ignition (engine knock) and variable mixture composition and properties.

CHAPTER THREE

MODELLING OF MIXTURE PREPARATION PROCESSES IN A CARBURETTED SPARK IGNITION ENGINE

3.1 Introduction

Mixture preparation processes are mainly the atomisation and evaporation of the liquid fuel and the mixing of the generated fuel vapour with air to produce the required combustible mixture prior to ignition. In the carburetted spark ignition engine this mixture is prepared in both the intake system and the engine cylinder.

Fuel is introduced to the relatively high velocity air stream at the caburettor jet leading to the production of a wide range of droplet sizes. As the fuel is exposed to air most of the light fractions are immediately vaporised leaving the heavier fuel components to traverse the manifold as droplets or deposit in the wall film. Fuel is deposited on the carburettor and manifold walls as a result of the highly turbulent flow. If the engine is operating at small throttle opening, most of the early wall film is re-entrained to the mainstream and the fuel is re-atomised due to the high shearing forces at the throttle plate. An increase in the wall film quantity is expected if any bend or branching point exists in the manifold. In the inlet port, the rate of fuel evaporation is enhanced due to the relatively high wall temperature.

The remaining liquid fuel will be introduced to the high temperature environments in the cylinder during the intake stroke, leading to a high evaporation rate. During the compression stroke, fuel evaporation continues until a point is reached where it is found that fuel vapour condensation is possible, especially at high cylinder pressures.

The present chapter examines the models used to describe the processes involved in the mixture preparation process in both the intake system and the engine cylinder. A droplet combustion model is also included.

3.2 Fuel Composition and Properties

Fuel atomisation, evaporation and combustion are strongly affected by the composition of the fuel. In all it's forms, petrol consists mainly of hydrocarbons with variable amounts of impurities. Generally, however, this basic form of petrol is not immediately suitable for use in an internal combustion engine as it does not inhibit such things as "knock", formation of "gum", nor does it contain anti-rust additives, anti-icing additives or contains upper cylinder lubricants.

However, in the present work the only compounds to be considered are the hydrocarbons, of which the normal petrol contains approximately 36 different types[41,42]. The effects of chemical and physical properties of fuels on the mixture preparation and combustion processes have been recognised and reported in the literature. Litchy[72], Taylor[73], Obert[74] and Goodger[75] reviewed the early work on fuel properties and presented the studies which have been carried out into basic fuel properties methods of measurement, effects on engine performance and variation with fuel composition. The basic properties of interest are specific gravity, viscosity, surface tension, vapour pressure, latent heat of evaporation and calorific value.

Fuel specific gravity, surface tension and viscosity have a considerable effect on fuel atomisation and metering. Vapour pressure and latent heat of evaporation

have a significant effect on fuel evaporation, mixture homogeneity and distribution both between the individual engine cylinders and within each cylinder. While chemical properties affect the rate of flame propagation, cylinder pressure and temperature.

Kraus and Richard[76] investigated the effects of the change in fuel composition on the emissions of carbon monoxide, unburnt hydrocarbons and nitric oxides in vehicle exhausts. They concluded that fuel viscosity, vapour pressure and specific gravity have significant effects on exhaust emissions, but the magnitude of the effect depends on the design of the intake system.

With light hydrocarbons (gaseous fuels) the problems of mixture preparation are mainly confined to mixing, while with the liquified gaseous fuels, some heat supply may be necessary to make up for the latent heat absorbed. With intermediate hydrocarbons the volatility is such that the liquid fuel may be introduced into the air stream under a very small pressure difference with little attempt to increase the liquid surface area and so permit sufficient evaporation. Petrol, as mentioned earlier, contains all types of hydrocarbons, therefore, it should be subjected to all of the above processes in order to achieve the required degree of evaporation.

As the modelling of all petrol components is practically impossible, a representative fuel model must

include components covering a wide range of boiling temperatures. Many of the components in petrol, particularly the heavier ones, are present in small quantities which contribute little to the overall evaporation[41]. Finlay et al.[41] lumped together some of the low concentration heavier fractions and produced a fuel model of 16 components. This model is adopted in the present work. The 16 components are listed in table (3.1) together with their mass fractions and boiling temperatures. The methods used to calculate the properties of the individual components and the weighted mean properties of the fuel are given in appendix (A).

3.3 Atomisation of Liquid Fuels

In order to ensure high rates of liquid fuel evaporation in the intake system, the liquid fuel must be finely atomised and well distributed in the flowing air. Atomisation of liquids in a gas stream has been studied by a number of researchers[77,78]. Three stages can be distinguished in the atomisation process[77].

1. Initiation of small disturbances at the surface of the liquid, in the form of local ripples.

2. Action of air pressure and tangential forces on these disturbances, forming ligaments which may break up into drops.
3. Further disintegration of these drops in movement through air.

Theoretical and experimental investigations of atomisation process indicate that the following flow and geometric parameters affect the process:

1. Physical properties of the atomised liquid and the flowing gas.

2. Relative velocity between the two fluids.

3. the dimensions of the atomiser.

In the present study the carburettor used is a constant depression one in which air atomisation is the principal process. The droplets are formed initially when the stream issuing from the fuel jet encounters the air passing underneath the piston. At small throttle openings, droplets are re-atomised by the shearing effect of the flow past the throttle plate. Another important but different type of droplet generation is by wall film re-entrainment; this will be discussed in a different section (sec 3.5).

The work of Nukiyama and Tansawa[78] represents the most extensive series of experiments on air atomisation. Drop size-distribution and average drop size were determined for a range of liquid properties, flow conditions and atomiser size and configurations. Drop sizes were measured by collecting samples on small oil-coated glass slides. The effects of flow conditions and liquid properties on the Sauter mean diameter, d_{32} were correlated by the expression:

$$d_{32} = \frac{5.85 \times 10^{5}}{V_a - V_L} \sqrt{\frac{\sigma_L}{\rho_L}} + 7.742 \times 10^{3} \left(\frac{\mu_L}{\rho_L \sigma_L}\right)^{.45} \left(\frac{\dot{V}_L}{\dot{V}_a} \times 10^{3}\right)^{1.5} \qquad (3.1)$$

where

d_{32} is the Sauter mean diameter, (μm),

V_a, V_L are the air and liquid velocities, (m/s),

σ_L is the liquid surface tension, (Kg/s^2),

ρ_L is the liquid density, (kg/m^3),

μ_L is the liquid viscosity, (kg/m.s),

$\dot{V}_a, \dot{V}_L$ are the volume flowrates of air and liquid respectively, (m^3/s).

From this expression, it is seen that for small values of $(\dot{V}_L/\dot{V}_a)$, atomisation is a function only of relative velocity, surface tension and liquid density. At higher values of $(\dot{V}_L/\dot{V}_a)$, droplet size increases and liquid viscosity influences atomisation. Finlay et al.[41] suggested the following form for eqn. 3.1 when the liquid is petrol:

$$d_{32} = \frac{3.045 \times 10^3}{V_a - V_L} + 30\left(\frac{\dot{V}_L}{\dot{V}_a} \times 10^3\right)^{1.5} \qquad (3.2)$$

At the carburettor jet the fuel is relatively stagnant, eqn. (3.2) may be written as:

$$d_{32} = \frac{3.045 \times 10^3}{V_a} + 9.487 \times 10^5 \left(\frac{\rho_a}{\rho_f} \frac{1}{A/F}\right)^{1.5} \qquad (3.3)$$

where A/F is the air/fuel mass ratio and ρ_f is the fuel density.

The Sauter mean diameter in eqn. (3.1) was calculated from the experimental data using the expression:

$$d_{32} = \frac{\Sigma d_d^3 \Delta N_d}{\Sigma d_d^2 \Delta N_d} \qquad (3.4)$$

where ΔN_d is the number of droplets having diameters between $(d_d - \frac{\Delta d_d}{2})$ and $(d_d + \frac{\Delta d_d}{2})$.

3.4 Fuel Evaporation

The evaporation of the atomised fuel is the second major step in the mixture preparation process. Fuel evaporation may occur by either of the low temperature or the high temperature mechanisms. The first mechanism occurs when the temperature of the surroundings is substantially the same as that of the fuel. Under this condition the evaporation rate is determined by diffusion processes, the predominant fuel property being the vapour pressure. The high temperature evaporation occurs when the difference in temperature between the fuel and the surrounding atmosphere is considerable. Godsave[11] found that the volatility of the fuel does not have a dominant effect in determining the evaporation rate in this case. Instead, the rate is determined by the rate of heat transfer to the fuel, and so the important fuel characteristic is the heat necessary to raise the temperature of the fuel to it's boiling point and evaporate it.

A model of a single-component fuel droplet vaporising into static atmosphere under steady state conditions is shown in Fig. 3.1 Vapour diffuses to the ambient atmosphere at a saturation pressure corresponding to the droplet temperature. It is assumed that droplet temperature is at a value below that of the surroundings, so that heat is transferred to the droplet at a rate just enough to supply the required heat for evaporation. For the condition of

spherical symmetry, the differential heat and mass transfer equations for a spherical surface at a distance, r from the droplet centre is given by[132]:

$$\frac{dm}{dt} = \frac{4\pi K}{L+C_p(T-T_s)} r^2 \frac{dT}{dr} \qquad (3.5)$$

$$\frac{dm}{dt} = \frac{4\pi PDM_w r^2}{RT} \frac{d}{dr} \left[\ln\left(1-\frac{P_v}{P}\right)\right] \qquad (3.6)$$

where:

- L is the latent heat of evaporation at droplet surface temperature,
- C_p is the vapour specific heat,
- T is the temperature at the stagnant film around the droplet,
- T_s is the droplet surface temperature,
- K is the mixture thermal conductivity,
- r is the radial distance from droplet centre,
- D is the diffusivity of vapour in air,
- M_w is the molecular weight of fuel,
- P is the ambient pressure,
- R is the universal gas constant,
- P_v is the vapour pressure.

In the derivation of these equations it is assumed that:

i. a quasi-stationary state exists such that the vapour concentration and temperature gradients around the droplet, at every instant, are those corresponding to equilibrium values for the existing droplet size, and

ii. the temperature in the droplet interior is constant at it's equilibrium value.

Assuming that C_p , K and D/T are constants and represent the mean values between droplet surface and the surroundings, the integration of eqns. 3.5 and 3.6 and the introduction of correction factors ϕ and α yields:

$$\frac{dm}{dt} = \frac{2\pi k d_d}{L} (T_g - T_s)\phi \qquad (3.7)$$

$$\frac{dm}{dt} = \frac{2\pi D M w d_d}{RT} (P_{v,s} - P_{v,\infty})\alpha \qquad (3.8)$$

where:

$$\phi = \frac{\ell n \left[1 + \frac{C_p (T_g - T_s)}{L}\right]}{\frac{C_p}{L} (T_g - T_s)} \qquad (3.9)$$

$$\alpha = P / \left[\frac{P_{v,s} - P_{v,\infty}}{\ell n \left(\frac{P - P_{v,s}}{P - P_{v,\infty}}\right)}\right] \qquad (3.10)$$

and

T_g is the ambient temperature,

ϕ is a correction factor for the effect of mass movement of the fuel vapour on the heat transferred to the droplet surface.

α is a correction factor for the difference in the calculated values of diffusion rates based on diffusion of one gas through a second stagnant gas and equimolar counter diffusion.

For evaporation into low temperature surroundings where the sensible heat change of the vapour between the droplet surface and ambient atmosphere is small compared with the latent heat of evaporation, the correction factor, ϕ approaches unity and eqn. 3.7 reduces to:

$$\frac{dm}{dt} = \frac{2\pi K d_d}{L} (T_g - T_s) \qquad (3.11)$$

Similarly, for evaporation where vapour pressure at droplet surface is small compared to the total pressure, the correction factor, α approaches unity and eqn. 3.8 reduces to:

$$\frac{dm}{dt} = \frac{2\pi D M_w d_d}{RT} (P_{v,s} - P_{v,\infty}) \qquad (3.12)$$

In the above quasi-steady model of droplet evporation it is assumed that droplet temperature is spacially uniform and temporally constant. The heat supplied is assumed to account for the heat required for evaporation only. In high temperature environment, however, the heat transferred to the droplet is sufficiently high such that the temperature

of the droplet is temporally varying. Many models[18-21] have been reported accounting for this phenomenon. For evaporation with droplet heating eqn. 3.5 becomes:

$$\frac{dm}{dt} = \frac{4\pi K}{H + C_p(T-T_s)} r^2 \frac{dT}{dr} \qquad (3.13)$$

where H is the slowly-time-varying effective latent heat of evaporation, that includes the latent heat of evaporation, L, plus the amount needed to heat the droplet interior per unit mass of evaporated fuel.

Secondly, most of the practical fuels are blends of many compounds with wide range of physical and chemical properties. In the calculation of evaporation rate for drops of multicomponent fuels the partial saturation vapour pressure of each component at the droplet surface is modified by the presence of the remaining components. This can be determined by assuming that the liquid mixture behaves as an ideal mixture such that Raoult's law:

$$\bar{P}_{i,s} = M_{fi} P_{i,s} \qquad (3.14)$$

applies, where M_{fi} is the mole fraction of fuel component i. Eqn. 3.14 states that the partial pressure of component i in a mixture is proportional to it's vapour pressure when it is in the pure state, the proportionality constant being it's mole fraction in the mixture.

Finally, the conditions during mixture preparation process in the engine are such that a relative velocity between the evaporating fuel and air always exists. Correlations of the droplet evaporation under forced convection are based on both heat and mass transfer relations. Accordingly, eqns. 3.11 and 3.12 become:

$$\frac{dm}{dt} = \frac{2\pi K d_d}{L} (T_g - T_s) Nu_h \qquad (3.15)$$

$$\frac{dm}{dt} = \frac{2\pi D M_w d_d}{RT} (P_{v,s} - P_{v,\infty}) \, Nu_m \qquad (3.16)$$

where Nu_h and Nu_m are the Nusselt number for heat and mass transfer respectively.

Several expressions for the Nusselt number of evaporating drops are found in the literature. The Ranz and Marshall[79] correlation has been adopted:

$$Nu_h = 1 + .3 \, Re_d^{1/2} \, Pr^{1/3}$$
$$Nu_m = 1 + .3 \, Re_d^{1/2} \, Sc^{1/3} \qquad (3.17)$$

where:

Re_d is the droplet Reynolds number,
Pr is the Prandtl number,
Sc is the Schmidt number.

3.5 The Liquid Wall Film

Normally, the fuel enters the cylinder of an engine by three routes: as a vapour, as droplets and as a liquid film flowing along the wall of the inlet port. The physical and chemical properties and the quantity of the liquid fuel in the film are important parameters in determining the engine performance and emissions. Film quantity and properties are not constants but vary with the mode of engine operation. They are influenced by the amount of heat supplied, air velocity, turbulence level and throttle plate setting.

The mechanisms of wall film generation and destruction in the intake system of an engine are not fully understood. No work has yet been reported on the rates of droplet deposition and re-entrainment, which are not only important in determining the wall film quantity, but also in the calculation of the momentum and energy interchange between the main-stream and the wall film. In the experimental part of the present work, however, it is revealed that:

1. For a straight manifold the wall film is mainly generated upstream the throttle plate due to one or more of the following reasons:

    a) poor atomisation at the carburettor nozzle leads to the generation of relatively large drops which cannot be carried by the air-stream and so deposit on the wall,

b) due to the combined effect of fuel viscosity and surface tension some of the fuel flows directly from the nozzle to the wall without being atomised.

c) the droplet deposition rate is very high due to the highly turbulent flow within the carburettor, and

d) the geometrical nature of the carburettor increases the probability of droplet impaction on the walls.

2. At partial throttle opening, the throttle plate increases the rate of droplet deposition due to both the deflection of the main flow towards the wall and the increase of turbulence level downstream of the plate. At small throttle openings, however, air velocity at the throat is so high that the wall film is sheared off to the main-stream.

3. In the manifold, the combined effect of wall film entrainment and evaporation is higher than droplets deposition, so that wall film quantity decreases as the length of the manifold increases. However, it never becomes zero. At small wall film thickness the net change in film flowrate is zero and the film reaches it's equilibrium thickness.

4. At bends, droplet impaction is high which increases the wall film flowrate. The entrainment from a sharp bend is found to be higher than that from a smooth

bend, so that the wall film quantity is higher after a smooth bend for the same manifold length.

The measured wall film mass flowrates have been correlated with an equation of the form:

$$\bar{m}_{ff} = A_o + A_1\dot{m}_{ff} + A_2\dot{m}^2_{ff} + A_3\dot{m}^3_{ff} \qquad (3.18)$$

where:

$\bar{m}_{ff}$ is the wall film rate of change = $Q_e + Q_v - Q_d$

Q_e, Q_v and Q_d are the entrainment, evaporation and deposition rates respectively.

A_o, A_1, A_2 and A_3 are correlation parameters, whose values depend on the total fuel in the system.

An equation to predict the initial wall film mass flowrate at the throttle plate has been derived:

$$\dot{m}_{ffi} = A \exp(B\dot{m}_{ft}) \qquad (3.19)$$

where:

$\dot{m}_{ft}$ is the total fuel mass flowrate,

A and B are correlation parameters, whose values depend on the throttle plate setting.

A smooth and sharp bend factors have also been determined. Details of the methods used to derive these equations are given in chapter (5). Eqns. 3.18 and 3.19 are sufficient for the prediction of the wall film mass flowrate

at any point within the intake system; however, individual values for Q_e, Q_d and Q_v are required in the calculation of energy interchange between the wall film and the mainstream.

Generally, four different mechanisms are known for the deposition of suspended particles (liquids or solids) on the wall of the carrying duct: diffusional, gravitational, electrostatic and inertial forces[80]. For the deposition of fuel droplets on the manifold wall, however, the diffusional and electrostatic forces are not important. This is because droplet sizes are large enough to ignore the diffusional effects and that the earthed metallic manifold wall overcomes the generated electrostatic charges.

Theoretical and experimental studies[27,80,82-84] on the deposition of suspended particles have assumed that the process is unidirectional, (i.e. the deposited particles are not re-entrained). For such a condition the following equation is commonly used for the deposition rate:

$$Q_d = K_d C \qquad (3.20)$$

where K_d is the mass transfer coefficient and C is the droplets concentration within the gas stream.

Relations for K_d have been suggested by many researchers, however, no general agreement is noted. In addition to the usual problems associated with experimental

accuracy, McCoy and Hanratty[82] pointed that results in horizontal flows could be quite different from those of vertical flows because of the influence of gravity. Very little work has been reported on the deposition in horizontal flow. Among these are the works of Friedlander and Johnstone[80] and Sehmel[84] which are of no interest here since their experiments were carried out using very small particles.

Alexander and Coldern[27] carried out experiments on the deposition of 27 μm water drops on the wall of a horizontal pipe carried in an air stream at velocities of 25-100 m/s. The deposition rate was estimated by examining the change in the radial profile of the droplets flux: the mass transfer coefficient, K_d was correlated by:

$$K_d = 8.34338 \times 10^{-4} V_a^{1.17} \quad (m/s) \qquad (3.21)$$

where V_a is the air velocity, (m/s).

On the other hand, droplet entrainment may occur in one or both of two mechanisms: wave entrainment and entrainment by the release of bubbles[85]. In annular two-phase flow the interface between the main-stream and the wall film is not smooth but covered with a complex pattern of waves. McManus[24] found that the amplitude of the waves might be several times greater than the mean film thickness. A wavy film can be entrained in several different ways such as roll-wave shearing off, wave undercutting, droplet impingment and liquid bridge

disintegration[85]. For horizontal flow the shearing off of the roll-wave crests is the most important entrainment mechanism[86,87].

Many factors are known to affect droplet entrainment, the most powerful of these are the main-stream velocity and the thickness of the wall film. There is no reliable method for entrainment rate calculation. There are, however, many methods to correlate the entrainment rate such as those of Hewitt[88], Dallman and Hanratty[89] for vertical flow and of Akagawa et al.[28] for horizontal flow. Akagawa et al. correlated the entrainment rate to the main-stream velocity and the wall film thickness in an equation of the form:

$$Q_e = 4.57 \times 10^{-7} h_m^{3.5} V_a^{9} \rho_f \ (kg/m^2.s) \qquad (3.22)$$

where h_m, V_a and ρ_f are the mean film thickness, (m), gas velocity, (m/s), and the density of the liquid in the film, (kg/m^3).

Liquid film thickness can be related to the film mass flowrate if the distribution of the film around the manifold periphery is known. In horizontal annular flow, gravity acts in a direction normal to the flow and this produces a circumferential flow in the film which is superimposed on the axial flow. That is, the horizontal annular flow tends to be asymmetric even if the liquid is injected uniformly around the periphery. This asymmetry is well illustrated by the results of McManus[24] and Finlay et al.[33].

However, many factors affect this behaviour and force the film to be uniformly distributed. Pletcher and McManus[90] suggested that secondary flows of the gas phase may cause upwards liquid transport from the bottom of the tube. A further mechanism which affects the redistribution of the film under gravitational effects is that of droplets entrainment. Since the film is thicker at the bottom of the tube, higher waves exist and more entrainment occurs. Redeposition of the droplets on the upper part of the tube occurs and a continuous cyclic process is set up in which the uniform distribution of the film is established.

In the present work the film is assumed to be uniformly distributed around the manifold periphery. Hence, film thickness may be related to it's mass flowrate by:

$$h = \frac{\dot{m}_{ff}}{\rho_f V_f \pi D_m} \qquad (3.23)$$

where V_f and D_m are the wall film velocity and manifold diameter repectively. In eqn. 3.23 both, h and V_f are unknowns. It is shown in appendix (B) that:

$$V_f = \frac{f_g \rho_g V_a^2}{\mu_f} h \qquad (3.24)$$

where f_g, ρ_g and μ_f are the gas phase friction factor, density and liquid film viscosity.

The size of the entrained droplet is important in determining the mass and heat transfer rates. Kataoka et al.[86] reviewed many of the available entrained droplet size correlations and set their own correlation for the volume mean diameter as:

$$D_{vm} = .01 \frac{\sigma_f}{\rho_g j_g^2} R_{eg}^{2/3} \left(\frac{\rho_g}{\rho_f}\right)^{-1/3} \left(\frac{\mu_g}{\mu_f}\right)^{2/3} \qquad (3.25)$$

where j_g is the gas flux.

In a recent study, Azzopardi[91] carried out several series of experiments to determine the effect of gas velocity, drop concentration, film flowrate and tube diameter on drop size in an annular two-phase flow. Film flowrate and tube diameter have been found to have very little influence on the sizes of drops. Azzopardi suggested an empirical equation to calculate drop size:

$$d_{32} = \lambda \left[\frac{15.4}{We^{.58}} + 3.5 \frac{G_{Le}}{\rho_L V_a}\right]$$

where $\lambda = \sqrt{\sigma_L/\rho_L g}$

$W_e = \rho_L V_a^2 \lambda/\sigma_L$ is the Weber number

G_{Le} is the entrained liquid mass flux.

As the present model assumes a monosized drops, it is therefore assumed that the entrained droplets will have the same size as that of the droplets which already exist in the flow.

Finally, the evaporation rate from the liquid film is assumed to follow the low temperature evaporation model mentioned in sec.3.4. The Nusselt number, however, is taken as that of forced convection in tubes for Reynolds number $\geq$ 4000, that is;

$$N_{uh} = .023 R_e^{.8} P_r^{.4} \qquad (3.27)$$

$$N_{um} = .023\ R_e^{.8}\ S_c^{.4}$$

3.6 Mixture Preparation Model in the intake System

From the literature survey on mixture preparation, it is clear that little work has been done on the modelling of fuel evaporation and transportation in the intake system of a carburetted spark ignition engine. It was decided to adopt the model proposed by Boam and Finlay[42] to study mixture preparation within the intake system. This is because:

1. The model assumes a multi-component fuel which is more representative of the actual case than simpler single component fuel models.

2. The model treats the liquid fuel as entrained droplets plus wall film which is more practical than dealing with droplets only.

3. The model is supported by good agreement between the predicted overall evaporation and the measurements of Collins[29] and Pao[30] on a running engine.

However, a new wall film deposition and entrainment model has been suggested and incorporated into the Boam and Finley model. The annular two-phase, multi-component flow of air, fuel vapour, fuel droplets and wall film found in the induction system is assumed to be one-dimensional, steady and turbulence free. It is additionally assumed that:

1. Air and the multi-component fuel vapour are perfectly mixed and behave as ideal gas.

2. The droplets are spherical, monosized, with the Sauter mean diameter to represent the size, and uniformly suspended in the mixture.

3. Internal circulation of the fuel within the droplet is so fast that the droplet temperature and composition are maintained spatially uniform but temporally varying.

4. No combustion or other chemical reaction takes place.

5. Droplet coalescence is ignored.

6. Secondary atomisation at the throttle plate is possible.

7. Liquid fuel transferred from the main-stream to the wall film and vice versa is assumed to mix perfectly with the surrounding liquid.

8. The manifold is represented by a circular,variable cross-sectional area pipe and the complex geometric area of the carburettor is assumed to be as shown in Fig. 3.2 following Finlay et al.[41].

9. Following Boam and Finlay[42], the throttle plate is treated as a convergent-divergent nozzle. The flow past the throttle plate is assumed to be a constant enthalpy expansion to the required manifold pressure. Down-stream of the throttle plate a recovery length is assumed at which the flow area is less than the geometric area of the manifold. This length is considered to be proportional to the degree of the throttle plate opening (see Fig. 3.2).

10. The curved inlet port is modelled by a variable cross-sectional area pipe of equivalent length ($\theta.r$). These later parameters are obtained from cylinder head drawings supplied by Ricardo Consulting Engineers plc. Wall film deposition is increased by a bend factor obtained during tests on a Ricardo E6 engine using a variety of manifold configurations with fuel supplied from an SU carburettor. These tests are described together with the analysis in chapter 5. Heat flux through the inlet port wall, valve stem and valve head is considered to be always present. The inlet valve is treated as a convergent-divergent nozzle in a manner similar to the throttle plate. Swirl effect is neglected, but it can be considered by increasing the inlet port length assuming that the effect of swirl is to increase the path of the flow.

11. Wall film is assumed to be present only down-stream the throttle plate. It starts at the throttle plate with a maximum value which depends on the air/fuel ratio and throttle setting.

12. The drag on the droplet is mainly caused by the difference between the local velocities of the droplet and the gas stream. The drag coefficient for the droplet is assumed to follow the correlation of Ingebo [92]:

$$C_d = 27\ \bar{Re}_d^{.84} \qquad (3.28)$$

where Re_d is the droplet Reynolds number.

13. The density of the air-vapour-liquid fuel droplets mixture is calculated using the formula suggested by James[93] for two-phase flow:

$$\rho_m = \frac{1}{\frac{x^{1.5}}{\rho_g} + \frac{(1-x^{1.5})}{\rho_L}} \qquad (3.29)$$

where:

$x = \dfrac{\dot{m}_g}{\dot{m}_g + \dot{m}_L}$ is the mixture quality

$\dot{m}$ is the mass flowrate,

ρ is the density,

and g,L are for gas and liquid phases.

14. Film thickness is assumed to be very small compared to the manifold diameter and the shear stress in the liquid film is taken to be constant and equal to the wall shear stress. This leads to that the friction factor between the main stream and the film is equal to that between the main stream and the manifold wall. For the calculation of the friction factor the Colebrook correlation [94] is used.

$$\frac{1}{\sqrt{f}} = -2\text{Log}_{10}\left(\frac{\varepsilon/D_m}{3.7} + \frac{2.51}{Re_m\sqrt{f}}\right) \qquad (3.30)$$

where f is the friction factor,

ε is the surface roughness,

Re_m is the main stream Reynolds number.

15. It is assumed that fuel vapour is saturated at the fuel surface (droplet or film) and the saturation pressure is given by the Clausius-Clapeyron relation as:

$$P_{st,i} = \exp\left[\frac{L_i}{R_{v,i}}\left\{\frac{1}{T_{b,i}} - \frac{1}{T_s}\right\}\right] \quad (\text{atm}) \qquad (3.31)$$

where

L is the latent heat of evaporation,

R_v is the fuel vapour gas constant,

T_b is the boiling temperature,

T_s is the fuel surface temperature,

i is of the i^{th} fuel component.

16. Vapour is transferred by diffusion and convection from the liquid fuel surface. The binary diffusion coefficient of fuel component, i, is calculated using the correlation of Slattery and Bird[95]:

$$D_i = \frac{2.745 \times 10^{-8}}{P} \left[\frac{M_{w,i} + M_{wa}}{M_{w,i}\, M_{wa}}\right]^{1/2} (P_{c,i} P_{ca})^{1/3} (T_{c,i}\, T_{ca})^{.495} T^{1.823} \quad (m^2/s) \qquad (3.32)$$

where

M_w is the molecular weight,

P is the total pressure, (atm),

P_c is the critical pressure, (atm),

T_c is the critical temperature, (^{0}K),

T is the system temperature, (^{0}K),

a is for air.

17. In the calculations of heat transferred between the main stream and the liquid fuel (droplet or film), the adiabatic temperature, T_{aw} is required. This is calculated using the formula given by Kays and Crawford[96]:

$$T_{aw} = T \left(1 + r \frac{\gamma - 1}{2} M_a^2\right) \qquad (3.33)$$

where:

γ is the adiabatic exponent,

M_a is the Mach number,

r is a dimensionless "recovery factor" which is a function of Reynolds and Prandtl numbers.

$r = p_r^{1/2}$ for laminar flow.

$= p_r^{1/3}$ for turbulent flow.

The value of T_{awd} is calculated using droplet Reynolds and Mach numbers Re_d and Ma_d, while T_{awf} is calculated using manifold Reynolds and Mach numbers Re_m and Ma_m.

Boam and Finlay applied the laws of conservation of mass, energy and momentum to both liquid and gas phases and obtained the following equations:

1. The conservation of energy applied to air and fuel vapour gives:

$$\frac{dT_a}{d\ell} = \left[\frac{\alpha_d n \pi d_d^2}{V_d} (T_d - T_{aw,d}) + \pi D_m \alpha_f (T_f - T_{aw,f}) - \right.$$

$$\left. -i\sum_{1}^{16} C_{pv,i} \left\{\frac{\dot{m}_{de,i}}{d\ell} (T_d - T_a) + \frac{\dot{m}_{fe,i}}{d\ell} (T_f - T_a)\right\} + \right.$$

$$+ \frac{1}{2} \sum_{i=1}^{16} \left\{ \frac{\dot{m}_{de,i}}{d\ell} (V_a^2 - V_d^2) + \frac{\dot{m}_{fe,i}}{d\ell} V_a^2 \right\} -$$

$$- V_a \frac{dV_a}{d\ell} \left(\dot{m}_a + \sum_{i=1}^{16} \dot{m}_{v,i} \right) - V_d \frac{dV_d}{d\ell} \sum_{i=1}^{16} \dot{m}_{d,i} \Big]^* \cdot$$

$$\frac{1}{\left[\dot{m}_a Cp_a + \sum_{i=1}^{16} \dot{m}_{v,i} Cp_{v,i} \right]} \qquad (3.34)$$

where

$$\alpha_d = \frac{K_a}{d_d} \left(2 + .6 Re_d^{1/2} \, Pr_a^{1/3} \right)$$

$$\alpha_f = \frac{K_a}{D_m} \times .023 \, Re_m^{.8} \, Pr_a^{.4} \qquad (3.35)$$

and

T	temperature
ℓ	distance from fuel jet
α	heat transfer coefficient
n	number of droplets/sec passing any section
d_d	droplet diameter
V	velocity
D_m	manifold diameter
C_p	specific heat
M	mass flowrate
K	thermal conductivity
f	of film
d	of droplet

v of vapour

aw adiabatic

e by evaporation

2. The conservation of energy applied to liquid fuel film gives:

$$\frac{dT_f}{d\ell} = \frac{1}{\sum_{i=1}^{16} \dot{m}_{f,i}\, C_{pf,i}} \left[\pi D_m \{H - \alpha_f (T_f - T_{aw,f}) + Q_d\, Cp_d \right.$$

$$\left. (T_d - T_f)\} + \sum_{i=1}^{16} Li \frac{d\dot{m}_{fe,i}}{d\ell} \right] \qquad (3.36)$$

where

Q_d deposition rate

L latent heat of evaporation

H manifold wall heat flux

3. The conservation of energy applied to liquid fuel droplets gives:

$$\frac{dT_d}{d\ell} = \frac{1}{\sum_{i=1}^{16} \dot{m}_{d,i} Cp_{d,i}} \left[- \frac{\alpha_d\, \pi d_d^2}{V_d} (T_d - T_{aw,d}) + \sum_{i=1}^{16} Li \right.$$

$$\left. \frac{d\dot{m}_{de,i}}{d\ell} + Q_e \pi D_m\, Cp_f\, (T_f - T_d) \right] \qquad (3.37)$$

where Q_e is the entrainment rate.

4. The conservation of mass applied to air and fuel vapour gives:

$$\rho_a V_a A_c + \sum_{i=1}^{16} \rho_{v,i} V_g A_c = \dot{m}_a + \sum_{i=1}^{16} \dot{m}_{v,i} \tag{3.38}$$

from which, if $V_a = V_g$

$$\frac{1}{V_a}\frac{dV_a}{d\ell} + \frac{1}{A_c}\frac{dA_c}{d\ell} + \frac{\{\frac{d\rho_a}{d\ell} + \sum_{i=1}^{16} \frac{d\rho_{v,i}}{d\ell}\}}{\{\rho_a + \sum_{i=1}^{16} \rho_{v,i}\}} = \frac{\sum_{i=1}^{16} \frac{\dot{dm}_{v,i}}{d\ell}}{A_c V_a \{\rho_a + \sum_{i=1}^{16} \rho_{v,i}\}} \tag{3.39}$$

where

A_c	cross-sectional area
ρ	density
a	air
v,i	vapour of i^{th} component

5. The conservation of momentum applied to the system gives:

$$A_c \frac{dP_T}{d\ell} - \pi r_h f \rho_m V_a^2 + [\dot{m}_a + \sum_{i=1}^{16} \dot{m}_{v,i}] \frac{dV_a}{d\ell} +$$

$$+(V_a - V_d) \sum_{i=1}^{16} \frac{\dot{dm}_{de,i}}{d\ell} - \dot{m}_d \frac{dV_d}{d\ell} - V_a \sum_{i=1}^{16} \frac{\dot{dm}_{fe,i}}{d\ell} +$$

$$+ \pi D_m V_d (Q_d - Q_e) = 0 \qquad (3.40)$$

where P_T total pressure

r_h hydraulic radius

ρ_m mixture density

6. Applying the partial pressure law yields:

$$\frac{dP_T}{d\ell} = \frac{dP_a}{d\ell} + \sum_{i=1}^{16} \frac{dP_{v,i}}{d\ell} \qquad (3.41)$$

7. Differentiation of air and vapour gas laws yields:

$$\frac{1}{P_a}\frac{dP_a}{d\ell} - \frac{1}{\rho_a}\frac{d\rho_a}{d\ell} - \frac{1}{T_a}\frac{dT_a}{d\ell} = 0 \qquad (3.42)$$

and

$$\frac{dP_{v,i}}{d\ell} = \frac{R_{v,i}}{\dot{m}_a R_a} \frac{\left[\frac{d\dot{m}_{de,i}}{d\ell} + \frac{d\dot{m}_{fe,i}}{d\ell}\right]\left[P_T - \sum_{i=1}^{16} P_{v,i}\right]^2}{\left[P_T + P_{v,i} - \sum_{i=1}^{16} P_{v,i}\right]} \qquad (3.43)$$

where

$$\frac{d\dot{m}_{de,i}}{d\ell} = \frac{\pi n d_d^2}{V_d} \beta_{d,i} (\bar{P}_{std,i} - P_{v,i}) \qquad (3.44)$$

$$\frac{d\dot{m}_{fe,i}}{d\ell} = \pi D_m \beta_{f,i} (\bar{P}_{stf,i} - P_{v,i}) \qquad (3.45)$$

$$\frac{d\dot{m}_{v,i}}{d\ell} = \frac{d\dot{m}_{de,i}}{d\ell} + \frac{d\dot{m}_{fe,i}}{d\ell} \qquad (3.46)$$

$$\beta_{d,i} = \frac{D_i}{d_d \, R_{v,i} \, T_d} \left(2 + .6 \, Re_d^{1/2} \, Sc_i^{1/3}\right) \tag{3.47}$$

$$\beta_{f,i} = \frac{D_i}{D_m \, R_{v,i} \, T_f} .023 \, Re_m^{.8} \, Sc_i^{.4}$$

and

P	partial pressure
$\bar{P}_{st}$	saturated partial pressure
R	gas constant
D	diffusion coefficient
S_c	Schmidt number
β	mass transfer coefficient.

8. Equating the rate of change of momentum to the drag force on the droplets gives:

$$\frac{dV_d}{d_\ell} = \frac{.75 \, C_d \rho_a \, (V_a - V_d)^2}{d_d \, \rho_d \, V_d} \tag{3.48}$$

where

C_d is the Ingebo drag coefficient.

9. The application of continuity of mass to the fuel droplets yields:

$$\frac{d_d}{d\ell} = \frac{2}{d_d^2 \, \rho_d n} \sum_{i=1}^{16} \frac{\dot{m}_{de,i}}{d\ell} \tag{3.49}$$

10. The mass flowrate of liquid fuel in droplets

$$\dot{m}_d = \frac{n \pi d_d^3 \rho_d}{6} \qquad (3.50)$$

Whence

$$d_d = \left(\frac{6\dot{m}_d}{n\pi \rho_d}\right)^{1/3}$$

Full details of the model are given in Ref. (42). Equations 3.35 - 3.50 were integrated from the carburettor jet to the required intake system length using a fourth-order Runge-Kutta method.

3.7 Modelling of Fuel Evaporation and Combustion Inside the Engine Cylinder

To complete the study of fuel droplet life history, fuel evaporation and combustion inside the cylinder is modelled. The period under consideration is that during the intake process, compression stroke and during the flame propogation process. The combustion of the droplets within the flame zone is also modelled. Physically, this period corresponds, as far as the evaporation process is concerned, to the situation involving a droplet located few millimeters downstream the inlet valve just before the intake process starts until this droplet is traversed by the flame front.

In Fig.3.3 the intake stroke model is shown. The model may be broken down into the following stages:

1. Initially, the cylinder contains residuals at pressure, P_1, temperature, T_1, and mass, m_1.

2. As the crank shaft rotates through a step $d\theta$, the cylinder draws fresh mixture containing a number of droplets, N_a (with initial SMD, d_1 and initial temperature, T_{d_1}) and fuel vapour of mass, Vap_a, which depends on the achieved total evaporation in the intake system. The mass of the fresh mixture drawn and hence the number of the droplets and fuel vapour mass are functions of the step length, system geometry

and the thermodynamic conditions in both the cylinder and the inlet port. The pressure, temperature and mass in the cylinder are updated according to the thermodynamic model (described in chapter 4) to P_2, T_2 and m_2 with fuel vapour concentration:

$$C_{vap_2} = \frac{Vap_a}{m_2} \quad .$$

3. Practically, the evporation process takes place within step (2) at varying cylinder conditions from P_1, T_1 and m_1 to P_2, T_2 and m_2 at different fuel vapour concentrations and other droplet related parameters. In the model it is assumed that the evaporation process takes place at mean cylinder conditions (i.e. $P = \frac{P_1 + P_2}{2}$, $T = \frac{T_1 + T_2}{2}$ and $m = \frac{m_1 + m_2}{2}$) and that the droplet parameters T_d and d are those at the start of the step. Due to the evaporation process, cylinder pressure, temperature, vapour quantity, droplet diameter and temperature will be changed to the final values of P_f, T_f, d_{a_1}, Vap_f, T_{da_1} .The predicted values of cylinder pressure, temperature, mass and fuel vapour mass are considered to be the initial values for the next step (P_1, T_1, m_1, Vap_1).

4. In the second step of crank shaft rotation droplets of number, N_b with the initial SMD, d_1 and temperature, T_{d_1} will undergo evaporation at:

$$P = \frac{P_1 + P_2}{2}, \quad T = \frac{T_1 + T_2}{2}, \quad m = \frac{m_1 + m_2}{2} \quad \text{and}$$

$$C_{vap} = \frac{(Vap_1 + Vap_b)/2}{m}$$

with final conditions of:

P_3, T_3, m_2, Vap_2 (= Vap_1 + Vap_b + vapour produced in the process), d_{b_1} and T_{db_1}. The size and temperature of the droplets d_{b_1} and T_{db_1} produced in this step are different from d_{a_1} and T_{da_1} produced by step (3) due to the relatively smaller evaporation rate of segment (B). This is due to the lower cylinder temperature and higher vapour concentration at the time when segment (B) is introduced into the cylinder.

5. During the second step the droplets in segment (A) undergo their second stage of evaporation at:

$$P = \frac{P_3 + P_1}{2}, \quad T = \frac{T_3 + T_1}{2}, \quad m = \frac{m_1 + m_2}{2} \quad \text{and}$$

$C_{vap} = \frac{(Vap_2 + Vap_1)/2}{m}$ with final conditions of d_{a_2}, T_{da_2} and Vap_f (= Vap_2 + vapour produced in the process). Due to evaporation cylinder pressure and temperature are updated to P_f and T_f. The final values of this step are considered to be the initial values for the next step.

6. In the third step of the crank shaft rotation the droplets in the newly introduced fresh mixture (segment(c)) evaporate as in point (4) with final conditions of P_3, T_3, m_2, Vap_2, d_{c_1} and T_{dc_1}. Droplets in segment (B) evaporate for the second time as in point (5) with final conditions of:
P_4, T_4, m_2, Vap_3, d_{b_2} and T_{db_2}. This is followed by the third evaporation of the droplets in segment (A) at:

$$P = \frac{P_4 + P_1}{2}, \quad T = \frac{T_4 + T_1}{2}, \quad m = \frac{m_1 + m_2}{2} \quad \text{and}$$

$$C_{vap} = \frac{(Vap_3 + Vap_1)/2}{m} \quad \text{to the final conditions of:}$$

P_f, T_f, Vap_f, d_{a_3} and T_{da_3}.

As the intake process proceeds droplets which entered the cylinder at the start of the process may evaporate completely as a result of longer residence time in the cylinder. The mixture at the end of the intake process (trapped point) will therefore, contain droplets with wide range of sizes and temperatures. Using eqn. 3.4 a new Sauter mean diameter is found. A new droplet temperature is required as well. To obtain this a "Sauter mean temperature" is introduced here as:

$$T_{d_{32}} = \frac{\Sigma\ T_d^3\ \Delta N_d}{\Sigma\ T_d^2\ \Delta N_d} \qquad (3.51)$$

The intake stroke is followed by the compression stroke during which the increasing mixture temperature tends to enhance the evaporation rate while the increase in mixture pressure tends to retard it. A point may be reached at which the effect of pressure on the evaporation rate becomes more than that of the temperature and the vapour starts to condense on the droplet. There is no strong evidence in the literature against the condensation of the fuel vapour inside the cylinder. Indeed, Peters's[1] measurements of droplet size inside the cylinder indicates that the droplets were growing. Peters put the following explanations for the increase in droplet size:

a) Droplet expansion due to heating,

b) droplet collisions,

c) condensation of fuel vapour due to the increase in cylinder pressure,

d) different droplets have been monitored due to the effect of swirl.

However, Peters rejected the first three possibilities and suggested that the effect of swirl is the only factor in the observed phenomenon.

Further supporting evidence to the possibility of fuel vapour condensation is that of Law[21]. During the testing of his multi-component droplet evaporation model, Law has set the ambient fuel vapour concentration of all the components to zero "hence excluding the possibility of condensation for any species"[21].

The interchange of vapour between the droplet surface and the surrounding atmosphere will continue during the compression stroke until the spark is discharged. After the development of the flame front the combustion chamber is subdivided into two zones. Droplets in the unburnt zone continue to evaporate in the manner explained above, however, the evaporation rate might be greater due to the higher temperature. Droplets traversed by the flame front during flame propogation evaporate with combustion. In such type of evaporation ambient vapour concentration is no longer important, instead oxygen concentration is the controlling parameter. During combustion, it is assumed that the outwardly diffusing multi-component vapour reacts stoichiometrically and completely with the inwardly diffusing oxygen at an infinitely thin flame around the droplet. Droplets which survive this process are assumed to continue evaporating behind the flame front in an oxygen free atmosphere, forming part of the unburnt hydrocarbons.

The major assumption in the present evaporation and combustion model is that there is no relative speed between the droplet and the surrounding mixture. If such speed is found in the cylinder, this assumption leads to lower evaporation rate. While the measurements of Peters[1] indicated the presence of swirl in the cylinder, this does not necessarily imply droplet relative velocity. In the present work intake system evaporation model it is found that the relative velocity depends on the inlet valve lift. In the table below the relative velocity is given for two positions at different valve lifts:

	Air Velocity, Droplet Velocity (m/s)	
Valve lift	at the	6 mm
mm	throat	downstream
.645	172,46	70,52
4.97	25,20	13,20
10.69 (max)	12,14	9,13

droplet diameter ≈ 29 μm.

This table shows that the droplets are settling down very quickly and implies that the assumption of zero relative velocity is acceptable. Furthermore, at small valve lifts, where the relative velocity is high, the number of droplets entering the cylinder is not sufficient to affect the total evaporation rate. Finally, Peters[1] observed that droplets that enter the cylinder at low valve lifts, both at the beginning and end of the intake process, were larger than those entering at higher valve lift which,

in turn, reduces the evaporation rate of these droplets.

Evaporation rate is calculated using the "ideal mixture" model for multi-component fuel droplet evaporation proposed by Law[21]. This model is basically the classical "d^2- Law" model[11] modified to allow for droplet heating, which is expected to be an important factor in controlling the droplet evaporation rate. In this model it is assumed that as the cylinder temperature and pressure continuously increase, the droplet temperature will also increase. Part of the heat absorbed by the droplet is used for evaporation; the rest is used in heating up the droplet.

In addition to the assumptions detailed in section 3.6, it is assumed that diffusion and radial convection are the controlling transport processes in delivering heat from the ambient to the droplet surface, and subsequently in dispersing the fuel vapour from the surface to the ambient.

The "ideal mixture" model of Law[21] is as follows:

1. Assuming quasi-steady process and spherical symmetry for the gas-phase, the conservation of fuel vapour and energy yields (in non-dimensional form):

$$\dot{m}_F = \ell n(1 + B) \qquad (3.52)$$

where

$\dot{m}_F$ is the total mass evaporation rate

$$= \sum_{i=1}^{16} \dot{m}_i \; ; \quad \dot{m}_i = \dot{m}_i'/4\pi\rho_i D_i r_d$$

D_i is the diffusion coefficient of fuel component, i

r_d is the droplet radius

and B is the transfer number

$$= (T_\infty - T_s + \hat{Y}_{O,\infty}\hat{Q})/(\hat{L} + H) \qquad (3.53)$$

T is temperature $= C_p T'/L_r$

T' is the dimensional temperature,

L_r is the reference latent heat of evaporation.

The species-weighted quantities, designed by " ^ ", are

$$\hat{L} = \sum_{i=1}^{16} \Omega_i L_i \qquad \text{Latent heat of evaporation}$$

$$\hat{Q} = \sum_{i=1}^{16} \Omega_i Q_i \qquad \text{Heat of reaction} \qquad (3.54)$$

$$\hat{Y}_{O,\infty} = Y_{O,\infty}/\hat{\nu} \qquad \text{Oxygen mass fraction}$$

$$\hat{\nu} = \sum_{i=1}^{16} \Omega_i \nu_i \qquad \text{Stoichiometric oxygen/fuel ratio.}$$

where

Ω_i Fractional mass evaporation rate = $\dot{m}_i/\dot{m}_F$

$$= Y_{i,s} + (Y_{i,s} - Y_{i,f})(1 - Y_{F,s})/(Y_{F,s} - Y_{F,f}) \qquad (3.55)$$

where

Y	mass fraction
s	at droplet surface
f	at flame surface
i	of i^{th} component
F	of total vapour
∞	at ambient (cylinder).

The slowly time-varying heat input function required to heat the droplet, H, is given by:

$$H = \frac{(T_\infty - T_s + \hat{L} - \hat{Q}) + (1 + \hat{Y}_{o,\infty}) \quad [\hat{Q} - \hat{L}(1 - Y_{F,f})/(1 - Y_{F,s})]}{(1 + \hat{Y}_{o,\infty})(1 - Y_{F,f})/(1 - Y_{F,s}) - 1} \qquad (3.56)$$

In the above equations $Y_{i,f}$ is artificially set to $\neq 0$ so that generalized expressions are obtained which can be specialised to combustion, with $Y_{i,f} = Y_{F,f} = 0$, or pure evaporation, with $Y_{o,\infty} = 0$ and $Y_{i,f} = Y_{i,\infty}$.

2. Phase-change relations give:

the mole fraction $M_{fi} = \frac{\bar{P}_{i,s}}{P_{i,s}}$

where:

$\bar{P}_{i,s}$ is the saturated partial pressure given by eqns. 3.14 & 3.31

$P_{i,s}$ is the saturated pressure of component i.

The combination of eqns (3.14) and (3.31) yields:

$$X_{i,s} = \frac{M_{fi}}{P_\infty} \exp \{\frac{Cp_i L_i}{K_i} (\frac{1}{T_{bi}} - \frac{1}{T_s})\} \qquad (3.57)$$

and $X_{i,s}$ is related to $Y_{i,s}$ through

$$Y_{i,s} = X_{i,s} W_i / \{(1 - \sum_{i=1}^{16} X_{i,s}) + \sum_{i=1}^{16} X_{i,s} W_i\} \qquad (3.58)$$

where

$W_i = M_{wi}/M_{wa}$

M_{wi} is the molecular weight of i^{th} component

M_{wa} is the molecular weight of air.

3. Liquid phase balance give droplet radius:

$$R^3 = \{1 - \sum_{i=1}^{16} \int_o^t \frac{\dot{Rm}_i}{\rho_{Li,o}} dt\} \{\frac{\sum_{i=1}^{16} M_{fi} W_i/\rho_{Li}}{\sum_{i=1}^{16} M_{fi} W_i/\rho_{Li,o}}\} \qquad (3.59)$$

where

$$R = \frac{r_d}{r_{d,o}}$$

$t = t' \ (3\rho_i D_i)/(r^2_{s,o} \ \rho'_r)$ dimensionless time

ρ'_r reference vapour density

L_i liquid pure state

o at time zero.

droplet temperature

$$T_s = T_{s,o} + \int_0^t [(\dot{m}_F H)/(R^2 \bar{\rho}_L)]dt \qquad (3.60)$$

where

$$\bar{\rho}_L = \sum_{i=1}^{16} \bar{\rho}_{Li} \ ; \ \bar{\rho}_{Li} = \frac{\bar{\rho}'_{Li}}{\rho'_r} \text{ dimensionless density}$$

$$\bar{\rho}'_{Li} = \frac{M_{fi} \ W_i}{\sum_{i=1}^{16} M_{fi} \ W_i/\rho'_{Li}} \text{ partial density}$$

Full details of the methods used to derive these equations are given in Ref.(21). The equations are integrated using a step-wise technique.

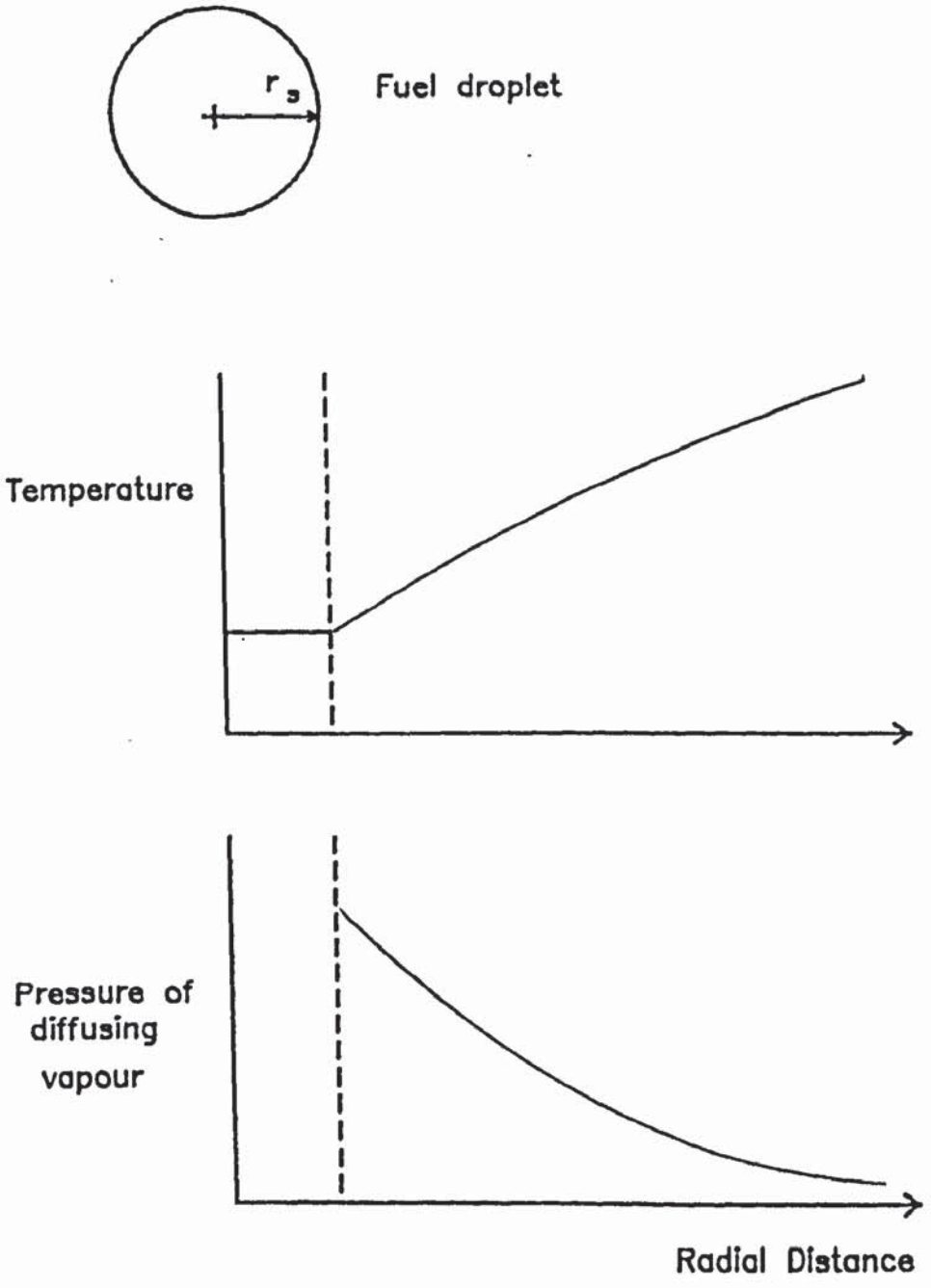

FIG. (3.1) Model for Evaporation of Droplet Under Static Conditions.

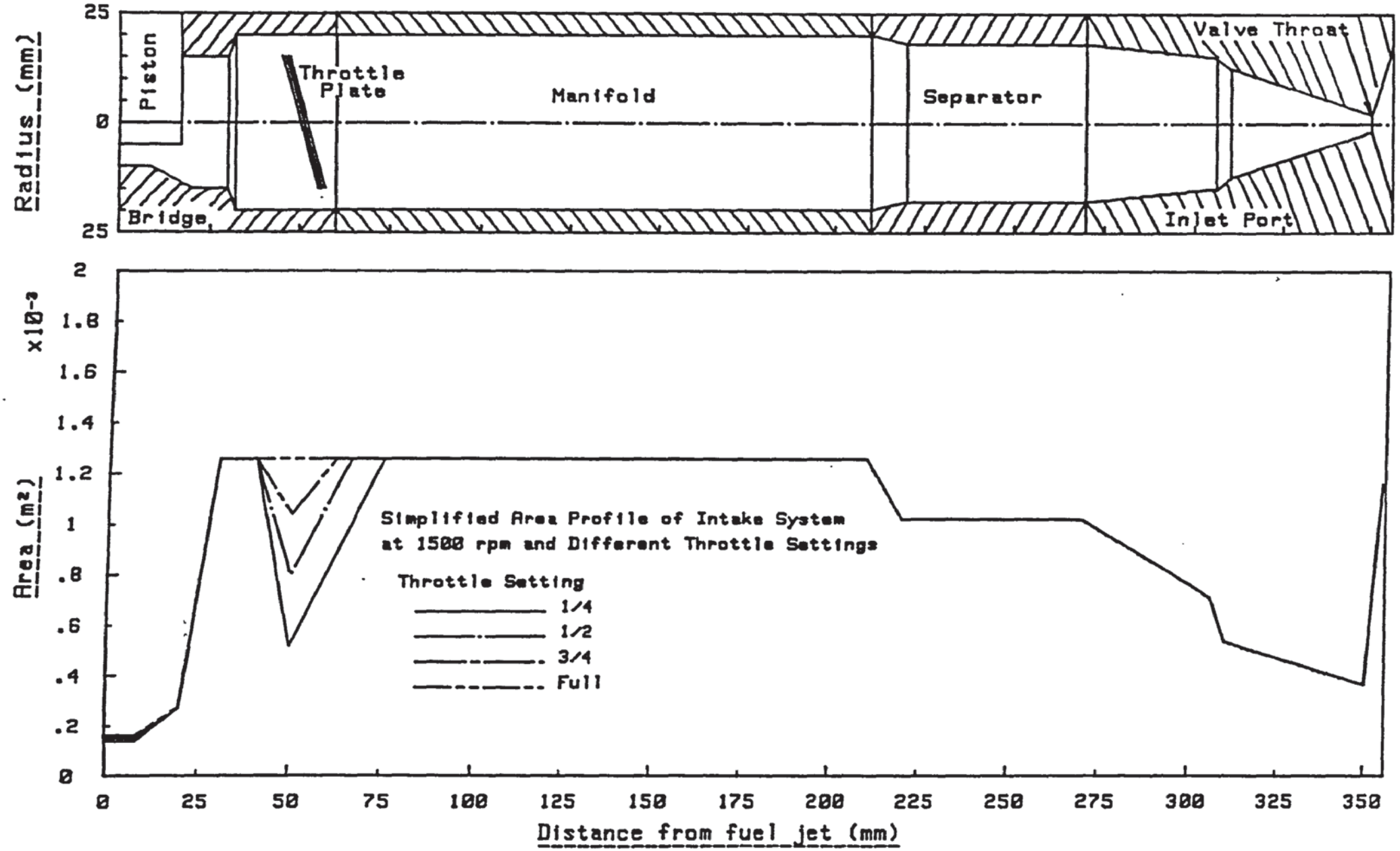

FIG.(3.2) Actual and Simplified Geometries used in Model

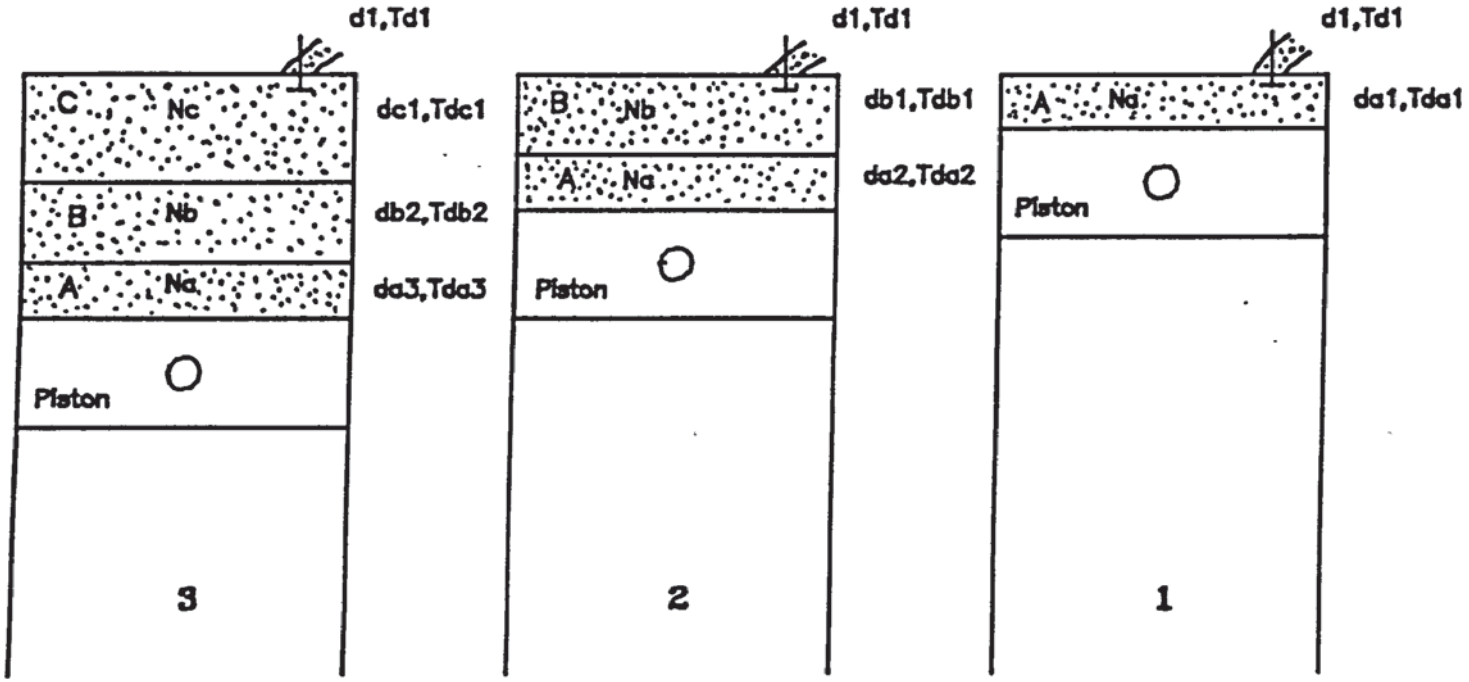

N ... number of droplets
d ... droplet diameter
Td... droplet temperature
A,B & C are the drawn fresh charge segments

FIG. (3.3) Intake Stroke Evaporation Model

The components are listed according to boiling point.

Mw = molecular weight
Tb = normal boiling point, °K
L = latent heat of evaporation ,MJ/gm.mol
Qvs = heat of combustion , GJ/Kgmol

No	Formula	Name	Mw	Tb	L	Qvs	Weight %
1	C_3H_8	Propane	44.097	231.1	18.773	2.044	.05
2	C_4H_{10}	Iso–Butane	58.124	261.3	21.296	2.658	1.44
3	C_4H_{10}	N–Butane	58.124	272.7	22.392	2.651	4.79
4	C_5H_{12}	2–Methyl Butane	72.151	301	24.685	3.264	7.59
5	C_5H_{12}	N–Pentane	72.151	309.2	25.773	3.272	8.88
6	C_5H_{10}	2–Methyl–2 Butene	70.135	311.7	26.304	3.134	2.38
7	C_6H_{14}	2–Methyl Pentane	86.178	333.4	27.781	3.879	8.21
8	C_6H_{14}	N–Hexane	86.178	341.9	28.852	3.886	7.13
9	C_6H_6	Benzene	78.114	353.3	30.76	31.694	2.85
10	C_7H_{16}	2,3–Dimethyl Pentane	100.2	362.9	30.388	4.489	3.45
11	C_7H_{16}	N–Heptane	100.2	371.6	31.697	4.5	4.14
12	C_7H_8	Toluene	92.141	383.8	33.179	3.772	11.16
13	C_8H_{10}	M–Xylene	106.168	412.3	36.358	4.374	15.17
14	C_9H_{12}	3–Ethyl Toluene	120.19	434.5	38.534	4.99	9.08
15	C_9H_{12}	Pseudo Cumene	120.19	442.5	39.246	4.978	5.03
16	$C_{10}H_{14}$	N–Butyl Benzene	134.22	456.4	39.246	5.614	8.85

Table (3.1) Composition of Fuel used to Simulate Petrol

CHAPTER FOUR

MODELLING OF THE SPARK IGNITION ENGINE CYCLE PROCESSES

4.1 Introduction

It has been shown in the review of previous work on mixture preparation in spark ignition engines that fuel evaporation is incomplete in the induction system. To study the in-cylinder mixture preparation processes and the effects of the remaining liquid fuel droplets on the combustion, engine performance and emissions it was necessary to develop a realistic cycle model to accommodate the proposed models of fuel evaporation.

The present chapter examines the models used to describe all the processes which are relative to energy transfer during the complete spark ignition engine cycle. The computational procedures involved are presented in chapter 6 and appendix (E).

The basic assumption made in this model is that combustion will only proceed in a mixture of air and fuel vapour, taking into account the vapour produced when the droplets are encountered by the flame during flame propagation. Any liquid fuel left behind the flame will continue to evaporate in an oxygen free atmosphere forming part of the unburnt hydrocarbons in the exhaust.

The model may be broken down into the following stages:

1. At the release point "Exhaust Valve Opening, EVO" cylinder contents start to leave the cylinder under the effects of pressure difference (blow down), and piston movement. Valve overlap period commences at "Inlet Valve Opening, IVO" and continues to "Exhaust Valve Closure, EVC", during which blowback via the inlet valve is possible. During the induction process the fresh charge, which is assumed to be a mixture of fuel vapour perfectly mixed with air and mono-sized fuel droplets uniformly suspended in the mixture, is drawn from the inlet port. As these droplets enter the cylinder at different cylinder conditions, depending on the time at which the entry occurs, evaporation rate from the droplets will be different. Additionally, different residence time in the cylinder will produce a mixture of multi-diameter droplets. At the trapped point "Inlet Valve Closure" a new Sauter mean diamater is calculated. Heat transfer between the working mixture and the surrounding surfaces is accounted for during these processes.

2. a. The induction process is followed by the compression process. As this proceeds, cylinder pressure and temperature increase. The rate of vaporisation is affected in a way that it is

enhanced by the temperature rise and retarded by the pressure rise. Except at the initial stages of the compression process, heat transfer is from the working mixture to the surrounding surfaces.

2. b. Due to the rise in mixture pressure and temperature and due to the changes in vapour fuel concentration, the auto-ignition period, which is assumed to be dependent on the physical and chemical properties of the mixture will be decreased.

3. When the mixture is ignited by the spark, there is a short delay before a self sustaining flame is formed. This period corresponds to the time required for the flame kernal to propagate through a mixture of volume equal to .001 of the total cylinder volume[67]. After the delay period is consumed the combustion chamber is subdivided into two zones, burnt and unburnt zones, separated by a spherical flame front. As the flame propagates across the combustion chamber fuel droplets in both zones continue to vaporise (pure evaporation) at the corresponding cylinder pressure and the appropriate burnt or unburnt temperatures, while droplets traversed by the flame front will evaporate with combustion. During this stage it is assumed that no heat is transferred between the burnt and unburnt zones but that each transfers heat to the surrounding surfaces.

The flame is assumed to propagate with laminar burning velocity through the boundary layer around the spark plug and the rate of flame propagation depends on the conditions in the cylinder (pressure, unburnt mixture temperature and fuel vapour concentration). When the flame front has crossed the boundary layer, it is considered to propagate with a higher burning velocity depending on the turbulence level in the cylinder.

When propagating across the combustion chamber the flame front encounters a variety of relatively cold surfaces. The interaction between the propagating flame front and these surfaces produces a thin layer of unreacted mixture. The fuel left in this quench layer is considered to form part of the unburnt hydrocarbons in the exhaust.

The increase in the pressure and temperature of the unburnt mixture ahead of the flame front decreases the auto-ignition delay, hence increases the probability of knock occurrence.

4. Flame propagation will proceed until one of the following alternatives occur:

   a. the flame traverses all the combustion chamber space in normal combustion burning the available vapour fuel, or

b. the auto-ignition period is consumed and knock occurs.

5. Expansion follows with an increase in the cylinder volume until the exhaust valve opens.

4.2 Flame Propagation

4.2.1 General

The assumption of a finite period of time for the combustion process to be completed in requires the ability to calculate the mass of charge burnt at any particular point of flame travel in the combustion chamber. This can only be achieved from the knowledge of the rate at which the flame propagates, the volume of the mixture traversed by the flame during a particular interval of time and the density and composition of the unburnt mixture.

The flame speed measured in an engine combustion chamber by ion probes or combustion photography is the sum of the burning velocity relative to the unburnt mixture and the transport velocity of the flame front due to the expansion of the combustion products. The fundamental quantity to be investigated in this section is, however, the flame front motion due to the reaction only, that is, the flame propagation relative to the unburnt mixture. It has been shown by many workers[97-99] that the two forms of

flame propagation (viz. laminar and turbulent) might exist in the combustion chamber of a spark ignition engine. Laminar flame propagation occurs at the two ends of the combustion process due to the presence of a laminar layer around the spark plug at the beginning of the combustion and near to the combustion chamber wall at the end of the flame travel. In the laminar layer the mixture is practically stagnant; thus until the flame propagates out of it into the more turbulent region of the chamber, the flame speed must be laminar in nature.

The effect of different flow parameters on the burning velocity has been studied experimentally and many expressions have been reported correlating the burning velocity to the mixture temperature, pressure, composition and turbulence level. For flame propagation in engines, it is generally assumed that:

i. the ratio of turbulent to laminar burning velocities is a linear function of engine speed, and

ii. the flame propagates in a spherical pattern from the spark plug.

The prediction of the laminar burning velocity is difficult for many reasons[107]. These are:

i. there is no complete theory which can readily be used. There are, however, a number of approximate

equations in the literature which approach the problem of flame propagation from various viewpoints,

ii. there is no data on the kinetics of the oxidation process under flame conditions, and very little data on transport properties at high temperature, and

iii. different methods of flame speed measurement give different values, so that it is difficult to compare data from different sources.

4.2.2 Laminar Flame Propagation

In view of the above mentioned difficulties in predicting burning velocities, various assumptions and approximations are made to simplify the problem. Based on the type of the simplifications used, two limiting mechanisms for laminar flame propagation were developed:

a. the thermal mechanism, and
b. the diffusional mechanism.

The thermal mechanism is based on the assumption that heat conduction is the most important physical process involved in the transfer of the reaction zone from one layer of the mixture to the next. The concentration of a given component at a point is assumed to be governed only by flow

and reaction processes. The Mallard and Le Chatelier[65] and Semenov[61] equations of laminar burning velocity are the original and most frequently used expressions based on the thermal mechanism. They are not used in this work for the following reasons:

a. the Mallard and Le Chatelier equation requires the knowledge of the ignition temperature and the reaction zone thickness which are difficult to obtain especially when dealing with multicomponent fuels and highly turbulent flow respectively.

b. both equations ignore the effect of pressure on flame speed, whilst it is widely accepted[68,102 103,106] that pressure has a non-neligible effect.

c. Bailey[100] attempted to use the Mallard Le Chatelier equation for his work on the combustion limitations of gaseous fuels in reciprocating engines. Some difficulties were encountered relating to the adjustment of temperatures: these were attributed to the exclusion of pressure-related effects on the burning velocity.

The diffusional mechanism maintains that the burning velocity is determined by diffusional processes. It is postulated that active particles and radicals (e.g. H', OH' and O'), produced by dissociation in the hot burnt gases and by chain branching, diffuse into the fresh mixture and cause

it to react explosively. the best known expressions based on this mechanism are those of Tanford and Pease[104] and of Manson[105]. Neither was used in this work however. This was because:

a. their accuracy of prediction is quite poor over the entire equivalence ratio range[107],

b. the Tanford and Pease expression requires detailed knowledge on the rate constants for the reactions involved, which are difficult to obtain,

c. in this work it is assumed that no pressure gradiant exist in the combustion chamber. The Manson theory, however, is based on the assumption of a small pressure drop across the flame front.

In view of the limitations in using any of the available theoretical laminar burning velocity expressions, it becomes necessary to base the rate at which the flame propagates in the combustion chamber on an empirical expression. Techniques for the measurement of flame speed may be considered under two categories: one in which the flame front is stable and stationary while the mixture is in motion through the flame, and one in which the mixture is initially quiescent and the flame propagates through it. Andrews and Bradley[108] presented a comprehensive survey of the different techniques for the measurement of burning velocity. The survey was carried out with particular

reference to the maximum burning velocity of methane-air mixtures.

The effects on the burning velocity of mixture temperature, pressure, equivalence ratio and fuel type have been studied using steady flow rigs or combustion bombs. It has been found that the initial temperature of the mixture has an appreciable effect on the burning velocity. It is generally found that burning velocity is a function of this temperature raised to a power between 1.4 and 2.1, the exponent varies with the temperature range covered. For propane-air mixtures in a temperature range 200-700^{0}K, Wanger et al.[109] suggested the expression:

$$S_L = 25 + .0085\ T_i^2 \qquad (4.1)$$

where

S_L is the laminar burning velocity (cm/s),

T_i is the initial mixture temperature (^{0}K).

and for methane-air mixtures in the same temperature range, Andrews and Bradley[106] suggested the expression

$$S_L = 10 + .000371\ T_i^2 \qquad (4.2)$$

The pressure dependence of burning velocity has been found by many investigators[68,102,103,106] to be of the form:

$$S_L = S_{La} P^n \qquad (4.3)$$

where S_{La} is the laminar burning velocity at one atmosphere and P is the mixture pressure. Under room temperature conditions, it has been found that the pressure exponent, n, is small ($\angle 1$) and negative for fuels with low burning velocities, and it is small ($\angle 1$) and positive for fuels with high burning velocities. The results of Goldenberg and Pelevin[102] showed that for a wide class of hydrocarbon-air mixtures the exponent is negative and varies within narrow limits of .25 - .3. Kuehl[68] found that this exponent is also dependent on mixture temperature. He found that for propane-air mixtures the value of the exponent approaches zero as the mixture temperature approaches the auto-ignition temperature.

Equivalence ratio effects on burning velocity have been studied by many workers[106,108-110,120,122,68]. It has been found that as equivalence ratio is increased the burning velocity passes through a maximum at an equivalence ratio between 1 and 1.3. The variation of burning velocity with equivalence ratio is more or less symmetrical about this maximum. For lean hydrocarbon-air mixtures, the burning velocity and equivalence ratio may be related by an expression of the form[110]:

$$S_L = A + B/\phi + C/\phi^2 + D/\phi^3 \qquad (4.4)$$

where A,B,C and D are pressure dependent correlation parameters and ϕ is the fuel-air equivalence ratio.

The above investigations provide data for various ranges of temperatures, pressures and equivalence ratios for different fuels. However, none provide data for simultaneous variations of all parameters, although, the available data[68] show that interaction of the variables must be taken into account in order to obtain generalized correlations. Recognising the need of such data, Kuehl[68] carried out an investigation to study the simultaneous effects of temperature, pressure and equivalence ratio on the burning velocity of propane-air mixtures. He proposed the following expression correlating the flame temperature, unburnt mixture temperature and system pressure:

$$S_L = \left[\frac{1.087 \times 10^6}{\left(\frac{10^4}{T_f} + \frac{900}{T_u}\right)^{4.938}}\right] P^{-.09876}$$

in which T_f, T_u and P are the flame temperature, ^0K, the unburnt mixture temperature, ^0K and the pressure, inch Hg repectively.

This expression was not used in the computer analytical model in this work for the following reasons:

a. it correlates data of lean propane-air mixtures which means that both equivalence ratio and fuel type are ignored,

b. pressure and temperature ranges at which the data was obtained is not comparable with those found in engines,

c. the use of flame temperature which is difficult to determine accurately. Indeed, Benson et al.[67] used the burnt zone temperature instead of T_f, but the problem arises from estimating the initial value of the burnt zone temperature.

Metghalchi and Keck[110,112] measured the burning velocities of mixtures of air with methanol, iso-octane, propane and indolene using the constant volume bomb method for equivalence ratios .8 - 1.5, over pressure range .4 - 50 atmosphere and temperature range 298 - 700^{0}K. They found that for temperatures above 350^{0}K, the data for all fuels could be fit within $\pm$ 10% by a simple power law of the form:

$$S_L = S_{Lr} \left(\frac{T_u}{T_r}\right)^{\alpha} \left(\frac{P}{P_r}\right)^{\beta} (1-2.1f) \qquad (4.6)$$

where

$$S_{Lr} = B_m + B(\phi - \phi_m)^2 \qquad (4.7)$$

is a fuel dependent reference burning velocity at reference pressure, P_r = 1 atm. and reference temperature, T_r = 298^{0}K.

B_m, B and ϕ_m are fuel dependent correlation parameters,

α, β are fuel independent correlation parameters,

$$\alpha = 2.18 - .8\ (\phi - 1)$$
$$\beta = -\ .16 + .22\ (\phi - 1) \qquad (4.8)$$

T_u is the unburnt mixture temperature

P system pressure,

f exhaust residuals mass fraction,

ϕ fuel-air equivalence ratio.

This expression will be used in the analytical model of the present work because it is simple and accounts for the most effective parameters in the combustion chamber during flame propagation. Additionally, Metghalchi and Keck have considered the effect of partially vaporised fuel which is important in this work. Jones and Evans[122] used this expression successfully in their work on the burning rates in spark ignition engines.

For the present work it is assumed that the equation for indolene provides the closest approximation to the laminar burning velocity of gasolene. The constants in equation (4.7) for indolene are:

B_m = 27.58 cm/s

B = -78.34 cm/s

ϕ_m = 1.13

4.2.3 Turbulent Flame Propagation

The fact that flame propagation can be considerably accelerated by turbulence has been familiar to the designers of internal combustion engines since early days[114], but a fundamental understanding of turbulent combustion has been lacking. The increased rate of burn of a turbulent flame over a laminar flame is normally accepted as being due to either one or a combination of the following three processes[115]:

1. the turbulent field may distort and wrinkle the flame front thereby markedly increasing its surface area. Turbulent burning theories which are based on this process are called Surface or Wrinkled flame front theories in which:

$$S_T = S_L \frac{A_T}{A_L} \qquad (4.9)$$

where S and A are the burning velocity and the flame surface area respectively and T, L are for turbulent and laminar.

2. turbulence may increase the rate of transport of heat and active particles, thus increasing the actual burning velocity.

3. turbulence may rapidly mix the burnt and unburnt mixtures in such a way that the flame becomes a homogenous reaction.

Theories based on processes 2 and 3 are defined as three-dimensional or volume turbulent combustion theories, the use of one of these is beyond the scope of this work. Thus, the turbulent burning velocity has to be based on a wrinkled flame front model. The work of Smith[116] on turbulent flame structure in engines supports the use of such a model. He found that the mean flame thickness is always greater than the laminar values and increases with engine speed due to the increase in turbulence density. The turbulent burning velocity is, therefore, the product of the laminar burning velocity calculated using Metghalchi and Keck expression (eqn.4.6) and a correction factor, K_f, thus:

$$S_T = K_f \times S_L \qquad (4.10)$$

The correction factor allows for many parameters affecting the rate of flame propagation in the combustion chamber which are not directly catered for in the Metghalchi and Keck expression. These primarily involve the aerodynamic conditions (viz. the turbulence and swirl)

existing in the combustion chamber. Many workers have found that this factor is a linear function of engine speed. A summary of the measured and predicted correction factors for different engines is given in table (4.1).

Benson et al.[67] suggested that this factor can be predicted by one of two methods. The best approximation of the value of K_f can be obtained by carrying out a number of calculations with different values of K_f and comparing the computed pressure-time diagrams and the experimental pressure-time diagrams. When the peak pressure in both the diagrams are matched the correct value of K_f is obtained. the other approximate method is followed in the case when no experimental pressure-time diagram is to hand. In this, K_f is adjusted until the computed pressure diagram gives a symmetrical burning time about TDC.

The value of K_f adopted in the present work is that found by Harrow and Orman[118] from experiments on the Ricardo E6 engine. This value was also used by Phillipps and Orman[64] in their Ricardo engine cycle simulation model. The technique used by Harrow and Orman to determine the value of K_f involved measurements of the flame speed in the combustion chamber using two ionization probes. The relation of Harrow and Orman is:

$$\frac{S_T}{S_L} = 1 + .002 \times N \qquad (4.11)$$

where N is the engine speed (rpm).

4.2.4 Flame Propagation Pattern

Knowledge of the pattern in which the flame spreads out from the ignition sourse is very important in the rate of burning and heat transfer calculations. It has been assumed in previous computer simulations of combustion in spark ignition engines[64,66,67] that the flame propagates spherically outwards from the spark plug, but from the works of Rassweiler and Withrow[121], Rabezzana et al.[58] and many others it is clear that the flame does not propagate spherically. Moreover, Beretta et al.[119] found that the flame centre is not always at the spark plug. Their data suggests that the flame centre moves rapidly when flame radius is less than 10 mm but stabilises for larger radii.

Numerous factors are known to exert some influence on the manner in which the flame propogates through the combustion chamber. Some of these are:

a. the geometrical design of the combustion chamber and inlet port which affect the swirl and turbulence intensities,

b. piston movement, and

c. charge homogeneity.

In the present work, however, the flame front is assumed to be spherical, or more exactly, that part of the sphere with its centre at the spark plug and contained within the geometrical limits of the combustion chamber. Turbulence is assumed to be of small-scale, that is, it does not affect the geometric shape of the flame front but merely makes it "ragged" and so increases its area. The justifications for assuming spherical flame propagation are:

a. the present work simulates the cycle of the Ricardo E6 engine which is equipped with a disc-shaped combustion chamber. This geometry reduces the effects of the combustion chamber on swirl and turbulence intensities, and

b. the effects of piston movement has been considered in the method used to calculate the required parameters.

Annand[120], reported a computational method to calculate the enflamed volume, flame front area and the wall surface area bounding the enflamed volume for a disc-shaped combustion chamber with the centre of the spherical flame at any chosen point on one of the flat surfaces. This method is adopted here with a modification to allow for the effect of piston movement. This modification consists of the updating of the chamber depth as the combustion process proceeds and setting a new range for the flame radius to

suit the new chamber depth. The method is described in appendix (c).

4.3 Unburnt Hydrocarbons Formation

4.3.1 General

The mechanism of formation of the unburnt hydrocarbons in the combustion chamber of a spark ignition engine varies with the mode of engine operation. Until recently, it was believed that one or more of the following mechanisms is the source of these emissions from a homogeneous charge engine:

a. at normal combustion chamber wall temperatures, the predominant mechanism is the quenching of the propagating flame at the walls. Daniel[123] found that the flame failed to propagate through the mixture located within about .05 to .38 mm of the combustion chamber wall,

b. at low wall temperatures, the UHC formation by wall quenching is augmented by fuel condensation[124,125],

c. a very small concentration of hydrocarbons can be formed as equilibrium products of the combustion reaction.[123],

d. the very high turbulent condition of the mixture in the combustion chamber may allow small pockets of unburnt mixture to pass through the reaction zone without being ignited[123,126],

e. incomplete burning of the charge at the presence of high exhaust gas residuals.

The wall quenching model of UHC formation has a stronger bases of support than any other mechanism. Experimental evidence has been found[123,127] which indicates that wall quenching of the combustion reaction occurs in an internal combustion engine. The apparent quench distances observed are in agreement with the quench distances from burner data at the same pressures and temperatures. In addition, the observed quench distances are of the right order of magnitude to account for the UHC found in the exhaust gas of an engine at many operating conditions.

Recently, however, this model has been substituted by a new understanding regarding the sources of UHC emitted by homogeneous-charge engines. It is now believed that crevice volumes and to a lesser extent oil films and/or surface deposits are the major sources of UHC emissions rather that wall quench layers[128]. This new understanding was obtained by applying newly developed measurement techniques and analysis methods. However, this model has not yet been

presented in a way which may be adopted for use in the UHC predictions under engine operating conditions. In the present work, therefore, it is considered that the UHC are produced from two sources:

1. The liquid fuel droplets which fail to vaporise completely in the flame zone and are left behind the flame front.

2. The flame quenching on the combustion chamber walls.

4.3.2 Flame Quenching

The quenching effect of relatively cold solid surfaces upon pre-mixed laminar flames has been explored by several workers. Friedman and Johnston[129] measured the quenching distance between two parallel plates for propane-air flames at different mixture pressures, temperatures and equivalence ratios and found that the increase in mixture pressure and temperature reduces the quenching distance; also there is an optimum equivalence ratio for minimum quenching distance.

By varying the initial composition in a constant volume bomb, Gottenberg et al.[130] found that the measured quenching distance increases in proportion to the amount of unreacted hydrocarbons. They also found that the quenching distance is affected by some of the bomb design and

operating parameters: it increases with the increase of the bomb surface area/volume ratio and decreases with the increase of burning velocity and wall temperature.

Potter and Berland[131] studied the effect of fuel type and burning velocity on the quenching distance. They found that:

a. the minimum quenching distance, for all hydrocarbons tested (saturated, unsaturated and aromatics), is obtained with rich fuel-air mixtures at equivalence ratio between.7 - .9, and decreases as molecular weight of fuel increases,

b. for stoichiometric fuel-air mixtures, the quenching distance varies inversley with burning velocity.

Daniel[123] was the first to demonstrate the existence of the quench layers in the combustion chamber of the spark ignition engine with photographs showing a decrease in flame luminosity close to the wall. He used the relations suggested by Friedman and Johnston[129], for laminar flame quenching distance, to calculate the thickness of the quench layer for several engine operating conditions. Daniel found that the calculated quench layer thicknesses are in fair agreement with the corresponding measured values using combustion photography.

Goolsby and Haskell[127] investigated the effects on quenching distance of the variation in equivalence ratio, manifold pressure, wall temperature, spark timing and fuel type using a CFR engine. The measured quench layer thicknesses ranged between .1 - 2 mm, and show strong dependence on equivalence ratio and manifold pressure.

4.3.3 Unburnt Hydrocarbons Formation Model

As mentioned earlier, the UHC sources considered here will be the liquid fuel droplets overtaken by the flame front and the flame quenching process. The UHC concentration at any time during flame propagation can be calculated as:

$$\text{UHC (\%)} = \left(\frac{m_{fd} + m_{fq}}{m_b}\right) \times 100 \qquad (4.12)$$

where

UHC (%) is the percentage of the UHC in the burnt charge,

m_{fd} is the mass of liquid fuel left from incomplete droplet combustion,

m_{fq} is the mass fuel trapped in the quench layer,

m_b is the total burnt zone mass.

The mass of the charge in the quench layer in an increment of time can be calculated from[70]:

$$m_q = \rho_u \left(\frac{A}{V}\right) \Delta V_b \, q_d \qquad (4.13)$$

where

m_q is the mass of charge (air + vapour fuel + liquid fuel + exhaust residuals) in the quench layer,

ρ_u is the unburnt charge density,

$\left(\frac{A}{V}\right)$ is the burnt zone surface area/volume ratio,

ΔV_b is the volume of charge traversed by the flame front during the time increment,

q_d is the quench layer thickness.

The thickness of the quench layer is predicted using the equation developed by Friedman and Johnston[129] viz.,

$$q_d = q_{dr} \left(\frac{P_r}{P}\right)^{\alpha} \left(\frac{T_r}{T}\right)^{\beta} \qquad (4.14)$$

where:

q_{dr} is the reference quench layer thickness at reference pressure, P_r and reference temperature, T_r,

P,T are the mixture pressure and temperature,

α,β are correlation parameters.

Friedman and Johnston reported the following numerical

values for the correlation parameters q_{dr}, α and β for propane-air mixtures at P_r = 1 atm and T_r = 300 K;

ϕ	q_{dr}(mm)	α	β
.7	.17	.8	1.5
1	.083	.9	.6
1.3	.084	.96	.49

From this data and the values of the quenching distance of hydrocarbon fuels reported in NACA report No. 1300 (ref. 132), Soliman[70] correlated the quenching distance for different hydrocarbon fuels using the following relation:

$$q_d = \psi\, q_{dr} \left(\frac{P_r}{P}\right)^{\alpha} \left(\frac{T_r}{T}\right)^{\beta} \qquad (4.15)$$

where:

ψ = $1.25(H/C - 3.26)^2 + .563$

H/C is the hydrogen /carbon atoms ratio

q_{dr} = $.92 - .7 \times \phi$ ($\phi \leq 1$)

= $.187 + .033 \times \phi$ ($\phi > 1$)

α = $.63 + .267 \times \phi$

β = $6.122 - 5.522 \times \sqrt{\phi}$ ($\phi \leq 1$)

= $1.386 - .786 \times \sqrt{\phi}$ ($\phi > 1$)

ϕ is the fuel-air equivalence ratio,

T_r = 300 K,

P_r = 1 atm.

4.4 Auto-Ignition Delay (Engine Knock)

4.4.1 General

Under certain operating conditions of a typical pre-mixed-charge spark ignition engine, large amplitude pressure waves are developed within the charge during the propagation of the turbulent flame. This phenomenon is called "knock" [135,136] and it affects engine efficiency, emissions, life and automobile drivability. The effect of the knock on engine life is mainly due to the increase in the rate of heat transfer to the combustion chamber walls. This is believed to be due to both the increase of flame temperature and the destruction of the boundary layer of the stagnant gas which normally protects the combustion chamber walls from direct contact with the flame.

Analysis of combustion data led to two general theories for the onset of knock[135]: the auto-ignition theory and the detonation theory. The auto-ignition theory postulates that due to sensitisation of the fuel-air mixture in the end gas region by preflame reactions, several portions of the charge undergo simultaneous auto-ignition, and this high speed combustion results in a local pressure imbalance and the characteristic gas vibration. On the other hand, the detonation theory implies that shock waves, are somehow developed during the propagation of the regular spark ignited flame-front,and initiate a reaction in the end

gas at detonation speed, when travelling through the unburnt mixture. However, as presented in a recent literature survey[136] the bulk of the experimental work supports the auto-ignition theory.

Theoretical research attempting to describe the detailed kinetics of the auto-ignition phenomenon[137,138], although extremely useful for understanding the problem, has not yet been able to produce practical tools for generalized knock prediction in engines. It is well known that even for pure hydrocarbons such as ethane[138], the kinetics of the pre-reactions leading to auto-ignition are very complex. Thus, a detailed analysis of this kind is hardly conceivable in the case of commercial fuels which are a mixture of a wide variety of hydrocarbons. The model used here is, therefore, based on empirical correlations of experimental data obtained either from engine tests or combustion studies of the auto-ignition phenomenon in a simulated engine-like conditions.

4.2.2 Description of the Auto-Ignition Knock Model

Auto-ignition delay has been defined by many workers [140-144] as a function of the mixture physical and chemical properties. It was decided to use the model proposed by Douaud[143,144] which relates the auto-ignition delay to the pressure and temperature of the end gas and to the equivalence ratio of the mixture. The model is simple and

makes use of an overall reaction rate which is valid for the pressure and temperature range encountered in spark ignition engines.

In this model the production rate of chain carriers ($d\alpha/dt$) as a function of their concentration α and the pressure and temperature of the end gas can be described by the equation:

$$\frac{d\alpha}{dt} = \alpha A' \, p^n \exp(-\frac{B}{T}) \qquad (4.16)$$

where

P is the mixture pressure

T is the mixture temperature

α is the chain carriers concentration

A' is a constant

n is the pressure coefficient

B is the temperature coefficient.

When pressure and temperature are constants, the integration of eqn. (4.16) between t_o and t_c yields:

$$\tau = t_c - t_o = AP^{-n} \exp(\frac{B}{T}) \qquad (4.17)$$

The time t_c for the occurence of auto-ignition corresponds to the critical value for the concentration of

the chain carriers α_c, and the time, τ is usually referred to as the auto-ignition delay.

Many investigators[140-142] have correlated the data of auto-ignition delay obtained at constant pressure and temperature studies for many fuels using eqn. (4.17).

When applied to time-variable pressure and temperature, the model (eqn. 4.16) can be written in an integral form provided that the critical concentration α_c obtained at time t_c of auto-ignition is independent of the pressure and temperature level. In this case, time t_c will be given by the equation:

$$1 = \int_{t_o}^{t_c} \frac{d_t}{AP^{\bar{n}}(t) \exp(\frac{B}{T(t)})} \qquad (4.18)$$

Livengood and Wu[145] determined the parameters A, n and B for a fuel using a compression machine and found that these values can explain the occurrence of knock in an engine using the same fuel. They computed the integral with the experimentally determined values of pressure P(t) and temperature T(t) of the end gas and compared t_c at which the value of the integral reached unity with the observed time of knock in the engine cycle.

When the delay parameters of a fuel are known, knock occurrence can be predicted by the thermodynamic simulation of the engine cycle which describes the pressure and temperature of the end gas. Unfortunately, the reported

values of these parameters differ widely in the literature for any given fuel. In addition, the available data is limited to few fuels, namely, n-heptane, n-dodecane, n-hexane,[142], benzene, iso-octane[141] and commercial petrol[144]. For the present work it was decided to use the reported parameters for the commercial petrol. The delay time can be predicted using the formula:

$$\tau = 7.2910^{-3}\ P^{-1.685}\ \exp\left(\frac{4341}{T}\right) \qquad (4.19)$$

where

τ is the delay time in seconds

P is the pressure (atm)

T is the temperature (^{0}K)

The effect of air/fuel ratio is also accounted for by the variation of the pre-exponent factor expressed by the following equation:

$$\frac{A_\phi}{A_{1.1}} = 1 + .9625\left(\frac{\phi}{1.1} - 1\right) + 5.445\left(\frac{\phi}{1.1} - 1\right)^2$$

$$+ 8.32\left(\frac{\phi}{1.1} - 1\right)^3 \qquad (4.20)$$

In this equation $A_{1.1}$ is the value of the pre-exponent factor, A for the fuel-air equivalence ratio, ϕ of 1.1 and A_ϕ is the value of A at any ϕ between .8 and 1.2.

In order to predict the onset of knock in the engine it is assumed that knock occurs when the auto-ignition delay is completed. the summation of the ratios of the increment of time and the instantaneous value of auto-ignition delay is used to predict the onset of knock. The auto-ignition delay is considered to be completed when:

$$\Sigma \frac{dt}{\tau} = 1 \qquad (4.21)$$

where dt is the time increment.

4.5 Heat Transfer

4.5.1 General

Heat transfer information is becoming increasingly important with the great emphasis on engine efficiency and because of the strong influence of heat transfer on exhaust emissions. In addition, heat transfer is important in estimating heat release rates and flame propagation from pressure-time data and in other engine simulation studies.

The amount and type of heat exchanged between the working mixture and the surroundings in an engine cylinder depends on the crank angle at which the exchange occurs. During the intake and compression strokes heat transfer, which for all practical purposes is entirely convective, is

normally small. Indeed, Lichty[72] has estimated it to be of the order of .5% of the heat of combustion. This is not very surprising in view of the comparatively low mixture temperatures during those two phases. In fact, during the intake stroke and the initial stages of the compression process, it is possible for the heat flow to be from the hotter surroundings to the cooler working mixture. As compression process proceeds, however, mixture temperature increases to become higher that the temperature of the surrounding surfaces and the heat flow is once again from the mixture to the walls.

During combustion and early expansion phases both convective and radiative heat transfer may be important. Mixture temperatures are much higher than the wall temperature and heat flow is from the working mixture and to the surrounding surfaces. Heat lost during these two phases has been estimated by many workers[147-151]. However the estimates vary because of the use of many different engine designs and operating conditions in the determinations. A summary of the estimated heat loss during the combustion and expansion phases, expressed as a percentage of the heat of combustion, is given in table (4.2).

4.5.2 Factors Influencing Heat Transfer

The processes inside the combustion chamber of a reciprocating internal combustion engine are very complex, involving rapid variation in mixture pressure, temperature, and local velocities. Heat flux into the walls varies throughout the engine cycle from a small negative value to a positive value reaching up to several megawatts per square metre, and also varies spatially due to differences in local mixture temperatures and velocities and doubtless also due to differences in orientation of the wall to the radiating flames.

Alkidas[152] measured heat flux at four positions on the cylinder head of a 4-stroke, V-8 spark ignition engine modified to operate on one cylinder. Tests were performed for both fired and motored operation of the engine. The primary engine operating variable was engine speed. It was found that:

i. peak heat flux varies considerably with measurement position. This spatial variation was considered to be principally attributable to the spatial variations of the temperature and velocity fields in the combustion chamber,

ii. advancing the spark timing increases the peak flux and advances the time at which this occurs in the cycle.

During the last stage of the expansion process the magnitude of the flux is independent of spark timing,

iii. the peak heat flux at each measurement position increases with the increase of engine speed.

Alkidas and Myers[153] studied the variations of heat transfer with air/fuel ratio and load (volumetric efficiency) using the same engine. They found that the local heat flux was not strongly affected by the variations in air/fuel ratio at constant conditions of engine speed and load. The peak heat flux reached a maximum at near-stoichiometric mixture, whereas at leaner or richer mixtures the heat flux decreased. This trend was caused by the burned gas temperature, which exhibits a similar variation with air/fuel ratio. Alkidas and Myers also found that an increase in volumetric efficiency from 40 to 60 percent resulted in an increase in peak heat flux of about 30%. This increase is primarily attributed to the increase of the convective heat transfer because of the increase in mixture density.

Overbye et al.[154] measured heat flux at several positions on the cylinder head of a CFR engine. Tests were performed at near stoichiometric air/fuel ratio and an engine speed of 830 rpm. The effect of intake manifold pressure, turbulence and wall deposits on heat flux were investigated. It was found that the effect of these

variables is dependent on whether the engine is fired or motored. Turbulence effect was found to be greater in the case of a firing engine, whilst the effect of manifold pressure was greater in the motored engine case.

Additionally, many other parameters and operating conditions can influence the magnitude of the heat flux. these include:

i. charge pressure, temperature and physical properties,
ii. engine size,
iii. compression ratio,
iv. fuel type,
v. exhaust pressure,
vi. combustion chamber shape,
vii. coolant temperature, flowrate and composition, and
viii. lubricating oil quantity and composition.

In engine cycle synthesis the need of an accurate instantaeous heat transfer expression led many investigators to try to correlate the measured heat flux. Many expressions have been reported; among these are of Nusselt[155], Eichelberg[62], Briling[156], Elser[157], Oguri[158], Overby[154] and Annand[159], to name a few.

Annand set out to derive his own heat transfer formula

after reviewing the previous work in this field and concluding that no formula satisfies all the requirements. He considered the formulae of Nusselt, Eichelberg and Briling to be unreliable because of dimensional incorrectness. Thus, they cannot be extrapolated to predict heat transfer rates under conditions far removed from those of the experiments on which they are based. He also faulted the formulae of Elser and Oguri because of the inclusion of incorrect terms, whilst Overby's formula was criticised because the wall temperature variation was not allowed for.

Recognising the limitations in attempting to include all the parameters which can influence heat transfer, Annand considered the following requirements to be of prime importance:

i. The convective and radiative components should be clearly distinguished since both are expected to vary not only from engine to engine but also in different parts of the same engine, and

ii. in convective heat transfer, the influence of Prandtl number is completely swamped by that of the Reynold's number.

From these considerations, Annand proposed that the total heat flux could be represented by an equation in the form:

$$\frac{q}{A} = a\frac{K}{D} R_e^b (T_g - T_w) + c^{\sigma}(T_g^4 - T_w^4) \quad KJ/m^2.s \qquad (4.22)$$

in which

q instantaneous heat transfer rate; KJ/s

A instantaneous area across which heat transfer occurs; m^2

K working mixture thermal conductivity; KJ/ms.K

D engine bore; m

R_e Reynold's number $= \frac{\rho V_p D}{\mu}$

ρ working mixture kg/m^3

μ working mixture dynamic viscosity kg/m.s

V_p mean piston speed $= \frac{2SN}{60}$; m/s

S engine stroke; m

N engine speed; rpm

T_g working mixture temperature; ^0K

T_w wall temperature; ^0K

σ Stefan-Boltzman constant
$= 5.68 \times 10^{-11}$ $KJ/m^2.s.^0K^4$

a,b and c are empirical constants.

Values of the constants a, b and c were determined statistically using Elser's measurements. Comparisons were also made with the measurements of Nusselt and Eichelberg, with some local heat flux measurements in spark ignition and compression ignition engines. These led Annand to suggest the following values for the constants:

b = .7

a = .35 to .8 for normal combustion; "a" increases with the increase of the intensity of charge motion.

c = 0 during compression

= .5714 for compression ignition engines

= .075 for spark ignition engines

during combustion and expansion.

4.5.3 The Application of Annand's Formula to the Computer Simulated Cycle Model

Annand's expression has been used to calculate the instantaneous heat transfer rate during the different phases of the Ricardo E6 engine cycle. The values of the constants a, b and c has been taken as:

a = .4

b = .7

c = .075 during combustion and expansion phases

= 0 during the rest of the cycle including gas exchange phase.

With the disc-shaped combustion chamber found in the Ricardo E6 engine and low level of swirl induced by the inlet system, mixture motion in the combustion chamber is expected to be very small. For this reason the value of "a" was chosen to be .4.

Combustion chamber wall temperatures are very important in heat transfer calculations. In practice, these vary not only from point to point in the chamber but also from one instant to another. Allowance for all these individual effects makes heat transfer calculations extremely complicated. To reduce the complexity of the present model the combustion chamber surface area is sub-divided into three main zones each having it's own assumed constant temperature, as follows:

i. the area of cylinder head surface (including the valves) involved in the heat flow at an instant of time, A_h at a temperature, T_h of 420 K,

ii. the area of piston surface involved in the heat flow at an instant of time, A_p at a temperature, T_p of 520 K, and

iii. the area of cylinder wall surface involved in heat flow at an instant of time, A_c at a temperature, T_c of 395 K.

These values for the temperatures T_h, T_p and T_c were considered by Johnson et al.[160] and Lucas and James[66] to be typical of those existing in spark ignition engines. Even if these are in error by $\pm$ 25 K however, the inaccuracies in heat loss estimations are only of the order of $\pm$ 2% [148].

In Annand's formula, T_w can be calculated from

$$T_w = \frac{A_c T_c + A_p T_p + A_h T_h}{A} \qquad (4.23)$$

where

$A = A_c + A_p + A_h$ is the total area.

During compression, expansion and gas exchange phases these areas are given by

$$A_p = A_h = \pi D^2/4$$

$$A_c = \pi D y$$

where y is the distance from the instantaneous piston position to the cylinder head.

During combustion period, however, a flame is propagating across the combustion chamber and the quantities, A_c, A_h and A_p in contact with both the burnt and unburnt fractions of the charge, are continuously changing. These areas are functions of the flame radius and piston position. The method used to calculate these areas has been discussed in a previous section (flame propagation pattern).

4.6 Prediction of Combustion Products Concentration

4.6.1 General

Knowledge of combustion products composition and properties are required for the thermodynamic cycle calculations. The dissociation of the products of combustion of hydrocarbon fuels produces various combinations of carbon, hydrogen, oxygen and nitrogen. The way in which these four elements are combined after combustion and the proportion of the various species in the burnt mixture depends on:

a. The proportions of these elements present in the original mixture,

b. the temperature and pressure, and

c. the extent to which chemical equilibrium has been approached.

In a high temperature combustion reaction between a hydrocarbon fuel and oxygen the following general equation may be written when the burnt mixture is assumed to consist of twelve species:

$$CyH_{4_x} + (y + x)\, O_2 \rightarrow n_1 N_2 + n_2 O_2 + n_3 CO_2 + n_4 H_2O + n_5 CO$$

$$+ n_6H_2 + n_7NO + n_8OH + n_9N + n_{10}H + n_{11}O + n_{12}A \qquad (4.24)$$

with

$$y = {}^{C_f}/_{12.01},\quad x = (1 - C_f)/4.032$$

and

$$C_f = \frac{m \times 12.01}{m \times 12.01 + n \times 1.008}$$

In these equations, m and n are the number of carbon and hydrogen atoms in a molecule of the fuel and n_i (i = 1 to 12) are the number of moles of:N_2, O_2, CO_2, H_2O, CO, H_2, NO, OH, N, H,O ,and argon respectively in the burnt mixture.

In practice, many other dissociated species are also present in the burnt mixture. However, the choice of the species to be included was made by choosing the twelve most significant of the sixteen species included in published data by AGARD[161].

Many models have been developed for predicting the concentration of the products of combustion. These models, either assume a complete equilibrium[162,163] which is not a valid assumption or use relatively complete kinetic solution [164,166] which is time consuming. The method used here is based on the system suggested by Way[167] and has the advantage of requiring fewer parameters to be estimated (only O/O_2 ratio): also it uses a combination of chemical rate equations for some slower reactions with chemical

equilibrium for faster reactions.

4.6.2 Kinetic System with Partial Equilibrium Model

The departure from chemical equilibrium, especially for species such as nitric oxide and carbon monoxide has been found experimentally to be extremely high[165]. In actual practice, the effect is to produce greater quantities of NO and CO than would be the case if equilibrium were to prevail. Measurements of Wimmer and McReynolds[168] and Huls and Nicol[169] indicated that the concentrations of these species correspond more closely to chemical equilibrium calculated at the peak combustion temperature. The measured concentration is, however, several orders of magnitude greater than the equilibrium concentration corresponding to the final exhaust temperature. The explanation of this lies in the non-equilibrium behaviour of these species during the combustion and expansion processes.

During the combustion process NO and CO are formed rapidly, and reach near chemical equilibrium levels at the combustion temperature. As the expansion process proceeds, and the temperature of the products decreases, NO and CO should, if chemical equilibrium is to be maintained, decompose. It appears, however, that the reactions by which they decompose is so slow relative to engine cycle events that significant decomposition does not take place.

The remaining species can be considered at equilibrium as the reactions by which these species decompose are extremely fast compared with the changes in the cylinder pressure and products temperature. Hence a sufficiently accurate kinetic treatment is possible which combines chemical kinetic equations for the slower reactions with equilibrium for the faster ones, with a considerable saving in computer time. Details of the model and the numerical method used are presented in appendix (D).

4.7 Gas Exchange Process

Most of the reported spark ignition engine cycle simulations are confined to the closed period of the cycle only. However, the trapped conditions in the cylinder have a powerful influence on the subsequent events of the cycle and depend on the valve areas, timing and the conditions in the inlet and exhaust manifolds. It is necessary therefore, to consider the open period of the cycle. Additionally, this is important in studying the evaporation of the remaining liquid fuel during the intake process.

Those who simulate the open period[67,170] have assumed that mass transfer through the inlet manifold, cylinder and exhaust manifold is the most important process during this period. The cylinder draws vapour fuel-air mixture in from the inlet manifold ready for compression. Following expansion the products of combustion are pushed

out to the exhaust manifold. This case might be true for diesel engines but not for a carburetted spark ignition engine where it is found that an appreciable amount of fuel is still in the liquid form prior to induction. A great deal of evaporation may occur during the induction process due to:

a. the probability of fuel atomisation at the inlet valve.

b. the contact between the flowing mixture and the relatively hot surfaces of the inlet and exhaust valves, cylinder wall and piston crown,

c. the mixing of the fresh charge with the hot residual gases.

The open period model consists of two sub-models: the thermodynamic model and the evaporation model. In this section the discussion is confined to the thermodynamic model as the evaporation model was discussed in chapter (3).

In addition to giving the mass flow into and out of the cylinder, the thermodynamic model calculates the cylinder pressure and temperature, heat transfer and work to the piston. The model assumes one dimensional, steady and pulsation free flow. To simplify the problem the fresh charge and combustion products have been assumed to remain unmixed throughout; this is not an assumption that can

introduce any significant error when the mass of residual gases is small.

Heat transfer from or to the mixture is accounted for using Annand's formula[159] as it is appreciated that the neglect of heat transfer gives a higher trapped mass for a given pressure. The equations used for flow through the valves are derived from adiabatic expansion through a nozzle. The equations are:

For inlet:

$$\dot{m} = C_{di}A_i \frac{P_a}{\sqrt{R_a T_a}} \sqrt{\frac{2\gamma_a}{\gamma_{a-1}} \left[\left(\frac{P_c}{P_a}\right)^{\frac{2}{\gamma a}} - \left(\frac{P_c}{P_a}\right)^{\frac{\gamma_{a+1}}{\gamma_a}}\right]} \qquad (4.25)$$

for subsonic flow when $\frac{P_c}{P_a} \angle \left(\frac{2}{\gamma_{a+1}}\right)^{\frac{\gamma_a}{\gamma_{a-1}}}$

and

$$\dot{m} = C_{di}A_i \frac{P_a}{\sqrt{R_a T_a}} \sqrt{\gamma_a \left(\frac{2}{\gamma_{a+1}}\right)^{\frac{\gamma_{a+1}}{\gamma_{a-1}}}} \qquad (4.26)$$

for sonic flow when $\frac{P_c}{P_a} \geq \left(\frac{2}{\gamma_{a+1}}\right)^{\frac{\gamma_a}{\gamma_{a+1}}}$

For exhaust

$$\dot{m} = C_{de}A_e \frac{P_c}{\sqrt{R_g T_g}} \sqrt{\frac{2\gamma_g}{\gamma_{g-1}}} \left[\left(\frac{P_e}{P_c}\right)^{\frac{2}{\gamma_g}} - \left(\frac{P_e}{P_c}\right)^{\frac{\gamma_{g+1}}{\gamma_g}}\right] \qquad (4.27)$$

for subsonic flow when $\frac{P_e}{P_c} < \left(\frac{2}{\gamma_{g+1}}\right)^{\frac{\gamma_g}{\gamma_{g+1}}}$

and

$$\dot{m} = C_{de}A_e \frac{P_c}{\sqrt{R_g T_g}} \sqrt{\gamma_g \left(\frac{2}{\gamma_{g+1}}\right)^{\frac{\gamma_{g+1}}{\gamma_{g-1}}}} \qquad (4.28)$$

for sonic flow when $\frac{P_e}{P_c} \geq \left(\frac{2}{\gamma_{g+1}}\right)^{\frac{\gamma_{g+1}}{\gamma_{g-1}}}$

where

C_d	discharge coefficient
A	valve flow area
P	pressure
T	temperature
γ	specific heat ratio
R	gas constant
i	inlet
a	air
e	exhaust
g	combustion products
c	cylinder

The flow area, A, at any crank angle is calculated from the valve lift at that angle and the valve configurations. Valve lift-crank angle data are expressed as fifth order equations derived from actual data supplied by Ricardo Consulting Engineers plc.

The coefficients of discharge used in the above equations are variables, depending upon the shape of the valves and passages and on the flow regime existing in the flow through the valve. In this work, however, these coefficients are considered to be functions of valve lift only since actual measurements[171] have shown little dependence of the coefficients on Reynolds number. For each valve an equation is derived from data of Ref.(171) to calculate the discharge coefficient at any valve lift.

Reference	Correction Factor	Engine
Harrow & Orman (118)	1+.002*N	Ricardo E6
Hodgetts (117)	1+.0017*N	Ford Zodiac Mark III
Benson et al (67)	1+.00234*N	CFR
James & Lucas (66)	1+.00197*N	Renault
Soliman (70)	1+.00314*N	Villiers 40 MAG 1045

N...Engine Speed, rpm

Table (4.1) Laminar to Turbulent Burning Velocity Correction Factor.

REF.	Heat Loss (% of heat of comb.)	
	During Combustion	During Expansion
147	4	6
148	5	20
149	6	7
150	5	10
151 *	15000/N	75000/N
72	7	9

* N...Engine Speed, rpm

Table (4.2) Heat Loss During Combustion and Expansion Phases

CHAPTER FIVE

EXPERIMENTAL WORK

5.1 Introduction

The objectives of the experimental programme in the present investigation were:

1. To devise a technique for liquid wall film separation and measurement.

2. To Investigate:
   a. the effects on wall film quantity of such parameters as air/fuel ratio, throttle plate opening, engine speed and intake manifold geometry.

   b. the effects of wall film on engine performance and emissions.

3. To correlate the wall film data with mathematical equations in such a way that values may be deduced for initial wall film quantity (at the throttle plate), bend factor, entrainment and deposition rates.

4. To obtain a comprehensive set of performance, pressure and emissions data which can be used as the basis of comparison for the theoretical cycle model developed during the research programme.

5.2 Wall Film Separation Technique

The liquid wall film characteristic of interest in the present investigation is the mean film flowrate. Many techniques to measure this quantity have been reported in the literature. These include the measurement of the liquid film mean thickness and velocity[172], liquid film sampling [173] and film separation[32,33,91,174]. Anderson and Russell[172] investigated the deposition of water drops on the wall of a horizontal pipe. They measured wall film mass flowrate by measuring it's thickness and velocity with a salt tracer technique. In his study of droplet mass transfer, Quandt[173] estimated entrainment by adding a dye to the liquid film at a given injection point, then sampling the film at successive downtream locations. The flowrate in the film was calculated by a simple mass balance from a knowlegde of the dye input rate and an estimate of the concentration of the dye in the liquid film at the point of dye injection. The latter quantity was estimated by back extrapolation of the sampling results.

Wall film separation is possible by extraction or using the slit method. In the extraction technique the liquid film is sucked through either a series of fine holes around the tube periphery[91] or by using a knife edged probe inserted on the duct internal wall[33]. These methods

are generally used when the film distribution is of interest, and if the liquid in the film is volatile material a correction factor is employed to compensate for the evaporation of the liquid during extraction[33].

Nightingale and Tsatsami[32] used brass tube inserts of diameter less than that of the inlet port incorporated between the manifold exit and the entry to the cylinder head to measure wall film flowrate. Using these inserts may result in a flow restriction which leads to higher flow velocity and turbulence level which in turn produce better combustion. This would produce a misleading representation of the effect of wall film separation on engine performance and emissions.

In the present work a slit method[174] was used for measuring film flowrate (Fig.5.1). The device consists of an annular gap in the manifold wall through which the film was allowed to flow. The entrained fuel is carried out beyond the gap by the gas phase. The thickness of the gap was made to be 2 mm which was expected to be more than the possible maximum wall film thickness. Since the pressure in the manifold is always sub-atmospheric, a pressure equaliser between the manifold and the air-tight measuring clinder was used, so that the liquid film flows out of the manifold collection chamber to the measuring cylinder under gravitational effects.

The intake manifold is divided into two parts separated by a small axial gap. Between the carburettor exit and the separator a constant internal diameter of 40 mm, equal to that of the carburettor exit, was used for all the manifold geometries which were investigated. Downstream from the gap the internal diameter was 36 mm to correspond with the inlet port of the engine. The downstream length was kept as short as possible to reduce the opportunity of further wall film deposition. The separated liquid film was collected in a chamber which was designed to be deep enough to prevent the sucking of the collected liquid fuel back to the main-stream at high engine speeds and small throttle openings. The measuring cylinder was located beneath the intake manifold (see plate 5.1) and connected to the manifold by two .4 mm diameter PVC tubes.

Evaporation from the separated fuel is possible, but it is expected to be very small due to:

1. the separated fuel flowing under gravity in a short tube of small diameter and low thermal conductivity.

2. When the film flowrate was high the time allowed for evaporation was small. If the flowrate was small, however, the measured volume was made less to reduce the test time and hence the time available for evaporation.

By using this technique, it was possible to measure wall film mass flowrates ranging from .5gm/s up to 22 gm/s at different engine operating conditions: results were repeatable with an accuracy of ± 5%.

5.3 Testing Equipment and Procedure

5.3.1 Equipment

Fig.5.2 and plate (5.1) show a schematic drawing and a view of the instrumentation used respectively. The engine was a Ricardo E6 engine equipped with an SU constant depression carburettor and coupled to a D.C. swinging field starter-dynometer. The specifications of the engine are:

Bore (mm)	76.2
Stroke (mm)	110
Swept Volume (cc)	507
Comp. Ratio	variable

For the purpose of the experimental programme a compression ratio of 8.5:1 was chosen.

The test rig was equipped with a standard range of instrumentation to measure fuel and air flowrates, engine speed and brake load. Exhaust gas was sampled by a .55 meter long stainless steel probe with sample inlet holes distributed over its length (end sealed). The probe was

positioned in the exhaust pipe with the upstream probe tip located about .5 meters from the exhaust port. Exhaust gas emissions (CO, CO_2 and UHC) were measured using Non-Dispersive Infra-Red analysers.

Cylinder pressure was measured using a water cooled peizo-electric AVL transducer coupled to a Kistler charge amplifier. Crank angle marker signals were obtained at20^0 intervals (10^0 intervals at TDC) and once per cycle trigger pulse signal using a crank shaft mounted slotted discs in conjuction with magnetic pick-up units. The pressure transducer, crank angle marker and trigger signals were recorded on a RACAL multi-channel tape recorder.

The pressure transducer was statically calibrated using a dead-weight tester over the pressure range 0-1200 psi, the relation between pressure and the output voltage of the transducer was linear. Static calibration was followed by a dynamic calibration on the engine in conjuction with a maximum pressure tester. This calibration was carried out during engine motoring where the maximun pressure tester was mounted in the spark plug position. In this test the maximum pressure was recorded and compared with that measured by the transducer. The dynamic effects were found to be negligibly small.

A linear transducer was fitted on the carburettor to measure the piston height for the determination of the area underneath the piston. The output voltage of this

transducer was calibrated against a micrometer, a linear relationship was found.

Wall film flowrate was measured by measuring the time required to fill a certain volume in the calibrated measuring cylinder. An average density of the separated liquid fuel during each test was measured using a density bottle. Wall temperature at three positions on the manifold were measured in order to calculate the heat input through the manifold wall. The positions were near to the carburettor, at a mid point and near to the inlet port. The average of these temperatures was used in conjunction with the room temperature to estimate the heat transferred from the room to the inlet manifold. This was found to be in the order of 2 watts maximum, which may be neglected without serious error.

Additional instrumentation consisted of K-type thermocouples to measure inlet air temperature, fuel temperature in the float chamber and a manometer to measure inlet manifold vacuum.

5.3.2 Test Procedure

The measurement of wall film flowrate requires a carefully planned test procedure since ambient and engine conditions strongly affect evaporation rate and hence the measured film quantity. Before and during the tests, the

following steps were taken to ensure better results:

1. The required fuel quantity for one test was kept in the test cell overnight to warm up the fuel to cell temperature: the temperature in the fuel store was slightly lower.

2. Engine warm up time was at least 45 minutes, meanwhile, film flowrate was measured in 10 minute intervals until a steady flowrate was reached.

3. Engine cell temperature was controlled by a manually operated ventilation system within $\pm 2^0C$.

4. If the temperature of the laboratory was low, fan heaters distributed in the laboratory were switched on until a satisfactory temperature was reached.

After familiarisation with the system, a series of tests were carried out to identify the limits of the variables and to study the effects of secondary parameters such as ignition timing, compression ratio and manifold axial gap. All these parameters were found to have negligible effect on the wall film mass flowrate. The principal tests carried out examined:

1. Five different manifolds (see plate (5.2)):
   a. straight manifolds of lengths 100, 150, and 200 mm,
   b. mitre bend manifold of length 200 mm,
   c. smooth bend manifold of length 200 mm.

2. Four throttle plate angular openings: 1/4, 1/2, 3/4 and full.

3. Constant engine speed of 1500 rpm.

4. Constant ignition timing of 30 deg. crank angle before TDC.

5. Variable air/fuel ratio between the rich and lean misfire limits.

Further tests were carried out to examine:

1. Mitre bend manifold, 1/2 throttle setting, at engine speeds of 1000 and 2000 rpm for different air/fuel ratios.

2. Straight manifold 150 mm, 1/2 throttle setting, constant air/fuel ratio and variable ignition timing from 40^0 before TDC to TDC in 5^0 intervals.

3. Mitre bend manifold, 1/2 throttle setting, 1500 rpm, wall film was not separated at different air/fuel ratios.

The procedure adopted for each test was as follows:

1. The throttle plate was set to the required position.

2. Initial values for atmospheric pressure and voltage from the carburettor piston height transducer for zero piston height were recorded.

3. The engine was warmed up at the required test speed.

4. The test may start from the rich or the lean limits of the mixture.

5. The following data were recorded: the times for total fuel and wall film; pressure drop across the orifice plate; load at the dynamometer; manifold pressure; manifold wall temperatures; air, fuel and exhaust temperatures; voltage from the carburettor piston height transducer; exhaust emissions (CO, CO_2, UHC); cylinder pressure; crank angle marker and trigger pulse signals.

6. Total fuel flowrate was changed using the mixture strength adjusting nut on the SU carburettor. Engine speed was set back to the initial value by the dynamometer. Sufficient time was allowed for the engine to stabilise at the new air/fuel ratio.

7. Steps 5 and 6 were repeated until misfire limit was reached.

8. New values for the parameters in step 2 were recorded.

The data was used to calculate the output power, air/fuel ratio at the carburettor (Total), in-cylinder air/fuel ratio, brake mean effective pressure, brake specific fuel consumption, film mass flowrate, % film flowrate, air velocity at the carburettor bridge, area under carburettor piston and heat input through the manifold wall.

Cylinder pressure data was later analysed using a Hewlett-Packhard 9825B Desk Top computer in conjuction with a transient recorder. For each condition in the test, ten cycles have been averaged to reduce the effect of cycle to cycle variation: this effect was found to be very small when wall film separation was in operation.

5.4 Analysis of Experimental Results

5.4.1 General

The effects of different engine operating conditions on the measured wall film mass flowrate are shown in Figs.5.3 - 5.20. The first six figures represent the basic data. The rest, however, are derived from these to simplify the analysis. It is found that using the absolute values of the film flowrate provides better representation of the actual trends of the results than using the percentage values. This is clearly shown in Figs. 5.8 and 5.9 which demonstrate the effect of engine speed on the wall film quantity at different total air/fuel ratios. As engine speed increases, Fig.5.8 indicates that the film mass flowrate increases, while Fig.5.9 shows that film percentage of total fuel decreases for a given air/fuel ratio.

The variation of film mass flowrate with total air/fuel ratio at constant engine speed (1500 rpm) and different throttle plate settings are shown in Figs. 5.3 - 5.7 for the five tested manifolds. These may be analysed as follows:

1. Wall film mass flowrate varies, approximately, exponentially with air/fuel ratio. The increase in wall film quantity with the increase of the system total fuel (as expressed by the decrease in air/fuel

ratio) is to be expected since droplet deposition rate is proportional to the droplets concentration in the mixture. It is also indicated that, in the absence of manifold wall heating, there is a minimum film quantity which is not an air/fuel ratio dependent. This minimum is attainable at air/fuel ratios of approximately 14:1 and over, it's value however is a system property (defined by intake system geometry and engine speed).

2. In all cases other than the mitre bend manifold the effect of throttle plate on fuel distribution and hence wall film quantity is clearly distinguished. Film flowrate is maximum at 1/2 throttle setting and decreases in the order 3/4, full and 1/4. This is believed to be due to the effect of the throttle plate in deflecting flow towards the manifold wall. Flow deflection is less for the 3/4 setting, zero for full throttle opening and it should be maximum at 1/4 throttle setting. The measured minimum film flowrate at 1/4 setting is, however, due to the higher air velocity and manifold depression which enhance both the rapid entrainment of the film back to the main-stream in the throttle plate region and the evaporation from the film.

3. For the mitre bend manifold, Fig. 5.7 indicates that the throttle plate has little influence on the distribution of the fuel in the manifold. Instead,

the fuel is redistributed at the bend, where high droplets impaction and entrainment rates might be expected.

4. A close look at Figs. 5.6 and 5.7 reveals a fact that supports the suggested mechanism of film entrainment at 1/4 throttle setting. In these figures the measured wall film for this condition is approximately the same as that for full throttle opening with the smooth bend and even more that that for the mitre bend manifold. This indicates that as the film is entrained in relatively large droplets (or even fuel sheets) which cannot negotiate the geometry of the bend their impaction rate, is therefore, higher and so more film is produced. This is also supported in Fig. 5.29 where the bend factor for 1/4 throttle setting is maximum.

As engine speed increases, total fuel flowrate increases and hence wall film quantity. This trend is shown in Fig. 5.8 for the mitre bend manifold at 1/2 throttle setting for three engine speeds of 1000, 1500, and 2000 rpm. Film mass flowrate at 1500 rpm is however, intersecting those of 1000 and 2000 rpm at the lean and rich regions respectively. This trend could possibly be attributed to measurement inaccuracies, but the results were repeatable (Fig. 5.12) and so some other phenomenon must be the cause. Fig. 5.9 indicates that film quantity may reach 45% of the total fuel in the system.

Figs. 5.10 and 5.11 are reproductions of Figs. 5.4 and 5.5 in the percentile form. These are plotted only to give an indication of the quantity of the fuel in the wall film. Fig. 5.12 shows the repeatability of the measurements. It is clear that due to the good control on the test conditions the results are repeatable within the acceptable experimental error.

Figs. 5.13 - 5.16 show the effect of manifold shape on film flowrate for the same manifold length (200 mm) at different throttle settings. For all throttle settings other than the 1/4, the smooth bend produces the highest film quantity. In the intake manifold design, it is well known that the bends should be sharp in order to throw wall film liquid back to the stream. The obtained results are, therefore, giving the expected trends. The effect of the bend on film quantity is very clear by the large difference between the film produced by the manifolds with bends and that produced by the straight manifold.

Figs. 5.17 - 5.20 show the effect of manifold length on film flowrate at different throttle settings. As manifold length increases film flowrate decreases, however, the rate of change is not constant but decreases as length increases. This is because:

a. entrainment rate is dependent on the film thickness which in turn is a function of film flowrate. This means that as manifold length increases entrainment rate decreases.

b. deposition rate is a function of droplets concentration in the mixture, which increases due to entrainment and decreases due to droplets evaporation. This affects the film mass flow rate in a way that to increase the deposition rate, but not more than the entrainment rate.

c. as manifold length increases, evaporation rate from the film decreases as the fuel left in the film becomes heavier.

The obtained results of the effect of manifold length on film flowrate are in good agreement with the measurement of Hayashi and Sawa[34].

Finally, the separated wall film was found to differ from fresh petrol in colour, smell and density. It was similar to the diesel fuel in colour and smell, it's mean density was 822 kg/m^3 while the mean density of the fresh petrol was 737 kg/m^3.

5.4.2 The Effects of Wall Film Separation

The effects of wall film separation on engine performance and emissions are shown in Figs. 5.21 - 5.23. Film separation reduces in-cylinder total fuel and hence weakens the mixture. This is shown in Fig. 5.21 in which the relation between the total air/fuel ratio and cylinder air/fuel ratio is approximately linear. This means that the added fuel at the carburettor is uniformly distributed between the film and the main-stream. At very rich mixtures, however, the in-cylinder air/fuel ratio is not strongly affected by the change in the total air/fuel ratio, the additional fuel being mainly supplied to the film.

In Fig. 5.22 the effects of wall film separation on the brake mean effective pressure, carbon monoxide, unburnt carbons, weak misfire limit and cycle to cycle variation (as expressed by the standard deviation of the peak pressure in ten cycles) are shown. The results indicate that engine power is higher, exhaust emissions are significantly reduced, cycle dispersion is almost eliminated and weak misfire limit is extended. The reduced cycle to cycle variation is clearly shown in Fig. 5.23 where cylinder pressures for ten cycles are plotted for three different air/fuel ratios.

Two possible explanations for the improved engine performance and emissions due to film separation exist:

1. The liquid film is usually introduced to the cylinder as large drops or even irregular sheets of liquid fuel. Mixing and evaporating fuel in this form is very difficult to achieve, hence incomplete combustion is expected which leads to the unsatisfactory engine performance and emission. Cycle to cycle variation might be due to the atomisation of the fuel in the film at the inlet valve being different from cycle to cycle as the result of transient pressure variation in the unsteady flow.

2. The fuel in the film is not suitable for combustion in the spark ignition engine since it represents the heaviest fractions of the petrol.

As mentioned in the literature survey, many investigators[3-7] found that complete evaporation of the fuel in the intake system reduces engine emissions and cylinder to cylinder maldistribution. These findings support point (1) above and eliminate point (2), since the fuel in the film has been introduced to the cylinder, but in the vapour form. No report on the effect of mixture quality on cycle to cycle variation has been found in the extensive literature survey.

5.5 Correlation of Wall Film Data

In the theoretical model of fuel evaporation and transportation in the intake system the wall film was assumed to be present downstream of the throttle plate only. The experimental results indicated that for a straight manifold, wall film flowrate decreases as the distance from the throttle plate increases. Moreover, the measurements of Finlay et al.[33] showed that at partial throttle opening wall film mass flowrate upstream of the throttle plate is much higher than that at 90 mm downstream. Therefore, an initial value for the wall film quantity at the throttle plate would be of assistance in studying the devlopment of the wall film within the intake system.

Wall film development downstream of the throttle plate may be explained with the aid of Fig. 5.24. In this figure, the liquid film, which is assumed to be uniformly distributed around the manifold periphery, has a mass flowrate of $\dot{m}_{ff_1}$ at point (1). This initial mass will be increased by $\dot{m}_{fd}$ due to droplet deposition and decreased by $\dot{m}_{fe}$ and $\dot{m}_{fv}$ due to entrainment and evaporation respectively. The final mass flowrate at point (2) is $\dot{m}_{ff_2}$, that is

$$\dot{m}_{ff_2} = \dot{m}_{ff_1} + \dot{m}_{fd} - \dot{m}_{fe} - \dot{m}_{fv} \qquad (5.1)$$

the net change in film flowrate between points (1) and (2) is:

$$\dot{m}_{ff_2} - \dot{m}_{ff_1} = \dot{m}_{fd} - \dot{m}_{fe} - \dot{m}_{fv} \qquad (5.2)$$

dividing eqn. (5.2) by the manifold surface area between the two points, A_{12} and re-arranging yields:

$$\text{Film rate of change} = \bar{m}_{ff} = \frac{\dot{m}_{ff_1} - \dot{m}_{ff_2}}{A_{12}} = Q_e + Q_v + Q_d \qquad (5.3)$$

where Q_d, Q_e, and Q_v are the deposition, entrainment and evaporation rates respectively. Values for these rates have not yet been reported for the flow found in the intake system of a carburetted engine.

Evaporation rate, however, has been ignored in studies involving non-evaporating liquids, the dangerous step is to ignore that in the case of petrol as it was done by Servati and Yuen[44] in their liquid wall film model. In the present work, it is found that evaporation from a 200 mm non-heated manifold wall film may reach 10% of the total fuel in the system (Fig. 5.25), which is non-negligible.

Finally, a bend factor is required to account for the effect of a bend on the wall film deposition rate, since the

conventional intake manifolds are basically a combination of straight ducts and different kinds of bends.

The experimental results have been analysed with the objective of establishing relationships to describe the initial wall film quantity, entrainment rate, deposition rate and the bend factor.

As air mass flowrate is dependent on throttle setting and engine speed, the data may be reduced and become more general if the air flowrate term is excluded. This was achieved by using the total fuel flowrate instead of air/fuel ratio as the independent variable: data was replotted as shown in Fig. 5.26 (as an example), the points were then fitted with best curves using the method of least squares. Values of wall film mass flowrate were then determined at different total fuel flowrates ranging from .02 - .04 kg/min (which correspond to total air/fuel ratios of 14.8 - 6.4), in .005 kg/min intervals.

5.5.1 Wall Film Flowrate at the Throttle Plate

This quantity was determined using the data of the three straight manifolds (100,150 and 200 mm) for the four throttle settings. Fig. 5.27 shows the film mass flowrate plotted against manifold length at 1/2 throttle setting for different total fuel flowrates. For each total fuel flowrate, three points are produced which may be connected

by many different equations. The final decision was, however, to connect each two points with a straight line, the slope of each line represents the film rate of charge, $\bar{m}_{ff}$ between the two points. As shown in Fig. 5.27, the slope is not constant throughout the measured zone, but it is higher within the 100 - 150 mm zone. The difference between the two slopes is represented by the angle, α, that is:

$$\alpha = B - A \qquad (5.4)$$

The slope is also dependent on the total fuel in the system as shown in Fig. 5.27. Except for very rich mixtures, the slope in the 100 - 150 mm zone decreases with the decrease in total fuel flow in the order of $B \succ L \succ M \succ N$. This is because as the total fuel flowrate increases wall film flowrate increases and likewise the entrainment and evaporation rates. With the rich mixture, however, deposition rate becomes more effective and retards the reduction in film flowrate, hence $B \succ K$.

Extrapolation of the lines back to the throttle plate was carried out assuming that the angles:

$$C = B + \alpha \text{ and } D = C + \alpha \qquad (5.5)$$

The justifications of this assumption are the observed trends in the measured zone and the simplicity of the process which produces no serious error. The determined initial wall film mass flowrates are shown in Fig. 5.28 for different throttle settings. It is found that the points may be correlated with an equation of the form:

$$\dot{m}_{ff_i} = A \exp B * \dot{m}_{ft} \qquad (5.6)$$

where

$\dot{m}_{ff_i}$ is the initial wall film mass flowrate at the throttle plate, (gm/min)

$\dot{m}_{ft}$ is the total fuel flowrate, (kg/min)

and

A and B are the correlation parameters, their values depend on throttle setting as follows:

Throttle setting	A	B
1/4	.903	63.57
1/2	3.43	44.52
3/4	3.1	44.22
Full	1.55	55.97

5.5.2 Determination of the Bend Factor

The bend factor is defined by the ratio of the film mass flowrates produced by equal lengths of bent and straight manifolds, that is:

$$B_f = \frac{\dot{m}_{ff_b}}{\dot{m}_{ff_s}}$$

where $\dot{m}_{ff_b}$ and $\dot{m}_{ff_s}$ are the film mass flowrates produced by bent and straight manifolds respectively. The measured wall film flowrates using the 200 mm straight, mitre and smooth bend manifolds were used to determine the bend factor. The calculated bend factor is shown in Fig. 5.29 for both the sharp and smooth bends at different throttle settings. The results indicate that:

a. except for the 1/4 throttle setting the smooth bend factor is higher than the sharp bend factor. This is believed to be due to the higher entrainment rate from the sharp bend,

b. generally, the bend factor is a weak function of total fuel flowrate. At high fuel flowrates, however, both bend factors tend to be equal,

c. maximum bend factor is at 1/4 throttle setting, its value being approximately 5 and 4.3 for the sharp and smooth bends respectively.

The results were fitted with equations of the form:

$$B_f = A_o + A_1 \dot{m}_{ft} + A_2 \dot{m}_{ft}^2 \qquad (5.8)$$

Values of the constants A_o, A_1 and A_2 depend on the throttle setting as follows:

Throttle setting	smooth bend			sharp bend		
	A_o	A_1	A_2	A_o	A_1	A_2
1/4	3.885	44.885	-771.43	4.345	52.25	-917.14
1/2	1.865	55.677	-1524.3	.762	64.8	-997.14
3/4	1.354	122.78	-2620	.228	149.4	-2674.3
Full	.632	149.43	-2777.14	-.623	185.8	-3011.4

5.5.3 Deposition, Entrainment and Evaporation Rates

The wall film rate of change is given by eqn. 5.3 as:

$$\bar{\dot{m}}_{ff} = \frac{\dot{m}_{ff_1} - \dot{m}_{ff_2}}{A_{12}} \qquad (5.9)$$

The values of $\dot{m}_{ff}$ have been calculated from the available data and plotted versus wall film mass flowrate as shown in Fig. 5.30 for different total fuel flowrates. The points were correlated with an equation of the form:

$$\bar{m}_{ff} = B_o + B_1 \dot{m}_{ff} + B_2 \dot{m}_{ff}^2 + B_3 \dot{m}_{ff}^3 \ (kg/m^2.s) \qquad (5.10)$$

where:

$\dot{m}_{ff}$ is the wall film mass flowrate (gm/min)

and $A_o = -2.369\ 10^{-4}$

$A_1 = 9.286\ 10^{-4}$

$A_2 = -2.36\ 10^{-5}$

$A_3 = 4.659\ 10^{-7}$

As shown in Fig. 5.10, the effect of total fuel flowrate on the film rate of change is small especially at lower wall film flowrates. However, this has been considered by determining different values for the coefficients of eqn. 5.10 for both the lean and rich limits of the mixture (dashed lines in Fig. 5.30). The values are:

	Lean mixture limit $\dot{m}_{ft}$ = .02 kg/min	Rich mixture limit $\dot{m}_{ft}$ = .04 kg/min
B_o	$-2.87\ 10^{-4}$	$-1.98\ 10^{-4}$
B_1	$1.125\ 10^{-3}$	$7.786\ 10^{-4}$
B_2	$-2.859\ 10^{-5}$	$-1.973\ 10^{-5}$
B_3	$5.643\ 10^{-7}$	$3.894\ 10^{-7}$

For mixtures between these limits and the mid value ($\dot{m}_{ft}$ = .03 kg/min) a linear interpolation is used to determine the film rate of change.

Eqn. 5.10 in conjunction with eqn. 5.6 are sufficient for the prediction of wall film development within the intake system downstream the throttle plate. However, the individual values for Q_e , Q_d and Q_v are required in the calculation of energy and momentum interchange between the liquid film and the main-stream.

Evaporation rate from the liquid film is already included in the mixture preparation model of the intake system (Chapter 3). The rate of film evaporation may be affected by many flow parameters such as fuel temperature, air temperature, manifold pressure, air velocity, manifold wall heating and liquid film composition. For the case of no wall heating, the remaining variables are functions of both throttle opening and the distance from the throttle plate. Fig. 5.31 shows the effects on the wall film evaporation rate of throttle setting and distance from the throttle plate. At the throttle plate, the fuel in the film contains more light fractions, hence evaporation rate is maximum and decreases with distance from the throttle plate due to the reduction in light fractions content of the film. This is applicable to all throttle settings, but with different rates of decrease since different manifold depressions and film initial values exist.

Throttle setting may affect evaporation rate through many routes. The smaller the throttle opening the higher manifold vacuum and the higher air velocity in the

manifold. These tend to increase the evaporation rate but also to reduce initial wall film, which reduces the evaporation rate. As the initial wall film mass flowrate is smaller, film content of light fractions is less and hence lower evaporation rate. Fig. 5.31 indicates that air velocity and manifold pressure are the dominant effects within the initial 20 mm of the manifold, but beyond this region initial film quantity starts to show a greater influence. For full throttle opening, however, droplet size in the manifold is expected to be larger since there is no secondary atomization. This may affect film evaporation due to the deposition of large droplets and hence more light fuel fractions.

As mentioned earlier, the calculation of film evaporation rate is included in the mixture preparation model and is performed for each length step as the calculations proceed. However, it is found that for a non-heated manifold wall the following mean values may be useful where there is no model available:

1/4	$1.14\ 10^{-3}$	
1/2	$1.57\ 10^{-3}$	$(kg/m^2.s)$
3/4	$1.56\ 10^{-3}$	
Full	$1.96\ 10^{-3}$	

Before explaining the method used to determine the deposition rate, a point should be made clear about the deposition and entrainment rates from a bent manifold. In the present model it is assumed that the entrainment rate from the smooth bend manifold is the same as that from the straight manifold. The bend factor is, therefore to increase the deposition rate only. The justification of this assumption is the observed trends of the measured film flowrate using the smooth bend manifold. The effects of air/fuel ratio and throttle setting are comparable in both the smooth and the straight manifolds, as shown in Figs. 5.5 and 5.6.

As mentioned earlier, the fuel is re-distributed at the sharp bend which means that the entrainment rate from the sharp bend manifold is higher than that from the smooth bend manifold. The difference, however, is accounted for in the smaller sharp bend factor, that is, the entrainment rate from the sharp bend is higher than that from the smooth bend by the difference in their bend factors at the same throttle setting.

The deposition rate was initially assumed to follow the Alexander and Coldren Correlation[27].

$$Q_d = 8.34338*10^{-4} V_a^{1.17} C \quad (kg/m^2.s) \qquad (5.11)$$

where

V_a is the air velocity (m/s)

C is the droplets concentration (kg/m^3)

Eqn. 5.11 will produce no effect on the wall film mass flowrate in a straight manifold if it is used in conjunction with eqn. 5.10, since the deposited fuel by eqn. 5.11 will be entrained by eqn. 5.10, that is,

$$Q_e = Q_d - Q_v + [B_o + B_1\dot{m}_{ff} + B_2\dot{m}_{ff}^2 + B_3\dot{m}_{ff}^3] \qquad (5.12)$$

However, the predicted values of Q_d and Q_e will only affect the energy interchange between the film and the mainstream. The true examination of eqn. 5.11 will be when using it to predict the deposition rate in the bent manifold. Since the deposition rate is increased by the bend factor, whilst the entrainment rate is the same as for the straight manifold, the deposited fuel by eqn. 5.11 in conjunction with the bend factor will not be entirely entrained by eqn. 5.10, i.e.

$$\text{the new deposition rate} = Q_d \times B_f$$

and

$$Q_e = Q_d - Q_v + [B_o + B_1\dot{m}_{ff} + B_2\dot{m}_{ff}^2 + B_3m_{ff}^3]$$

Subjected to this test, eqn. 5.11 failed to predict the measured wall film mass flowrate for the smooth bend manifold. It is found that the velocity exponent in eqn. 5.11 should be doubled and the constant should also be changed in order to obtain the measured values, i.e.

$$Q_d = 1.85 \times 10^{-3} V_a^{2.34} C \qquad (5.13)$$

The increase in the velocity exponent might be explained by the highly pulsating, turbulent flow found in the manifold which is in no way comparable with that used by Alexander and Coldren experiments.

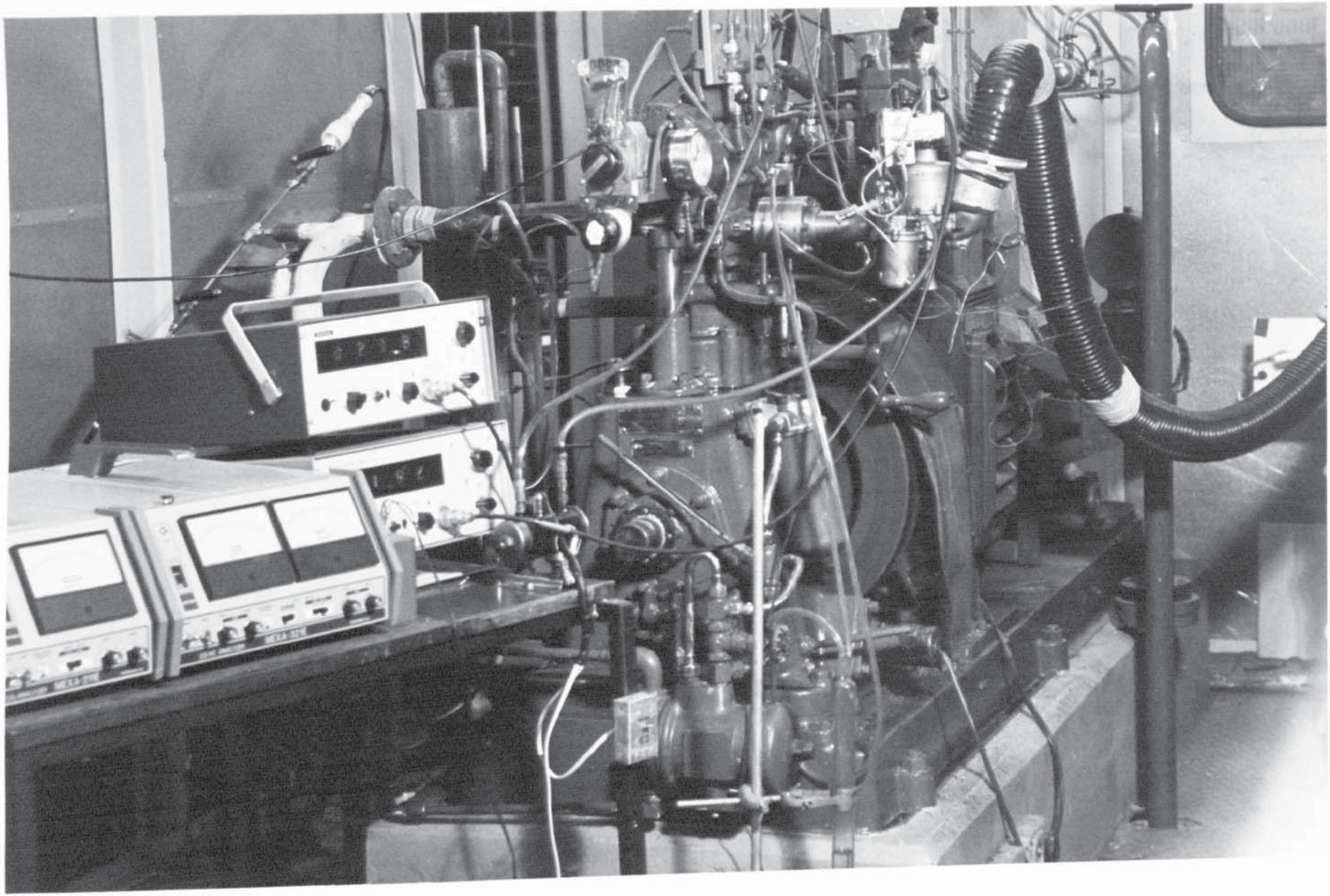

Plate (5.1) The Ricardo E6 Engine Test Rig.

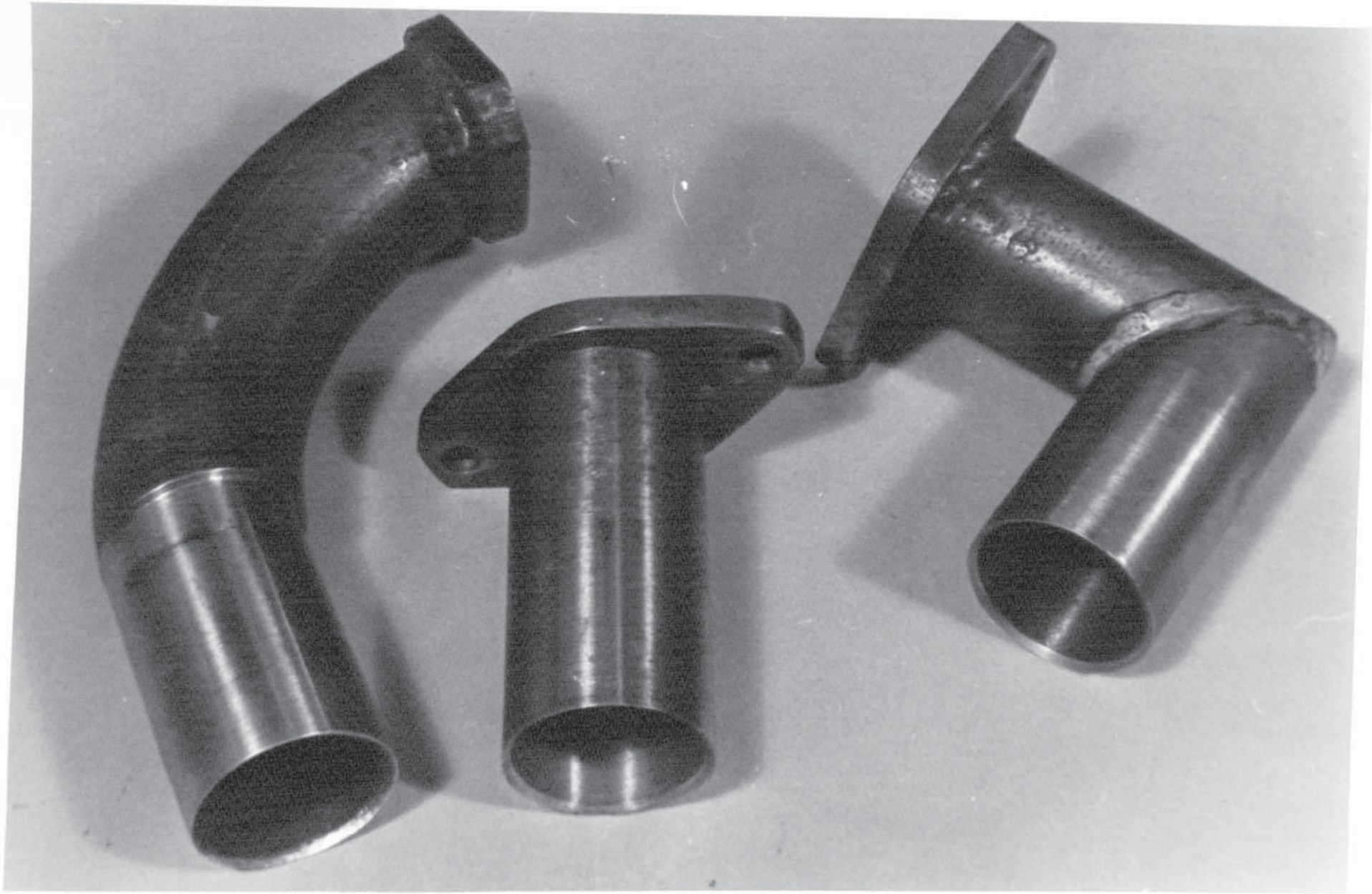

Plate (5.2) The Experimented Inlet Manifold Designs.

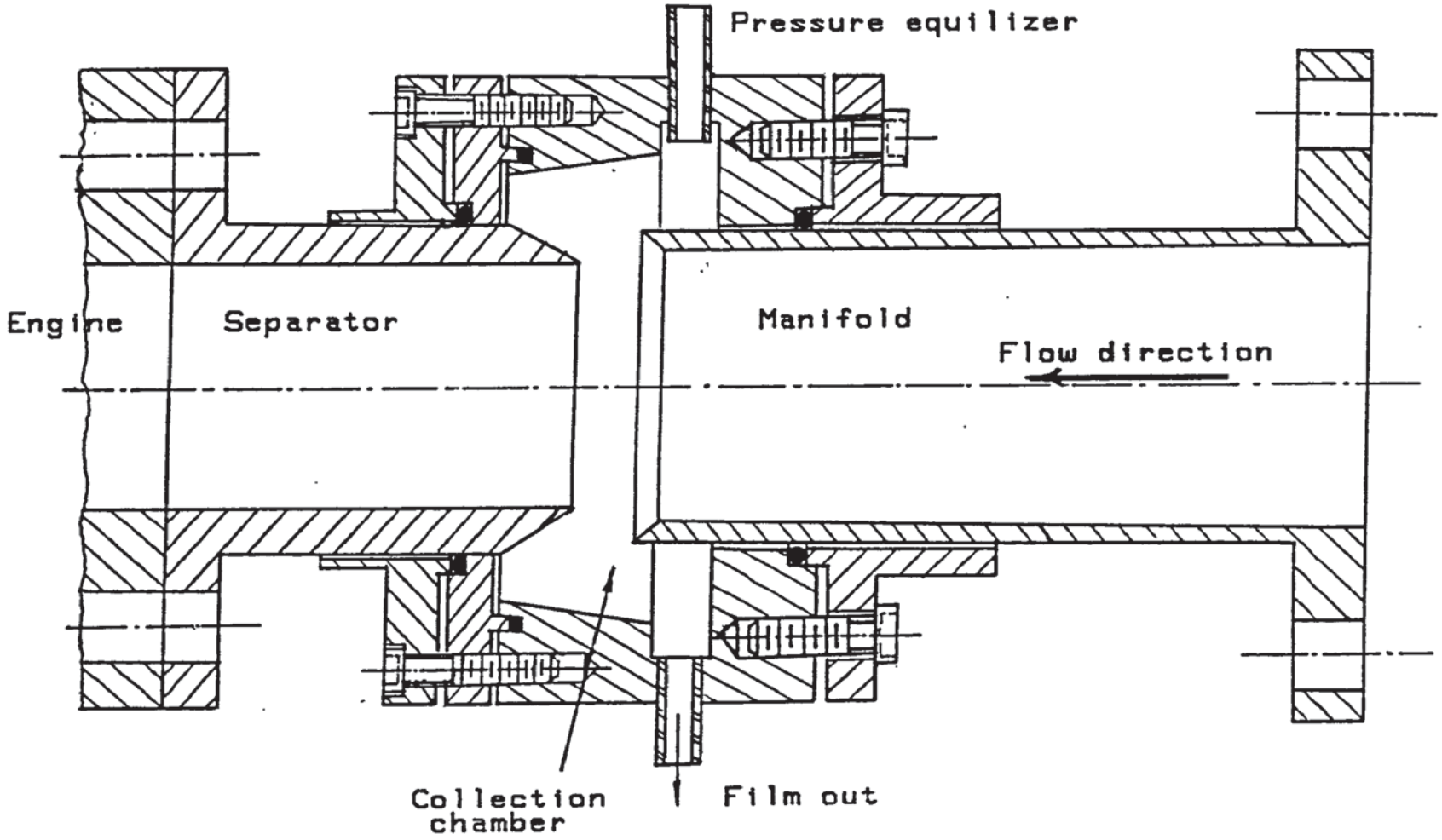

FIG.(5.1) Inlet Manifold With Film Separation Slit

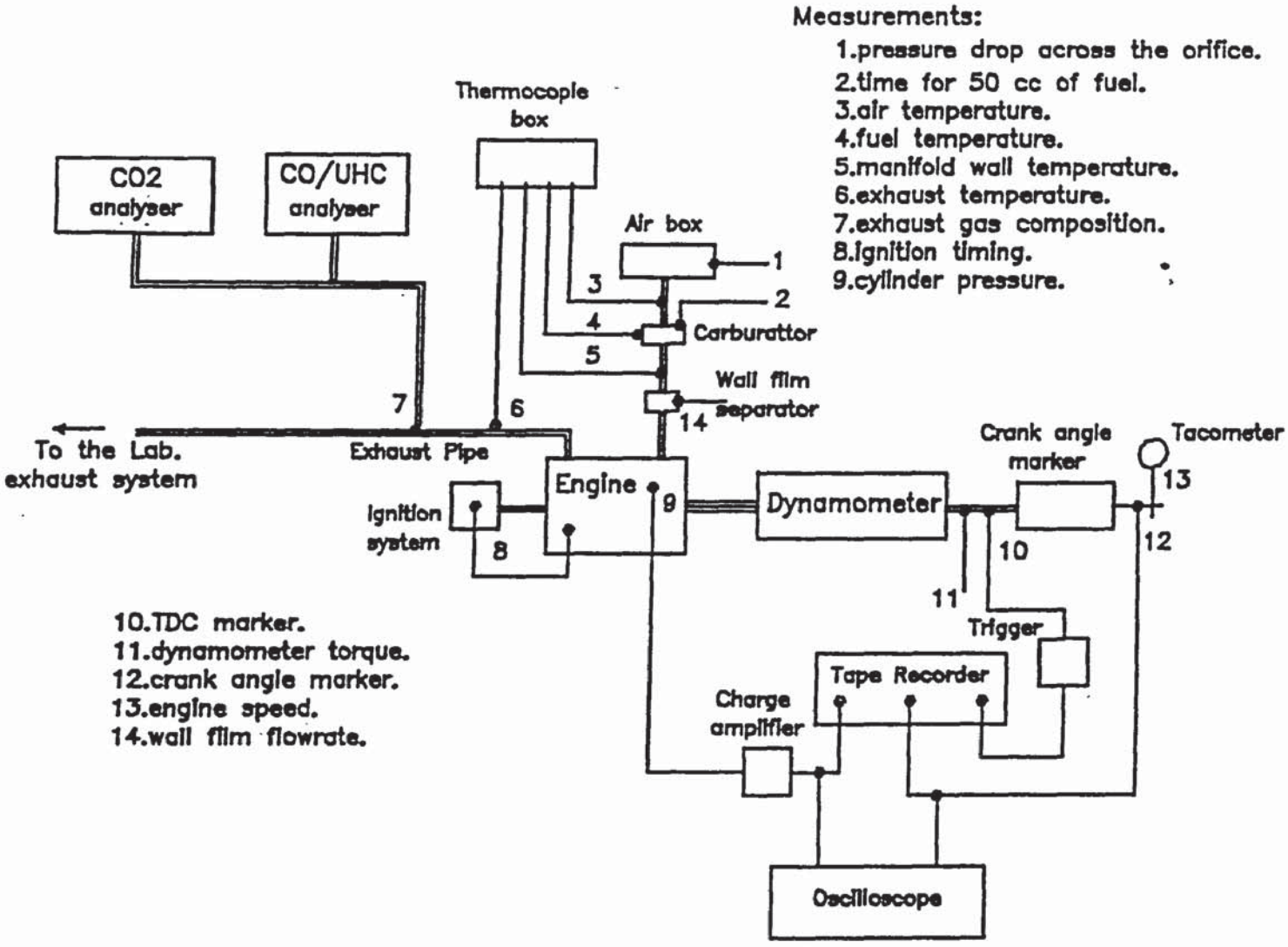

FIG. (5.2) Test Rig Layout.

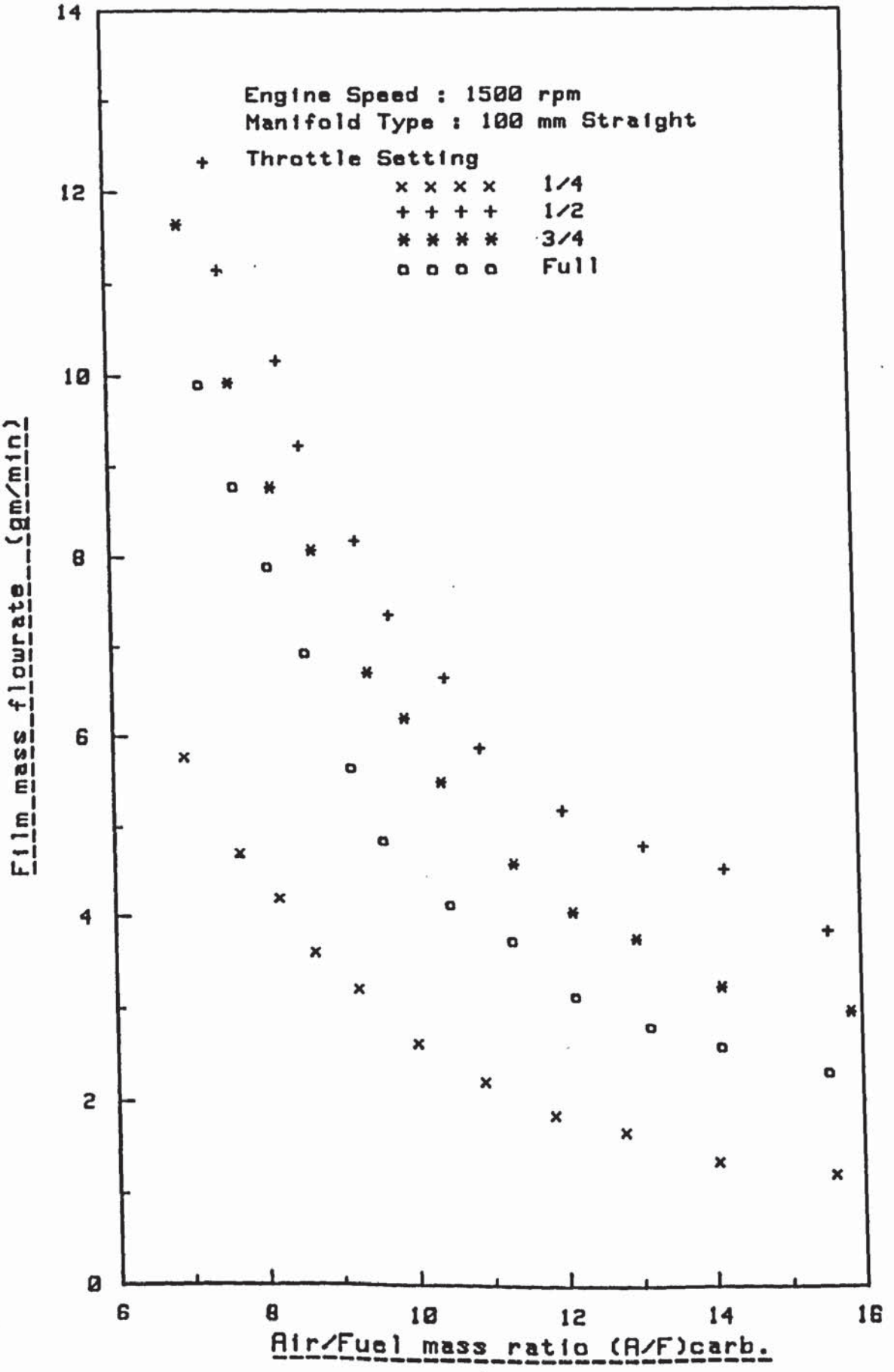

FIG. (5.3) Effect of Throttle Setting on Film Flowrate

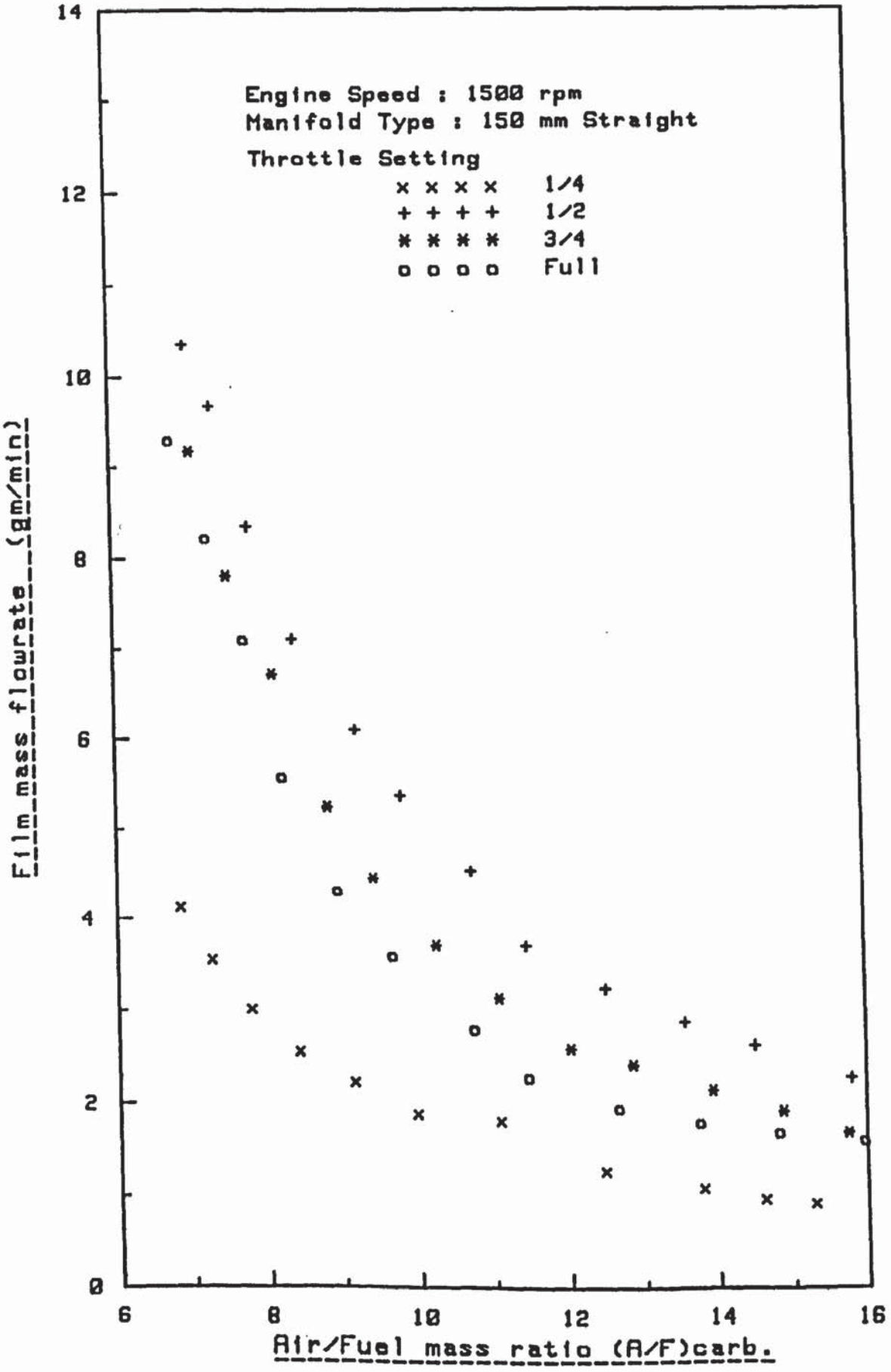

FIG. (5.4) Effect of Throttle Setting on Film Flowrate

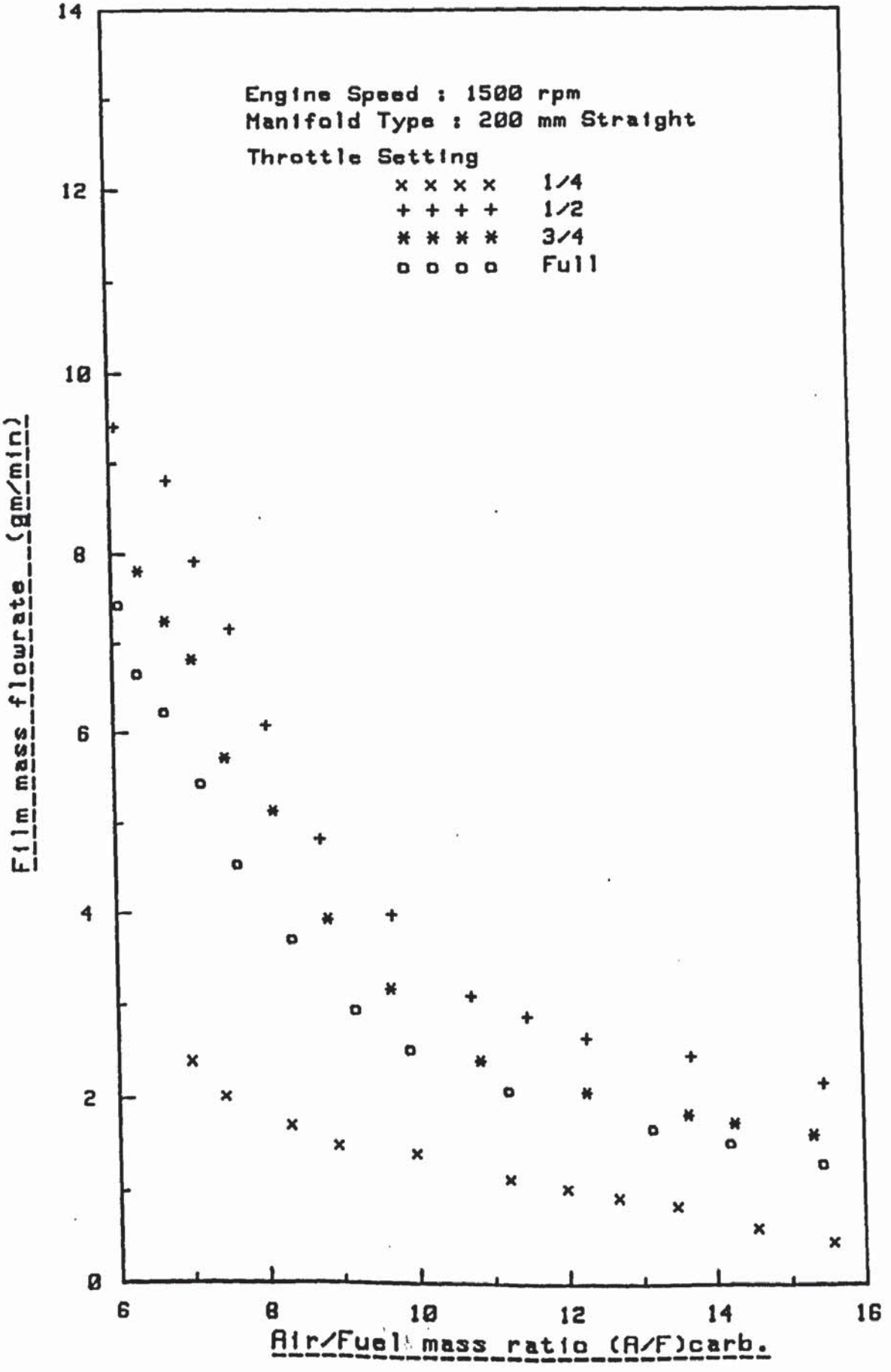

FIG. (5.5) Effect of Throttle Setting on Film Flowrate

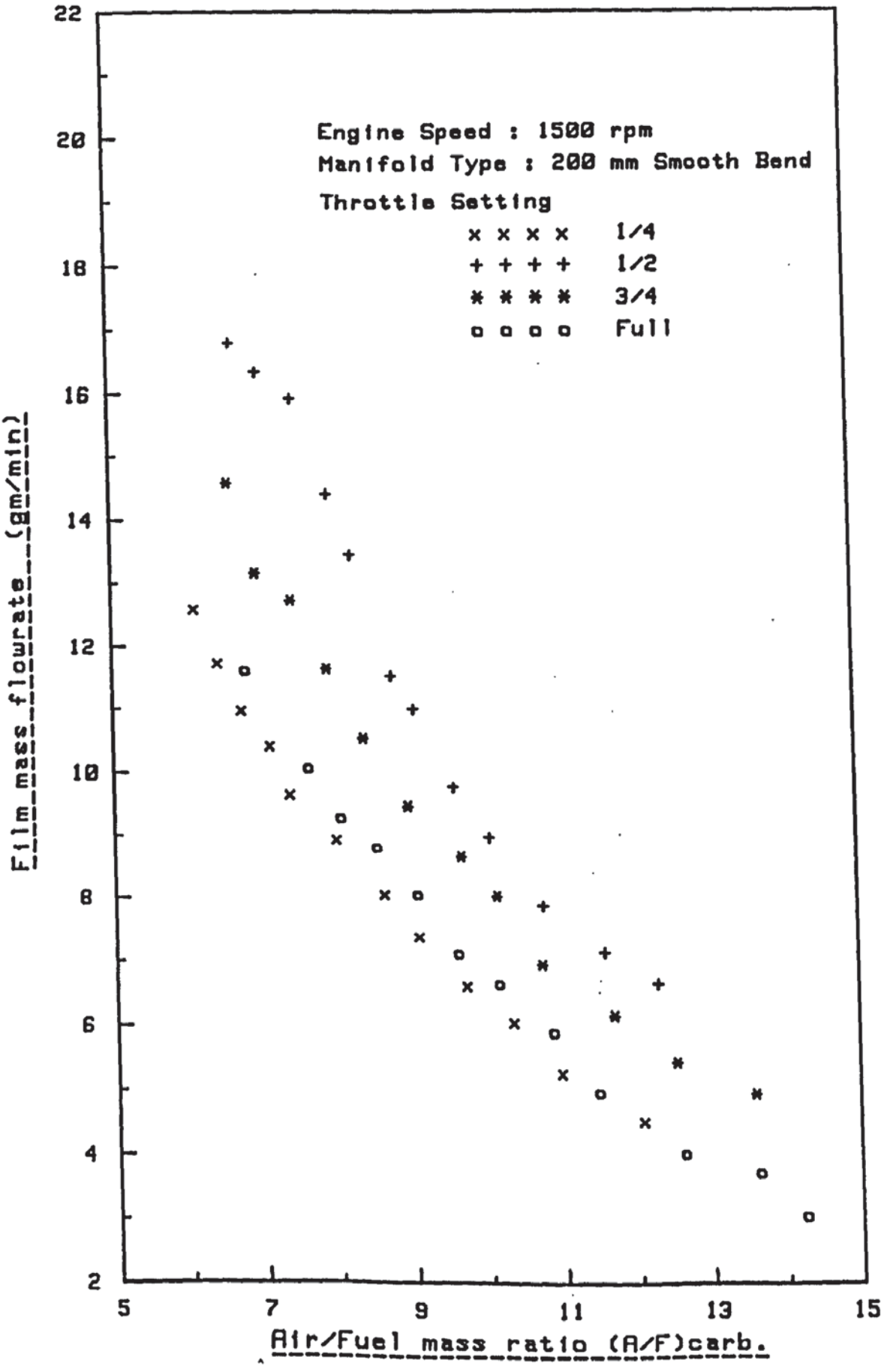

FIG. (5.6) Effect of Throttle Setting on Film Flowrate

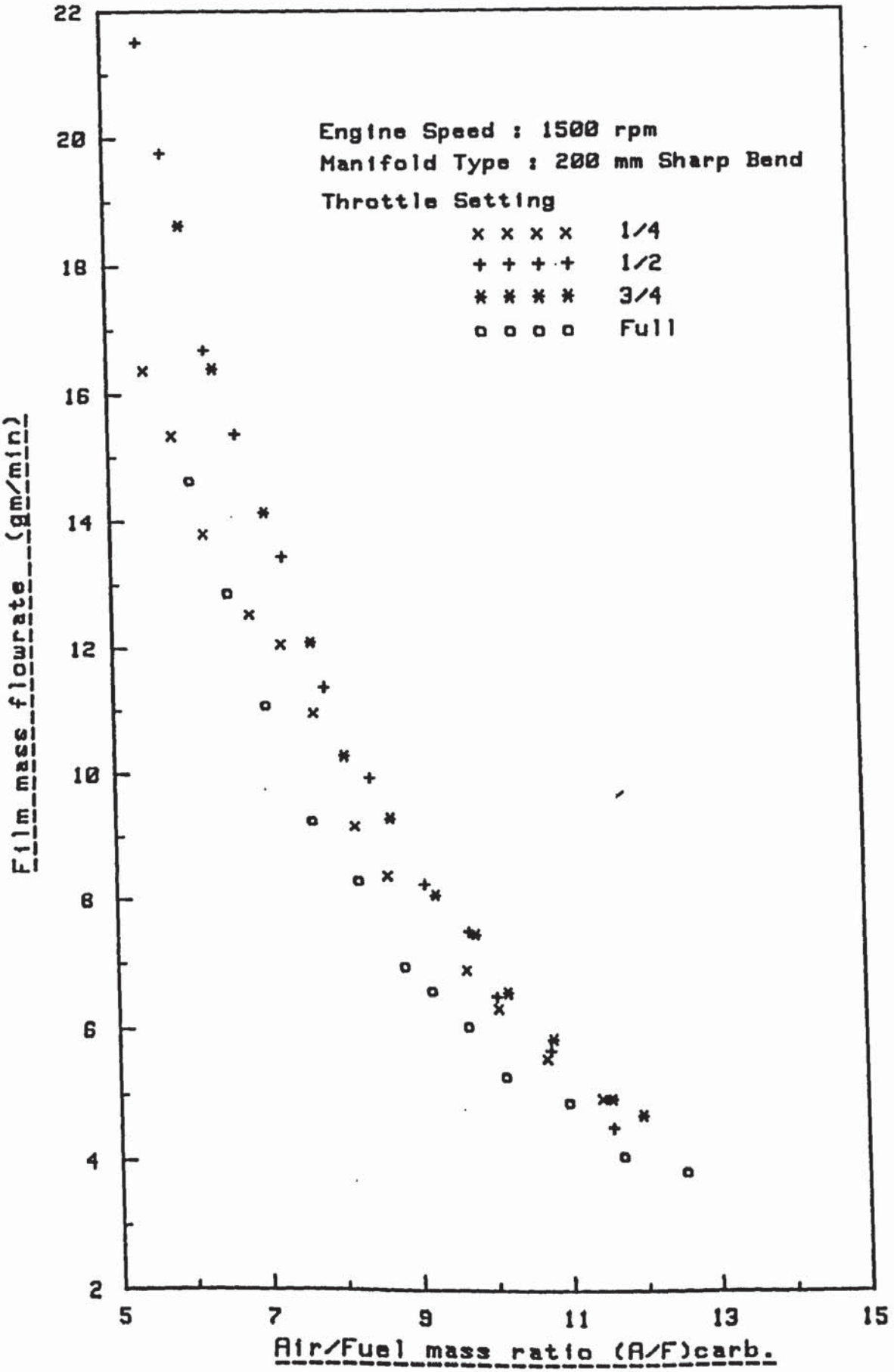

FIG. (5.7) Effect of Throttle Setting on Film Flowrate

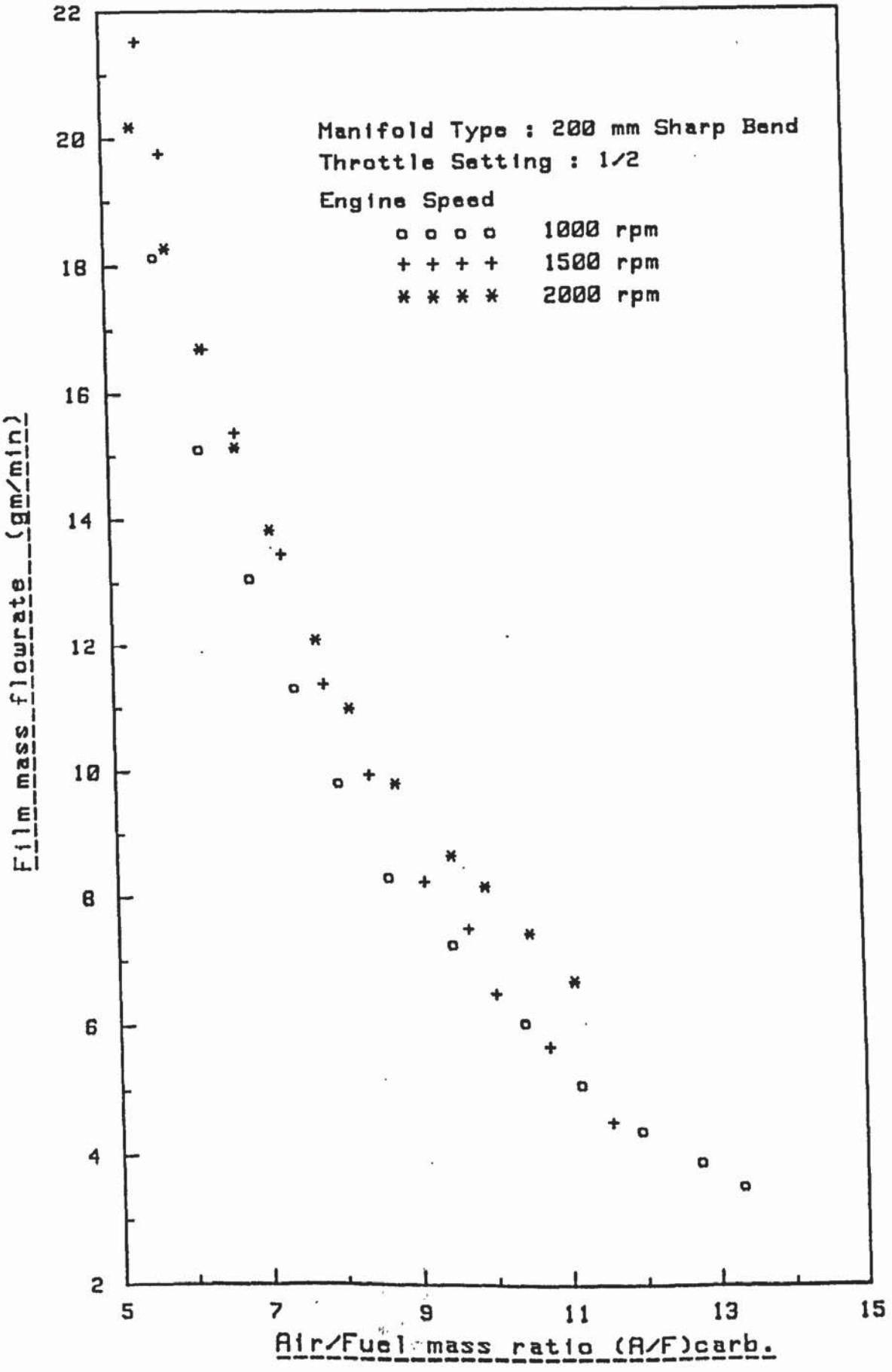

FIG. (5.8) Effect of Engine Speed on Film Flowrate

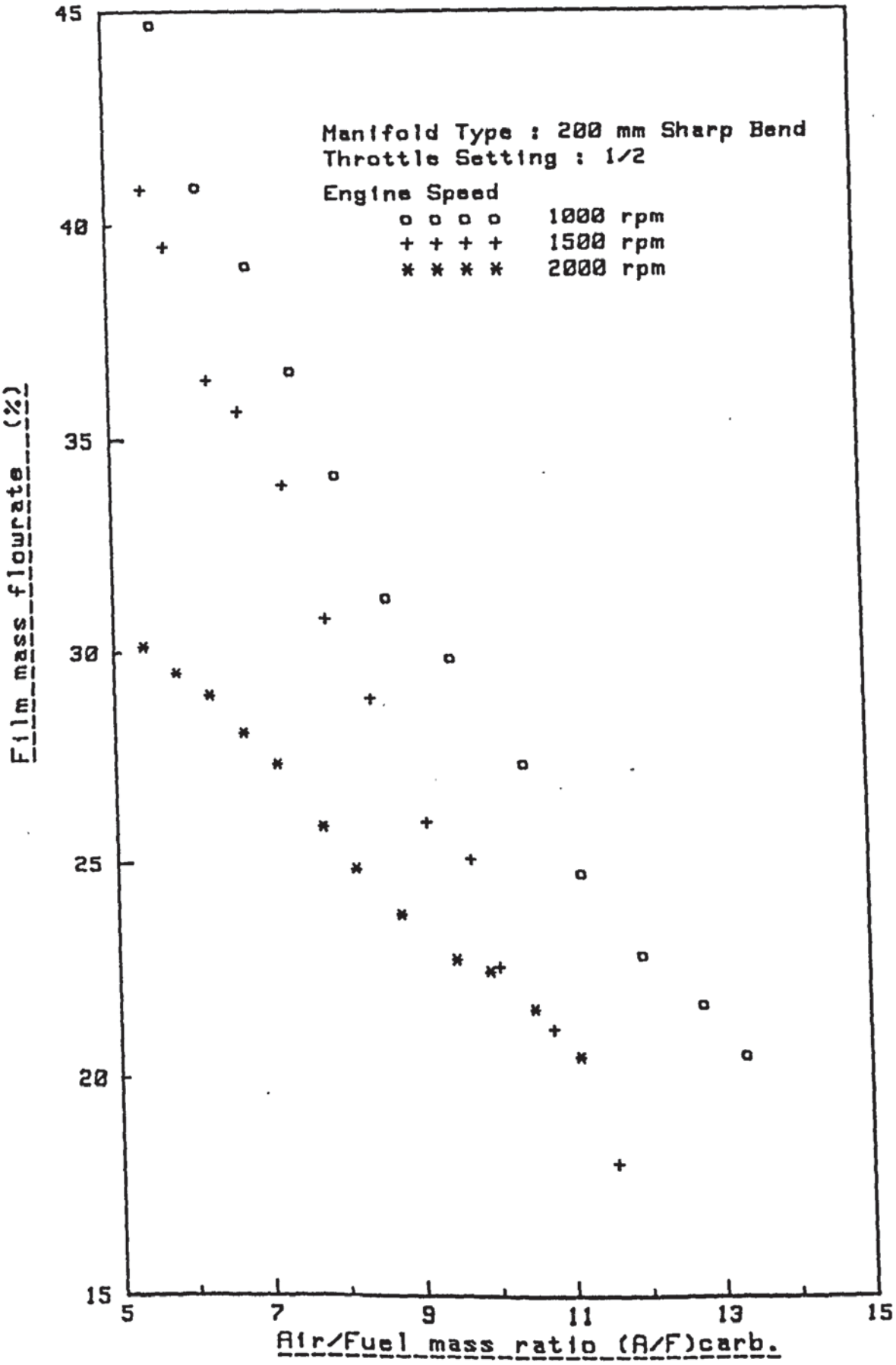

FIG. (5.9) Effect of Engine Speed on % Film Flowrate

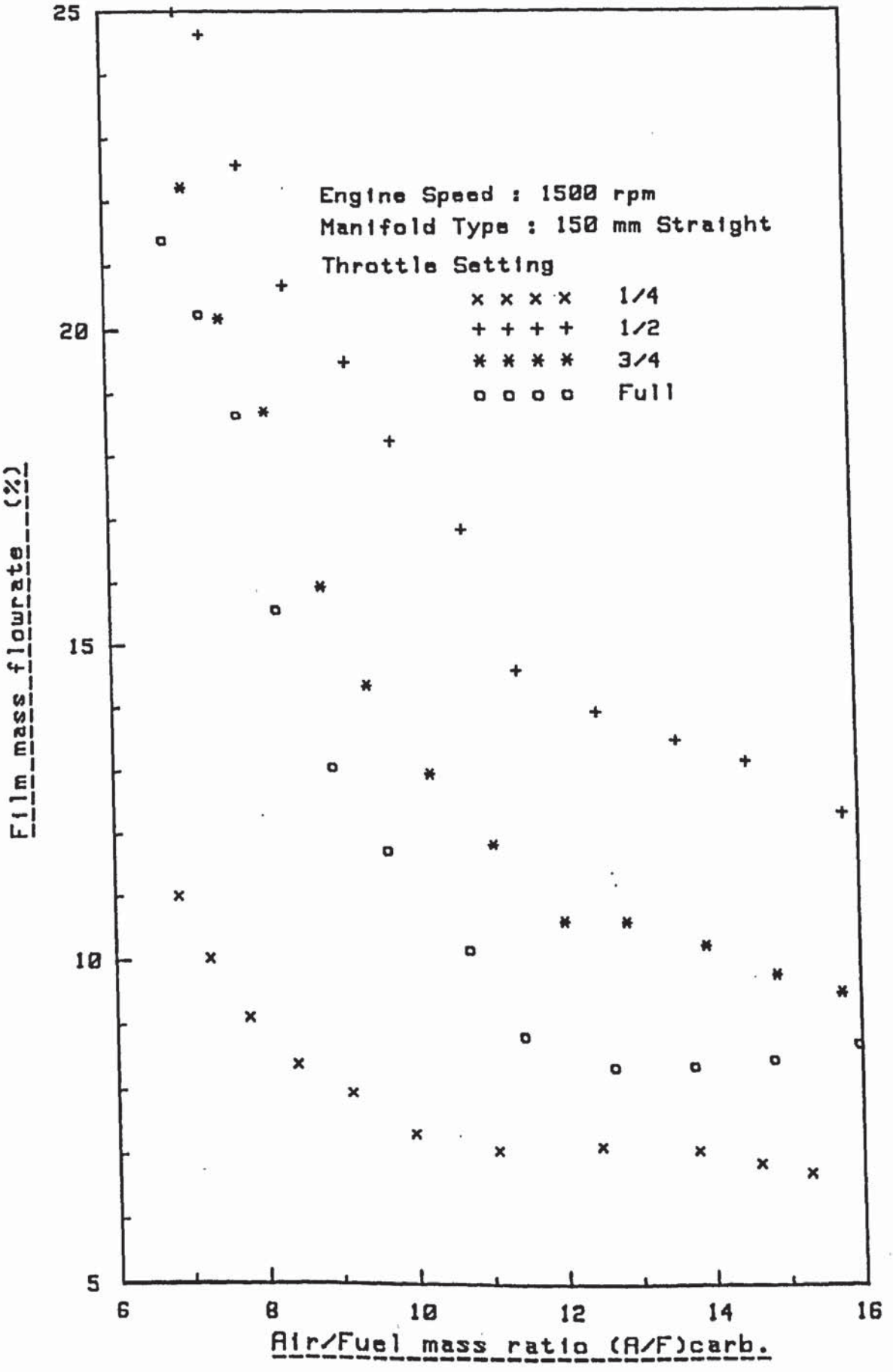

FIG. (5.10) Effect of Throttle Setting on % Film Flowrate

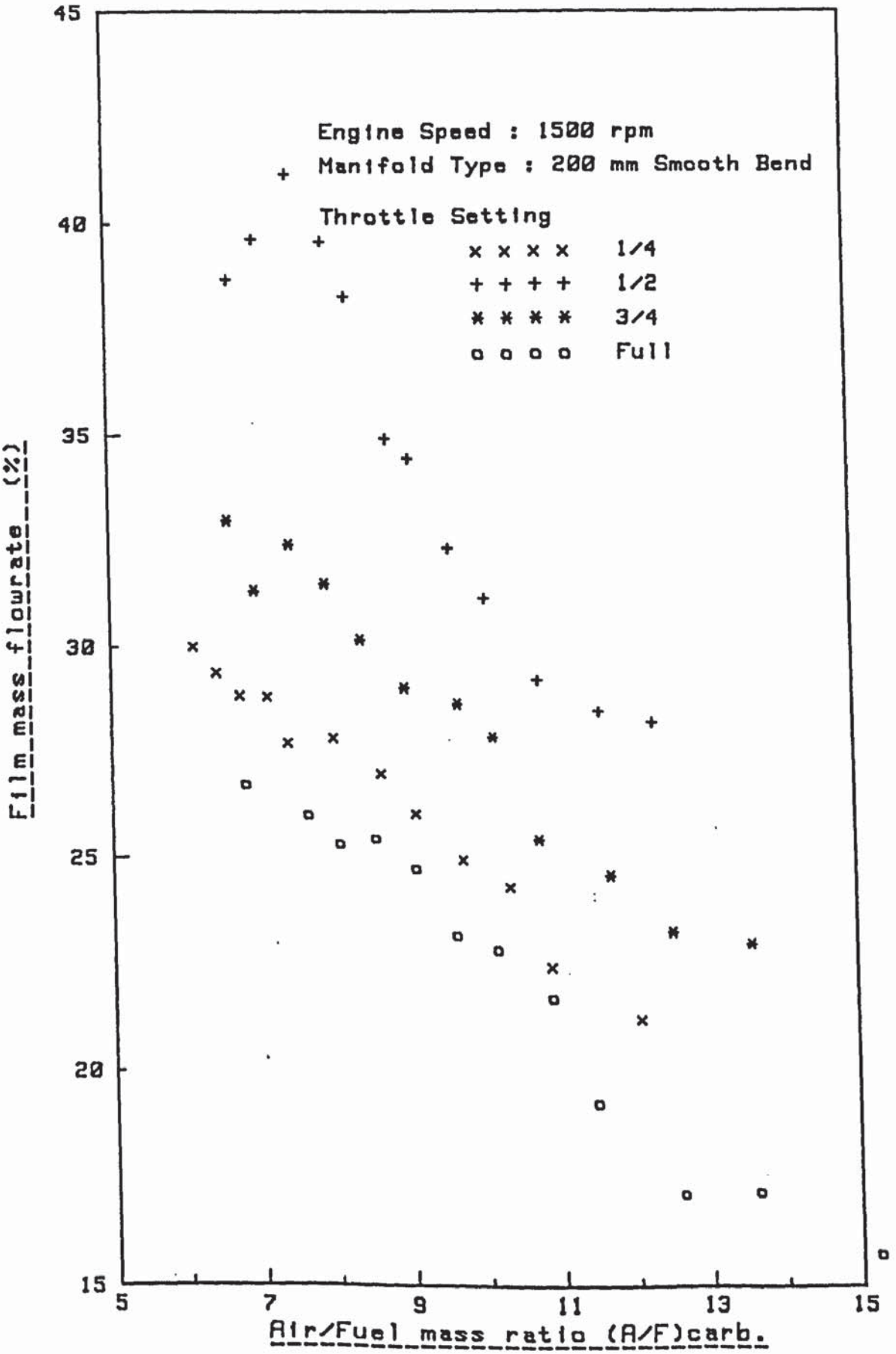

FIG. (5.11) Effect of Throttle Setting on % Film Flowrate

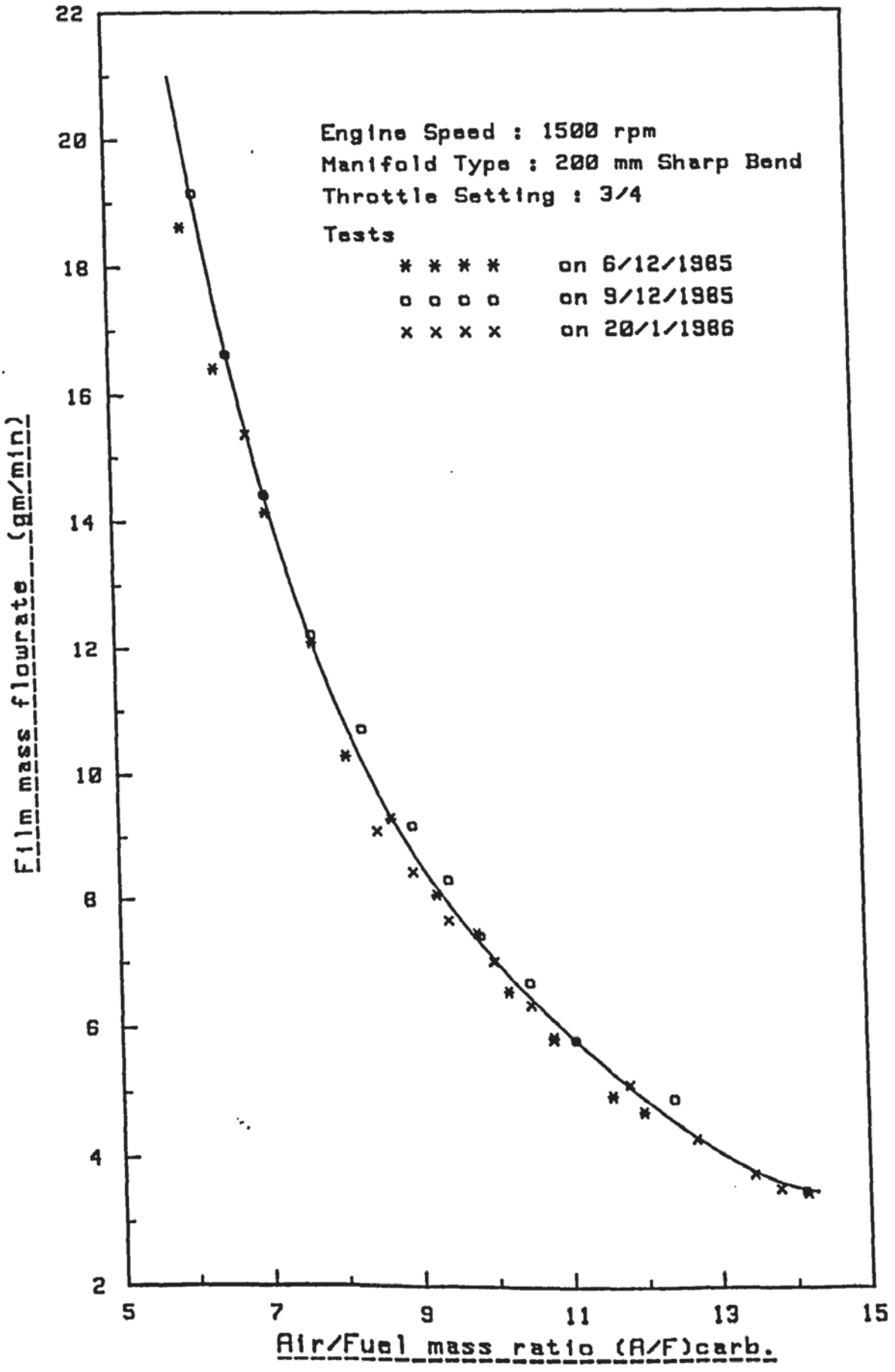

FIG. (5.12) Testing The Repeatability of The Measurements

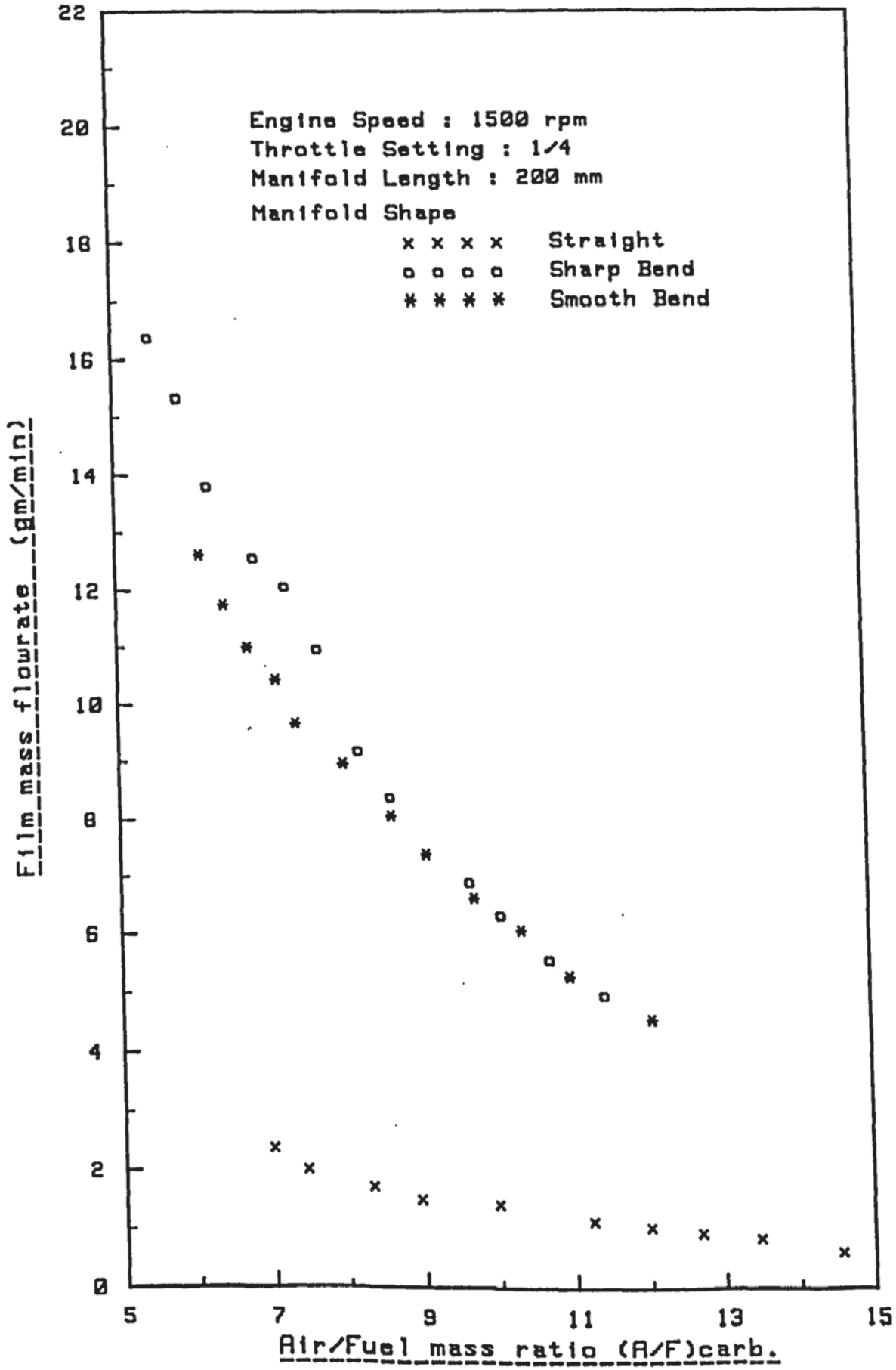

FIG. (5.13) Effect of Manifold Shape on Film Flowrate

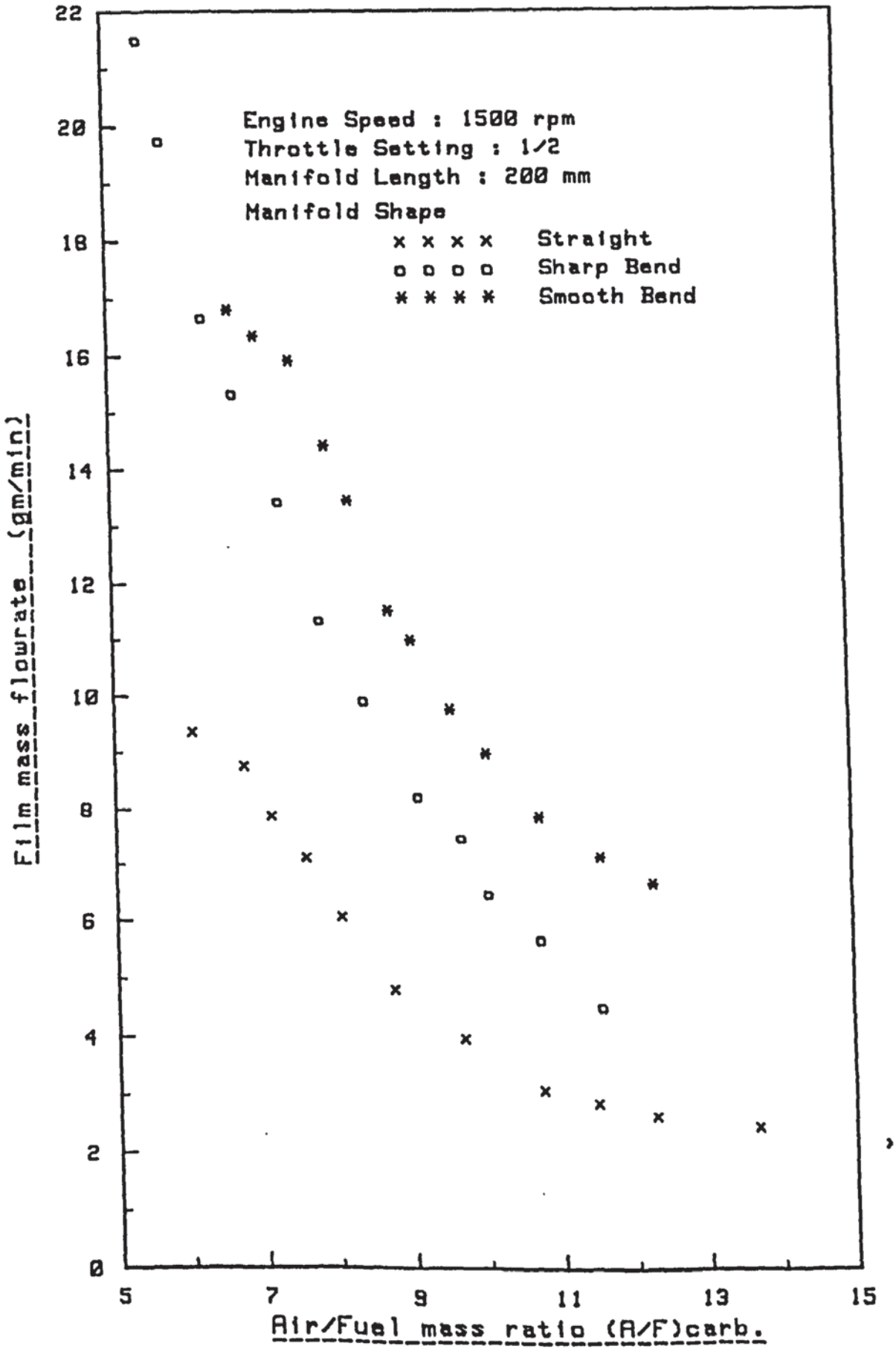

FIG. (5.14) Effect of Manifold Shape on Film Flowrate

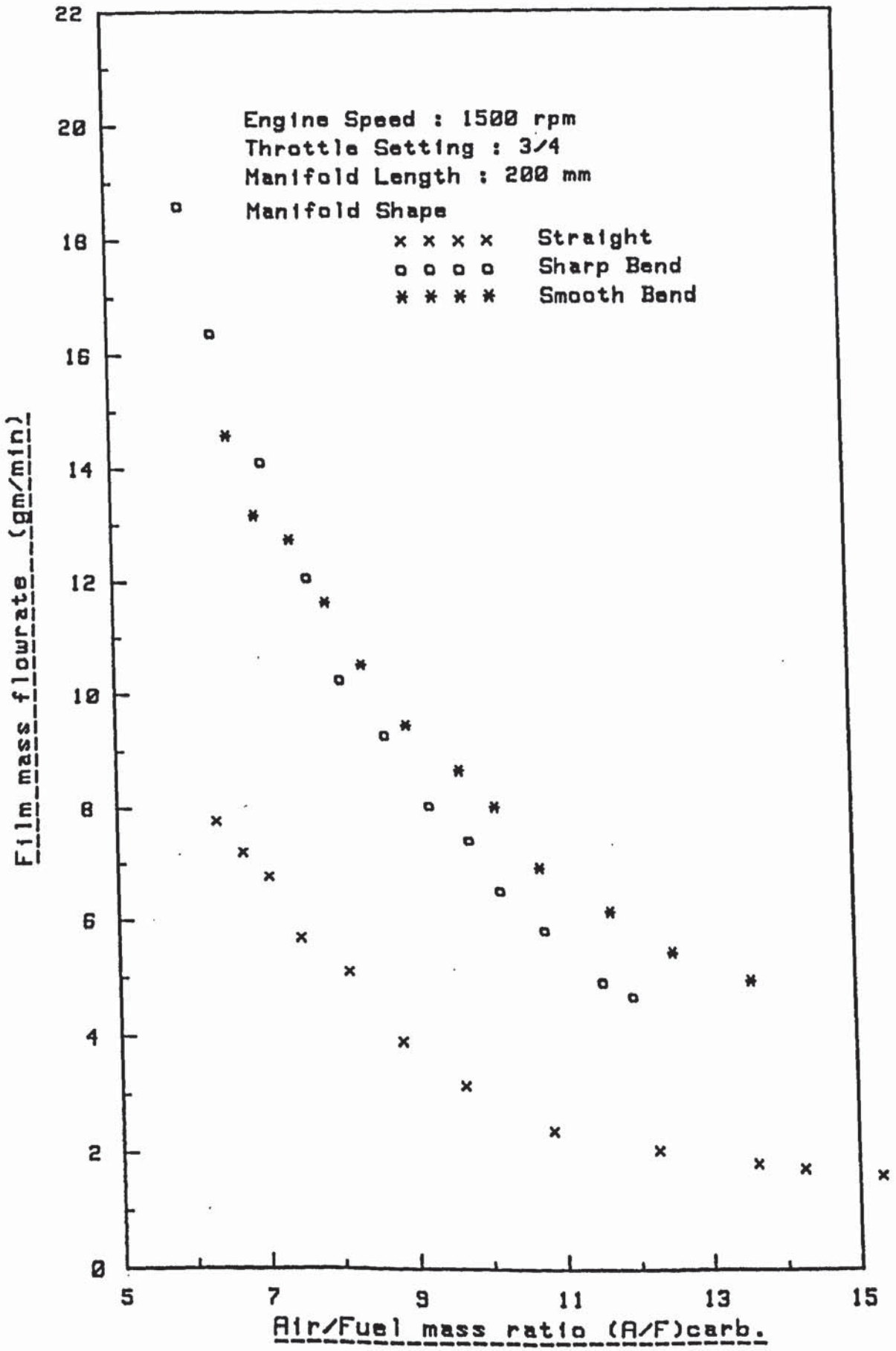

FIG. (5.15) Effect of Manifold Shape on Film Flowrate

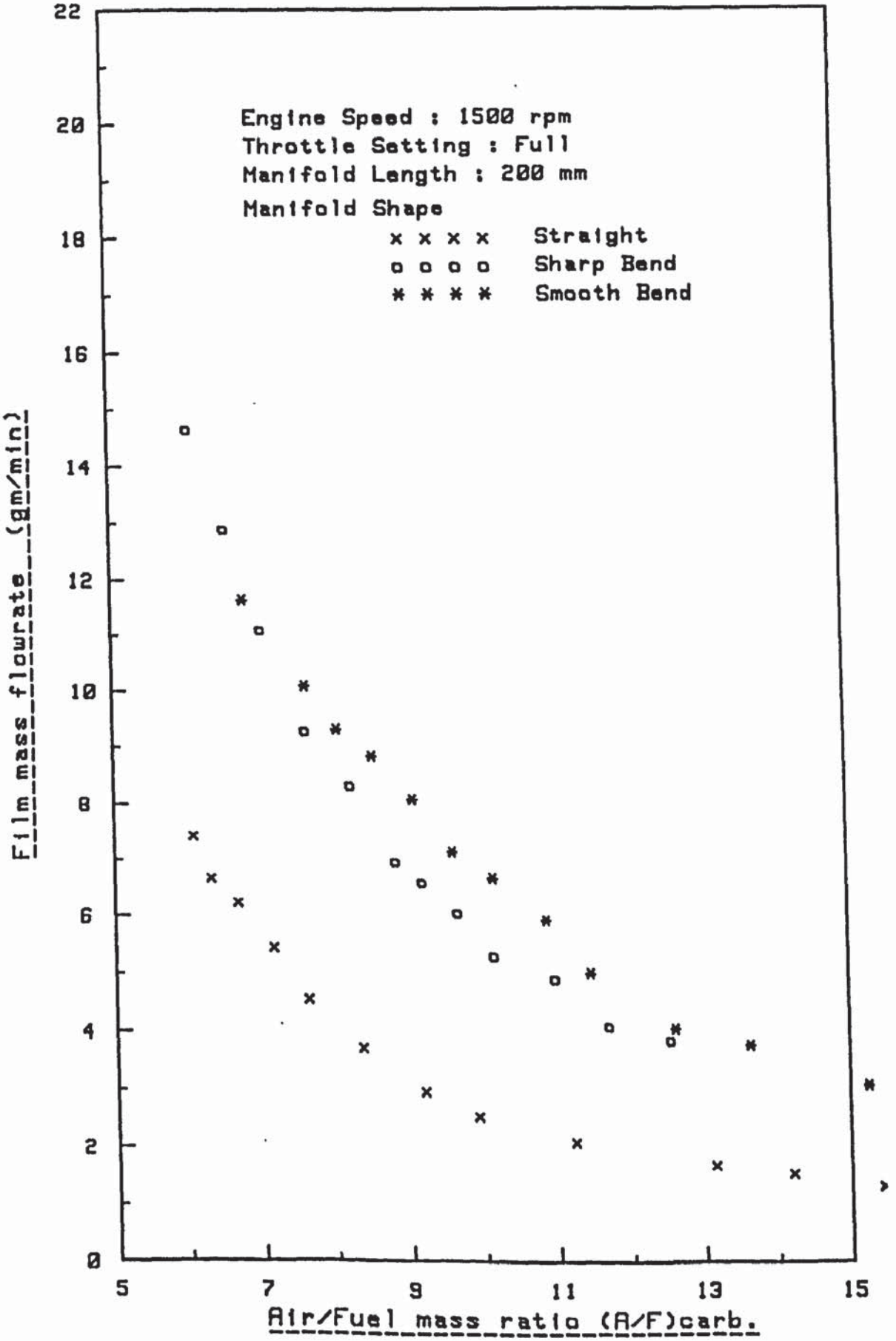

FIG. (5.16) Effect of Manifold Shape on Film Flowrate

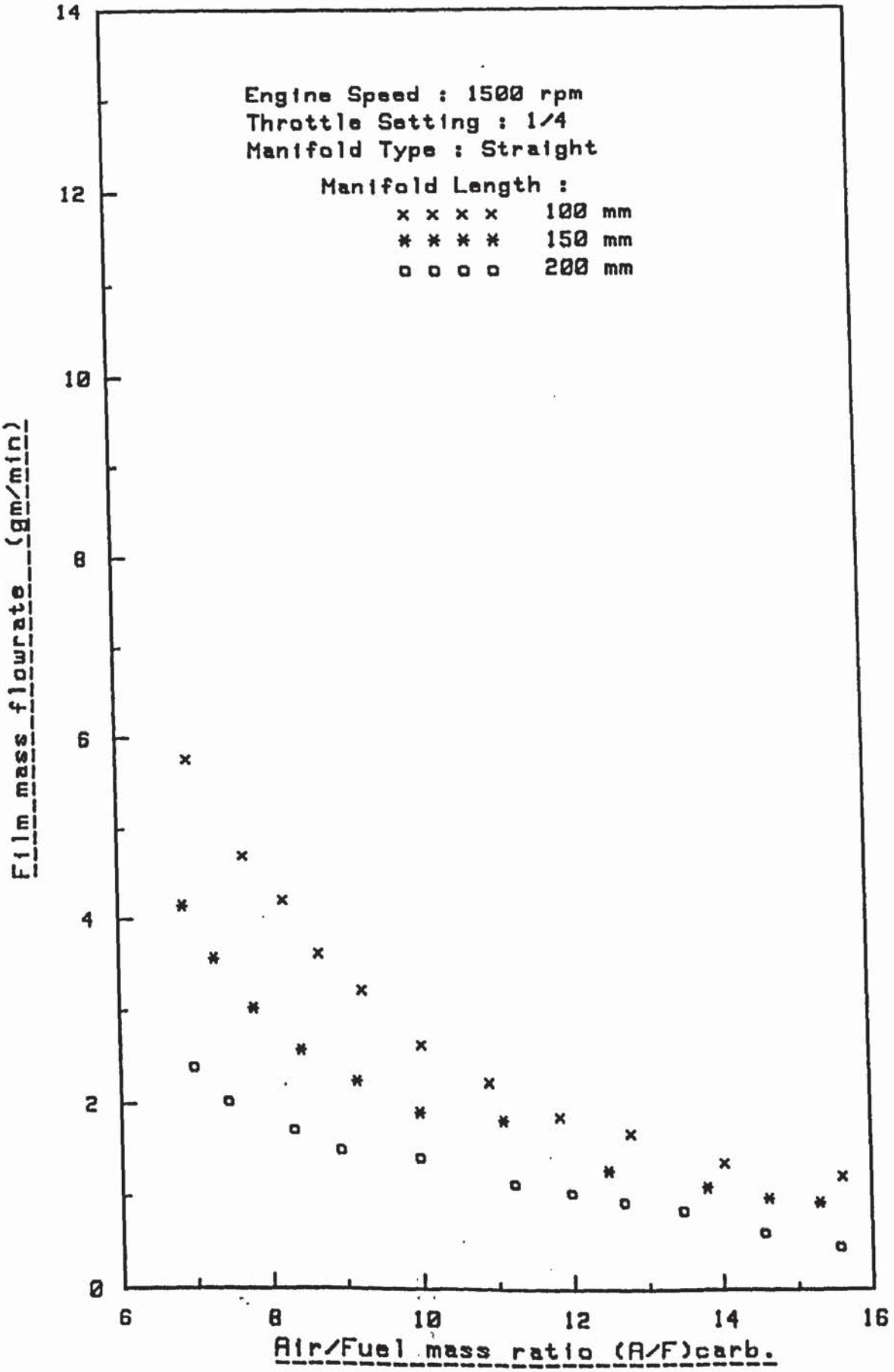

FIG. (5.17) Effect of Manifold Length on Film Flowrate

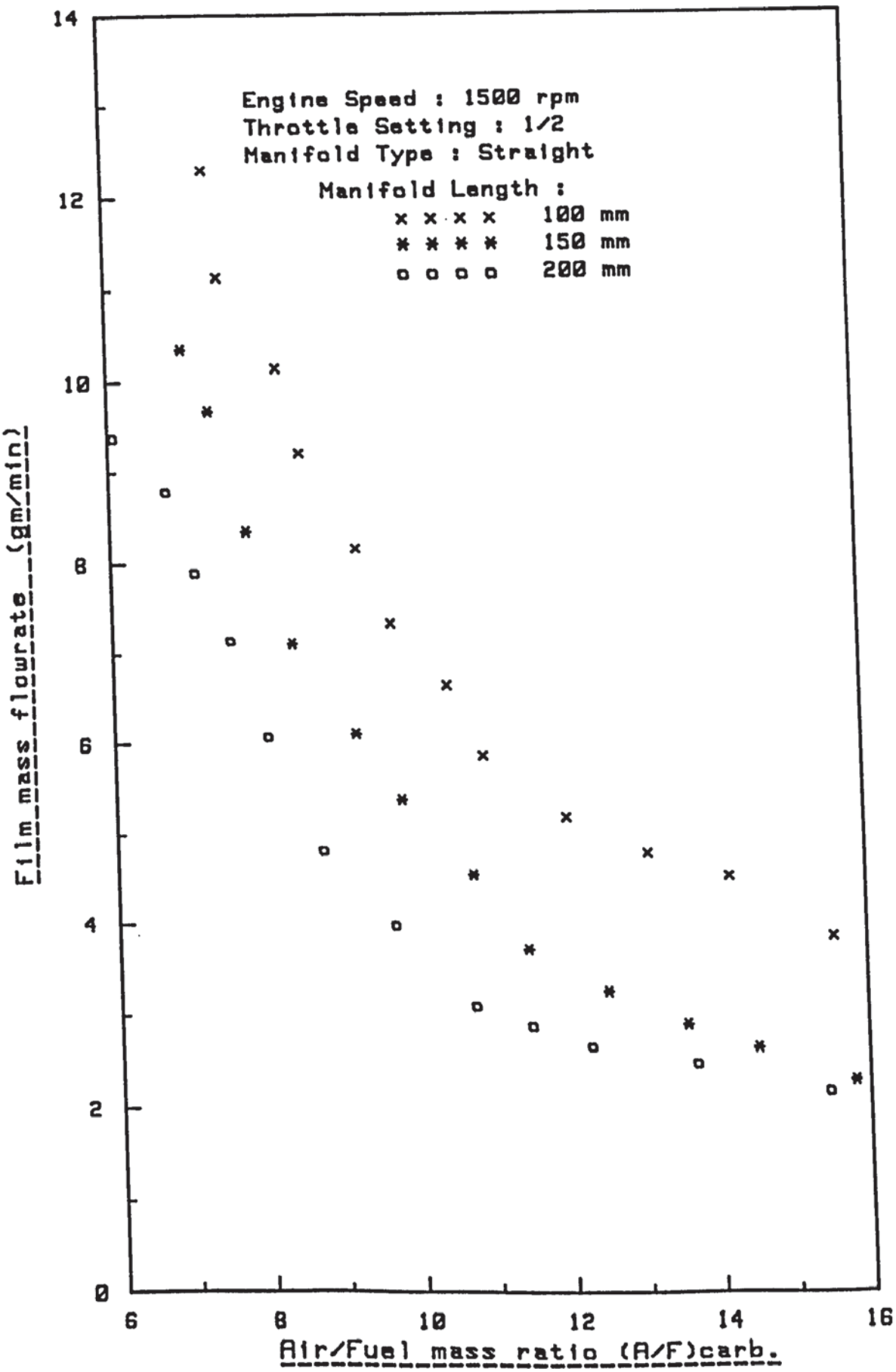

FIG. (5.18) Effect of Manifold Length on Film Flowrate

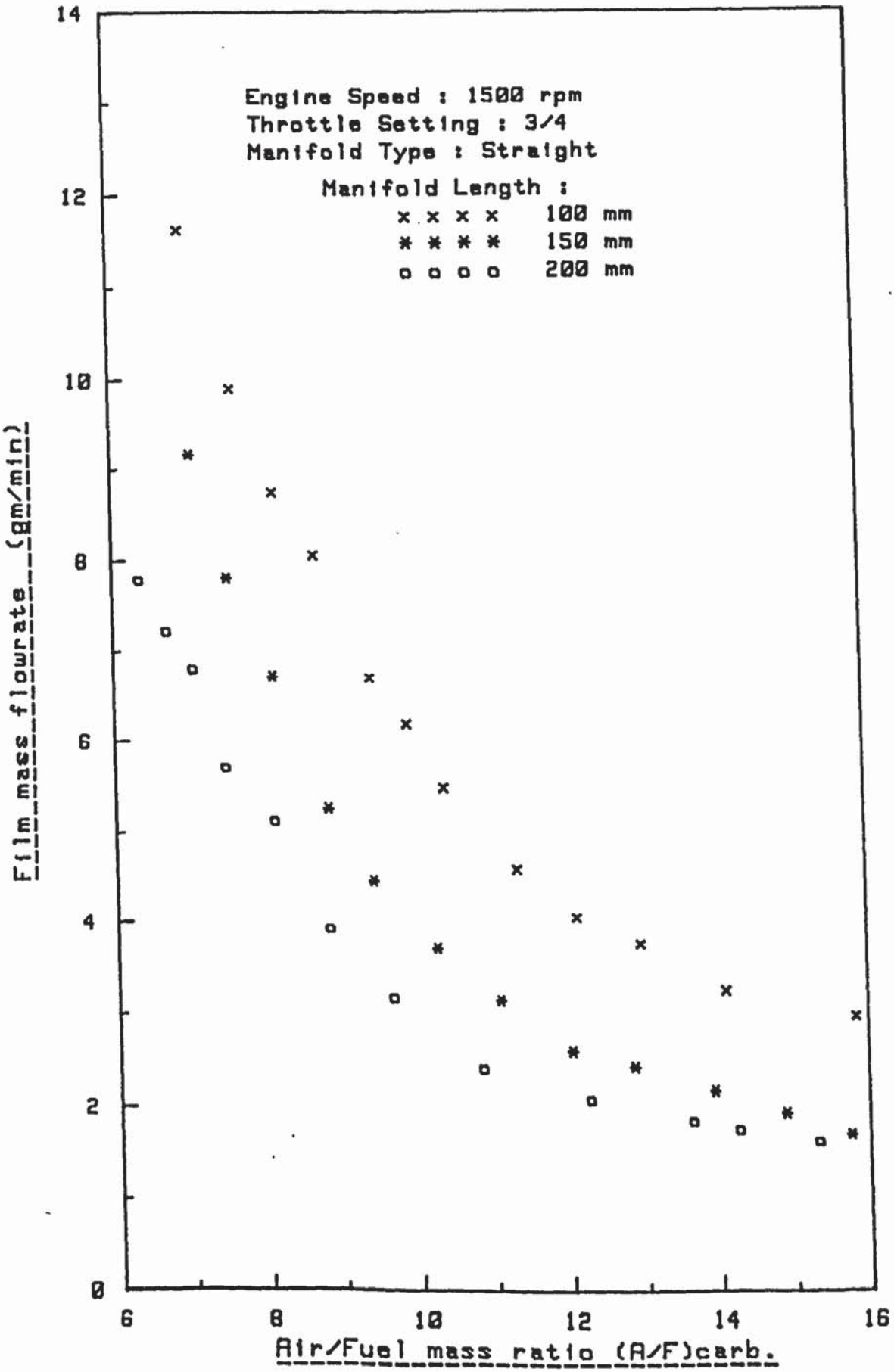

FIG. (5.19) Effect of Manifold Length on Film Flowrate

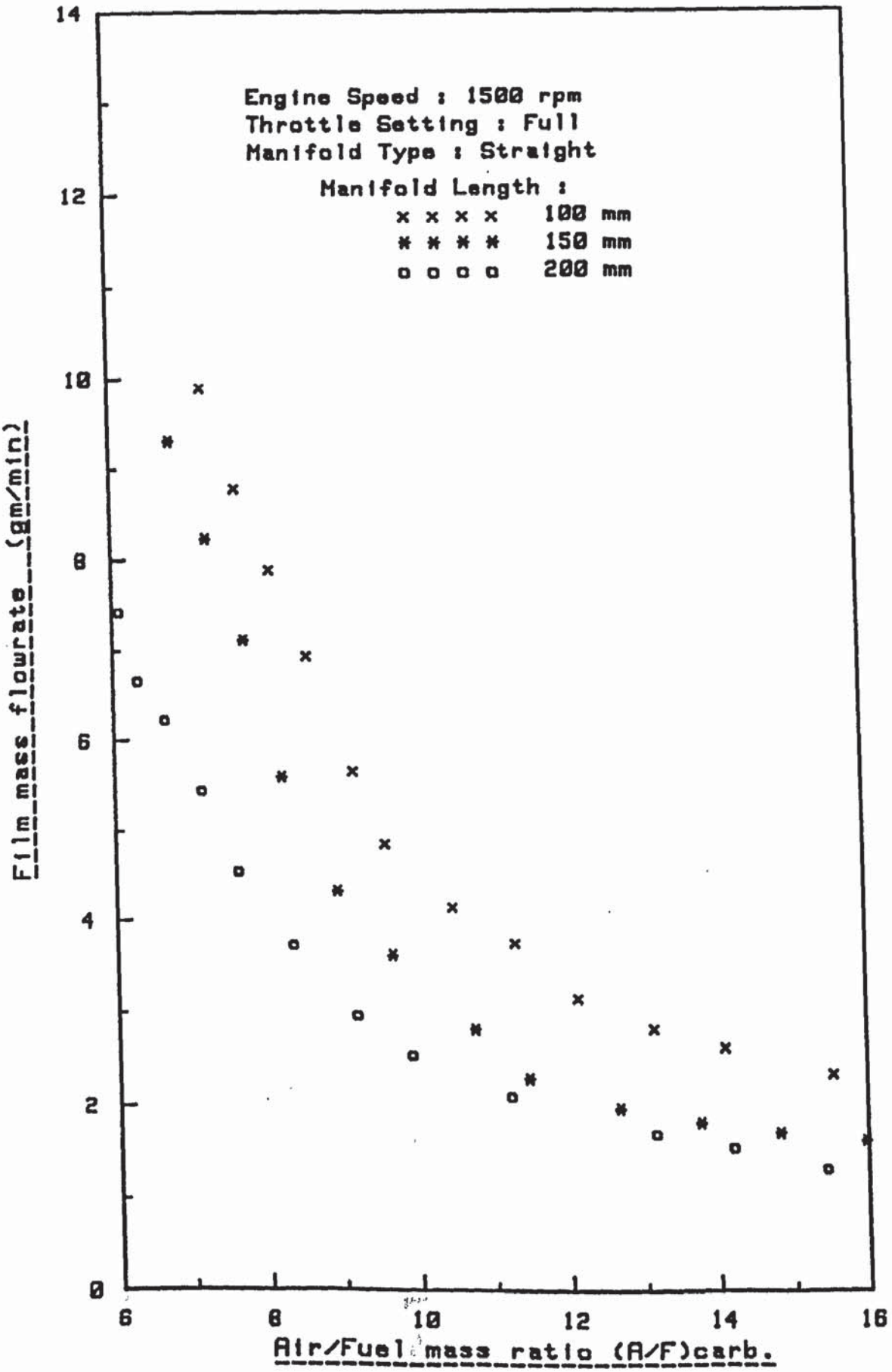

FIG. (5.20) Effect of Manifold Length on Film Flowrate

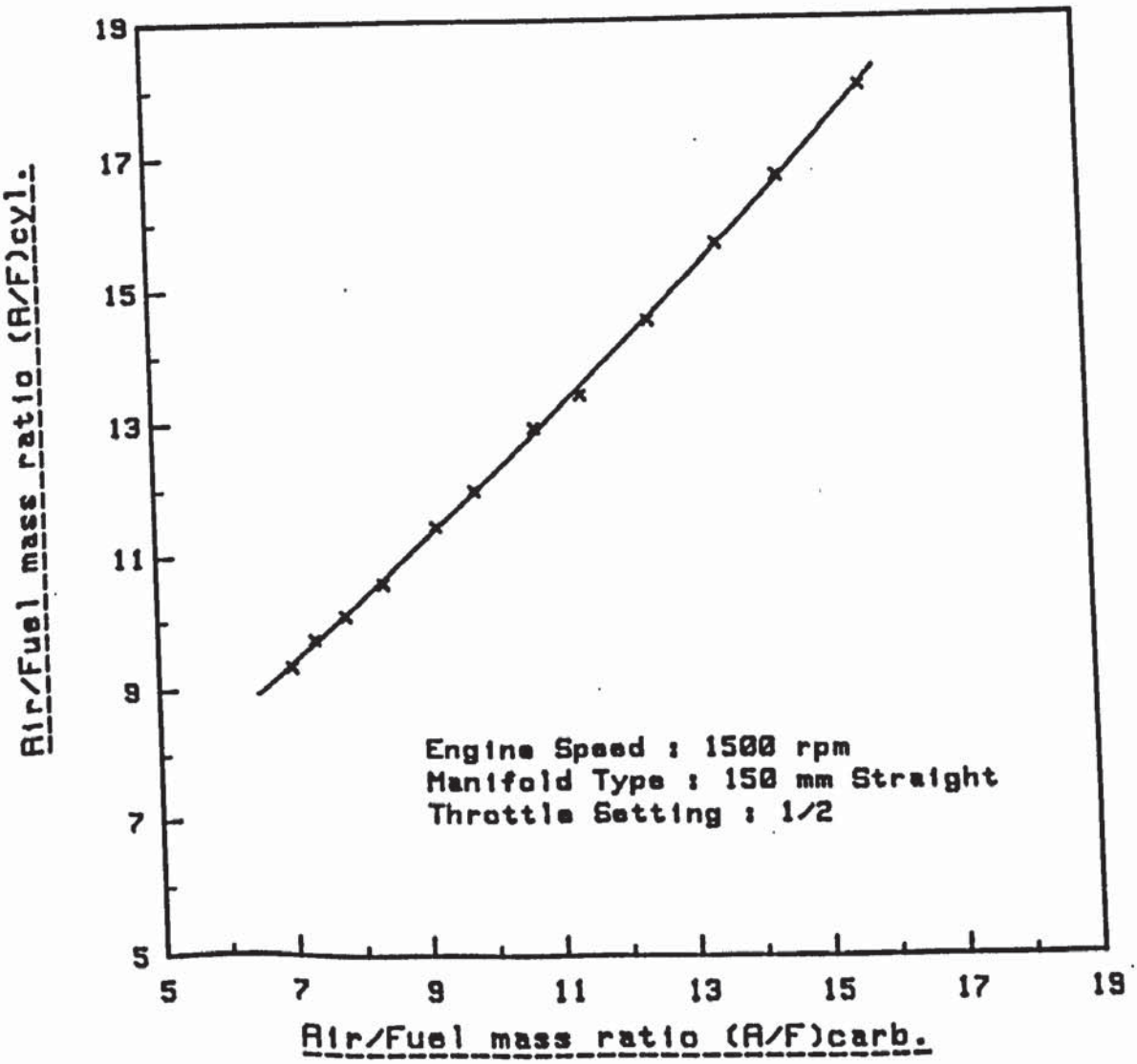

FIG. (5.21) Effect of Wall Film Separation on Cylinder A/F Ratio

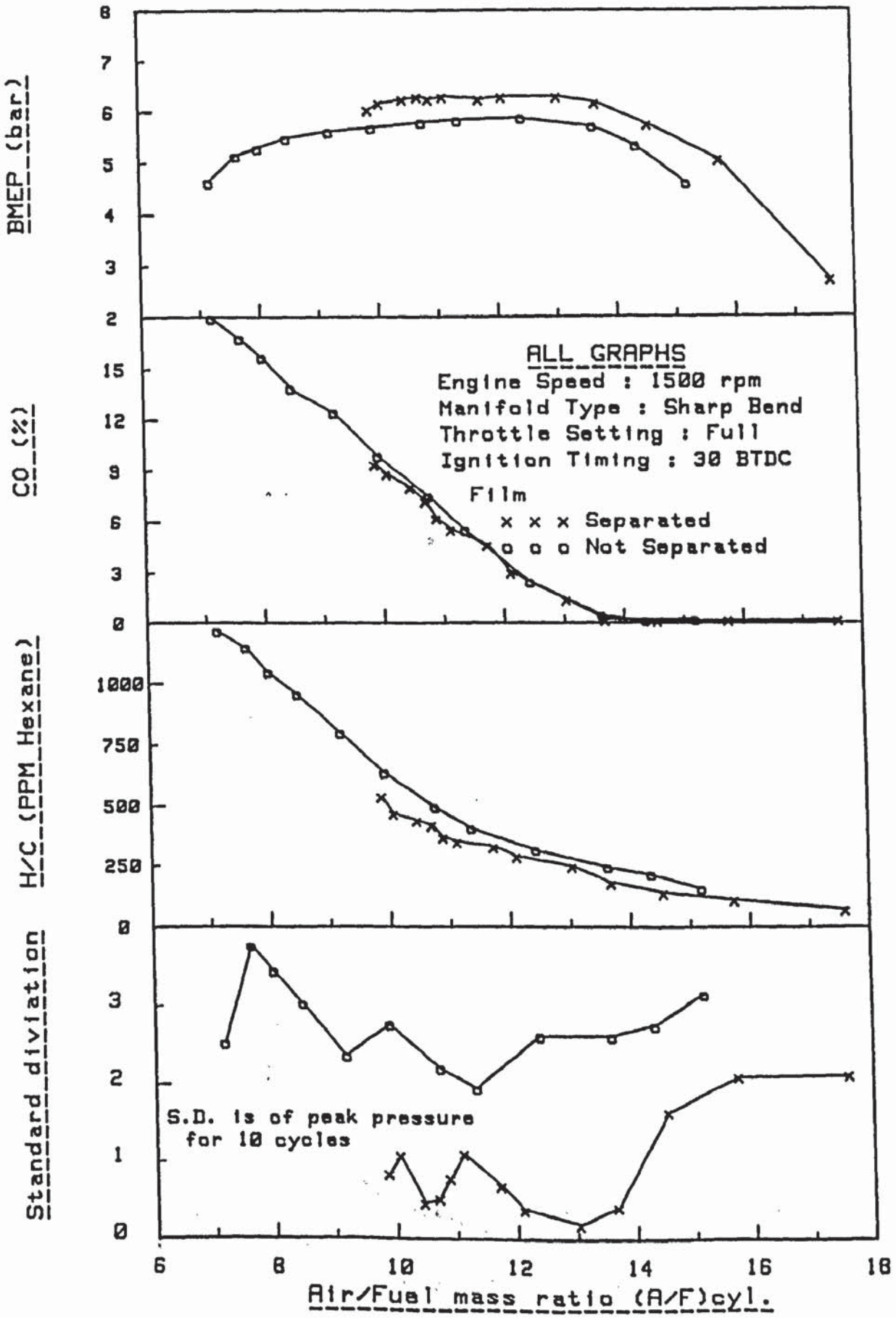

FIG. (5.22) Effect of Wall Film Separation on Engine Performance and Emissions

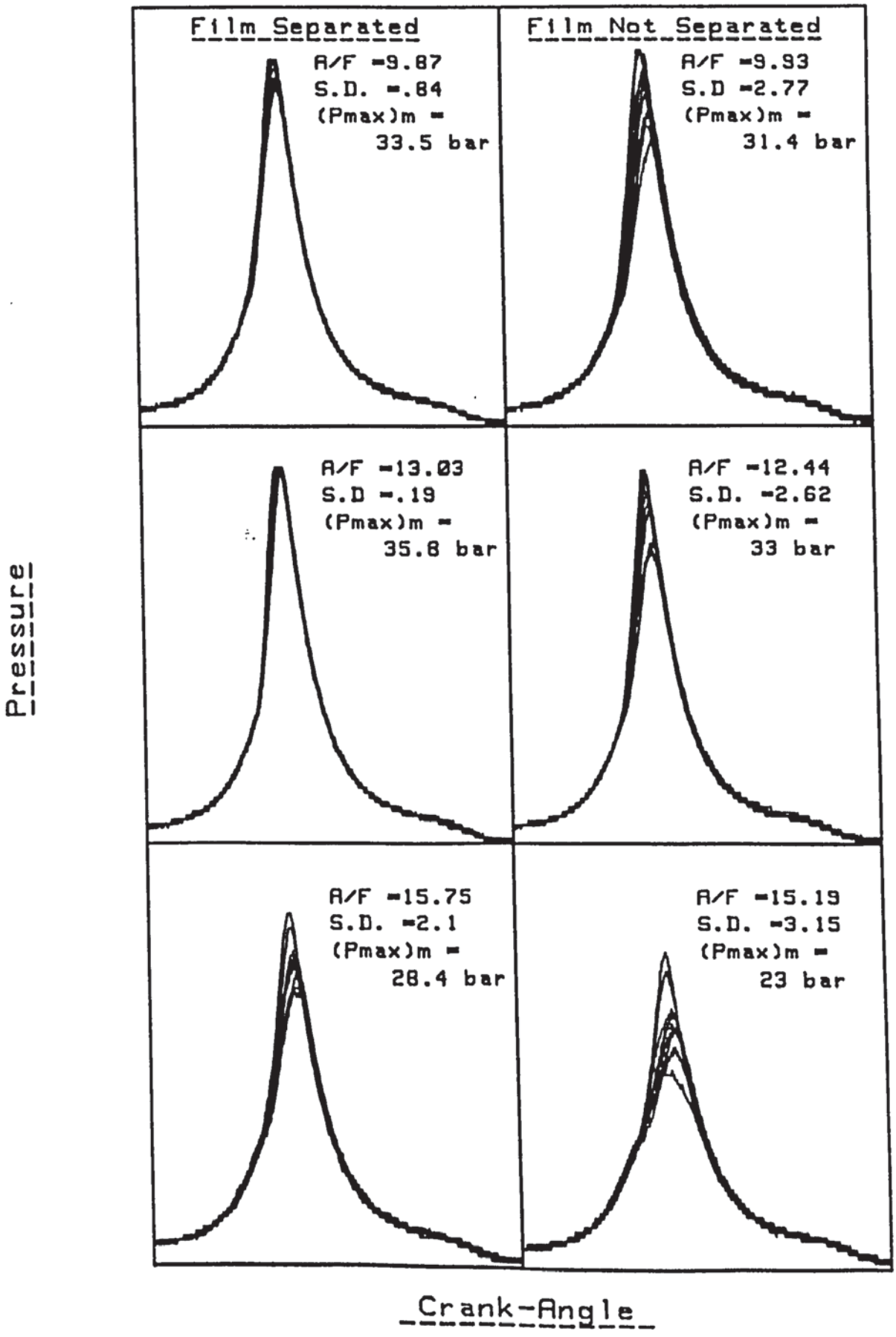

FIG. (5.23) Effect of Wall Film Separation on Cycle to Cycle Variation

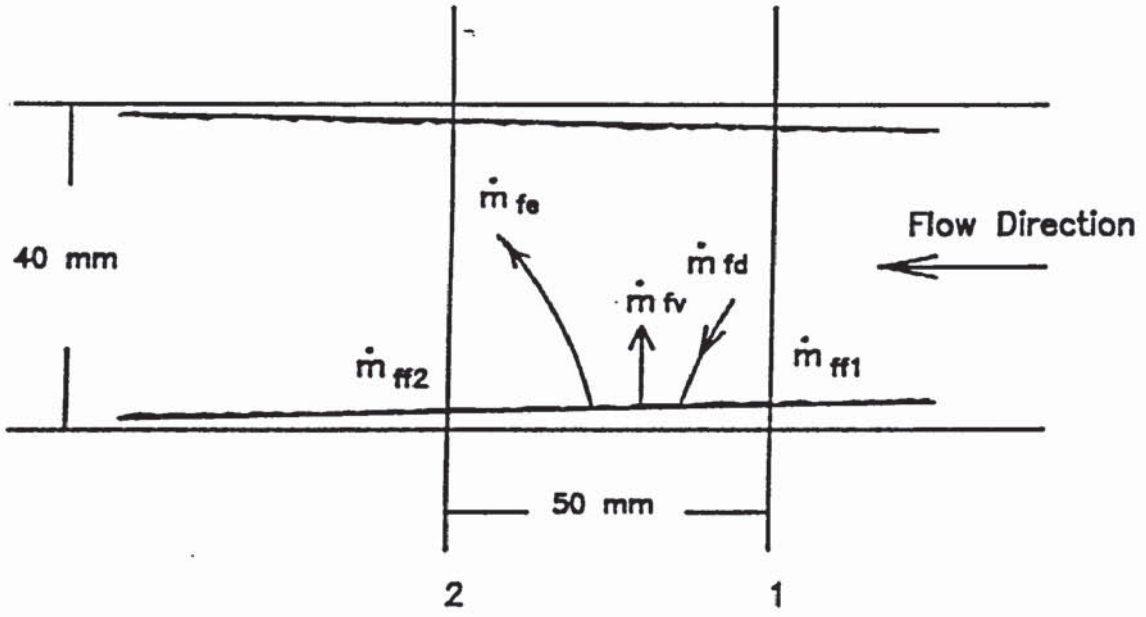

FIG. (5.24) Wall Film Model in the Intake Manifold

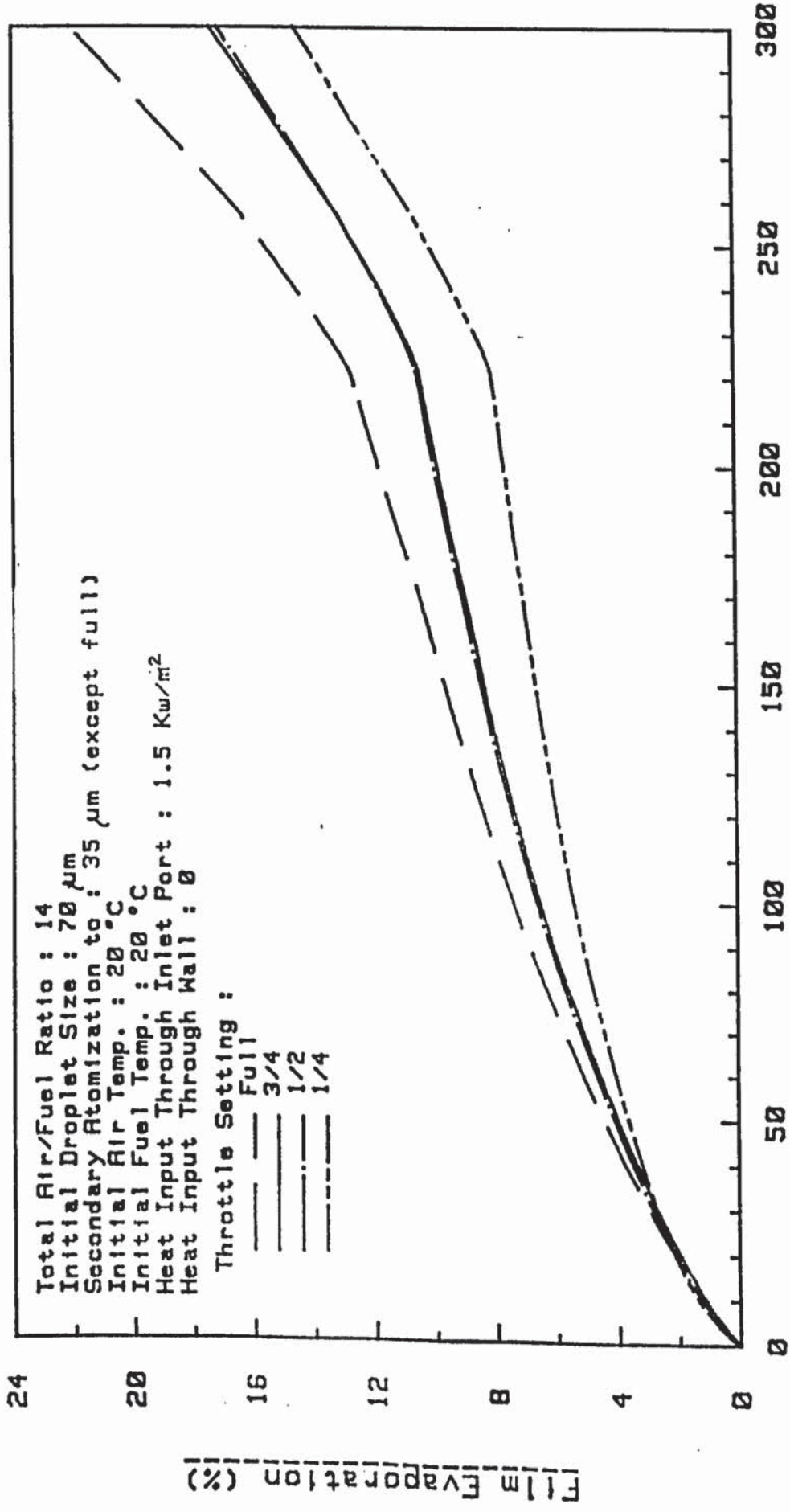

FIG. (5.25) Effect of Throttle Setting on Wall Film Evaporation

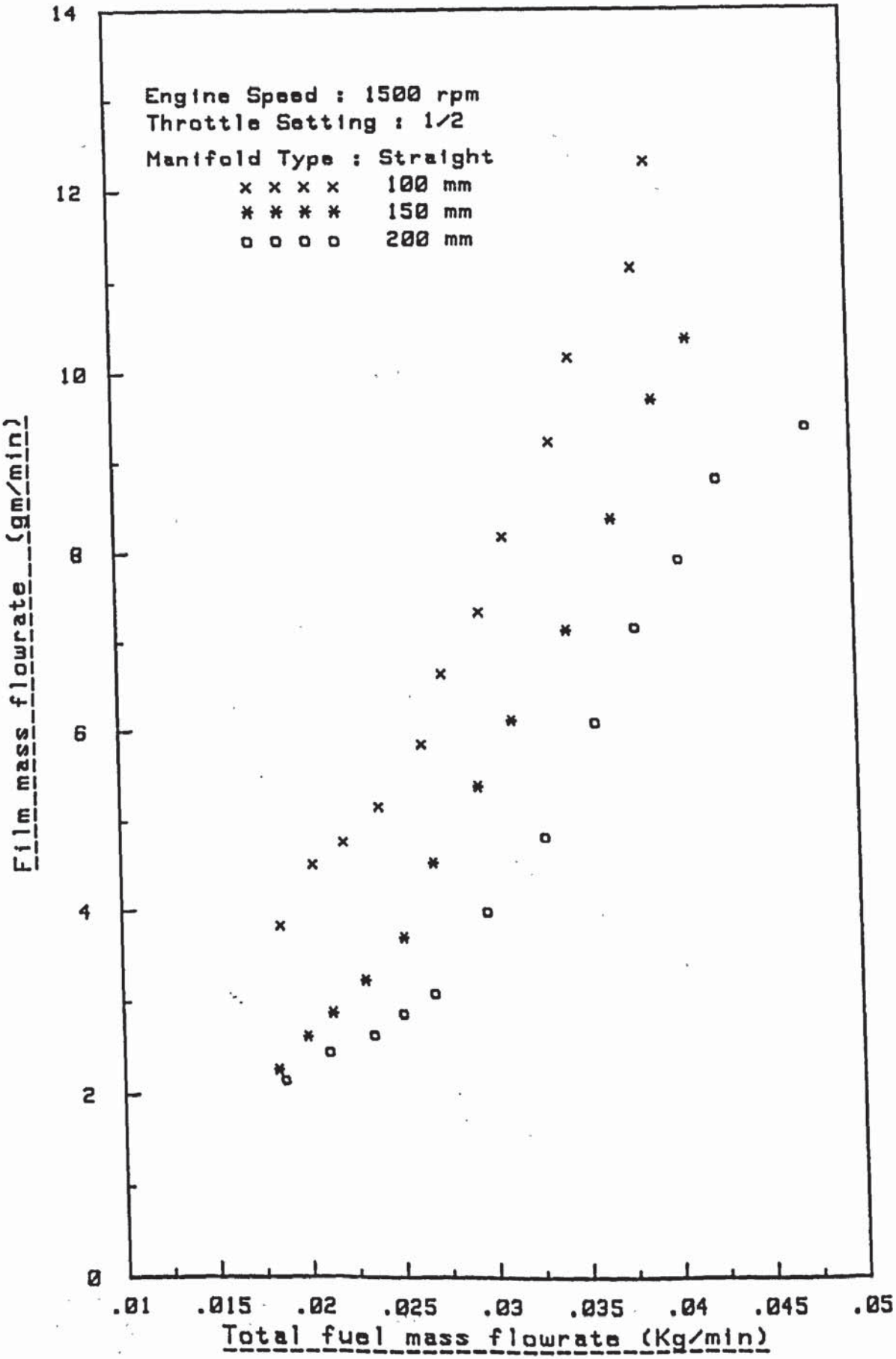

FIG. (5.26) Effect of Manifold Length on Film Flowrate

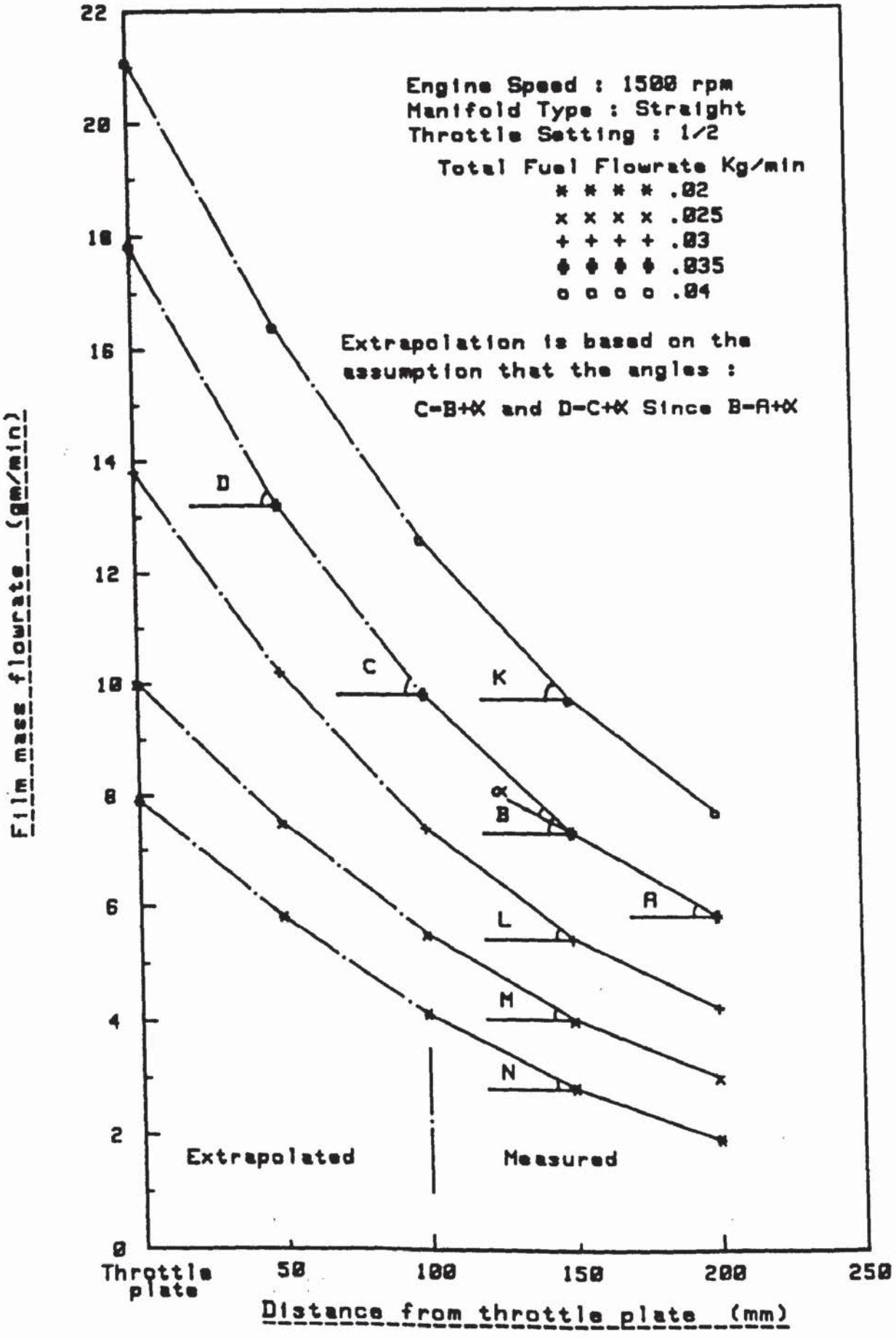

FIG. (5.27) Extrapolation of the Measured Film to the Throttle Plate

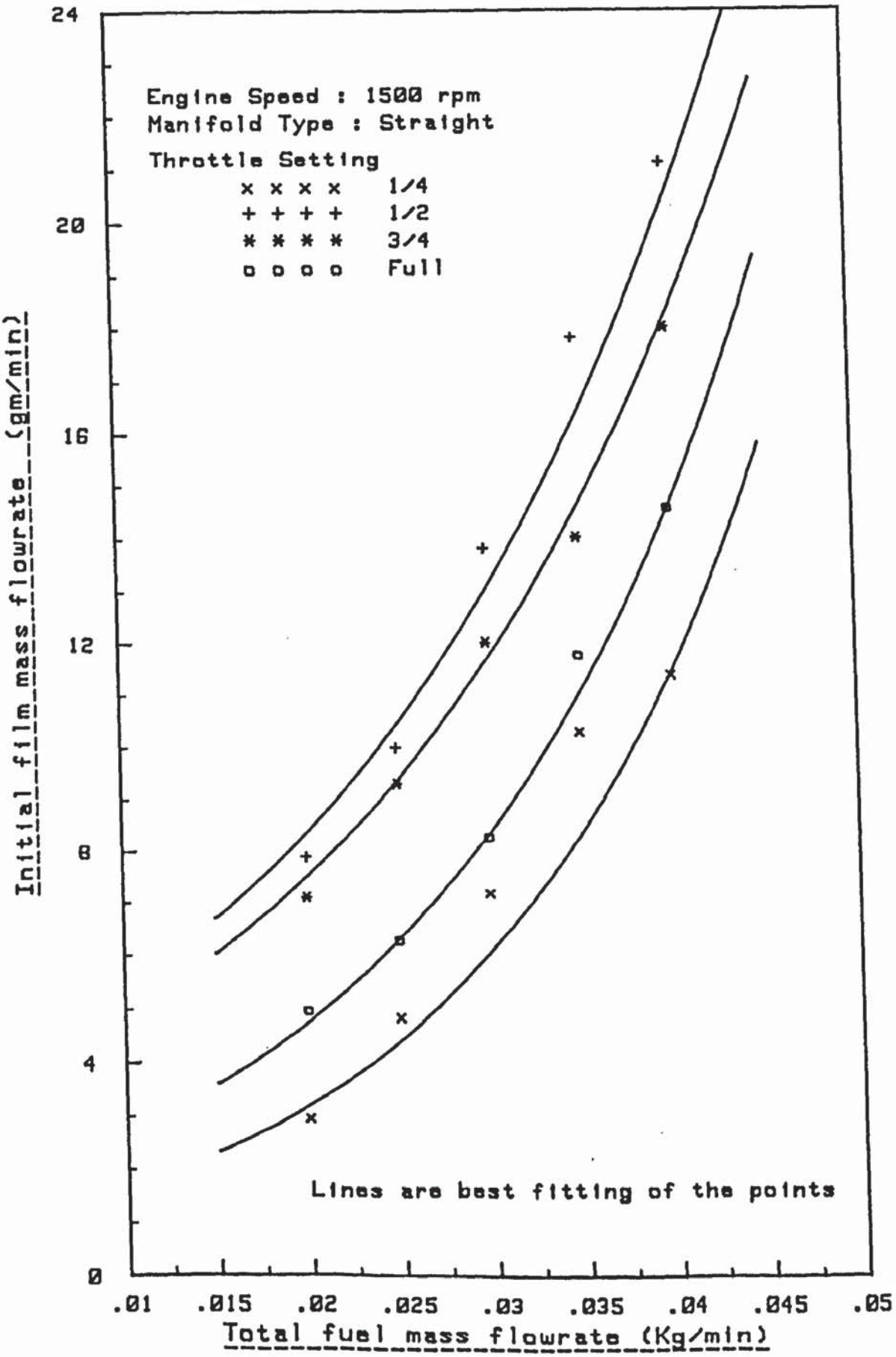

FIG. (5.28) Calculated Initial Wall Film at Throttle Plate

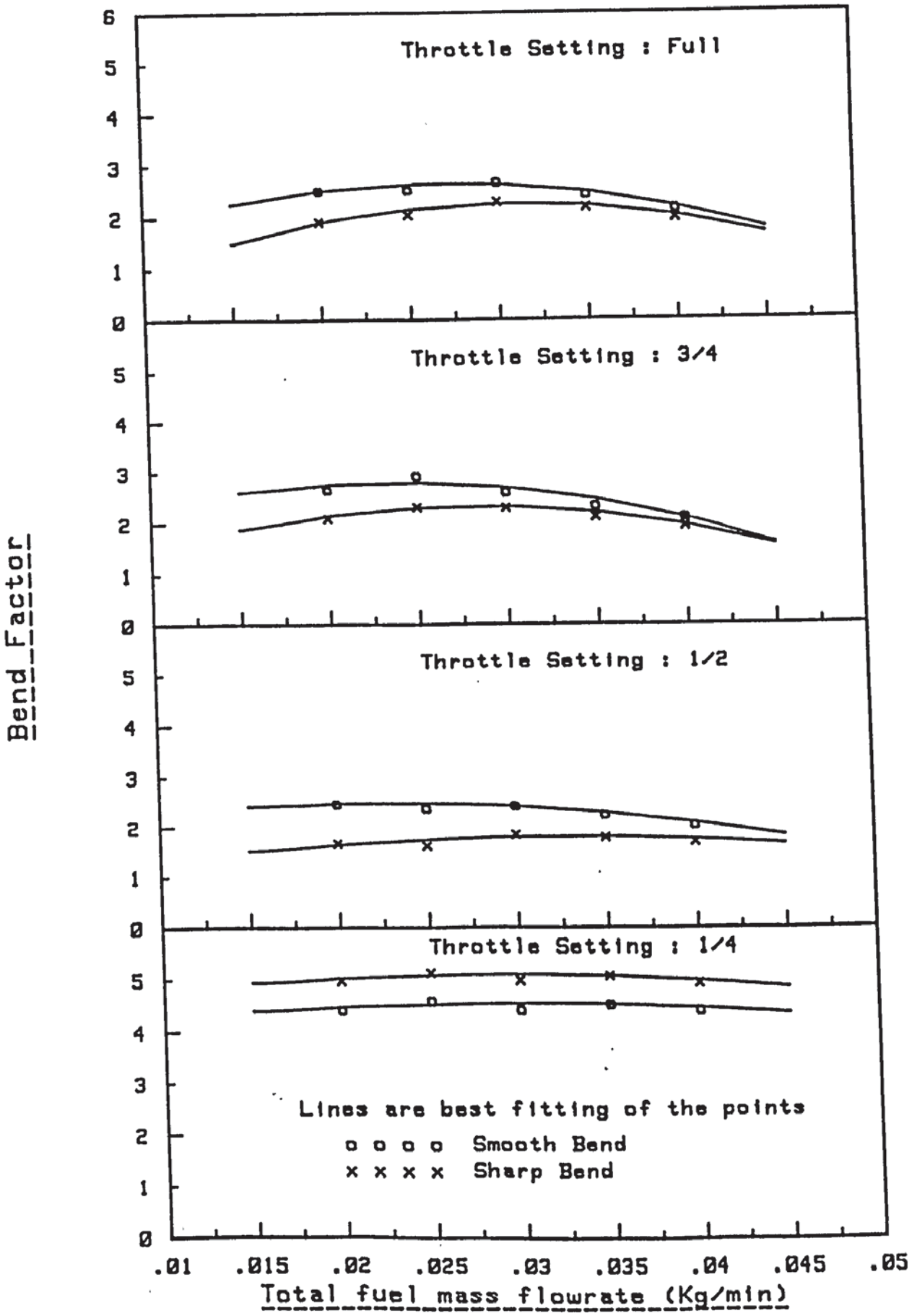

FIG. (5.29) Effect of Total Fuel Flowrate on The Bend Factor

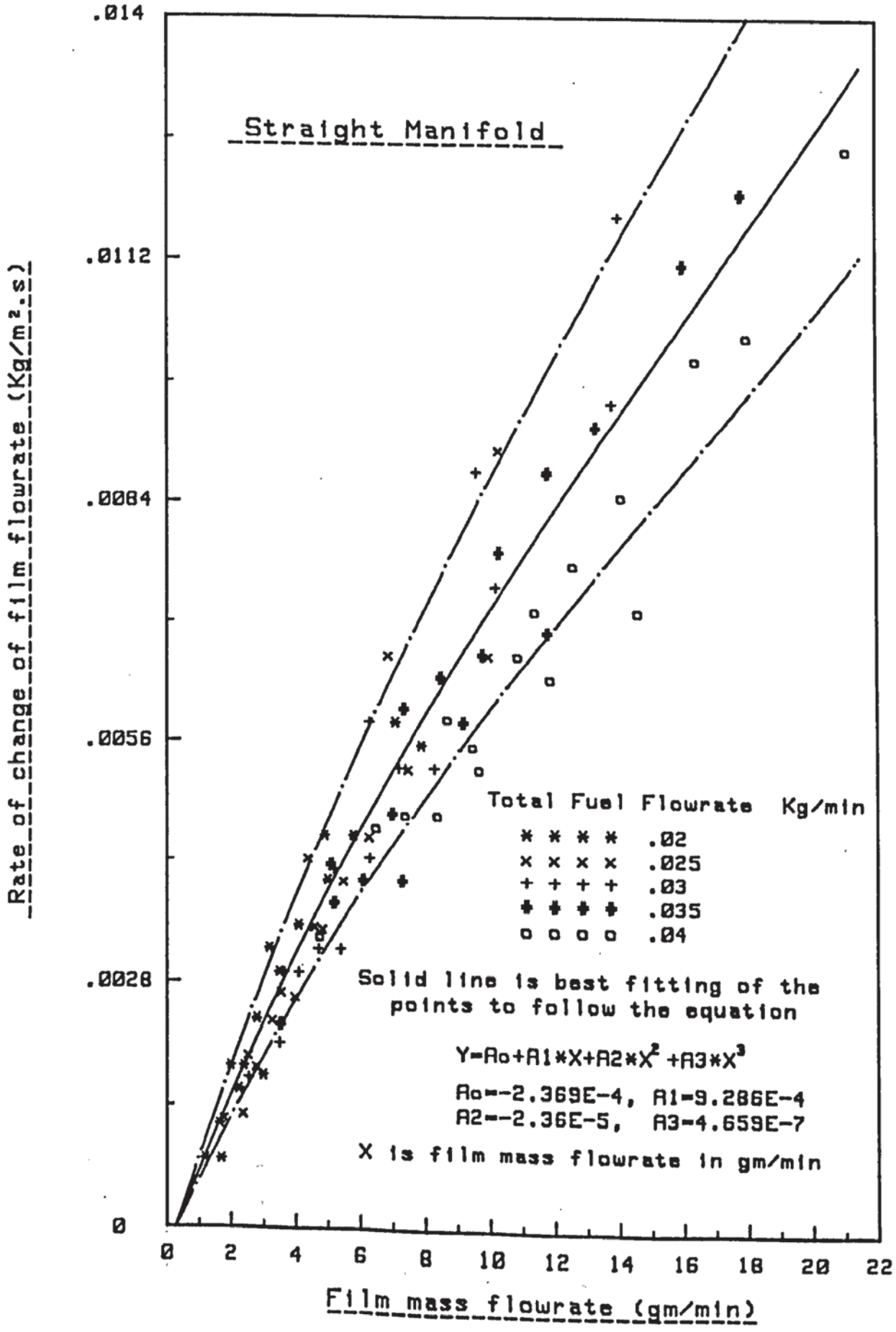

FIG. (5.30) Effect of Fuel Distribution on The Rate of Change of Film Flowrate

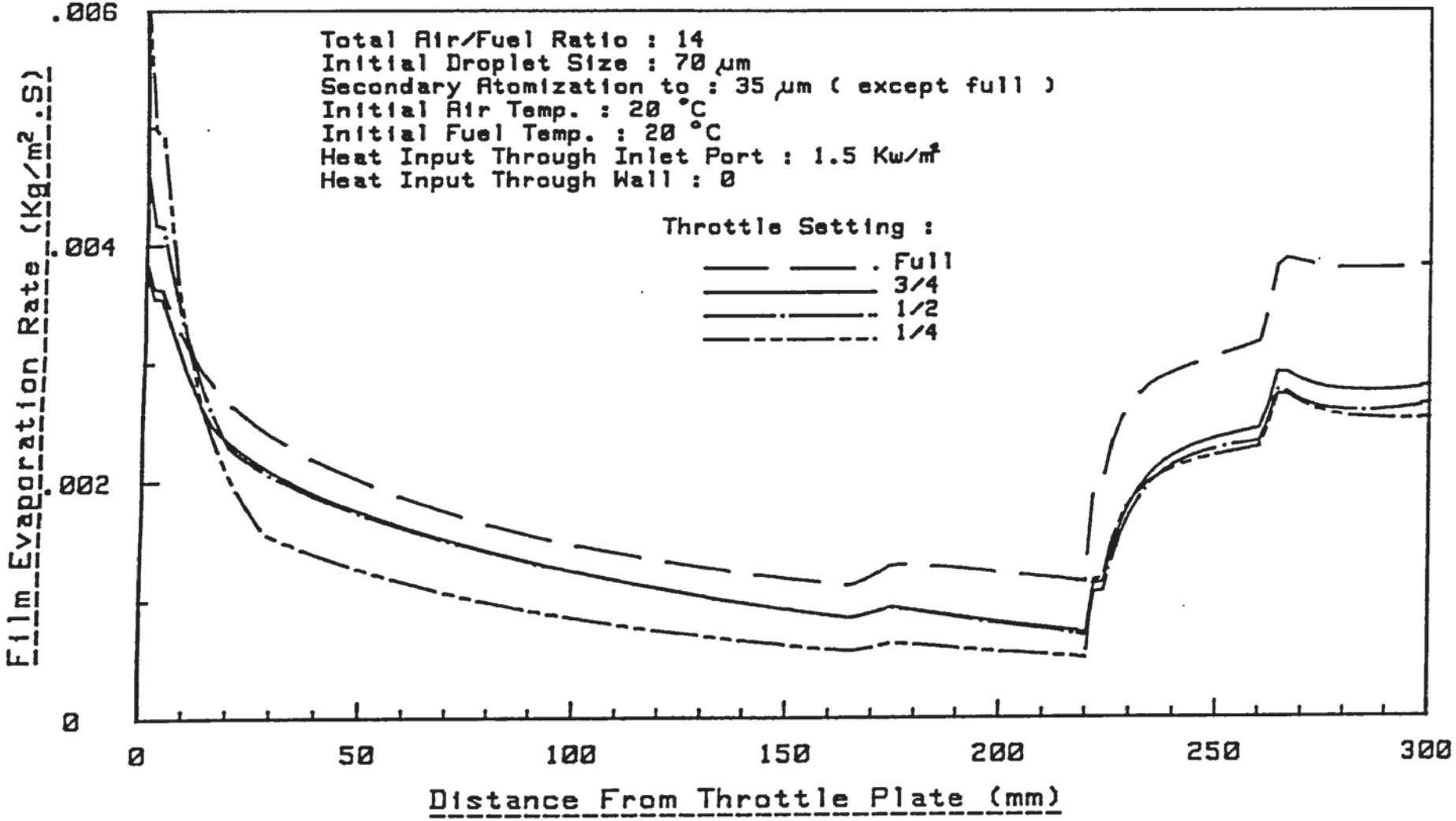

FIG.(5.31) Effect of Throttle Setting on Film Evaporation Rate

CHAPTER SIX

COMPUTER IMPLEMENTATION

6.1 Introduction

In chapters 3 & 4 and appendix (E), the mathematical models for mixture preparation and the engine cycle were established, together with the techniques used for solving the mathmatical equations. Accordingly, three main programs were structured and run on the HP 9845B Desk Top computer. The first program, INTSYS, deals with the calculations involved in the mixture preparation processes within the intake system (from the carburettor jet until a few millimeters downstream of the inlet valve). The second program, OPNSYS, is for the calculations, involved during the gas exchange period, while the third program, CLSYS, deals with the closed period of the cycle.

This chapter describes the implementation of the models in the form of structured computer programs from a global to a particular point of view. In the second section, the computer system around which the programs are structured are described. This is followed by a description of the interconnection of the programs comprising the complete computer implementation. The remaining sections provide the details of the individual programs and their major algorithms. To complete the documentation, program listings are provided in appendix (F).

6.2 Computer System Configuration

The computer system is the Hewlett-Packard 9845B Desk Top computer option 204. This incorporates 120K byte of system ROM and 187K byte of available Read/Write memory for program and data, and an enhanced language processor, which permits execution speeds of three times that of the standard model. The complete system schematic diagram is shown in Fig. 6.1. The external peripherals supported were an HP 9872A flat-bed plotter, a BENSON drum plotter and an HP 9885M flexible disc drive of .5m byte storage capacity. The language is an enhanced version of interpretive HP BASIC.

6.3 Programs Interconnection

In this section, the general global structure of the suite of modelling programs for the mixture preparation and cycle simulation is presented. The aim of which is to provide an appreciation of the programs interconnection in relation to their processes and the input/output requirements. The general structure of the programs interconnection is shown schematically in Fig. 6.2.

In addition to the three main programs, there is a group of minor programs which deal with further processing and the presentation of the fundamental data and simulation predictions. These are classed under the general heading of auxiliary programs. Data transfer between programs is either manually or via data files stored on the mass-storage units. Data is generated by one program is accessed by another further down the execution tree.

At the head of the flow diagram is the program INTSYS, by which the mixture preparation processes within the intake system are dealt with. Final predictions from INTSYS are required by the program OPNSYS further down the execution tree. The data is handled by this program in three separate groups, namely the intake system geometry, initial test conditions and the physical and chemical properties of the components comprising the mixture. At exit, the program generates data to be used by the program OPNSYS. An initial check on the validity of the predictions of this program is made by comparing the measured and the predicted liquid wall film mass flowrates.

Further down the execution tree is the program OPNSYS. The execution of this program starts at the release point (exhaust valve opening) with an initial estimate of the pressure and temperature of the cylinder contents at this point. In addition to the intake system flow conditions predicted by INTSYS, the input data for OPNSYS

comprise engine geometry and speed, combustion chamber wall temperatures and thermodynamic properties of charge components. The output from this program is the working mixture conditions at the trapped point (inlet valve closure).

The execution of the program CLSYS covers the period from the trapped point (inlet valve closure) until the release point (exhaust valve opening) passing through all of the closed period phases, viz. the compression, combustion and expansion strokes. The validity of the predictions of this program is checked by comparing the predicted pressure - crank angle diagrams and exhaust emissions (mainly the unburnt hydrocarbons) with those measured experimentally.

The three programs are interconnected through two loops. the first loop is between the programs OPNSYS and CLSYS, in which the initially assumed release pressure and temperature are checked. This is carried out by comparing the predicted release conditions by CLSYS with the assumed values, if these are within the prescribed accuracy, the next loop is performed. If not, however, new release conditions are assumed and the program OPNSYS is re-executed. This will continue as many cycles as required until the required accuracy is achieved.

The second loop is between the three programs in which the predicted pressure - crank angle diagram is validated. The pressure - crank angle predictions are compared with the measured values. If they are within the prescribed tolerance the predictions are accepted to be correct and the conclusions concerning mixture quality are drawn. If the accuracy is not satisfactory the next step will depend on whether the liquid film has been separated or not. If it has been separated the program INSYS will be executed using a new droplet size at the throttle plate (different degree of secondary atomisation). If the film has not been separated, the size of the droplets formed due to film disintegration at the inlet valve will be changed and the program OPNSYS is re-executed using the finally predicted release conditions (by the first loop). This method provides the means of predicting the process by which the film is disintegrated as well as the effect of air/fuel ratio on the size of the droplets entering the engine cylinder.

6.4 Program INTSYS

This program deals with the mixture preparation processes in the intake system. The non-linear differential set of equations described in sec. 3.6 are integrated using a fourth-order Runge-Kutta method. With this method, there is a danger of partial instability which can arise if an

insufficiently small step size is used. It is found that step size affects only some of the variables involved, namely, the velocity, diameter and temperature of the droplet and to a smaller extent the total vapour mass flowrate, as shown in Fig. 6.3. Computing throughout at the minimum step size would prove extremely time consuming, therefore, a variable step size was used. In the regions of the carburettor nozzle, throttle plate and inlet valve, where the probability of partial instability is very high, a step size of .1 mm was used. For the remaining regions it is found that a step size of 2 mm is acceptable.

The input data for this program are grouped as follows:

1. System geometry, defined by:-
   a. carburettor piston height (or area underneath the piston),
   b. carburettor cross-sectional area,
   c. throttle plate setting,
   d. manifold diameter, length and shape,
   e. inlet port length and inlet valve lift.

2. Flow conditions:

   a. air or total fuel flowrate,

   b. total air/fuel ratio,

   c. air velocity at the carburettor bridge,

   d. air and fuel temperatures,

   e. heat input through manifold wall,

   f. heat input through inlet port,

   g. wall film condition (separated or not),

   h. degree of secondary atomisation.

3. Chemical and physical properties of fuel and air:

   a. liquid fuel composition,

   b. fuel components molecular weight, boiling temperature, critical pressure and temperature, specific heat coefficients, latent heat of evaporation, Pitzer's acentric factor, carbon atoms, hydrogen atoms, critical volume, and the critical compressibility,

   c. air viscosity, thermal conductivity, specific heat, molecular weight, and the critical pressure and temperature.

When executed the program will only demand some of the above data, since the remaining are included in the program. The execution data are:

a. throttle setting (1/4, 1/2, 3/4 and 4/4), Thr$

b. manifold length, Mlenth$

c. manifold shape (s:straight, SM:smooth bend, SH: sharp bend), Mshape$

d. air mass flowrate, W_a

e. air/fuel mass ratio, Afr

f. initial air velocity, Avelocity

g. air and fuel temperatures, Atemp, Ftemp

h. is the film separated or not, FsepS

i. manifold pressure, Pman

j. heat input through manifold wall, Hl

k. secondary atomisation, Dsecondary

After performing some initial calculations (mainly the calculations of droplet size and number), the initial conditions at the carburettor nozzle (L = o) are arranged as follows:

1. For J = 1 to 16: where J is fuel component

Xx1 (O,J)	droplet evaporation rate, (kg/s)
Xx1 (1,J)	film evaporation rate, (kg/s)
Xx1 (2,J)	total evaporation rate, (kg/s)
Xx1 (3,J)	vapour pressure, (N/m^2)
Xx1 (4,J)	vapour density, (kg/m^3)

2.

Xx(0)	droplet velocity, (m/s)
Xx(1)	droplet diameter, (m)
Xx(2)	droplet temperature, (^{0}K)
Xx(3)	film temperature, (^{0}K)
Xx(4)	total pressure, (N/m^2)
Xx(5)	air pressure, (N/m^2)
Xx(6)	air density, (kg/m^3)
Xx(7)	air velocity, (m/s)
Xx(8)	air temperature, (^{0}K)

The flow chart of a step calculation is shown in Fig. 6.4. At the beginning of the step the program checks if the total length of the intake system has been exceeded. If so, program termination occurs after printing out the required data. Otherwise, an examination of the flow position is performed; if it is within the inlet port the heat input through the wall is redefined. The selection of step size according to flow position is carried out followed by examining the flow position relative to the throttle plate. If the flow is within the plate region the convergent/divergent nozzle flow calculations are performed to determine the conditions downstream the throttle plate. The initial wall film mass flowrate and the bend factor are then calculated together with the new droplet number considering the secondary atomisation.

If the flow is in the manifold and within a distance less than the prescibed wall film separation point, the subroutine "Film" is executed to calculate the deposition and entrainment rates. If the liquid film is not to be separated the execution of the subroutine "Film" will continue throughout. However, if the liquid film is separated the subroutine "Film" will not be executed beyond the separation point, at which the flow is updated due to film separation.

These are followed by executing the subroutine "Runge" by which the integration of the differential equations is performed. After performing the integration a print out of the required output is obtained. The print out is normally arranged to be at 2 mm intervals along the length, but it can be done at any required intervals.

The output data which are required by the next program OPNSYS are:

1. For each fuel component
   a. fuel mass in the vapour form,
   b. liquid fuel in the droplets,
   c. liquid fuel in the film.

2. Droplet size and temperature.

3. Manifold pressure and temperature.

The functions of the subroutines called in are as follows (referring to sec. 3.6 for notations):-

Runge

Runge 1, Runge 2, Runge 3, Runge 4

(Perform a step calculation in the Runge-Kutta method)

Functions 1: calculates

$$\frac{d}{d\ell}\left(\dot{m}_{de,i};\ \dot{m}_{fe,i};\ \dot{m}_{ve,i};\ P_{v,i},\ \rho_{v,i}\right) \text{ for } i = 1 \text{ to } 16$$

Functions 2: calculates

$$\frac{d}{d\ell}\left(V_d;\ d_d;\ T_d;\ T_f;\ P_t;\ P_a;\ \rho_a;\ V_a;\ T_a\right)$$

Initials: calculates

$$P_r;\ R_{ed};\ R_{em};\ \alpha_d;\ C_d;\ Sc_i;\ \beta_d;\ \beta_f;\ \rho_m;\ T_{awf};\ T_{awd};\ f.$$

Seg: calculates

$$\sum_{i=1}^{16}\left(P_{v,i};\ \dot{m}_{ve,i};\ \rho_{ve,i};\ \dot{m}_{d,i} * Cp_{Li};\ \dot{m}_{de,i};\ \dot{m}_{ve,i} * Cp_{vi};\right.$$

$$\left.\dot{m}_{f,i} * Cp_{f,i};\ \dot{m}_{fe,i};\ \dot{m}_{d,i};\ \dot{m}_{f,i}\right)$$

Segd: calculates

$$\sum_{i=1}^{16} \frac{d}{d\ell} (\dot{m}_{de,i};\ \dot{m}_{ve,i};\ \dot{m}_{fe,i};\ \dot{m}_{de,i} * L_i;\ \dot{m}_{fe,i} * L_i)$$

$$\sum_{i=1}^{16} \{ \frac{d\dot{m}_{de,i}}{d\ell} (V_a^2 - V_d^2) + \frac{d\dot{m}_{fe,i}}{d\ell} V_a^2 \}$$

$$\sum_{i=1}^{16} Cp_{v,i} \{ \frac{d\dot{m}_{de,i}}{d\ell} (T_d - T_a) + \frac{d\dot{m}_{fe,i}}{d\ell} (T_f - T_a) \}$$

Data 2: calculates

- new air properties,
- $\rho_{L,i}$; $P_{std,i}$; $P_{stf,i}$; D_i; $Cp_{L,i}$; $Cp_{v,i}$

Segma 1 calculates fuel component mole fraction in the
Segma 2 droplet and in the film respectively

Rowf: calculates the molar mean density of the liquid fuel.

Film: calculates the wall film deposition and entrainment rates.

Area: calculates the geometric area, Ac and dAc/dℓ.

Printout: perform the printing out of the data.

6.5 Program OPNSYS

This program deals with the calculations involved during the gas exchange process with special emphasis on the evaporation process during the intake stroke. Pressure, temperature and mass in the engine cylinder are calculated by solving the first law of thermodynamics for the open system together with the convergent/divergent nozzle equations. The model used to calculate fuel evaporation and the final droplet size and temperature has been discussed in sec. 3.7. The input data for this program is:

1. For each fuel component:

    a. fuel mass in the vapour form,
    b. mass of liquid fuel in the droplets,
    c. mass of liquid fuel in the film.

2. Droplet size and temperature at inlet valve.

3. Inlet manifold pressure and temperature.

4. Exhaust manifold pressure and temperature.

5. Cylinder pressure and temperature at the release point.

6. Engine geometry and speed.

7. Valves geometry and the valve lift - crank angle data (in the form of polynomial equations).

8. The wall temperature of the combustion chamber components.

9. Physical, chemical and thermodynamic data of the flow components.

The flow chart for this program is shown in Fig. 6.5. The execution starts at the release point with an initial estimation of the combustion products pressure and temperature. At the begining of each step the program executes the subroutine "Thermo" by which the changes in the cylinder pressure, temperature and mass due to piston movement, heat transfer and flow through valves are calculated. During the overlap period the exhaust process is given priority and the basic steps are broadly:

a. rotate crank shaft through a small angle,
b. calculate pressure and temperature changes according to adiabatic process,
c. calculate heat transferred,
d. re-calculate pressure and temperature according to constant volume process,

e. calculate mass increment passed through exhaust valve,

f. re-establish pressure and temperature,

g. calculate mass increment passed through inlet valve,

h. calculate final pressure and temperature.

At exit from the subroutine "Thermo" the program examines the possibility of "blow back" through the inlet valve which might occur during the initial stages of the intake stroke. This is dealt with by determining the total mass of the products passed through the inlet valve during this period. The intake of the fresh charge will not commence until this mass has been completely re-introduced to the cylinder. Evaporation rate calculations during the intake process are separately performed on the newly and the previously induced fuel as explained in sec. 3.7. The cylinder pressure and temperature are updated due to fuel evaporation after each evaporation process.

The outputs from this program are the mixture conditions at the trapped point (inlet valve closure). These include:

1. Cylinder pressure, temperature and mass.

2. Droplet size and temperature (SMD and SMT).

3. Total evaporation of each fuel component.

4. Exhaust residual mass fraction.

The program main subroutines are:

Evap: calculates the evaporation rate from the previously induced fuel segments.

Diam: calculates the final Sauter - mean diameter and temperature.

Mflow 1
Mflow 2 calculates the mass increment passed through the inlet and exhaust valves respectively.

Overlap: deals with the valve overlap period.

6.6 Program CLSYS

The outline of the program CLSYS is described by the flow charts shown in Figs 6.6 - 6.8. This program calculates cylinder pressure, temperture and mixture composition by solving the first law of thermodynamics together with the fuel evaporation model described in sec. 3.7. The simulated cycle phases are:

1. The compression stroke.

2. Ignition and initiation of two zones in the combustion chamber.

3. Flame propagation throughout the combustion space.

4. The expansion stroke.

The execution of this program starts at the trapped point (inlet valve closure). The state of the mixture at this point is the output data from the previous program OPNSYS. The general structure of the program is shown in Fig. 6.6. An initial examination on the present crank angle is carried out. If this is less than the nominal spark angle the program will proceed with the calculations of the compression stroke which comprise:

a. rotate crank shaft through a small angle,
b. calculate pressure and temperature changes according to adiabatic process,
c. calculate heat transferred,
d. re-calculate pressure and temperature according to constant volume process,
e. calculate evaporation rate from the liquid fuel,
f. update cylinder pressure and temperature,

g. calculate work done during the step and the final mixture internal energy,

h. examine the validity of the first law of thermodynamics. If this is within the prescribed accuracy go to (i). If not, however, apply the Newton-Raphson method to estimate the temperature at (b) and repeat the step until the required accuracy is achieved.

i. calculate the auto-ignition delay, and continue for the next crank step.

At the nominal spark angle the program executes the subroutine "Initiation", by which the ignition and initiation of two zones in the combustion chamber is performed. In the present model, ignition of the fuel is said to take place when a finite volume of the burnt mixture exceeds .001 times the total cylinder volume (swept volume plus clearance volume). At the end of the step an examination of the final burnt volume is made. If this is less than .001*Vtot the mixture is considered not to have been burnt and the compression process carries on for the next crank angle increment. The process continues for as many crank angle increments as necessary until the burnt volume $\geq$ .001 * Vtot when combustion is said to have commenced. The mathematical model of this process is described in appendix (E). The computer implementation of the process is carried out as shown in the flow chart of Fig. 6.7, which may be summarised as follows:

a. rotate crank shaft through a small angle,

b. calculate the pressure and temperature of the mixture according to adiabatic process,

c. calculate heat transferred,

d. re-calculate the pressure and temperature according to constant volume process,

e. calculate flame speed and radius,

f. calculate burnt volume and mass,

g. burn the available vapour fuel in the burnt volume and calculate product temperature, pressure and composition (it is assumed that combustion is initiated in the vapour fuel only),

h. expand the burnt zone until pressure equilibrium is attained,

i. calculate the final pressure, burnt zone temperature, unburnt zone temperature and burnt volume,

j. check if the final volume is $\geq .001 * V_{tot}$,

k. calculate evaporation rate and ignition delay.

At exit from the subroutine "Initiation" and if the combustion has commenced the main program continues executing the subroutine "Combustion" in the subsequent crank angle increments after examining the following control points:

1. The exhaust valve: if it is opened program termination occurs.

2. The burnt fraction: if the burnt fraction is $\geq .999$ * Vtot then combustion termination occurs and the expansion stroke starts. The program will execute the subroutine "Expansion" at the subsequent stages.

3. Knock: if the auto-ignition delay is consumed knock is said to have occurred and expansion with full products is commenced.

During combustion the chamber is sub-divided into two zones, the burnt and the unburnt zones which are defined by their own temperatures and composition with a common cylinder pressure. Within the combustion step a third zone is initiated as the flame front propogates through the unburnt mixture (this is called the combustion zone). Fuel droplets in this zone are assumed to be surrounded by the flame and their evaporation is a high temperature one (with combustion). Fig. 6.8 shows the flow chart of a combustion step which is carried out in the following stages:

a. rotate a crank shaft through a small angle,
b. for each zone,
   i. calculate pressure and temperature according to adiabatic process,
   ii. calculate heat transferred to the combustion chamber walls,

iii. re-calculate pressure and temperature according to constant volume process,

c. calculate flame speed and radius,

d. calculate the new volume of the burnt zone,

e. calculate the volume and mass of the combustion zone,

f. calculate the air, vapour fuel, residual masses and the number of fuel drops in the combustion zone,

g. calculate flame quenching to determine the amount of fuel (vapour and droplets), air and residuals trapped in the quench zone. The trapped fuel is considered to form part of the unburnt hydrocarbons,

h. calculate the evaporation from the droplets in the combustion zone. The remaining liquid in the drops (incomplete evaporation) will form the second source of the unburnt hydrocarbons,

i. burn the available vapour fuel and calculate the combustion zone pressure and temperature,

j. expand the combustion zone into the burnt zone until pressure in both zones is equilibrated, then mix the products in both zone to determine the new burnt zone temperature (now the chamber is divided into two zones only with their own pressures and temperatures),

k. perform pressure equilibrium between the burnt and unburnt zones and find the final temperatures, cylinder pressure and burnt volume,

L. if the final burnt volume is $\geq$ .999 * Vtot, combustion termination occurs.

At exit from the subroutine "Combustion" and if the combustion stroke has not been terminated, the main program executes the subroutine "Evaporation" to calculate the evaporation rate from the fuel droplets in the unburnt zone at mean step pressure and temperature. This is followed by the execution of the subroutine "Ignition delay" to calculate the auto-ignition delay.

The computer implementation of the expansion stroke is the same as that for the compression stroke, but the dissociation of the combustion products are calculated during each phase in the step.

The program CLSYS contains thirty subroutines and subprograms, their functions are indicated by their names. The following, however are the major subroutines:

Flame : calculates the burnt volume and the surface areas surrounding the burnt and unburnt volumes. The inputs of this subroutine are the flame radius, piston position, cylinder diameter and the spark plug position.

Diss: calculates the partial equilibrium of combustion products. The inputs are the product temperature, burnt zone volume, number of moles of air and the equivalence ratio.

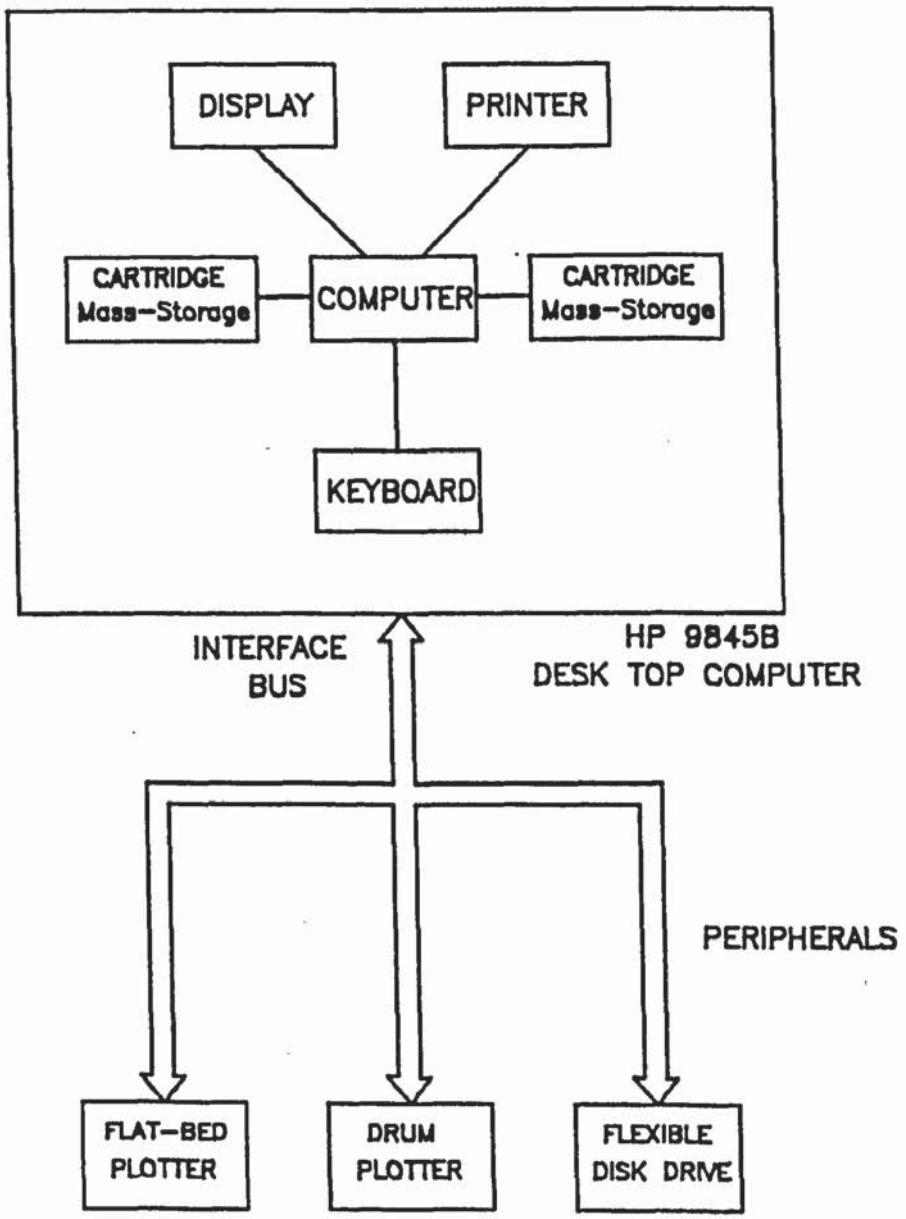

FIG. (6.1) Computer System Configuration

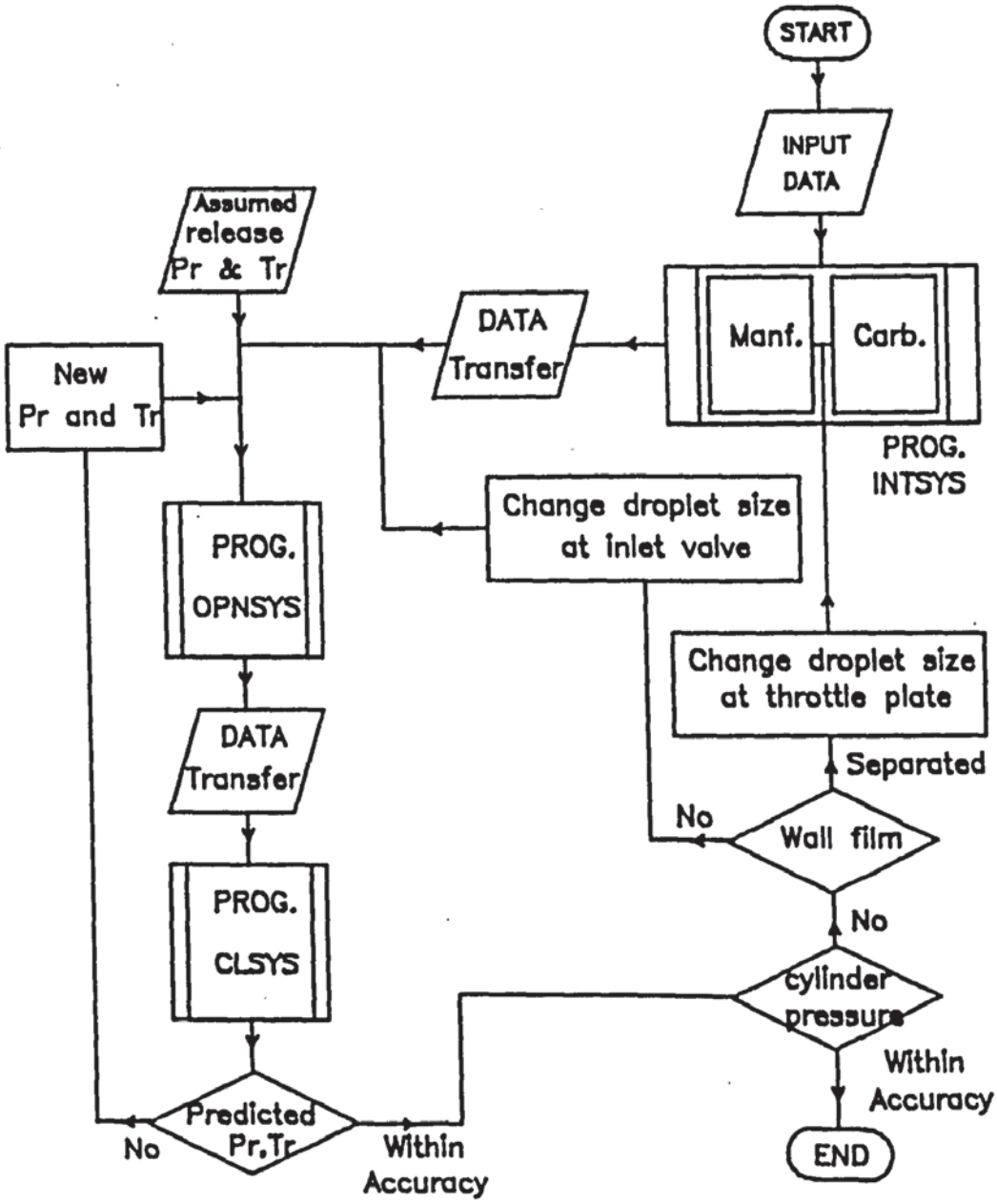

FIG. (6.2) Programs Interconnection

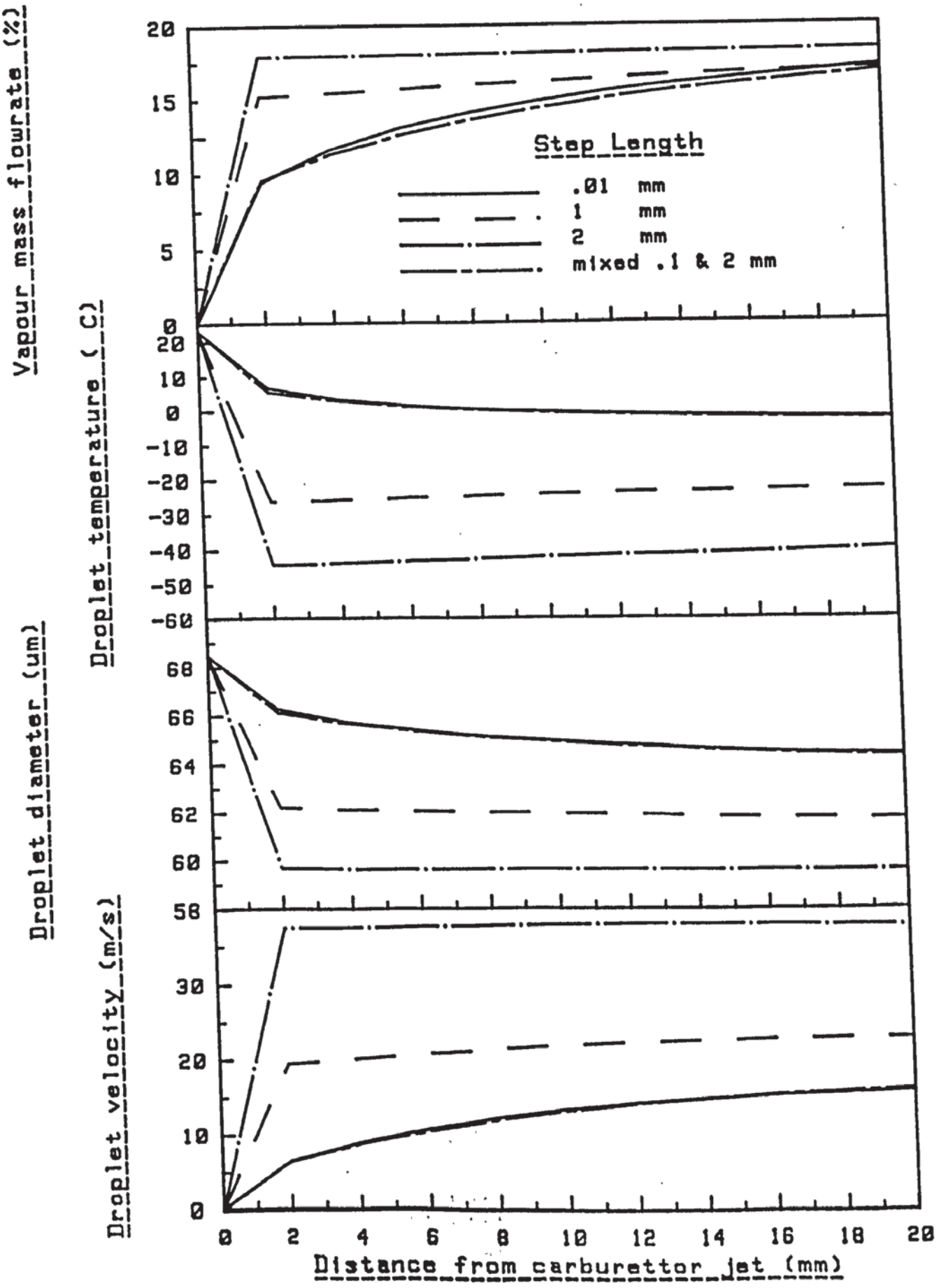

FIG. (6.3) Effect of Integration Step Length on Some of the Flow Parameters

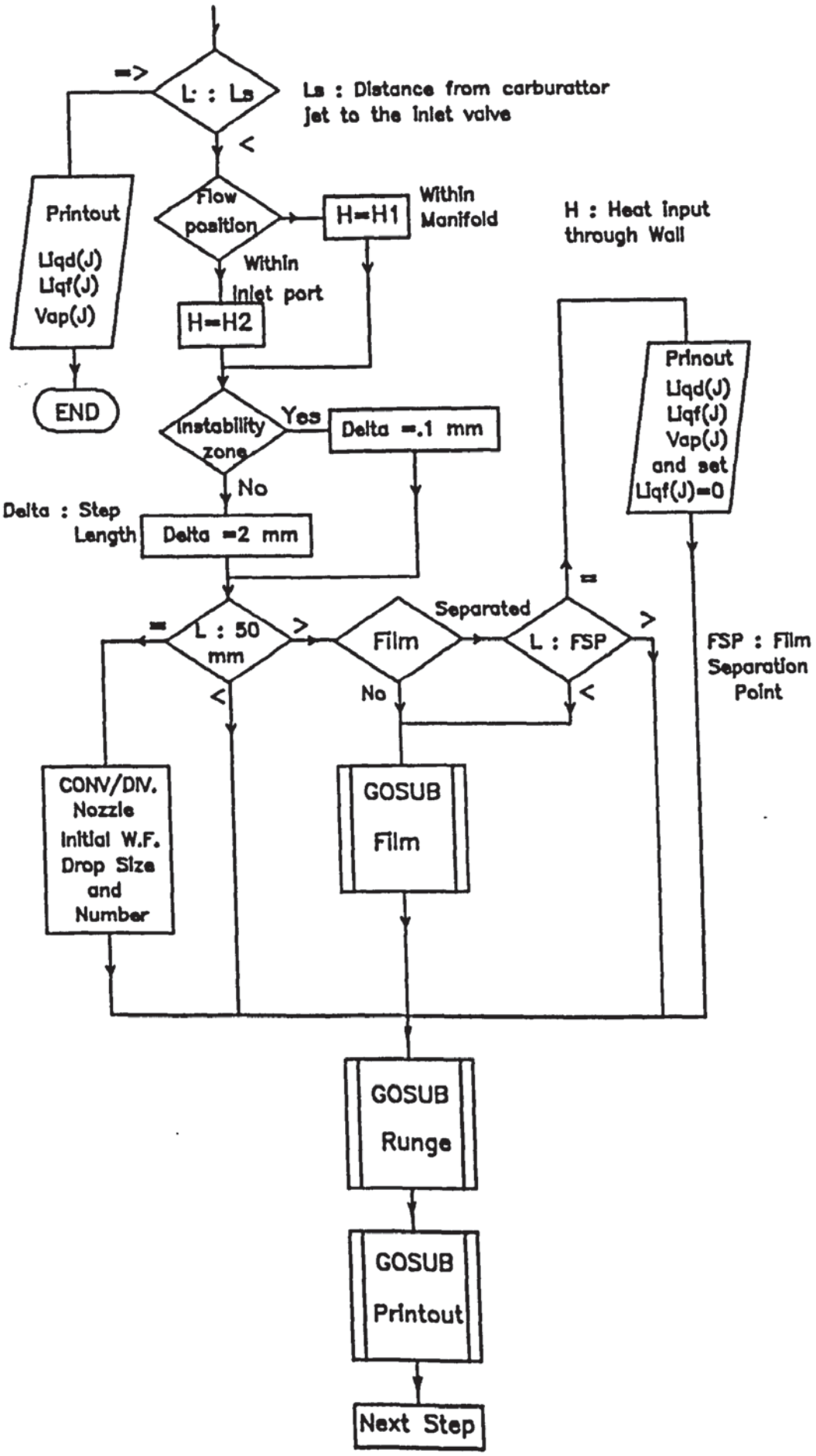

FIG. (6.4) A Step Calculation in the Program INTSYS

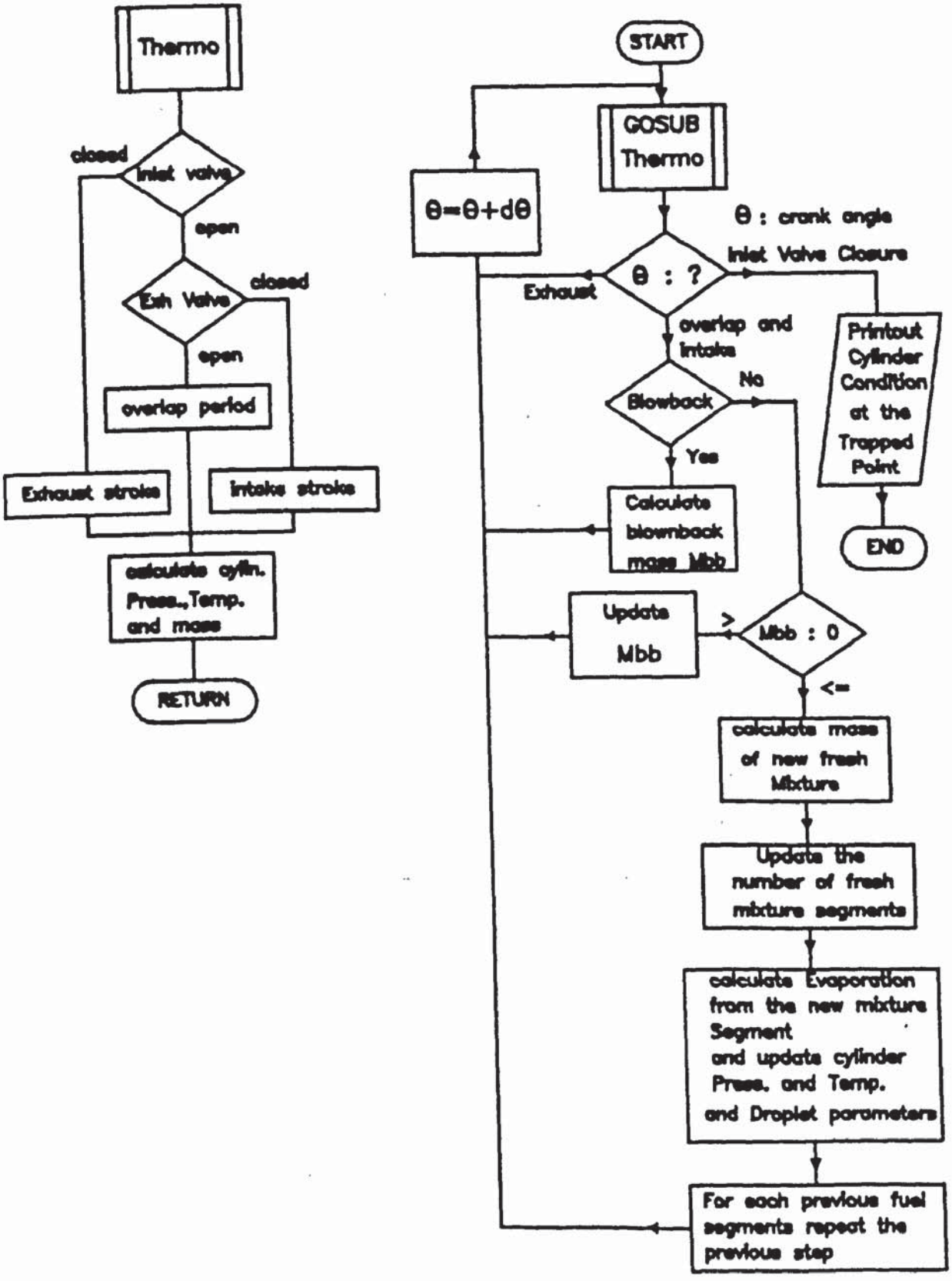

FIG. (6.5) Flow Chart of the Program OPNSYS

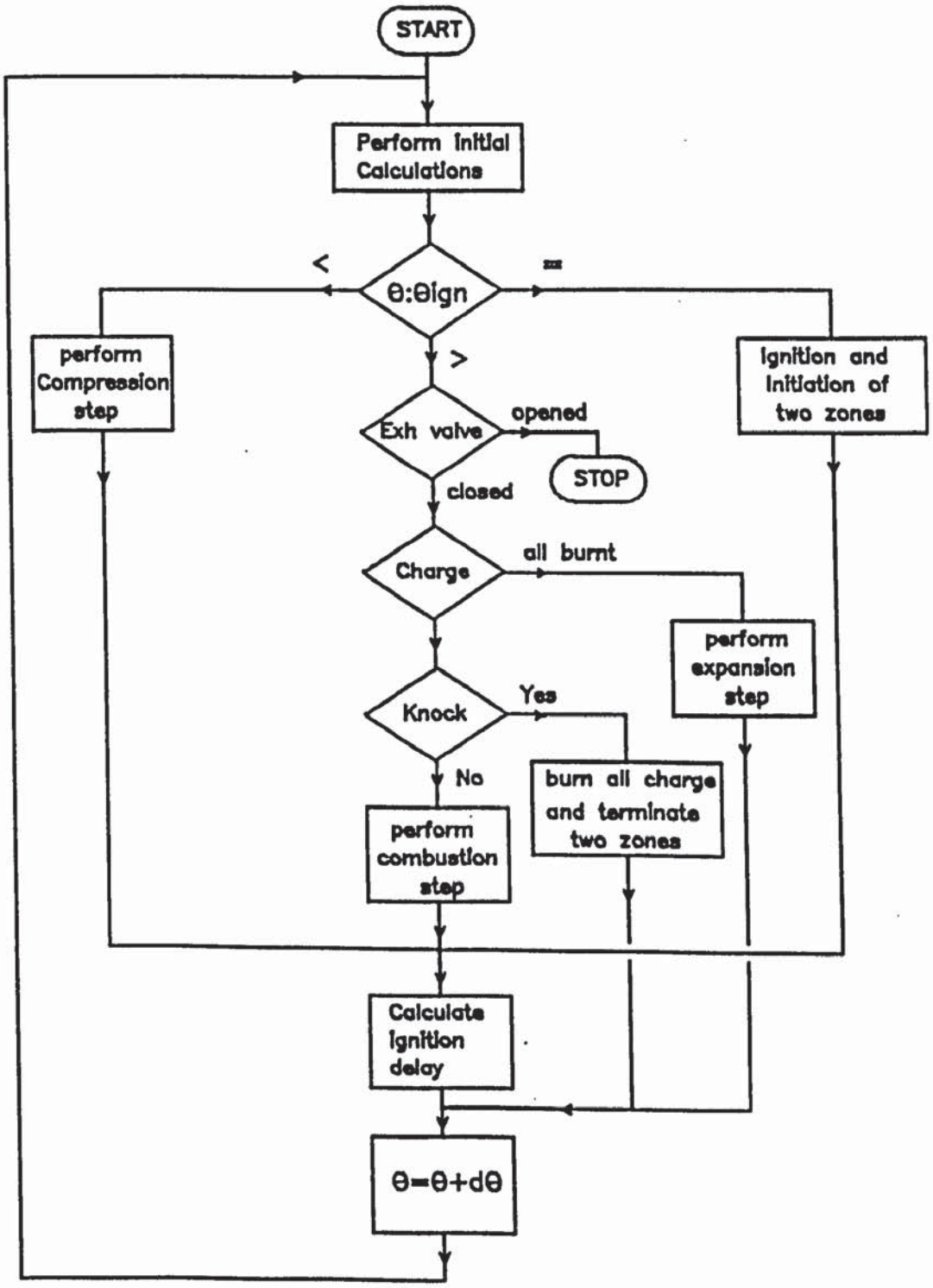

FIG. (6.6) Flow Chart of the Program CLSYS

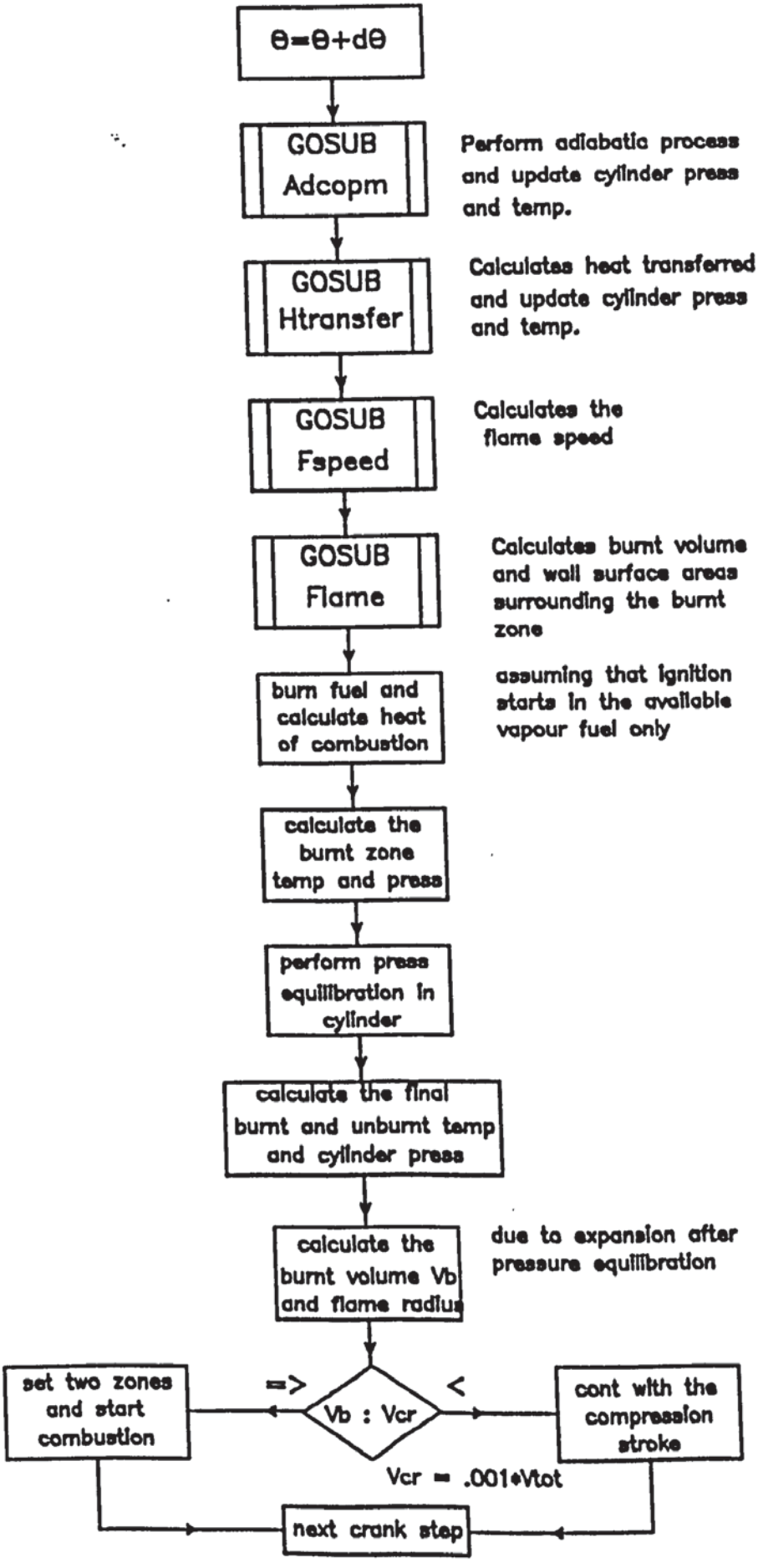

FIG. (6.7) Ignition and Initiation of Combustion

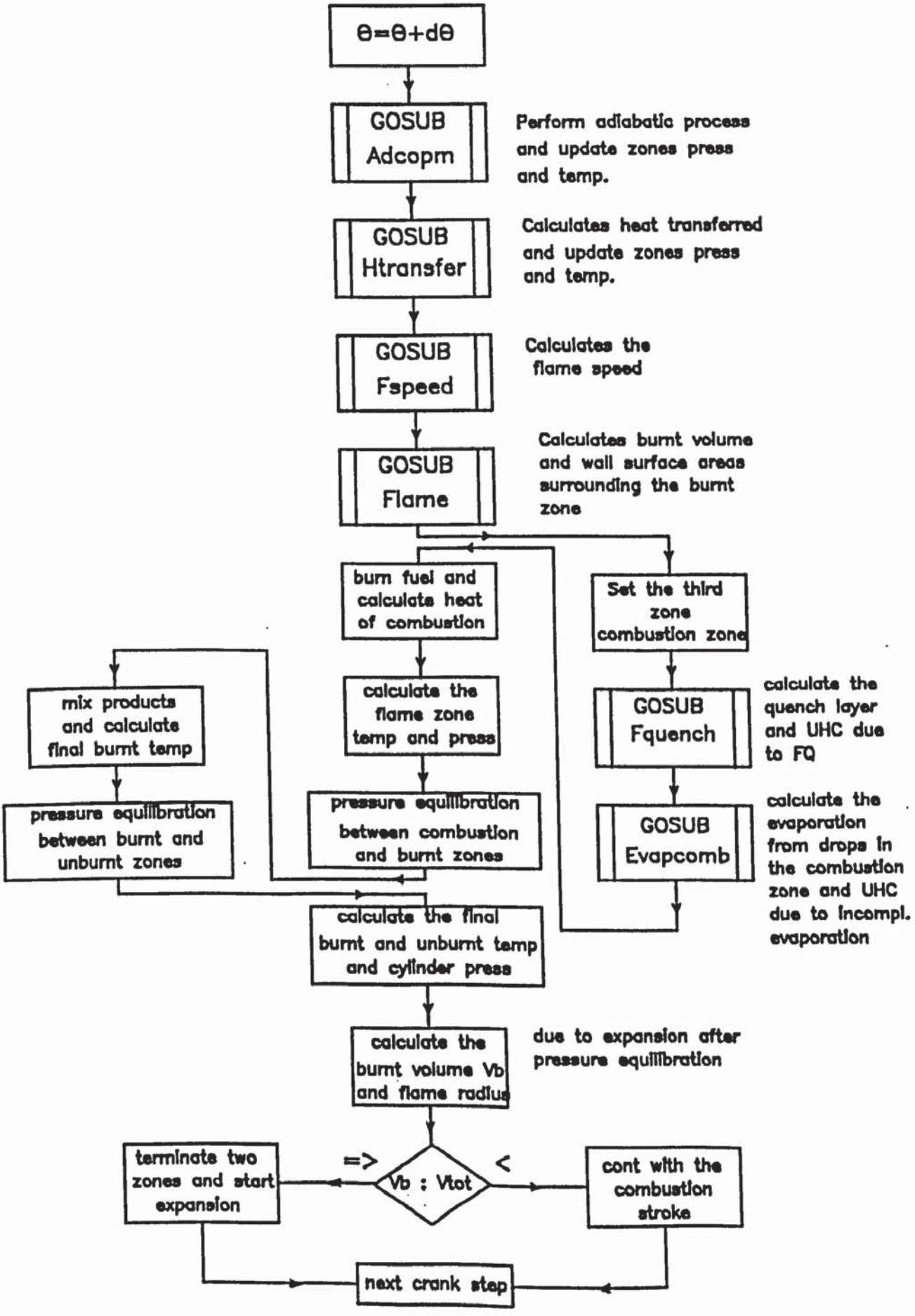

FIG. (6.8) Flow Chart of A Combustion Step

CHAPTER SEVEN

ANALYSIS OF PREDICTED RESULTS

7.1 Introduction

Before performing any parametric study using the computer programs developed during the present research, it was considered desirable to test the accuracy of both the suggested and adopted models so that, if any large scale discrepancies occur between the computed and experimental results, these are well noted and the limitations of the models are fully realised. The choice of parameters to be included in the comparison depends on many factors, among these are the availability of the appropriate experimental equipment and the possibility of the measurement of the particular parameter.

The accuracy of the models has been determined by comparing the predicted and measured values of:

(i) liquid wall film flowrate,

(ii) pressure-crank angle diagrams,

(iii) exhaust emissions, in particular, carbon monoxide and unburnt hydrocarbons.

Additionally, the accuracy of numerous subroutines which form parts of the models have been already tested by other researchers who developed the methods for the prediction of such factors as flame factor, heat transfer coefficient and many others, and chose appropriate correlations to ensure good agreement between the measured and predicted results.

Because no close experimental measurement could be made of the spectrum of fuel droplets induced into the engine cylinder it was necessary to establish an implicit correlation, using measured pressure - crank angle diagrams and exhaust emissions to establish the appropriate SMD of fuel droplets, as described in Chapter 6 (sec. 6.3).

The parametric studies are confined to mixture preparation and the effect of the prepared mixture on engine performance and emissions since numerous conventional parametric studies of the engine cycle have been reported in the literature[64-71]. The present parametric studies have been performed with a particular objective, that is, to gain clearer ideas on the best method of solving the problems associated with the liquid wall film.

7.2 Program Testing

There is no experimental data on engine performance during the gas exchange period either from previous researchers or the present experiments. The programs to be tested in this section are,therefore, the program INTSYS, which deals with the mixture preprration processes in the intake system, and the program CLSYS, which deals with the calculations involved during the closed period of the cycle. However, the three programs are linked together such that the output of one program is used as input for the next in an iterative closed cycle which permits the implicit testing of the program OPNSYS as part of the sequence.

7.2.1 Liquid Wall Film Flowrate

The only output from the program INTSYS to be considered is the liquid wall film mass flowrate. However, the predicted overall evaporation in the intake system is in good agreement with that measured by Collins[29] and Pao[30] in running engines. The total evaporation predicted at 1/2 throttle setting and an engine speed of 1500 rpm ranged from 45% up to 70% depending on the size of the droplet in the mixture and the heat input through manifold wall, while the reported measured overall proportions are 69% at 1/2 throttle setting[29] and 70% at stabilised engine operation, after warm-up[30].

Figs. 7.1 - 7.4 show comparisons between the predicted and measured wall film mass flowrates for a straight pipe manifold at different total air/fuel mass ratios, throttle plate settings and manifold lengths. For all conditions tested the agreement between the computed and measured values is good, which suggests that the empirical equations derived during the present research are reliable. However, for both rich mixtures (A/F $<$ 8:1) and lean mixtures (A/F $>$ 14:1) the computed wall film flowrates are not identical to those measured, especially for the 200 mm manifold. This is believed to be due to the difficulties of measuring the very low wall film flowrate at the end of the long manifold at these operating conditions.

The degree of secondary atomization at the throttle plate used during the prediction of wall film flowrates in Figs. 7.1 - 7.4, was based on data reported in refs. (35) and (36) which indicate that for a constant engine speed secondary atomization is related only to throttle plate setting and the consequent manifold depression. Droplet size at the throttle plate was, therefore, varied from 30 μm at 1/4 throttle setting (manifold depression of 45 mm Hg) to 40 μm at 3/4 throttle setting (manifold depression of 30 mm Hg) with no secondary atomization at full throttle opening (Droplet size = 65 μm).

Since there is no effect of the droplet size on the predicted wall film quantity in a straight pipe manifold (this view will be explained later in the parametric study), the adopted degrees of secondary atomization did not affect the predictions in Figs. 7.1 - 7.4. Furthermore, the effect of air/fuel ratio on the size of the droplet was not identified. However, when the calculations proceeded to predict wall film flowrate in the manifold with 90^0 smooth bend, it is found that air/fuel ratio has an appreciated effect on the degree of secondary atomization at the same manifold depression. Although the effect of air/fuel ratio on both the initial quantity of the liquid fuel in the wall film and the concentration of the droplets in the mixture, and hence on the rates of droplet deposition and entrainment was considered during the derivation of the empirical equations (in fact it is the only major variable in addition to the throttle plate setting), it was not possible to predict accurately the measured wall film in the smooth bend manifold without altering droplet size.

The observed good agreement between the predicted and measured wall film quantity in the manifold with 90^0 smooth bend (Fig. 7.5) is, therefore, due to the adjustment of the droplet size at the throttle plate. The droplet sizes required to predict the measured wall film flowrate ranged from 25 μm at air/fuel ratio of 14:1 to 40 μm at air/fuel ratio of 6:1. It was expected that the effect of air/fuel ratio on droplet size would be higher at the 1/4 throttle

setting, but the same range of droplet sizes was used to predict film flowrates at this throttle setting. This is believed to be due to the inclusion of the effect of throttle plate setting in the bend factor.

Although the predicted droplet sizes are still within the range measured by Finlay et al.[35], but the observed effect of air/fuel ratio on droplet size is relatively high compared with that calculated using Nukiyama and Tansawa equation[78] (eqn. (3.1)). Using this equation the Sauter mean diameter would vary by approximately 3.5 μm by changing the total air/fuel ratio from 14:1 to 6:1. The difference might be due to that the equation of Nukiyama and Tansawa has been derived using data obtained from steady flow tests, while the flow in the intake system is pulsating and highly turbulent. The latter flow characteristics enhance droplets collision which is expected to be higher at lower air/fuel ratios due to the increase in droplets concentration in the mixture. The effect of air/fuel ratio on droplet size may also be attributed to the higher droplet evaporation rate at higher air/fuel ratios arising from the lower vapour concentration in the mixture.

Finally, air and fuel initial temperatures, initial air velocity and manifold depression which were used as input data in the preceding calculations are those measured experimentally during wall film measurements.

7.2.2 Pressure - Crank Angle Diagrams

In order to reduce computing time the comparison between the measured and computed pressure - crank angle diagrams is carried out using data obtained from tests on the 150 mm straight pipe manifold when the wall film is separated. The cases where the wall film is not separated are considered later in the parametric study. Furthermore, it is found, even if the wall film is separated, that at low air/fuel ratios the required droplet size to give the same measured pressure - crank angle diagram is high (much higher than the local droplet size at the throttle plate) which was attributed to the possibility of wall film re-generation in the inlet port. These cases have been treated as though the wall film is not separated. Finally, bends have been considered in all cases by treating the inlet port as a convergent 90^0 smooth bend.

The results of the comparison are shown in Figs. 7.6 - 7.15 for different air/fuel ratios and throttle plate settings. In general, release pressure and temperature were found to be only functions of throttle setting. Figs. 7.6 - 7.11 show the predicted pressures at 1/2 throttle setting for different air/fuel ratios. For each air/fuel ratio three predicted pressure - crank angle diagrams are plotted to show the effect of droplet size on cylinder pressure. The information given in each figure is that corresponding to the condition which gave the best predicted pressure.

The accuracy of prediction was considered in regard with both the peak pressure and the crank angle at which the peak occurred.

The effect of droplet size on predicted pressure is very clear. The larger surface to volume ratio of small drops must result in an increased availabiliy of fuel vapour for combustion. Good agreement is obtained over the entire air/fuel range tested except for the first two air/fuel ratios. In Fig. 7.6 and due to the lean mixture (cylinder A/F = 16.725:1), it is to be expected that cycle to cycle variation would be high so that it is difficult to predict cylinder pressure accurately. Furthermore, for both these air/fuel ratios (Figs. 7.6 and 7.7) it is concluded that droplet sizes should be slightly reduced to give higher pressures.

The predicted SMD of trapped droplets varied considerably with the total air/fuel ratio of the mixture from 17.32 μm at A/F = 14.5:1 to 94.27 μm at A/F = 7.02:1, consequently the trapped fuel present as vapour varied from 77.33% to 58.84%. Considering the ealier observed effect of air/fuel ratio on the predicted droplet sizes for the smooth bend, it is clear that the relatively large droplets predicted as necessary to give the measured pressures is not due to the effect of air/fuel ratio alone. It is believed that this is due to the re-generation of the liquid wall film in the inlet port due to the high

rate of droplet impaction with the bend and on the valve.

Liquid wall film re-generation down stream of the separation point may occur at any air/fuel ratio. However, it was not considered to happen unless the required secondary atomization to give the measured pressure exceeded the maximum predicted size for wall film deposition in the smooth bend, that is, 40 μm. Beyond this diameter, the secondary atomization is not altered; instead a tertiary atomization at the inlet valve is considered. The results indicate that the tertiary atomization occurs in relatively large droplets and this is believed to be due to the weak aerodynamic stripping action of the air/vapour core flow on the liquid wall film.

In Figs. 7.12 and 7.13 a comparison is made between the measured and computed pressures at 3/4 throttle setting for two different air/fuel ratios. The predicted trapped droplet sizes were 64.46 μm at A/F = 8.14:1 and 40 μm at A/F = 9.447:1. For the same total air/fuel ratio range, Figs. 7.14 and 7.15 show a comparison at 1/4 throttle setting. The predicted droplet sizes were 78.49 μm at A/F = 7.8:1 and 57.79 μm at A/F = 9.16:1. Comparing these sizes with those predicted at 1/2 throttle setting for the same range of air/fuel ratios (63.36 μm at A/F = 7.84:1 and 37.88 μm at 9.24:1) indicates that the effect of throttle setting on droplet size is negligible, except for 1/4 throttle setting. The large increase in the effect of air/fuel ratio at 1/4 throttle setting indicates that the

liquid wall film is entrained in relatively large droplets at this throttle setting. This can be considered as further support for the suggested mechanism of wall film entrainment discussed in chapter 5, and it is in good agreement with the measured film flowrates down stream bends.

7.2.3 Exhaust Emissions

Before comparing the measured and predicted exhaust emissions, it is considered desirable to show the variation of some combustion parameters, including the emitted species of interest, throughout the engine cycle. As shown in Figs. 7.16 and 7.17 the formation of exhaust emissions varies considerably with crank angle. The effect of droplet size on these parameters is also shown, and indicates that the larger the droplet size the higher the emitted unburnt hydrocarbons and combustion time and the lower the CO concentration, burnt zone temperature and flame speed.

Fig. 7.18 shows a comparison between the measured and predicted exhaust emissions obtained from the cycles in which the predicted pressures show best agreement with the measured values. The variation in the CO and CO_2 concentration is given at three points in the cycle:

a) at peak cylinder temperature,

b) at end of combustion,

c) minimum values for CO and maximum values for CO_2.

Unburnt hydrocarbons concentration is given only at the end of combustion where there is no further generation of these emissions.

The observed considerable discrepancy between predicted and measured values of CO and CO_2 is believed to be due to one or both of the following reasons:

a) the assumed kinetic model for CO formation, which implies that the rate of formation of CO is faster than the rate of decomposition. However, the non-equilibrium behaviour of CO is widely accepted so that the observed deviation might be due to the use of inadequate rate constants in the model.

b) the solution procedure for the CO model used in the computer program might be inadequate.

It is anticipated that the predicted CO and CO_2 concentrations do not strongly influence the remaining cycle parameters due to the small amounts of these species in the mixture.

The predicted unburnt hydrocarbons, on the other hand, show good agreement with the measured values in spite of the difficulties involved in the measurements due to cycle to cycle variation. The results support the unburnt hydrocarbons formation model which implies that the formation of these species is due to the flame quenching mechanism and the liquid fuel droplets failed to achieve complete evaporation in the flame zone.

7.3 Parametric Studies

Having established the reliability of the models used to study the mixture preparation and combustion processes, it was decided to perform a number of parametric studies to study the effect of various flow parameters on the preparation of the combustible mixture. The study was mainly performed to identify the best methods which might be used to solve the problems associated with the presence of the liquid wall film.

7.3.1 Mixture Preparation in the Intake System

The parameters involved in this study are:

a) the degree of secondary atomization (at the throttle plate),

b) heat input through manifold wall,

c) air and fuel initial temperatures,

d) total air/fuel ratio.

The study has been carried out under constant conditions of engine speed (1500 rpm), throttle setting (1/2), and heat input through inlet port wall (1.5 Kw/m^2) without separating the liquid wall film. The results are shown in Figs. 7.19 - 7.32.

The degree of secondary atomization at the throttle plate has a considerable effect on fuel evaporation and transportation in the intake system down stream the throttle plate. It is well known that increasing the surface area of the liquid fuel, by decreasing droplet size, enhances the rate of fuel evaporation: this is clearly demonstrated in Fig. 7.21. Fuel evaporation is also enhanced when the flow reaches the inlet port due to the relatively high rate of heat transfer to the liquid wall film. Evaporation rate within the inlet port, however, depends on the initial size of the droplet, which affects the composition of the liquid wall film; this will be discussed later.

The effect of the intake system geometry on the velocities of the air and droplets is shown in Fig. 7.20. It can be seen that at the throttle plate, since the flow area is large compared to that at the carburettor bridge and

inlet valve, the change in the air velocity is not high. The response of the droplets to the changes in the air velocity depends on the size of the droplet however, and the droplets of all sizes are settling down quickly a few millimeters down stream of the inlet valve.

The variation of air and fuel temperatures in the intake system is shown in Fig. 7.21. The sudden fall in fuel temperature at the carburettor jet is due to the high rate of evaporation from the light fractions of the fuel. The rise in droplet temperature at the throttle plate, especially at 15 μm, is due to the conversion of kinetic to thermal energy. This effect has been reduced due to droplet evaporation which reduces droplet temperature. The sudden increase in liquid wall film temperature in the inlet port is due to the effect of heat transfer through the inlet port wall, which is later reduced due to the decrease in the surface area from which the heat is transferred.

Manifold wall heating is a commonly applied method to achieve higher rates of fuel evaporation. In the model it is assumed that the heat is applied uniformly through the wall. the amount has been chosen according to the mass flowrates of fuel and air found in a single cylinder engine running at a speed of 1500 rpm. Fig. 7.22 shows the variation of overall fuel evaporation at different rates of wall heating and indicates that 10% more evaporation can be achieved by adding 2 Kw/m^2 of heat.

Due to the use of a multicomponent fuel comprising components with a wide range of boiling temperatures, it is reasonable to expect that the composition of the remaining fuel varies considerably with location. Fig. 7.23 demonstrates this fact and also shows that the remaining liquid fuel is not uniformly distributed between the droplets and the wall film. At the throttle plate, where the wall film is assumed to start, the distribution of the fuel between the droplets and wall film depends on the initial quantity of the liquid film. Each fuel component will contribute to form the film in its own proportion of the remaining liquid fuel. The distribution is then altered due to droplets deposition and entrainment and due to evaporation. The resulting fuel distribution indicates that the liquid wall film contains more heavy fuel fractions than the droplets.

Fig. 7.23 also indicates that more than 18% of the fuel is vaporised in the carburettor and that this proportion is mainly composed of light fuel fractions.

Heat may be added to the mixture in three ways[42]. These are:

(i) heating the liquid fuel before entry to the carburettor,

(ii) heating the air before entry to the carburettor,

(iii) heating the manifold wall.

Fig. 7.24 shows the effect on the overall fuel evaporation of adding the same amount of heat through these three routes. The air and fuel initial temperatures have been varied from 20^0C to 25.3^0C and 58.12^0C respectively. Heat addition to the fuel resulted in higher evaporation rate within the carburettor with no noticeable effect on the overall evaporation at the end of the intake system. On the other hand, the rate of fuel evaporation responded slowly to the increase in air temperature due to the time required to transfer the heat from the air to the fuel. The most effective method of achieving higher evaporation is by adding the heat through the manifold wall.

The size of the droplet present in the flow has no effect on the quantity of the liquid wall film in a straight pipe manifold as shown in Fig. 7.25. The present work experimental results and the reported work on liquid wall film indicate that:

(i) the rate of droplet deposition depends on the concentration of the droplets in the mixture and on the velocity of the main stream,

(ii) the rate of droplet entrainment from the liquid film depends on the thickness of the wall film and on the velocity of the main stream.

Initially, changing droplet size will have no effect on the main stream velocity which suggests that this factor should be neglected. Droplet size, however, will affect the number of the droplets in the mixture and droplet velocity which, in turn, affects droplet concentration. In the straight part of the manifold under study, droplet velocity is not significantly affected by changing the size of the droplet (see Fig. 7.20). Additionally, the increase in the number of droplets, due to the decrease in droplet size, will not affect the overall mass of the fuel in the droplets, therefore, this, in turn, will not affect the mass transferred by the droplets to the wall film.

Finally, any increase in the rate of droplets deposition will increase the thickness of the liquid film which, in turn, enhances the rate of droplets entrainment from the film. The interaction of these factors tends to maintain the quantity of the liquid wall film in a straight pipe manifold, to be a function only of the distance from the point of film formation. This, in turn, is a function of total fuel in the system and throttle plate setting.

Within the inlet port, however, the effect of droplet size on the quantity of the liquid film is considerable on account of droplet momentum. The smaller the droplet size the higher the velocity and the lower the droplets concentration which, in turn, reduces the rate of droplet deposition. Due to the effect of the bend factor (explained

in chapter 5), the increase in the rate of droplet deposition will not strongly affect the rate of droplet entrainment, as it did in the straight pipe manifold.

Although droplet size does not affect liquid film quantity in a straight pipe it, nevertheless, affects the composition. The larger droplets carry more light fuel fractions to the wall film, and the subsequent droplet entrainment is from the heavier fuel fractions. This is shown in Fig. 7.26 where the effect of secondary atomization on wall film evaporation is shown. The larger the droplet the higher rate of wall film evaporation.

The above discussion may well be applied in analysing the effect of manifold wall heating on the quantity of the liquid fuel in the wall film. Increasing the heat input through manifold wall will increase wall film temperature (Fig. 7.29), hence wall film evaporation rate (Fig. 7.28), but will not affect wall film quantity at a specified distance. The fuel evaporated from the film being at the expense of the dropwise fuel flow, as shown in Fig. 7.30. The higher the heat input the higher fuel evaporation from the film which, in turn, reduces wall film thickness. Depending on the quantity of the remaining liquid fuel in the film, either droplet entrainment is reduced or droplet deposition is increased to keep the same wall film thickness at a specified distance which is determined by the throttle plate setting and total fuel in the system. In the inlet port, although the rate of heat input is

constant,1.5 Kw/m^2 , the different rates of heat input through manifold wall causes different liquid film temperatures which, in turn, produces different rates of film evaporation.

The final parameter to be studied was the effect of total air/fuel ratio on fuel evaporation in the intake system. As air/fuel ratio is reduced, liquid fuel in the system is increased which, in turn, produces a higher quantity of liquid wall film as shown in Fig. 7.31. Light fuel fractions evaporate more readily from the droplets, with their high heat transfer/mass transfer coefficients, than from the wall film in a non-heated manifold wall. Therefore, the overall evaporation is expected to be less as air/fuel ratio is reduced as shown in Fig. 7.32.

7.3.2 Mixture Preparation During the Gas Exchange Period

This period is very important to the mixture preparation process, since the fuel is introduced to the cylinder during the intake stroke. The state of the liquid wall film at the time it is introduced to the cylinder must strongly influence the nature and quality of the mist inside the cylinder. The parameters which have the most powerful effect on fuel evporation inside the cylinder are the degree of tertiary atomization achieved earlier at the inlet valve and the temperature of the liquid fuel droplets. The

following parameters are, therefore, included in this parametric study:

(a) the degree of tertiary atomization,

(b) the temperature of the droplets emerging from the valve throat,

(c) pressure and temperature of the cylinder at the release point (exhaust valve opening).

Fig. 7.33 shows a typical predicted variation of cylinder pressure, temperature and fuel vapour concentration during the gas exchange period. Three different values of SMD have been used to represent the droplets introduced to the cylinder, with a common initial droplet temperature. Fuel evaporation is initially enhanced due to the high temperature of the cylinder contents at the beginning of the intake stroke. It is clear that the degree of tertiary atomization has a powerful influence on fuel evaporation inside the cylinder.

The effect of the initial droplet temperature on fuel evaporation and on cylinder pressure and temperature during the open period is shown in Fig. 7.34, while that of the manner in which a range of release conditions affect these parameters is shown in Fig. 7.35. It is seen that different release conditions affect the exhaust process but have little effect on the conditions during the intake stroke and hence fuel evaporation.

Cylinder volume and conditions vary continuously as fuel droplets are introduced during the intake stroke so that droplet evaporation rate dependent upon these varying cylinder conditions and on the residence times of the droplets in the cylinder. At the trapped point (inlet valve closure), the droplets found in the cylinder will, therefore, have a wide range of different sizes and temperatures. Figs. 7.36 and 7.37 show the predicted droplet size - number distribution at the trapped point for different degrees of tertiary atomization and droplet temperatures. For the case of 30 μm tertiary atomization the increase in droplet temperature produces wider size - number distribution with higher evaporation rate at the trapped point. The wider size - number distribution will produce higher evaporation rate during the compression stroke.

Figs. 7.38 and 7.39 summarise the effect of droplet size on some of the fuel parameters at the trapped point. It is clear that droplets of small size and high temperature achieve better evaporation during the intake stroke.

Final conclusions on the effects of liquid wall film disintegration cannot be drawn unless analysing the effects on mixture preparation and combustion inside the cylinder and this is discussed in the following section.

7.3.3 Mixture Preparation and Combustion

The processes involved during the closed period of the cycle are strongly affected by the conditions at the trapped point. Therefore the data obtained from the previous study are used directly to investigate the effect of mixture preparation on the combustion process and related parameters.

Figs. 7.40 and 7.41 show a typical predicted variation of some fuel parameters in a motored engine after a sufficient warming up time. It can be seen that fuel evaporation continues during the compression stroke until a point is reached where the effect of cylinder pressure starts to retard evaporation. Droplet temperature is not strongly affected by the increase in cylinder temperature, however, and small droplets show higher response. This may be attributed to the high surface to mass ratio of small droplets which permits rapid droplet heating.

The effect of droplet size on cylinder pressure has been discussed earlier and it is shown again clearly in Figs. 7.42 - 7.44. Figs. 7.42 and 7.43 indicate that droplets with diameters 20 μm or less at entry to cylinder have no effect on cylinder pressure due to their complete evaporation either during compression or in the flame zone. The effect of droplet size on cylinder pressure is small for diameters less that 30 μm , however, a sharp

decrease in peak pressure is noticed for sizes greater than 40 μm . This effect increases as droplet temperature is reduced.

Fig. 7.45 shows that for 10 μm droplets the increase in droplet temperature resulted in lower peak pressure which has not been so for other droplet sizes (Figs. 7.46 and 7.47). This is believed to be due to that complete evaporation prior to ignition has occurred so that the increase in droplet temperature resulted in higher vapour temperature which reduced the volumetric efficiency of the engine.

A summary of the effect of droplet size on combustion parameters is shown in Figs. 7.48 and 7.49. Droplets with diameters less than 20 μm have no effect on any parameter except NO formation. The effects increase slowly until 30 μm then rise sharply for larger droplet sizes. The slight increase in ignition delay and the reduction of NO emissions at 20 μm indicates that droplets of this size do not evaporate completely prior to ignition, but complete the process only in the flame zone. Finally, CO predictions indicate that there is an optimum droplet size for lowest CO emissions.

7.4 Concluding Remarks

As mentioned earlier, the models of earlier workers adopted to describe the thermodynamic aspects of the cycle have been tested and good agreement between the measured and predicted results has been reported. Program testings have, therefore, been carried out mainly to determine the quality of the mixture which has been burnt to give the measured pressures. The predicted droplet sizes for the entire range of air/fuel ratio tested are in good agreement with those measured in the inlet manifold of a carburetted engine and reported in the literature. Furthermore, the good agreement observed between the computed and measured unburnt hydrocarbons suggests that both the thermodynamic and mixture preparation models are working satisfactorily.

The size of the droplets produced by the tertiary atomization of the fuel at the inlet valve is very important in determing mixture quality in the cylinder. Smaller sized droplets produce higher cylinder pressures, higher cylinder temperatures and higher NO emissions, but they also lead to lower emissions of CO and unburnt hydrocarbons. A compromise should be made which suggests that heating the liquid film prior to entry to the cylinder and atomizing it into droplets of sizes below 35 μm provides the best overall results.

Finally, even if the thermodynamic models are not accurate quantitatively they, nevertheless, provided a complete qualitative study.

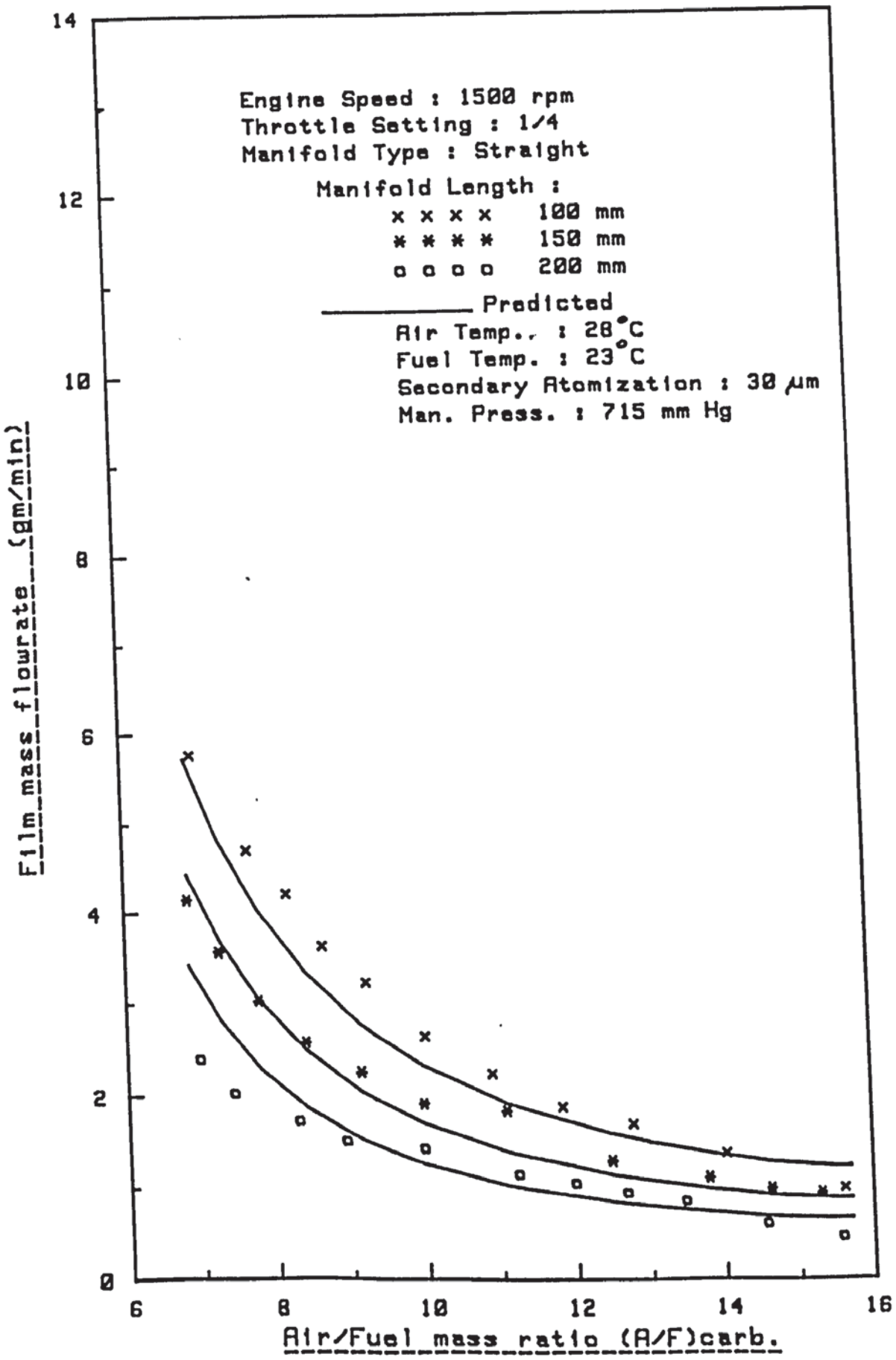

FIG. (7.1) Comparison Between the Measured and Predicted Film Flowrates

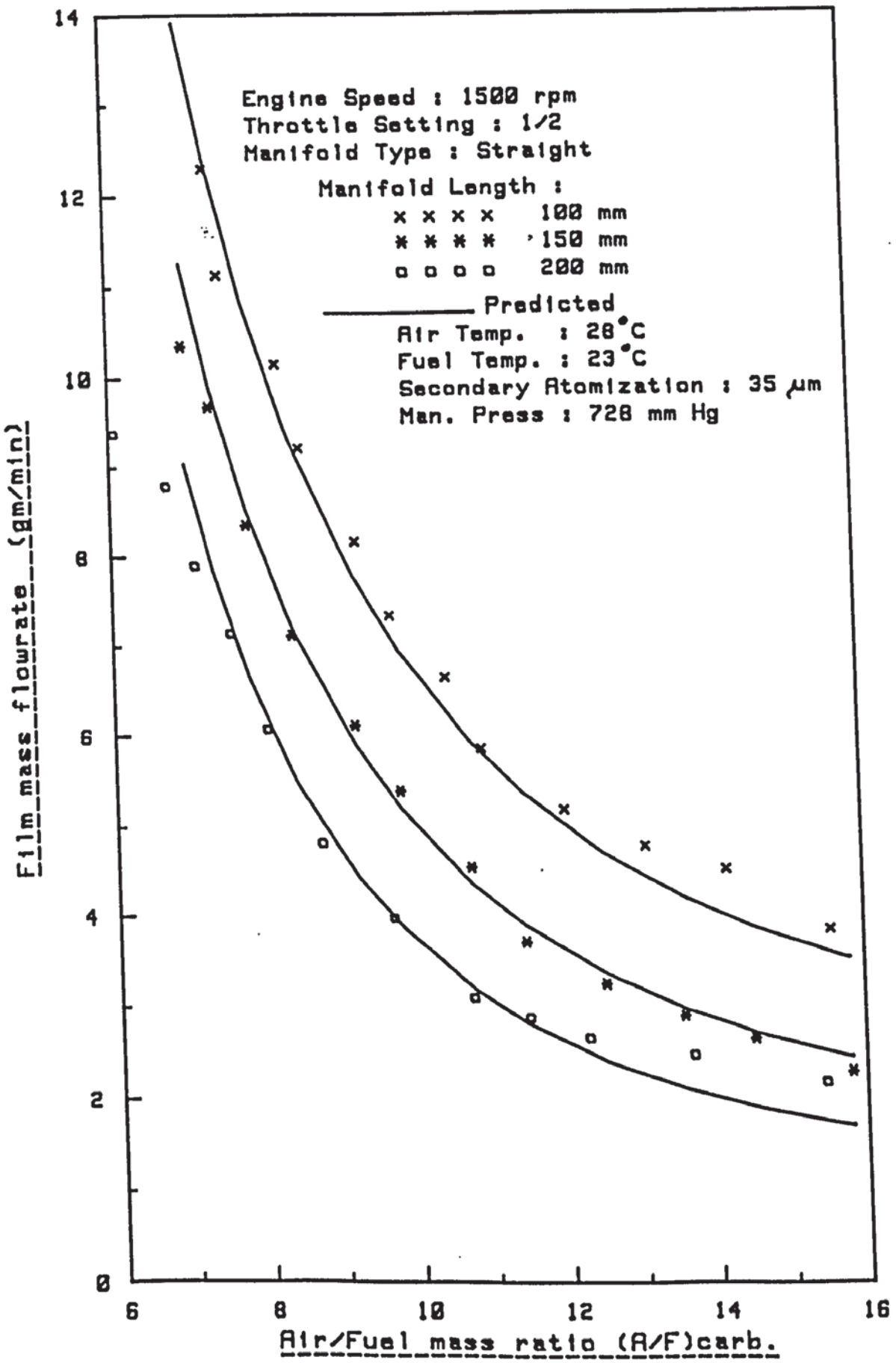

FIG. (7.2) Comparison Between the Measured and Predicted Film Flowrates

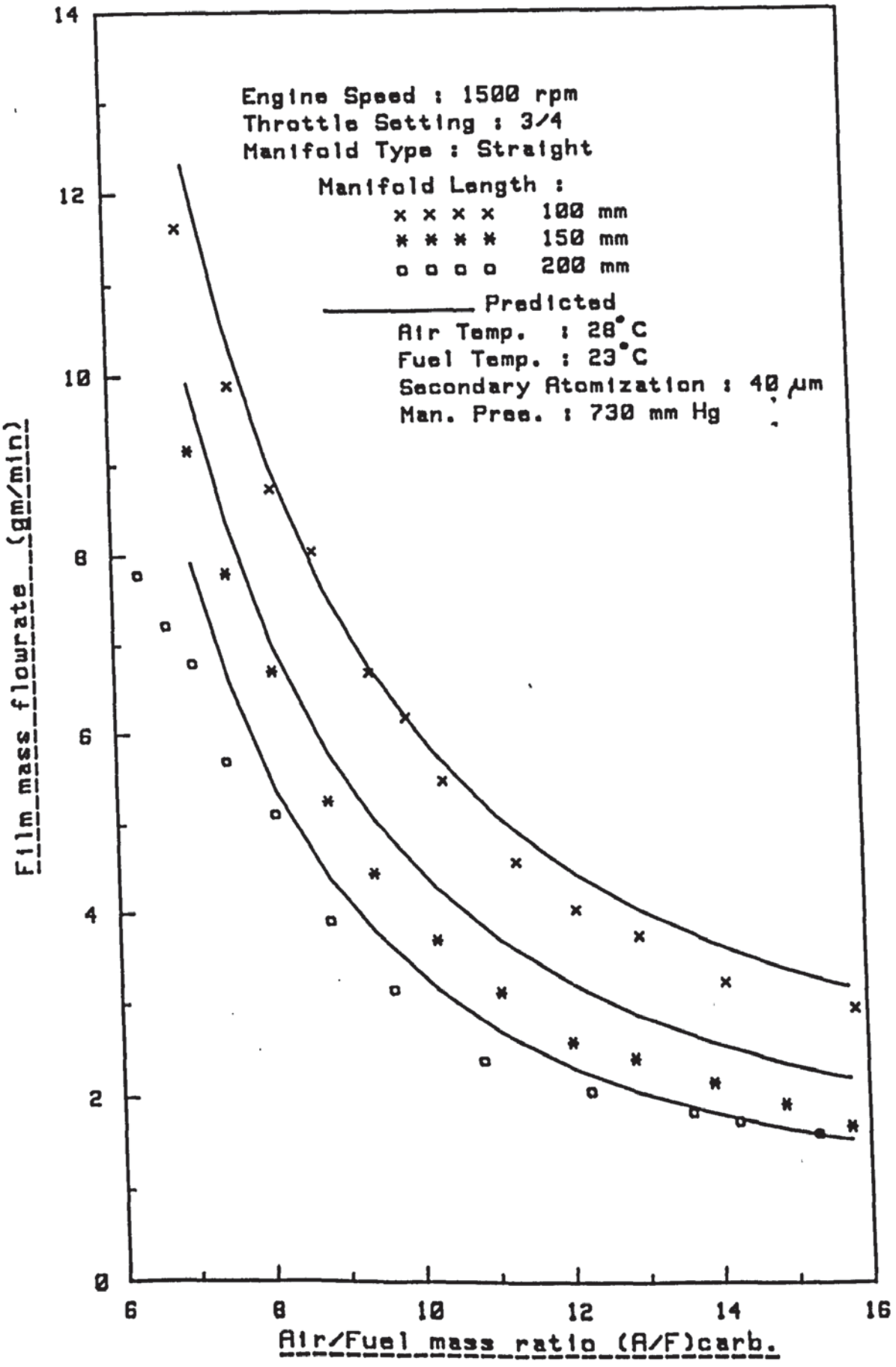

FIG. (7.3) Comparison Between the Measured and Predicted Film Flowrates

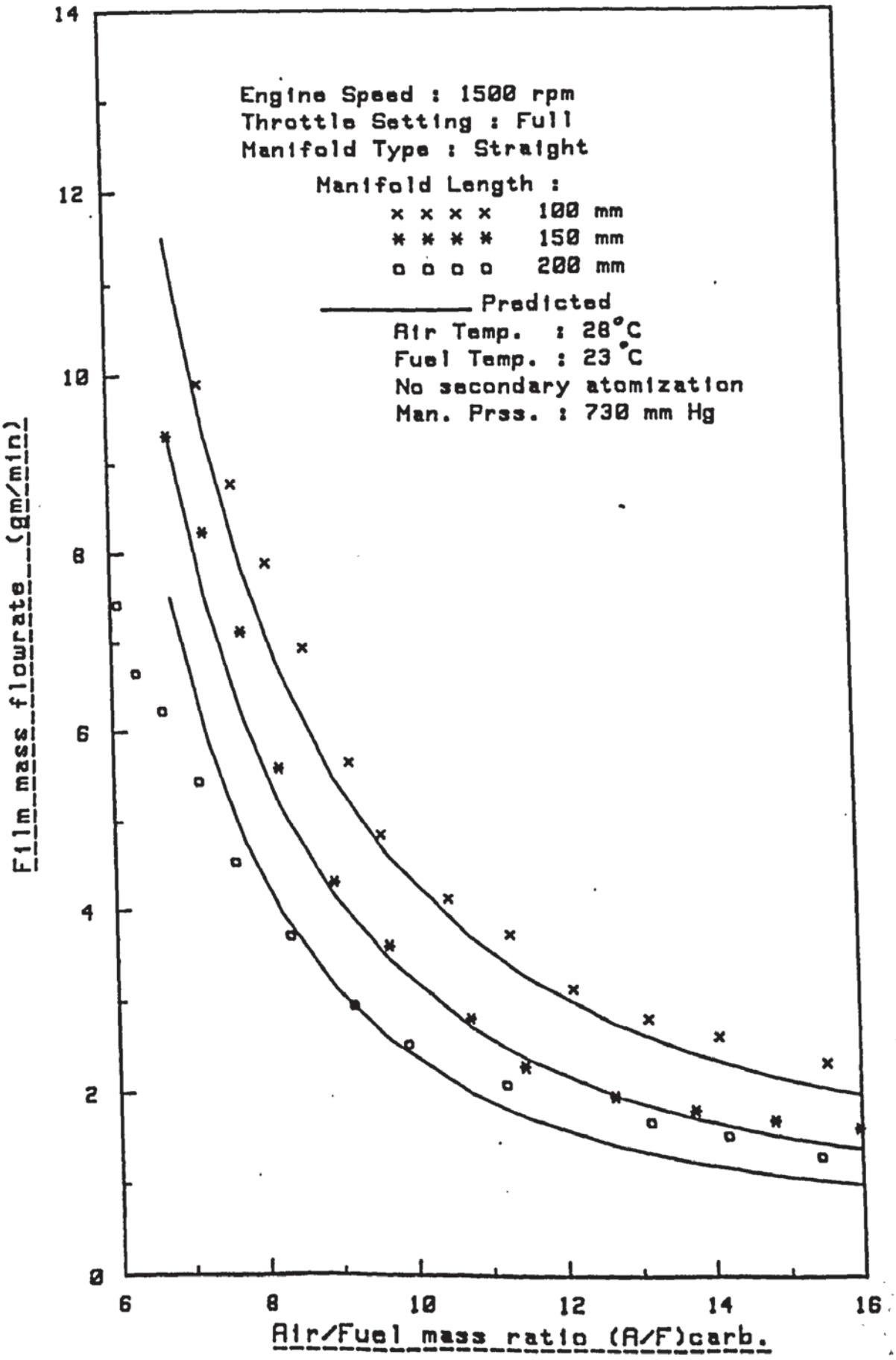

FIG. (7.4) Comparison Between the Measured and Predicted Film Flowrates

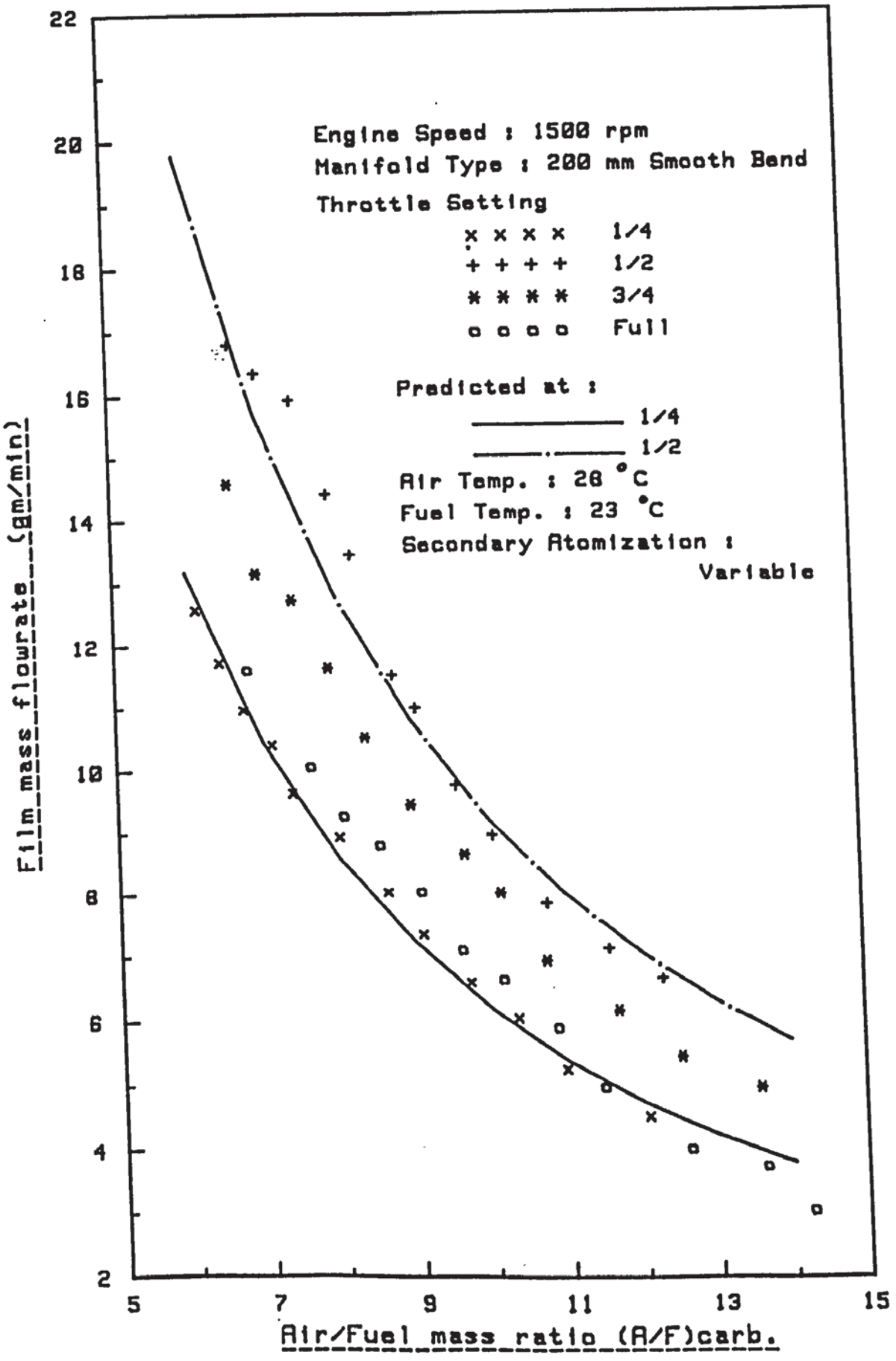

FIG. (7.5) Comparison Between The Measured and Predicted Film Flowrate

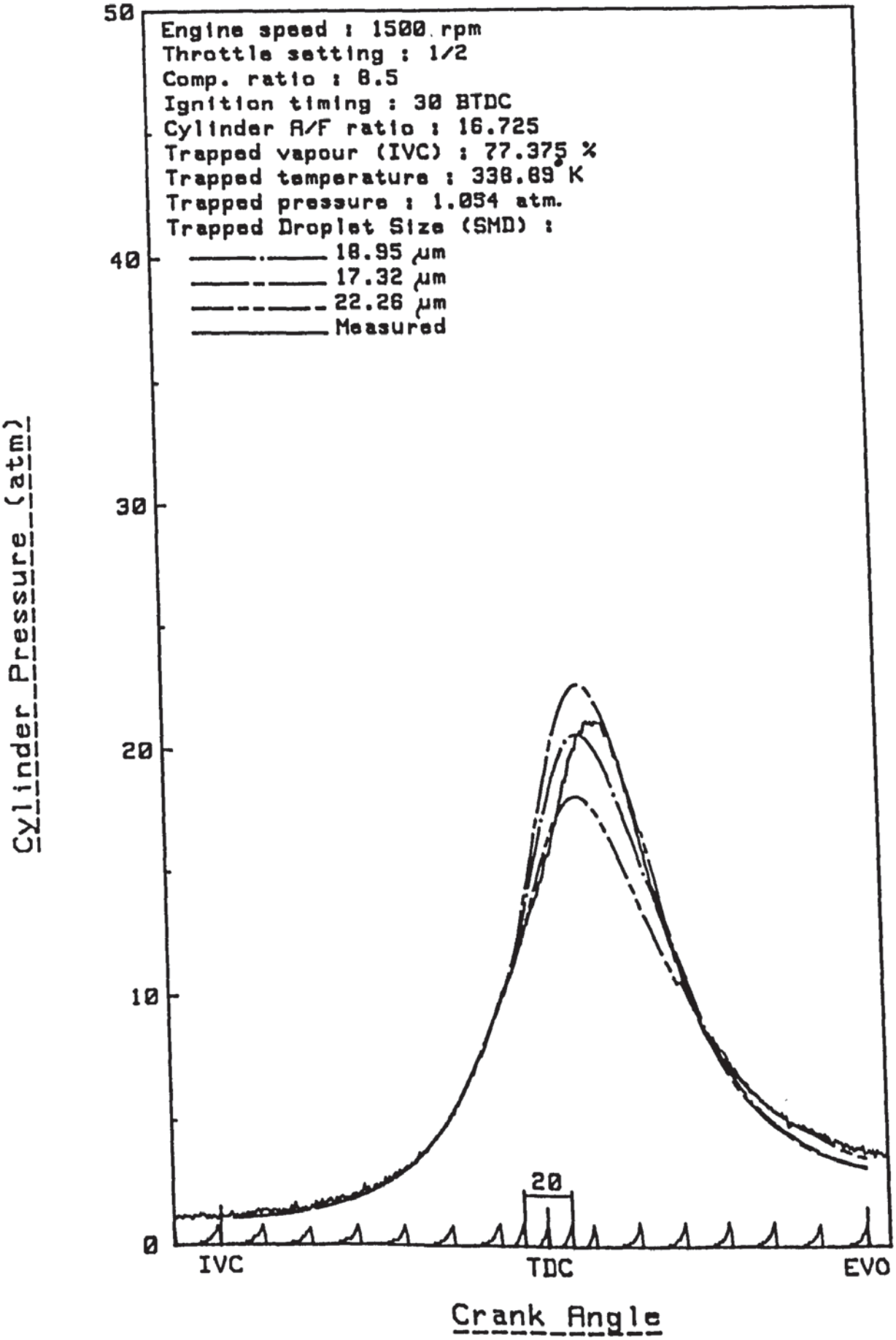

FIG. (7.6) Comparison Between The Measured and Predicted Pressure

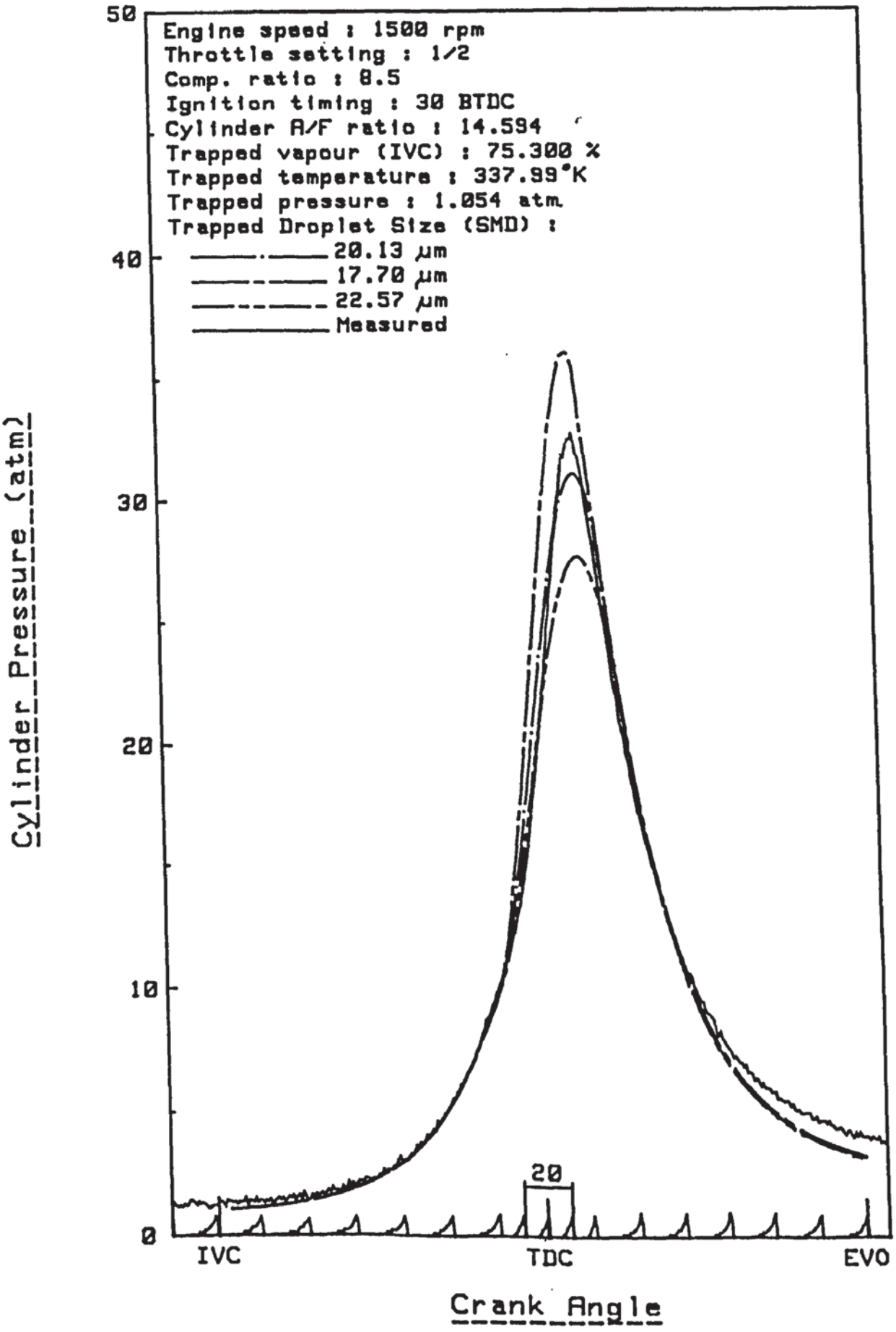

FIG. (7.7) Comparison Between The Measured and Predicted Pressure

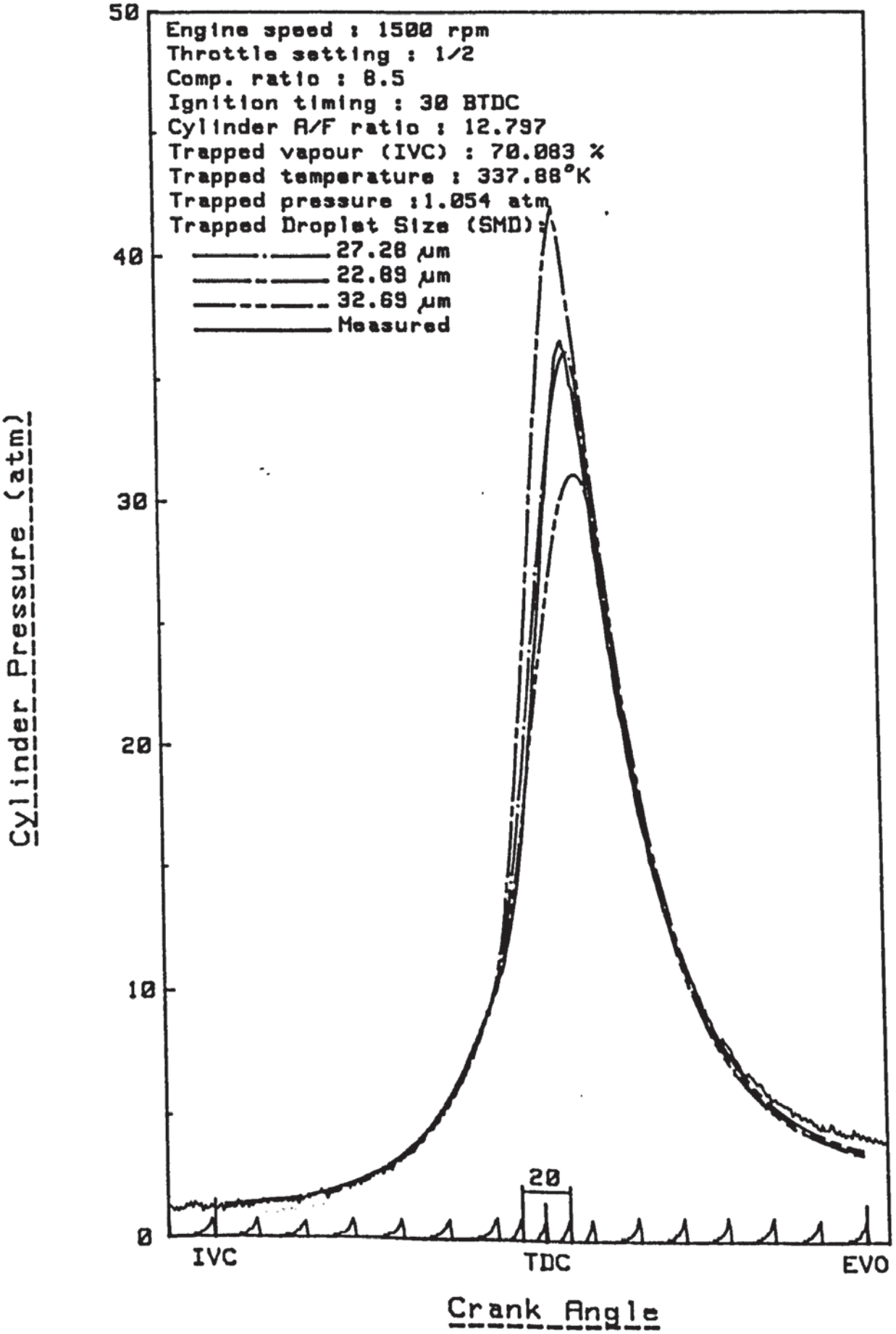

FIG. (7.8) Comparison Between The Measured and Predicted Pressure

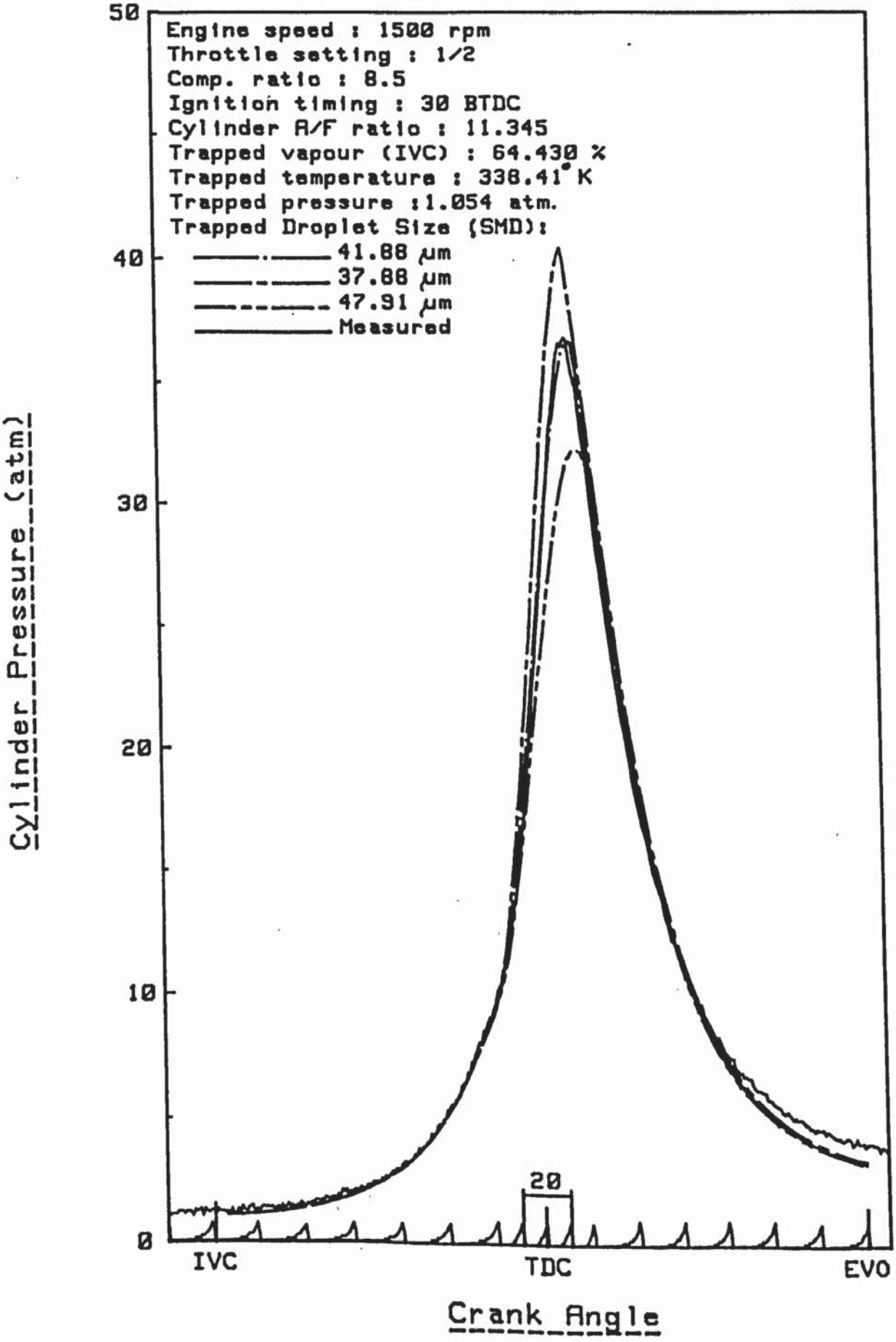

FIG. (7.9) Comparison Between The Measured and Predicted Pressure

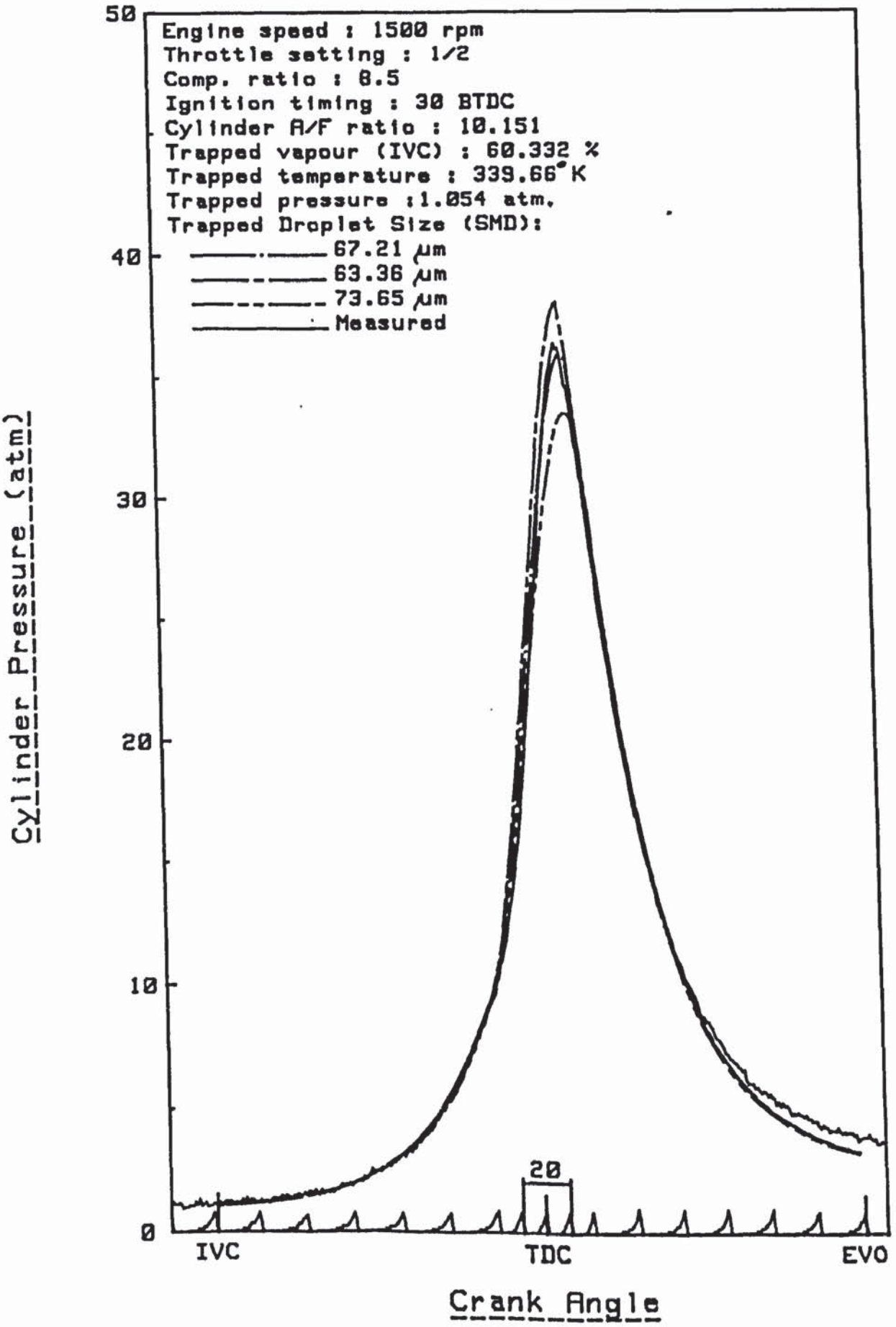

FIG. (7.10) Comparison Between The Measured and Predicted Pressure

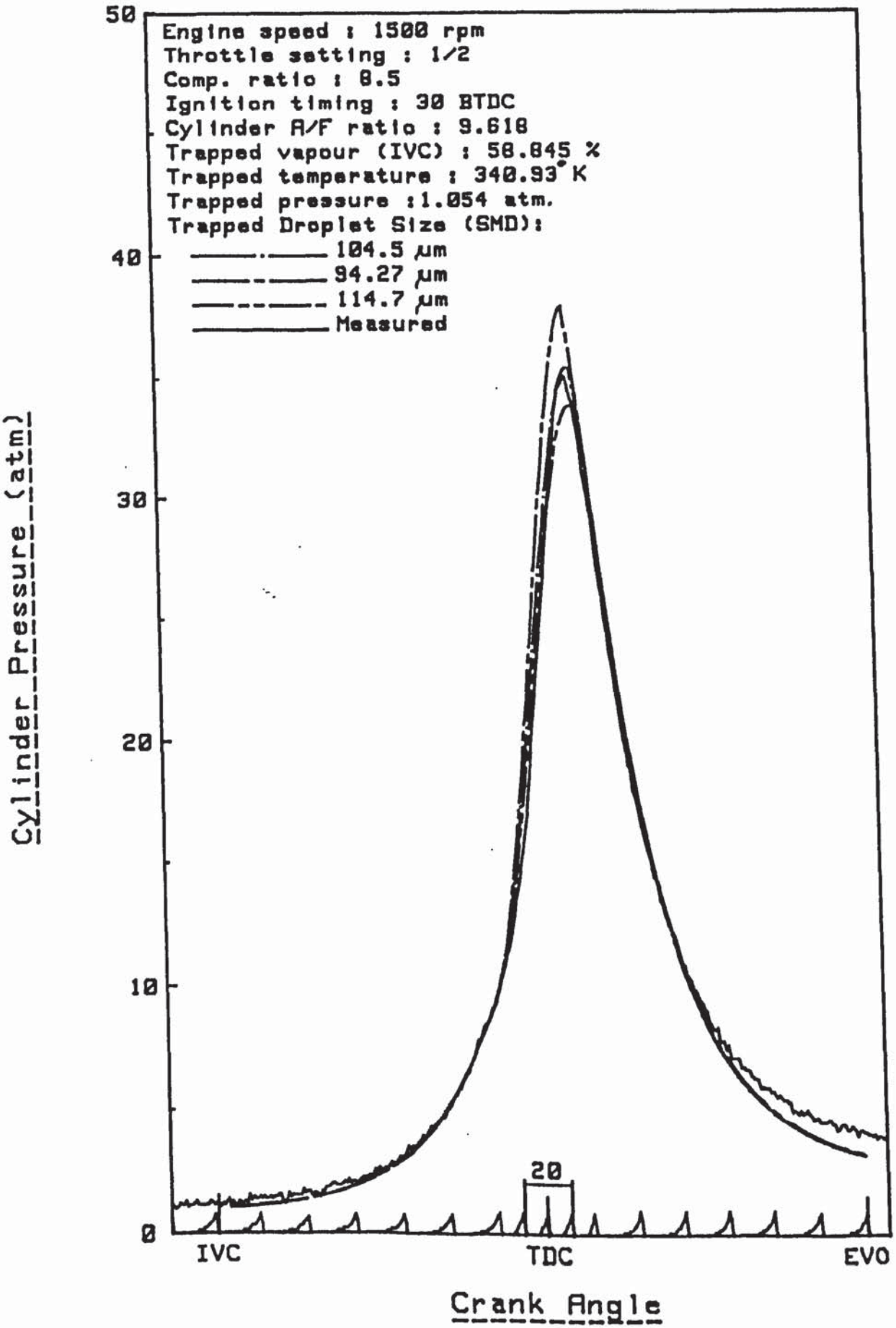

FIG. (7.11) Comparison Between The Measured and Predicted Pressure

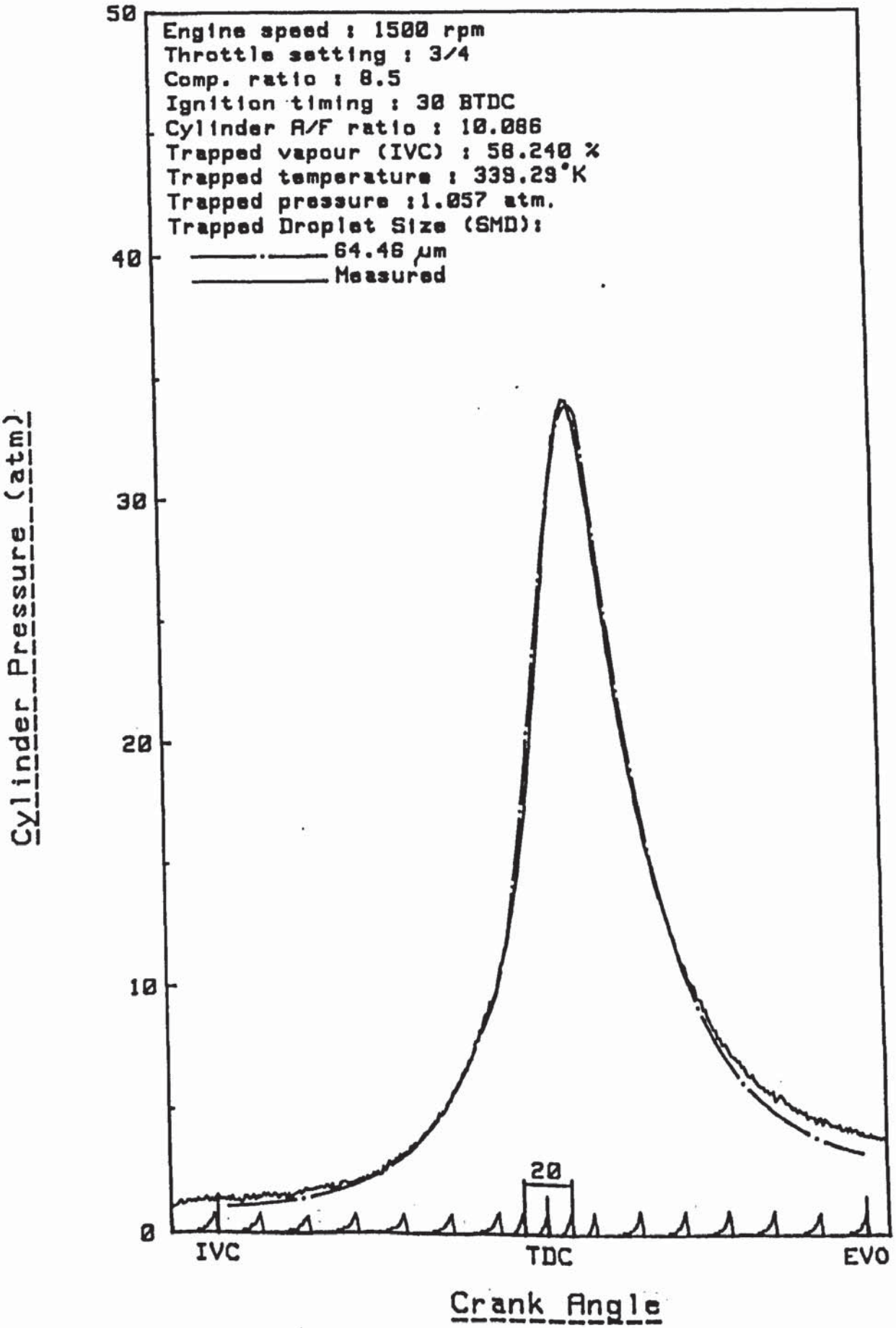

FIG. (7.12) Comparison Between The Measured and Predicted Pressure

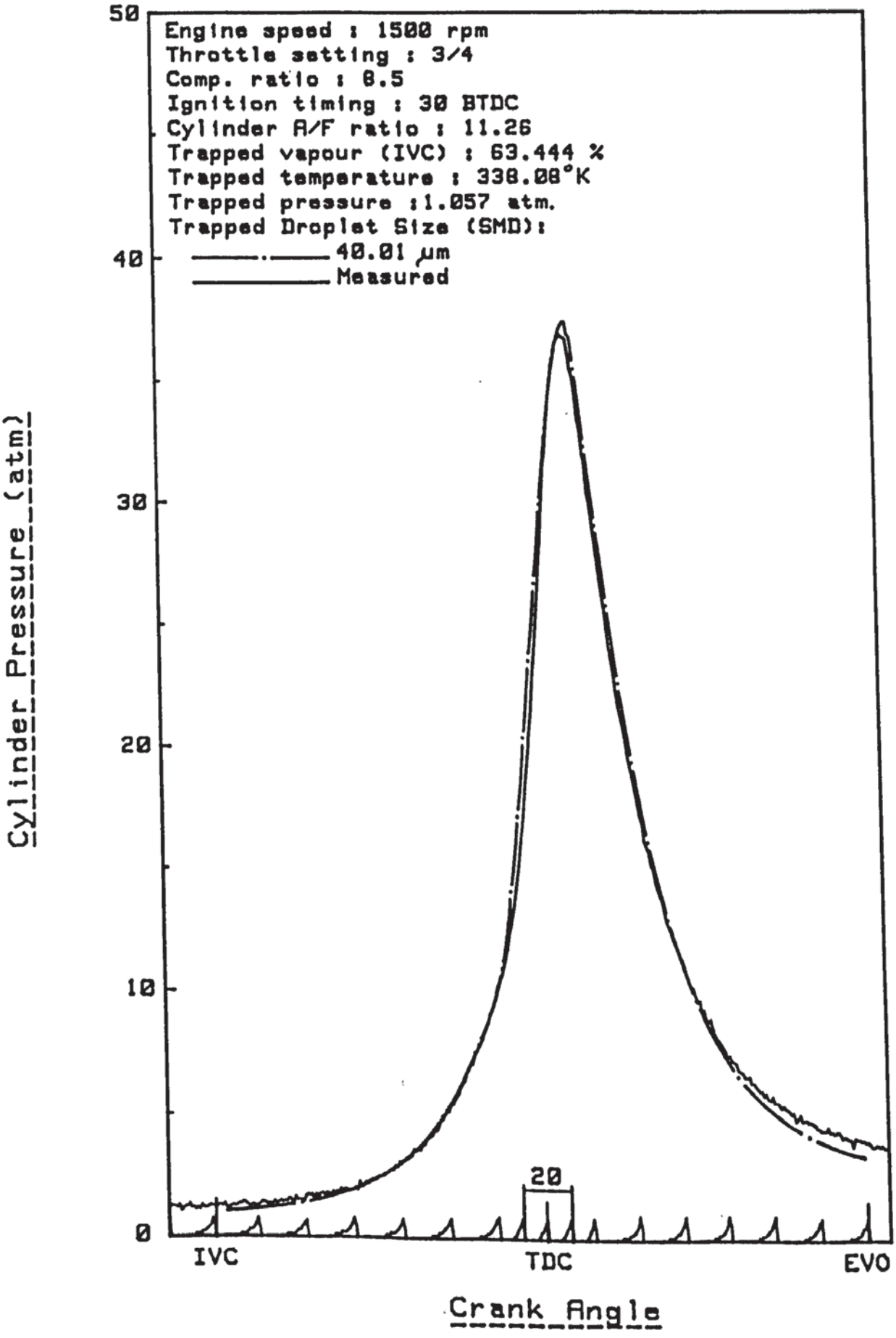

FIG. (7.13) Comparison Between The Measured and Predicteo

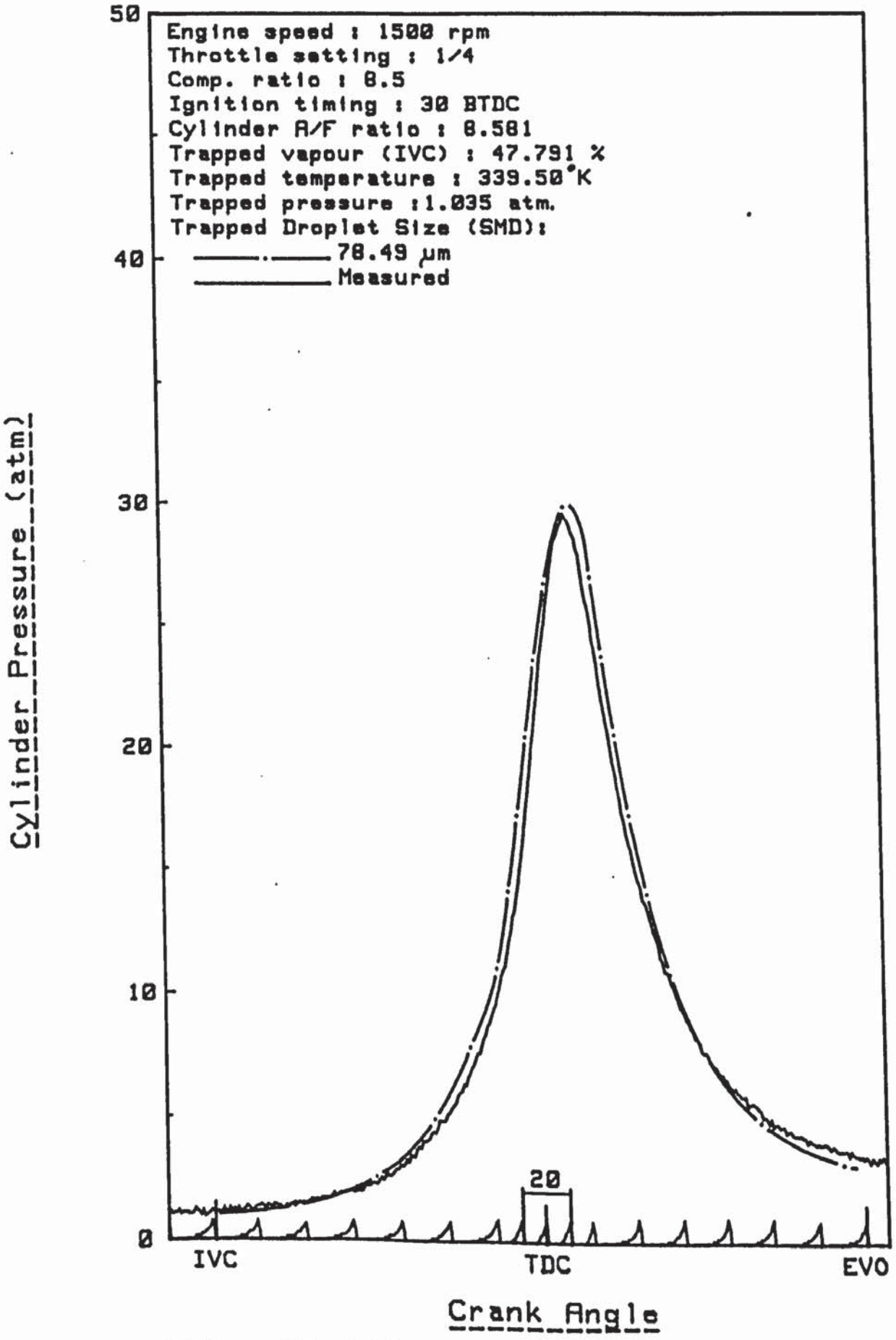

FIG. (7.14) Comparison Between The Measured and Predicted Pressure

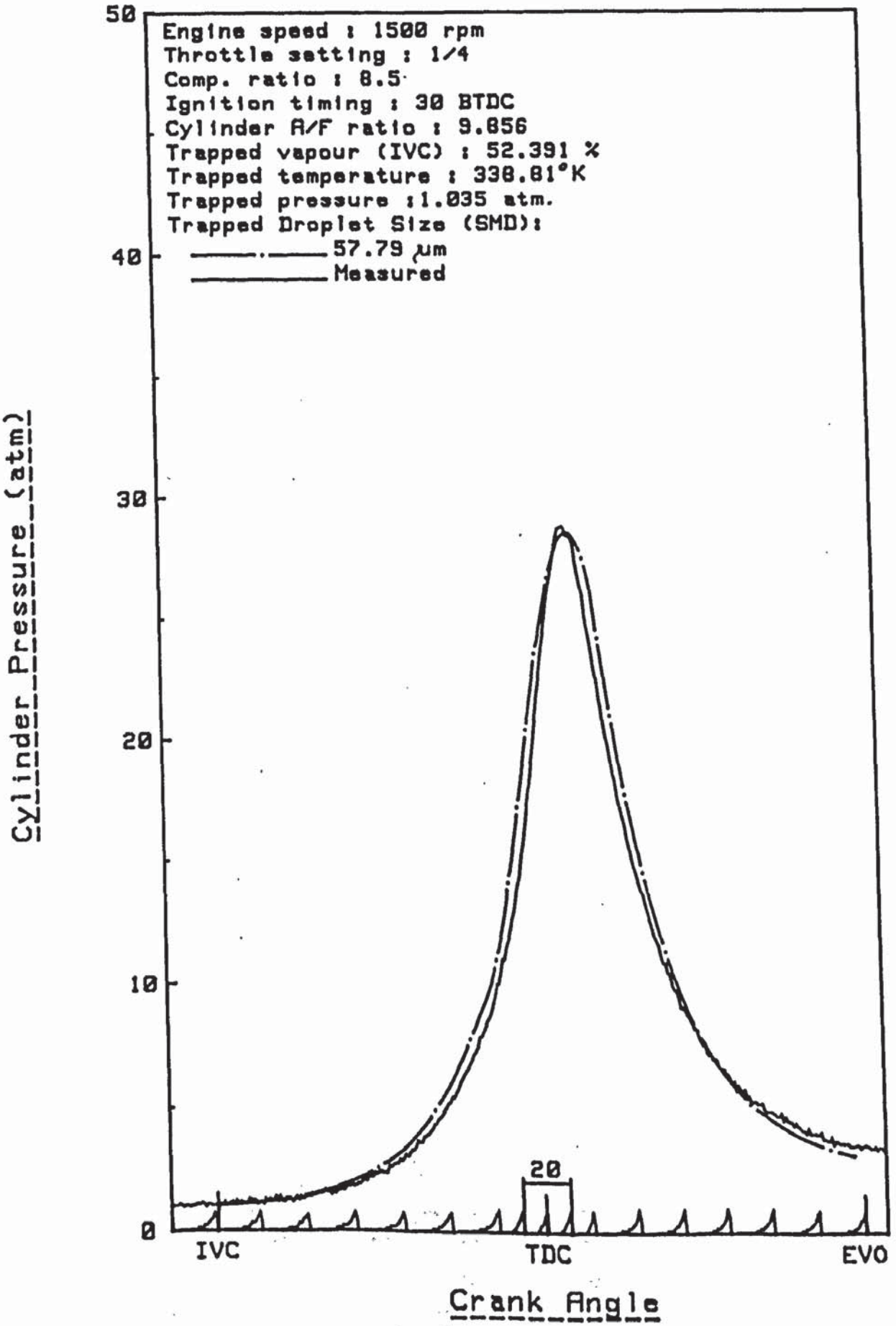

FIG. (7.15) Comparison Between The Measured and Predicted Pressure

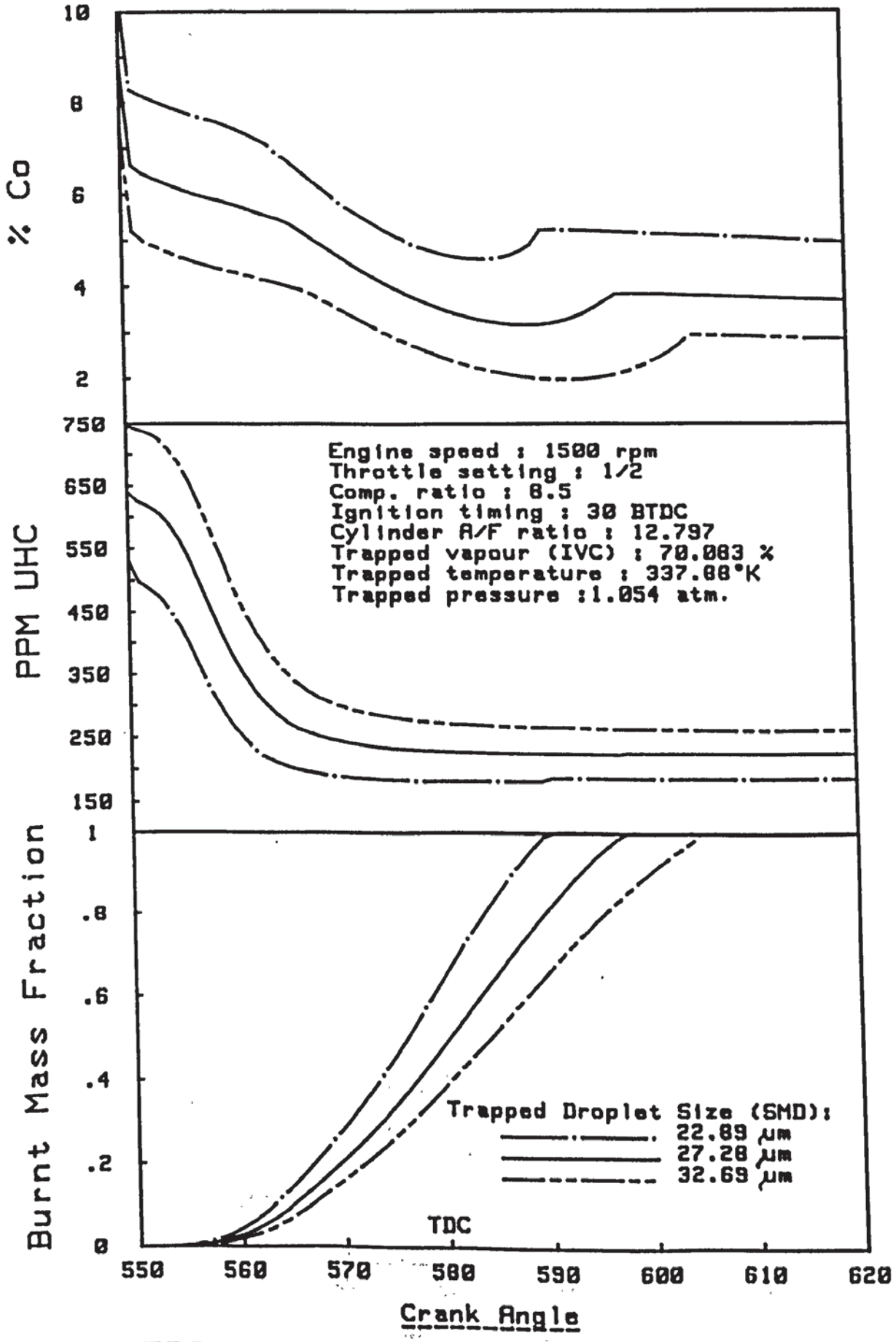

FIG. (7.16) Typical Variation of Combustion Parameters

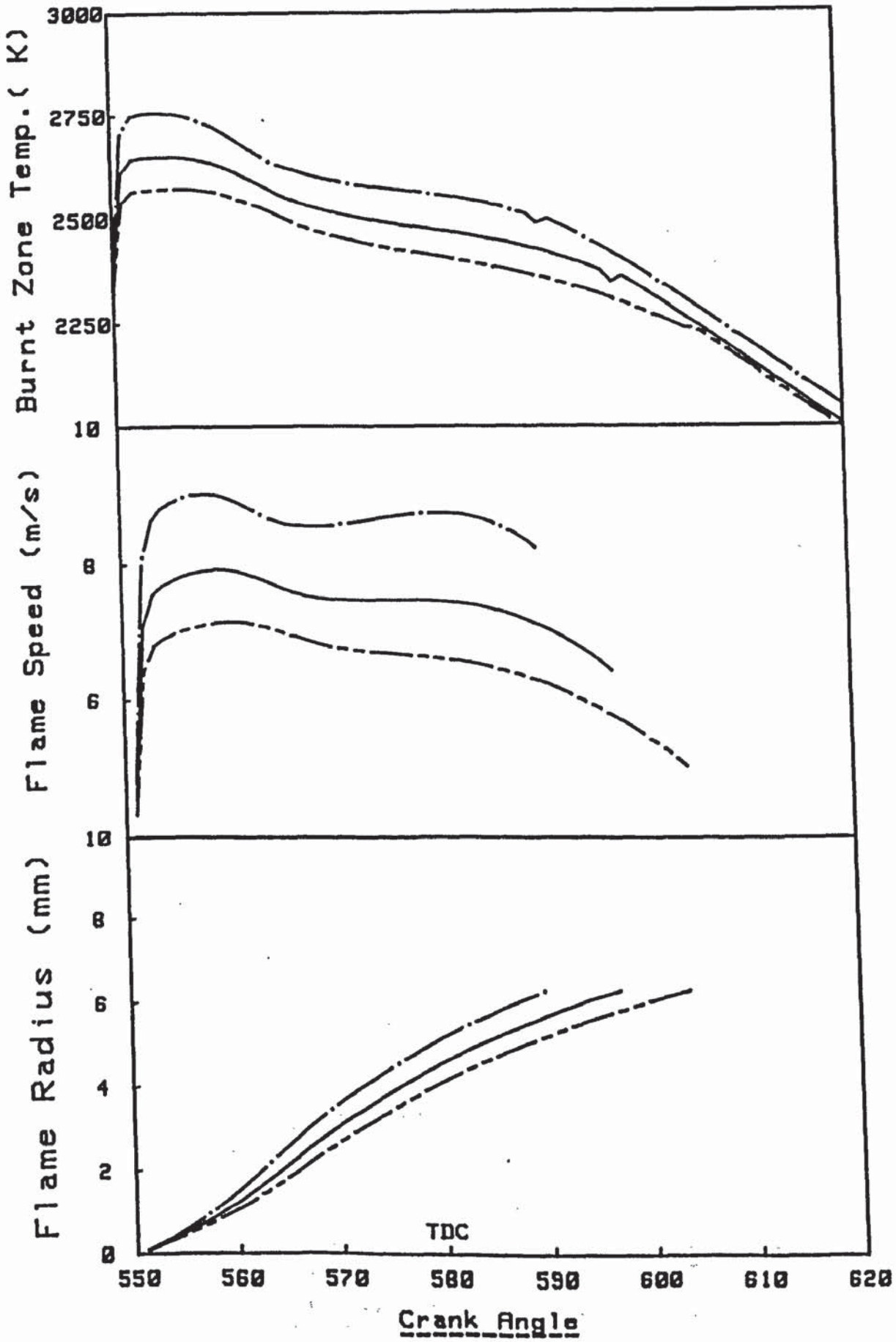

FIG. (7.17) Typical Variation of Combustion Parameters

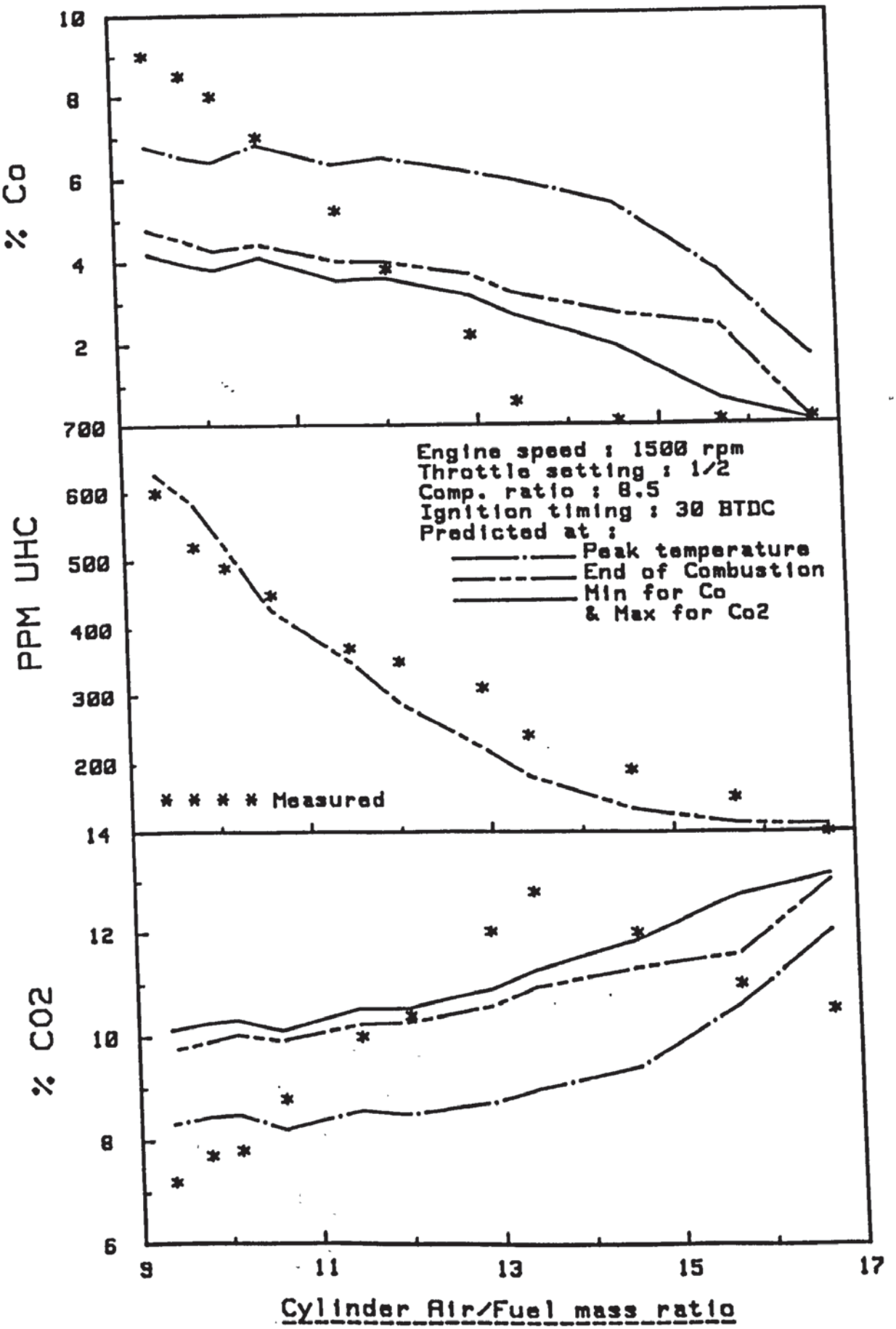

FIG. (7.18) Measured & Predicted Exhaust Emissions

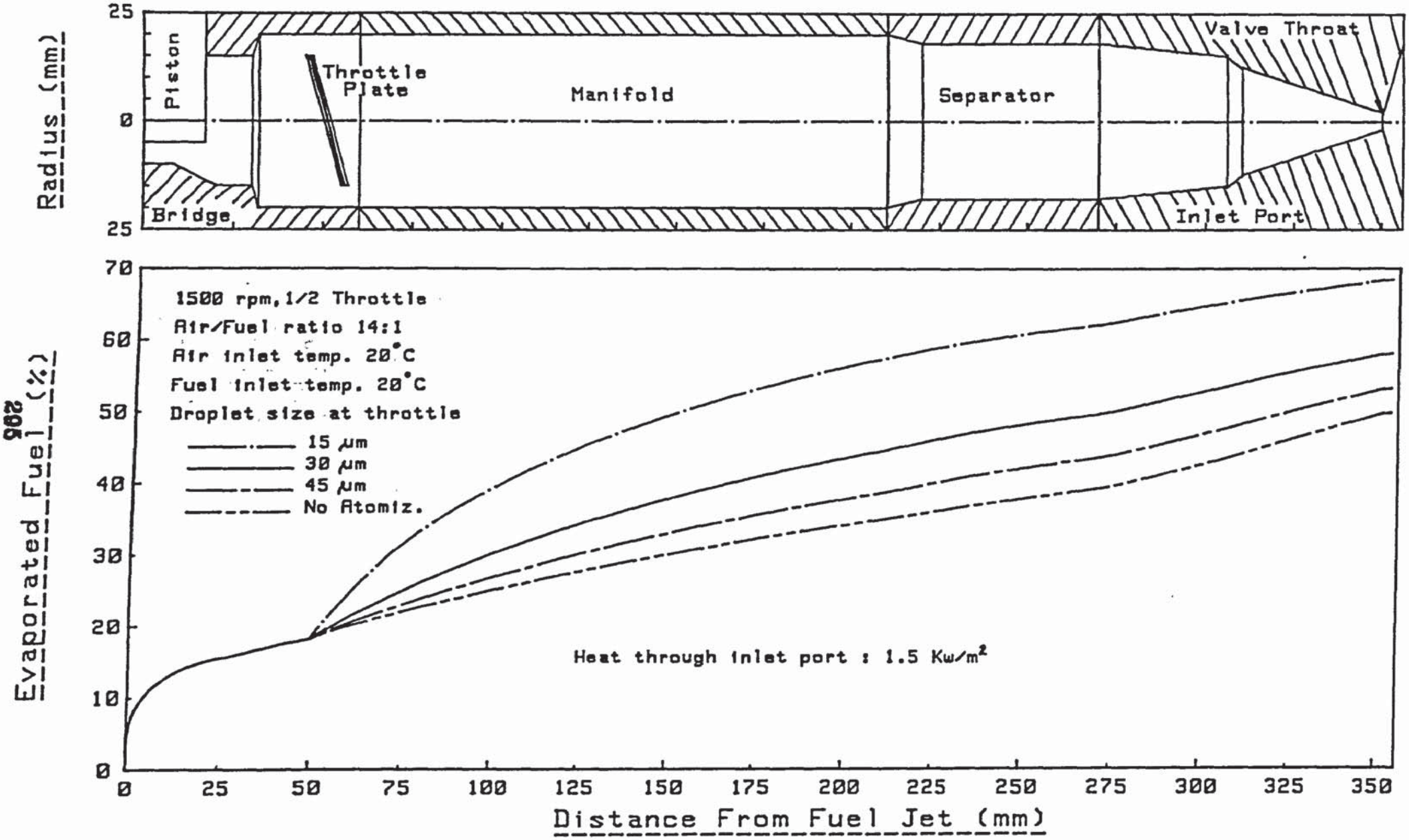

FIG.(7.19) Effect of Secondary Atomization on Fuel Evaporation

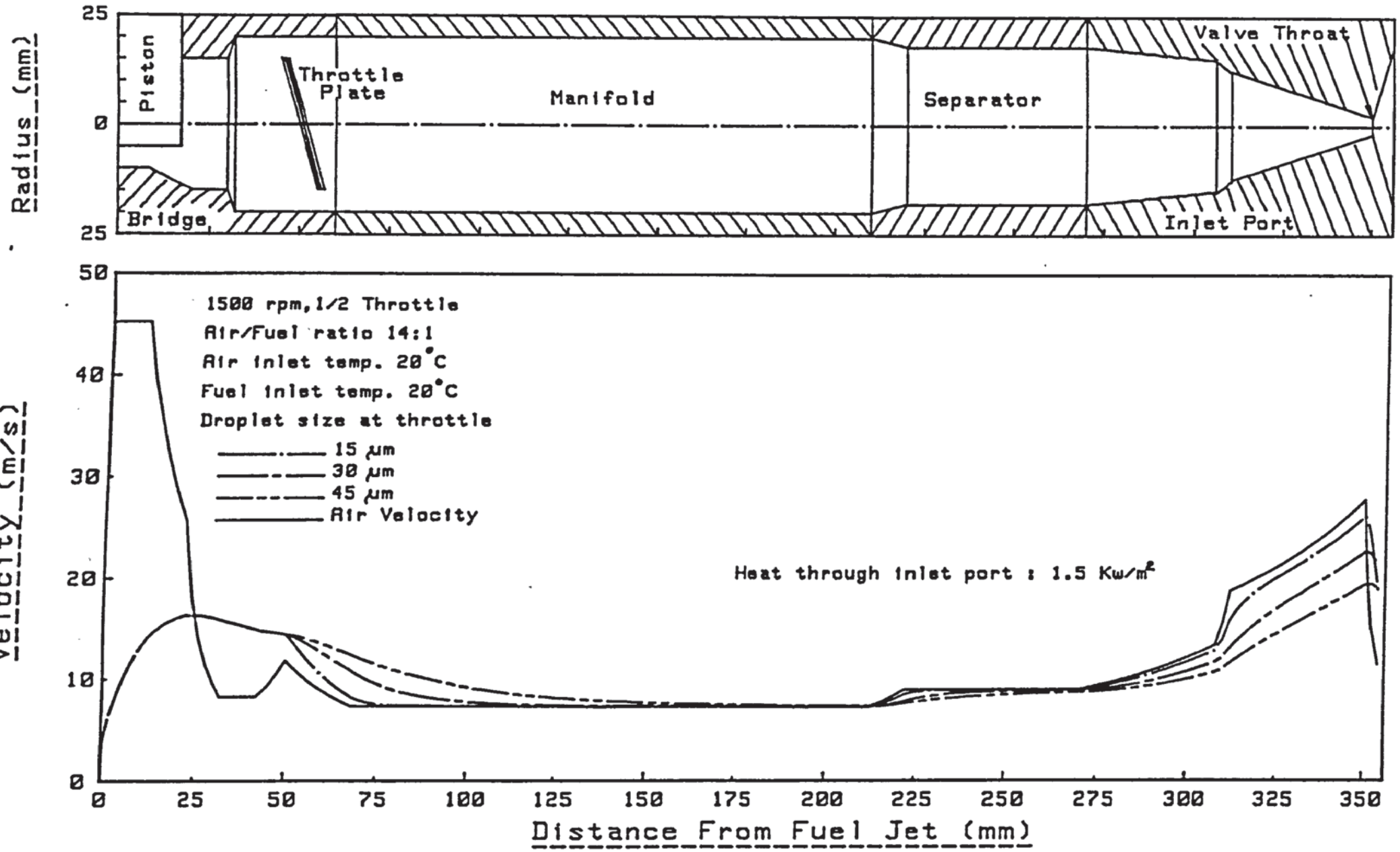

FIG. (7.20) Effect of Secondary Atomization on Droplet Velocity

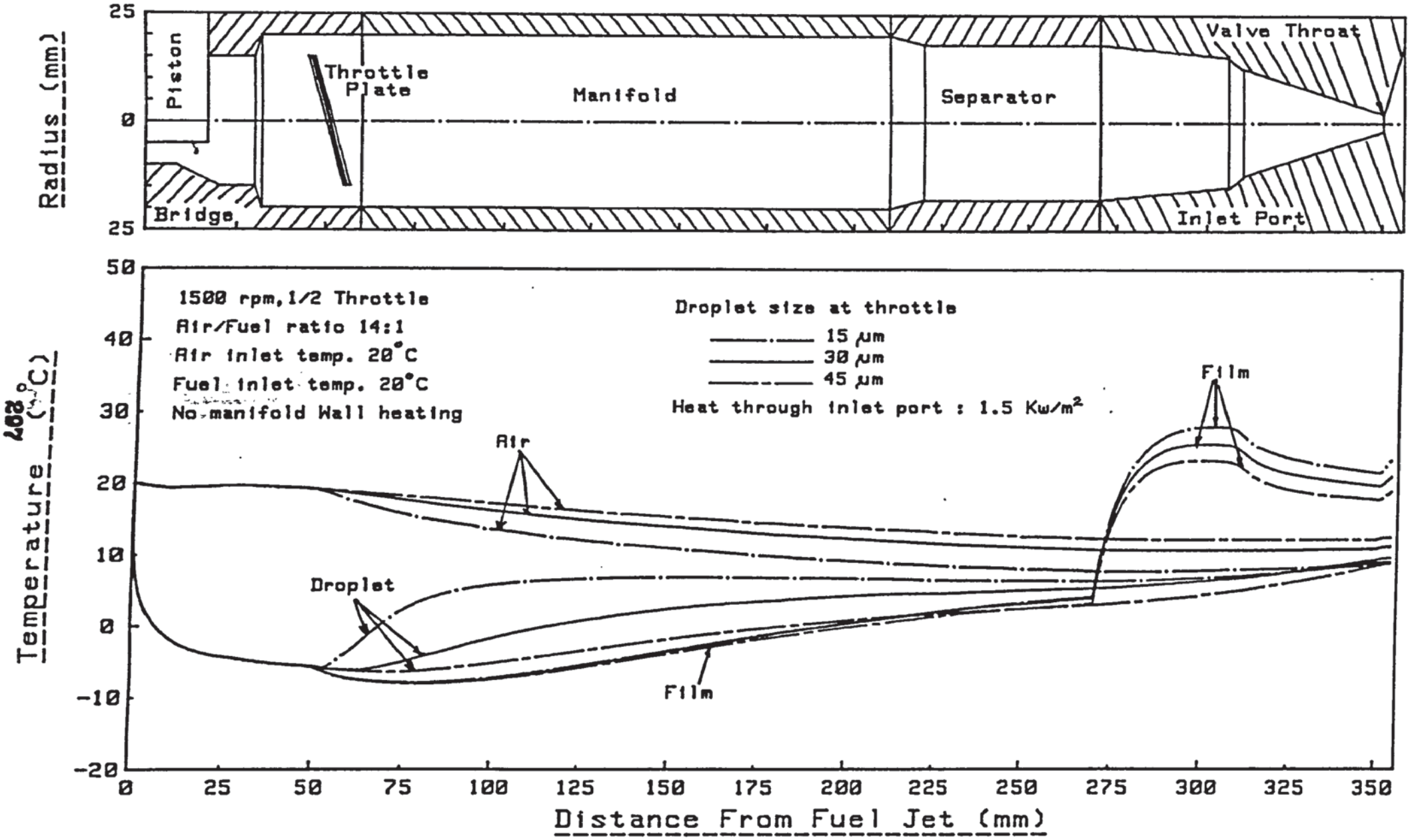

FIG. (7.21) Effect of Secondary Atomization on Fuel & Air Temperatures

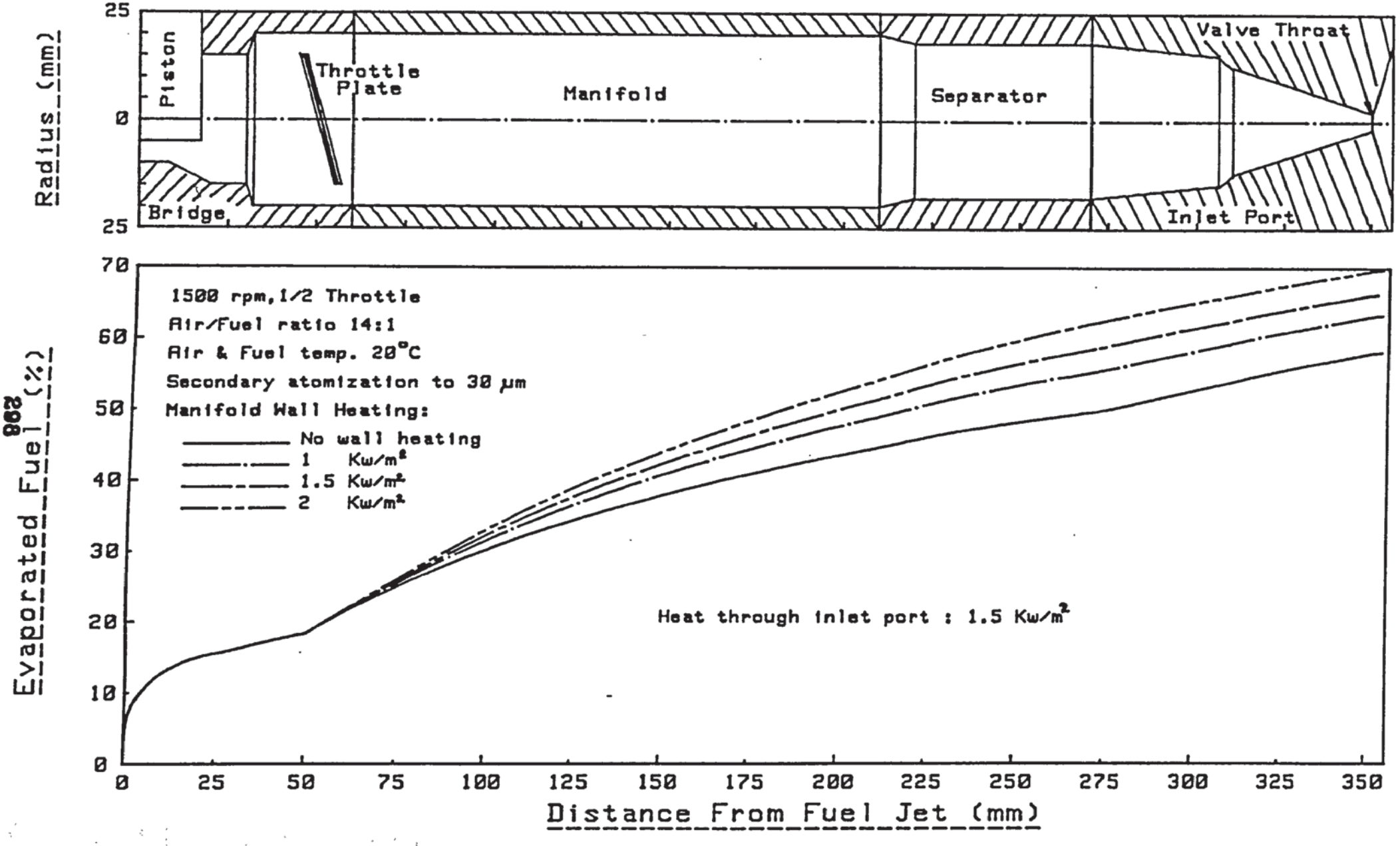

FIG (7.22) Effect of Manifold Wall Heating on Fuel Evaporation

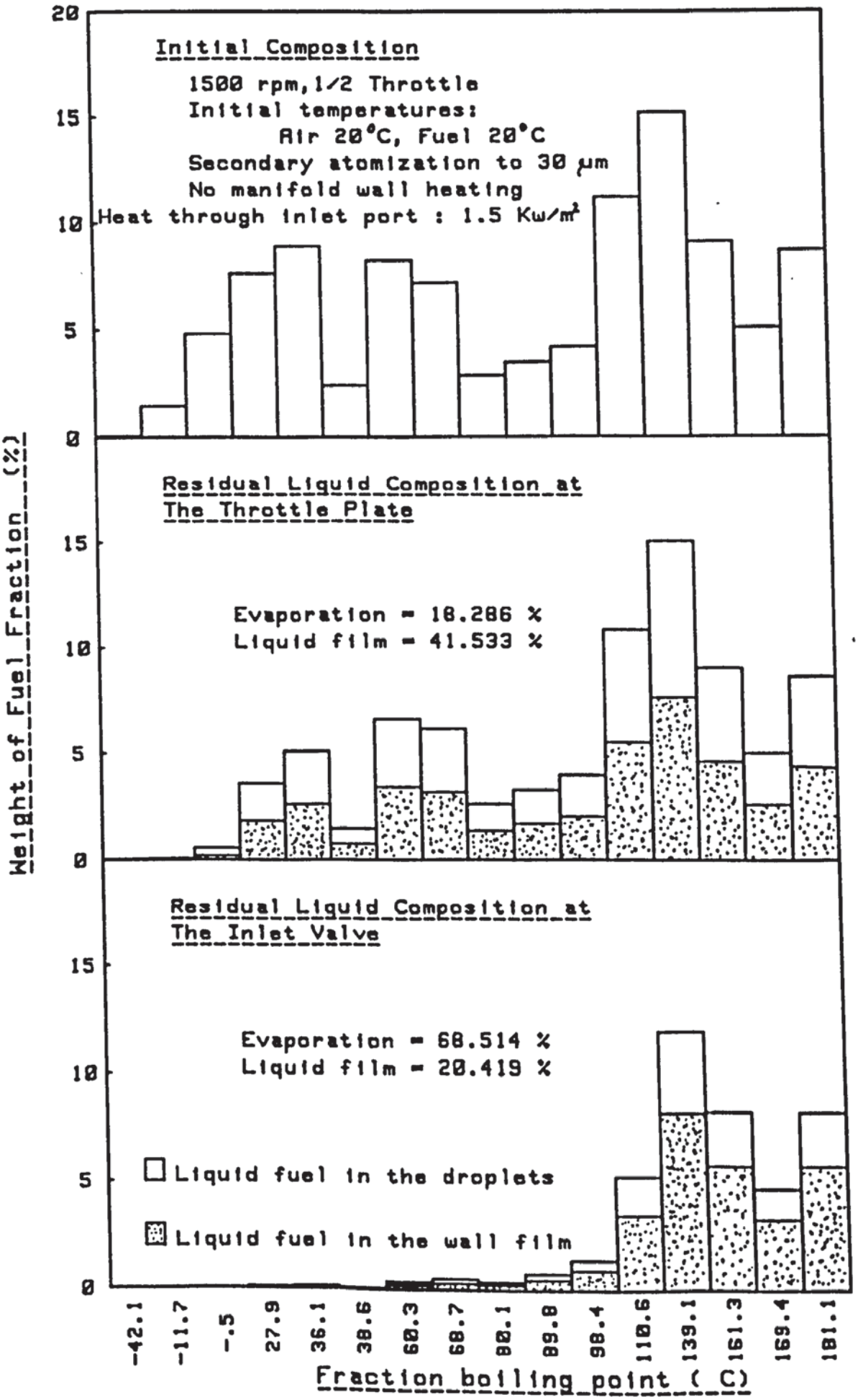

FIG.(7.23) Residual Liquid Fuel Composition at Various Locations in the Intake System

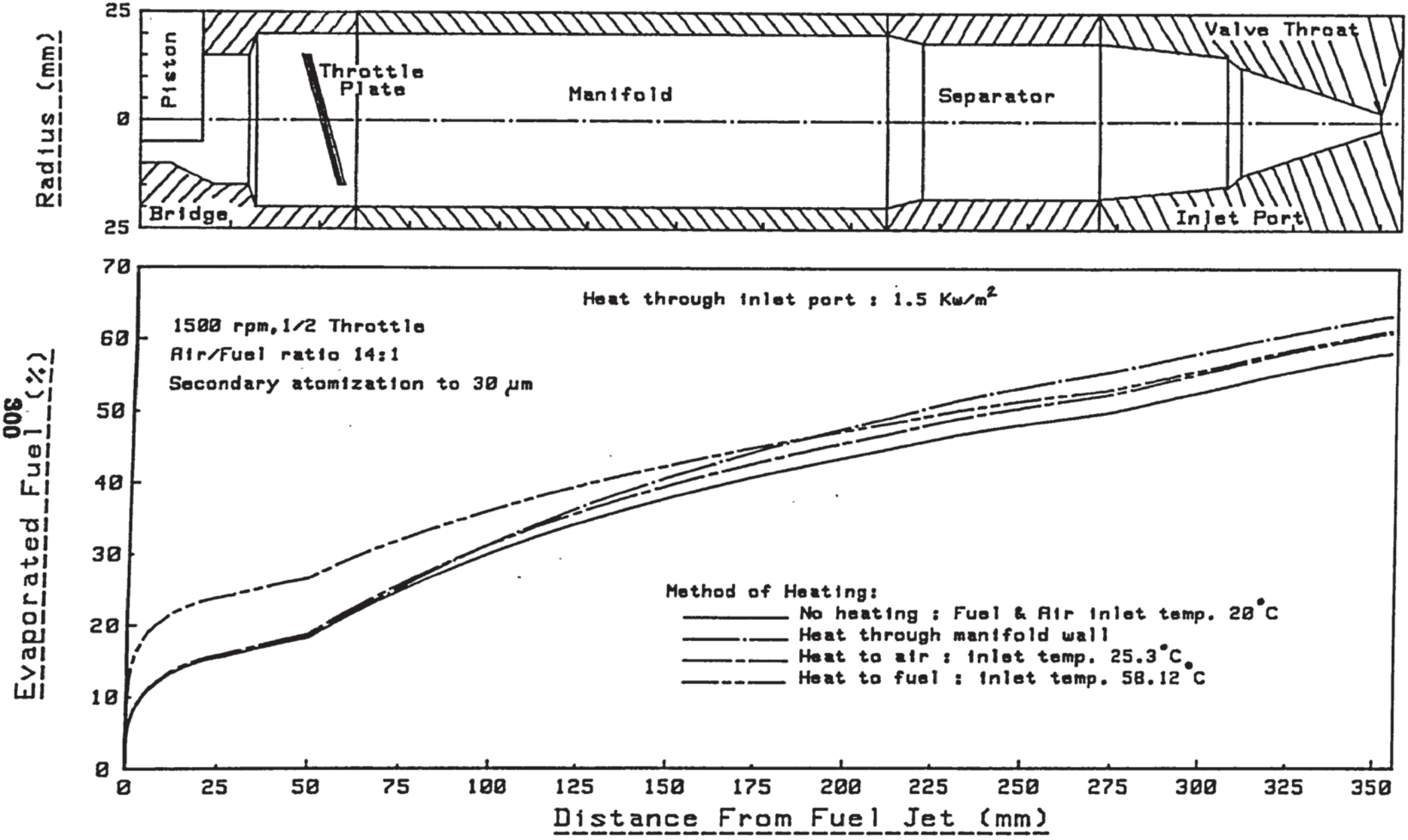

FIG.(7:24) Effect of Method of Heating on Fuel Evaporation

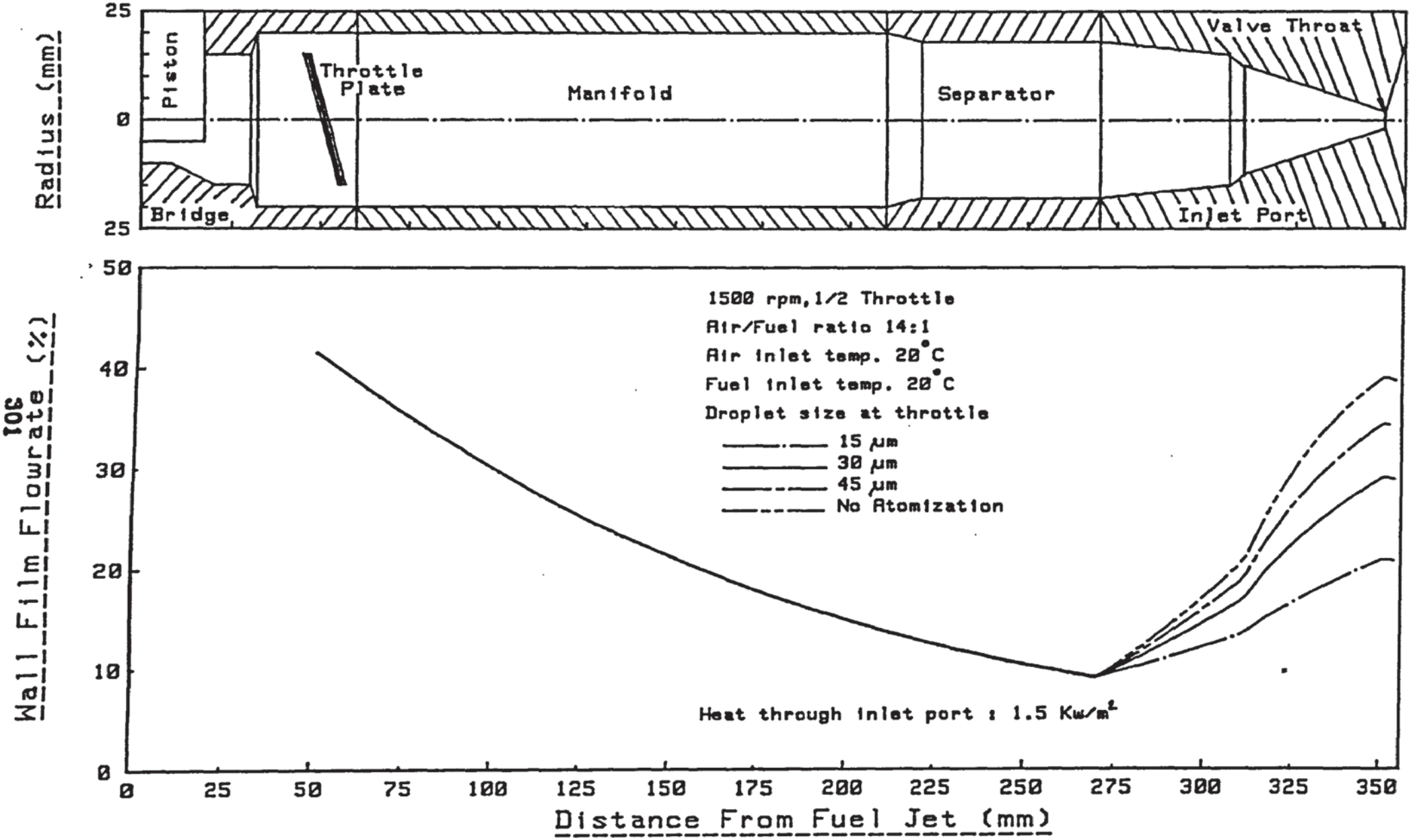

FIG.(7.25) Effect of Secondary Atomization on Wall Film Quantity

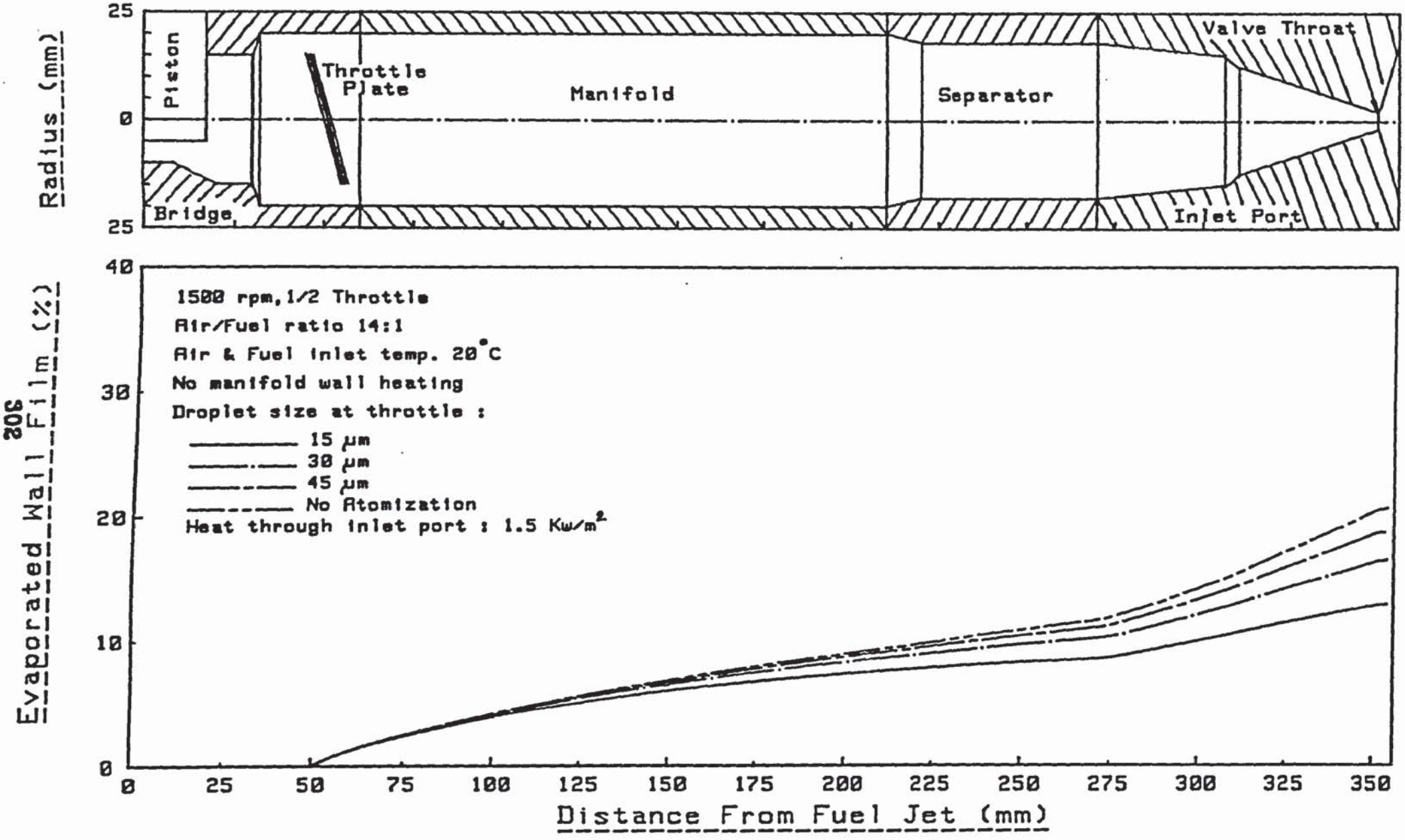

FIG. (7.26) Effect of Secondary Atomization on Film Evaporation

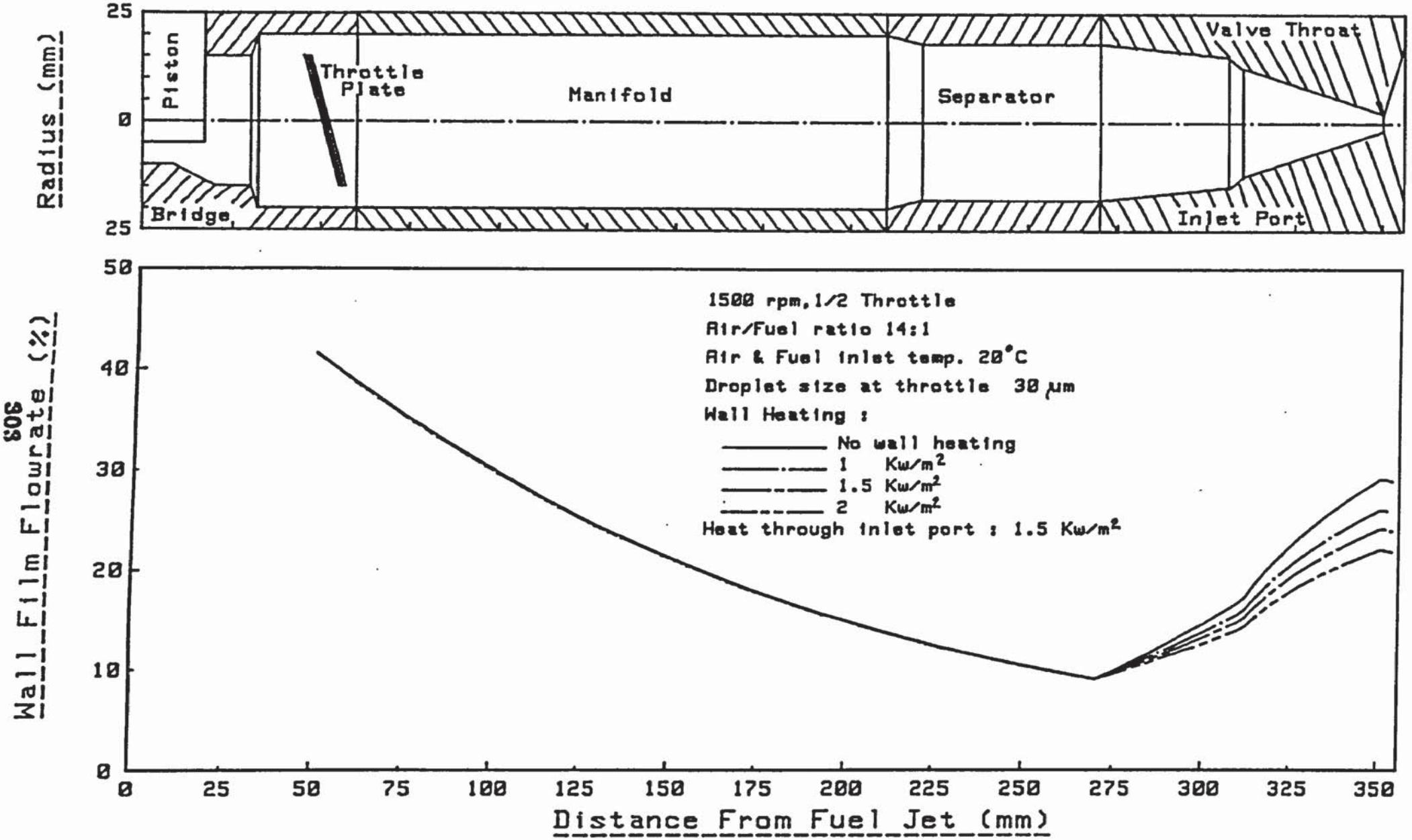

FIG. (7.27) Effect of Manifold Wall Heating on Wall Film Quantity

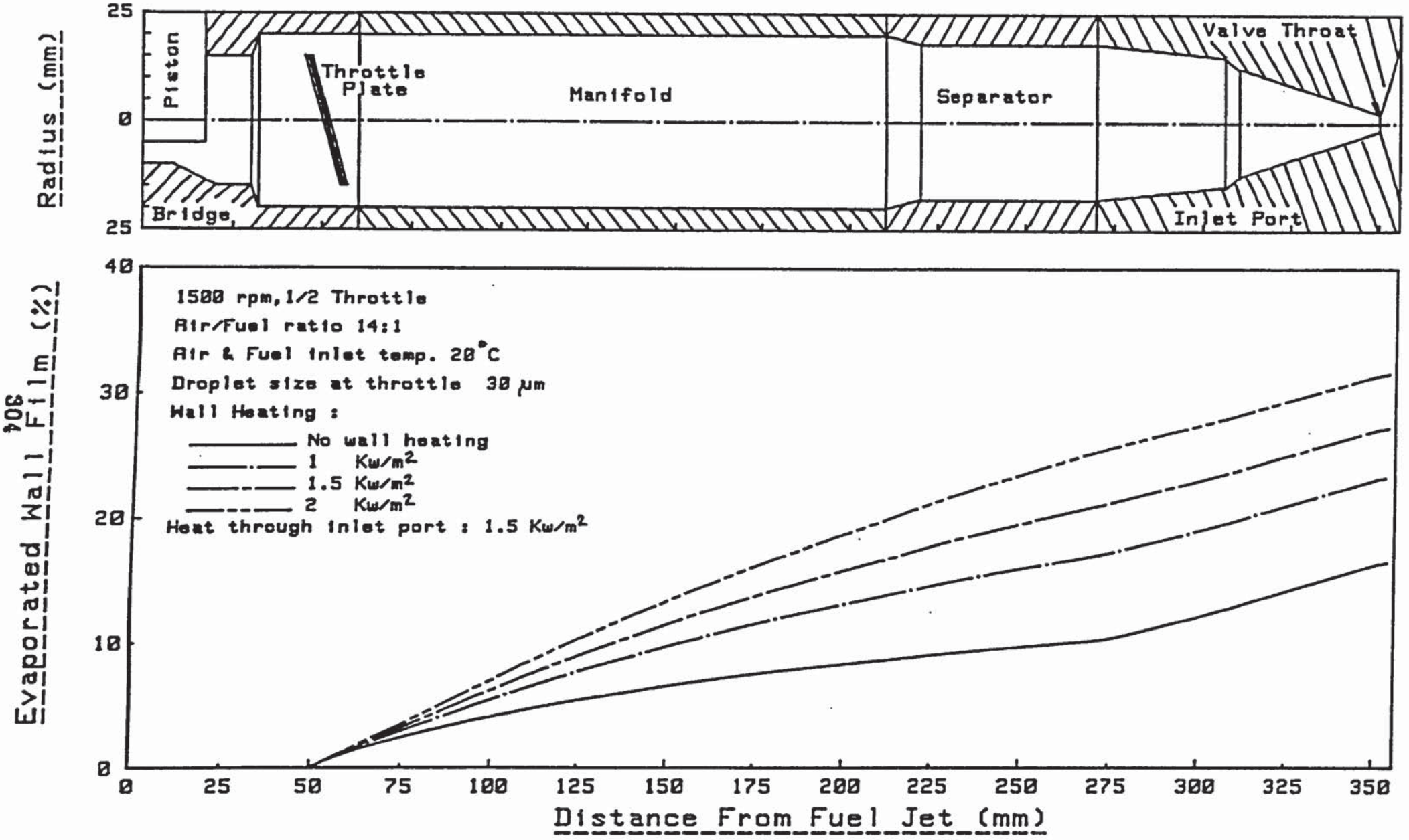

FIG. (7.28) Effect of Manifold Wall Heating on Film Evaporation

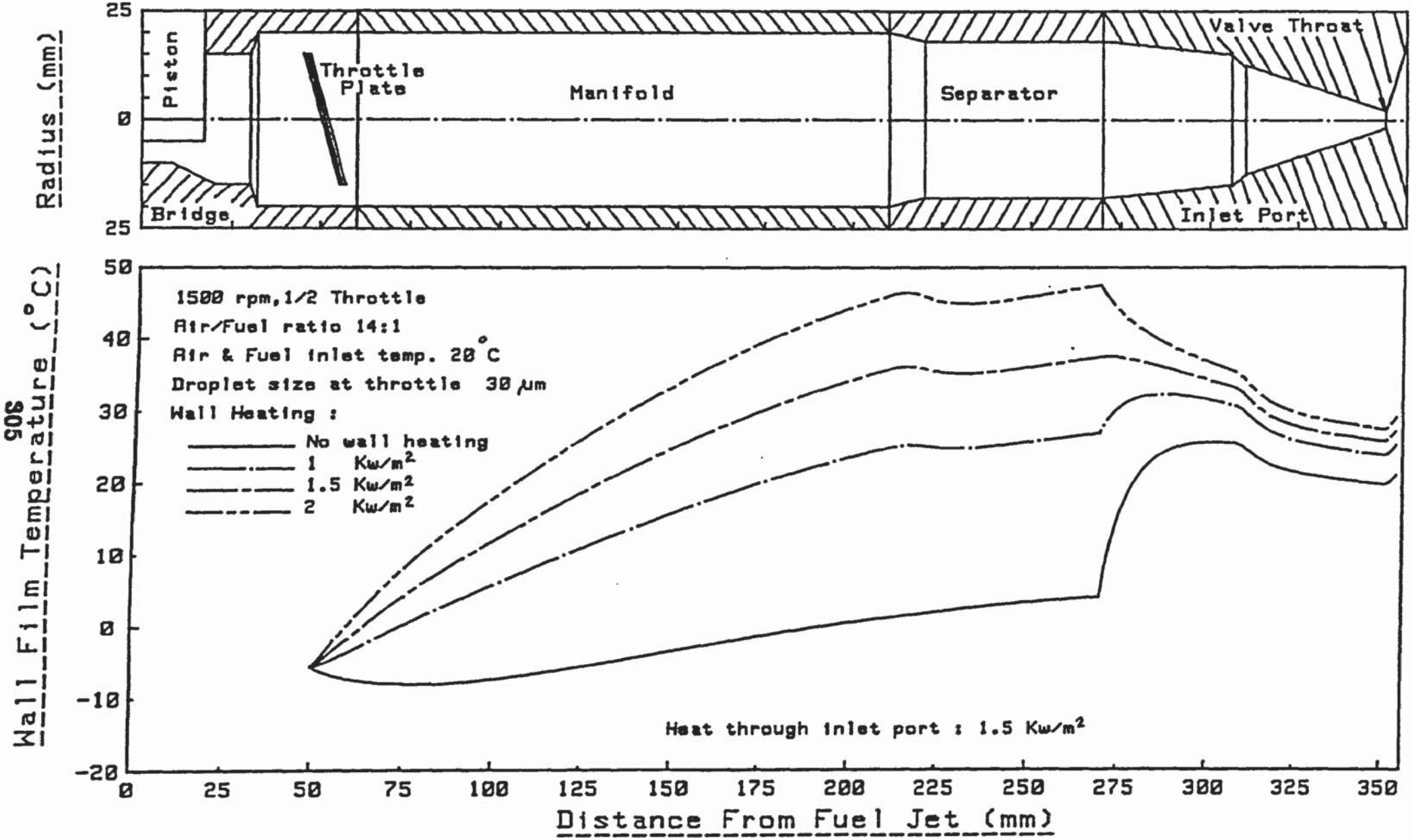

FIG. (7.29) Effect of Manifold Wall Heating on Film Temperature

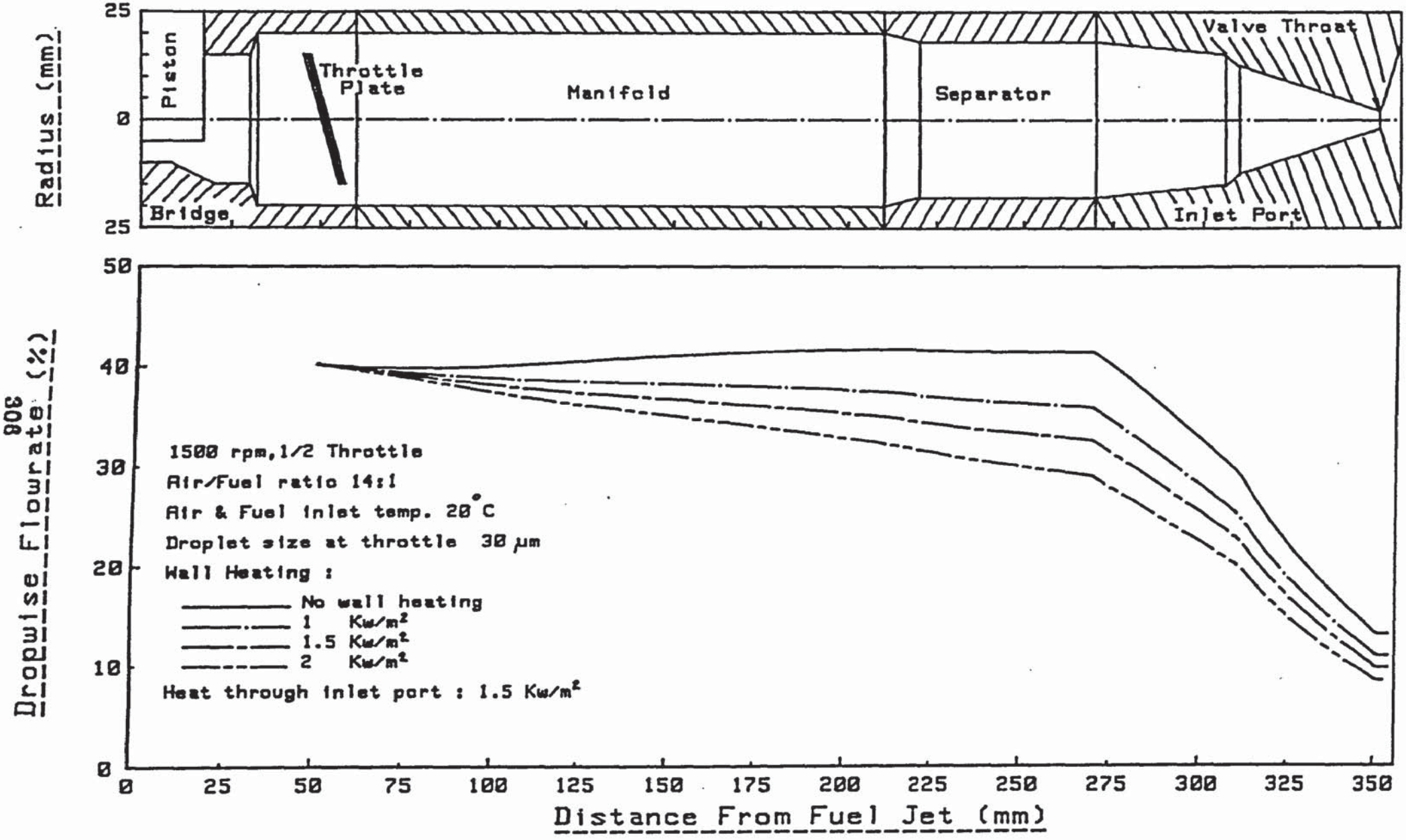

FIG. (7.30) Effect of Manifold Wall Heating on Dropwise Flowrate

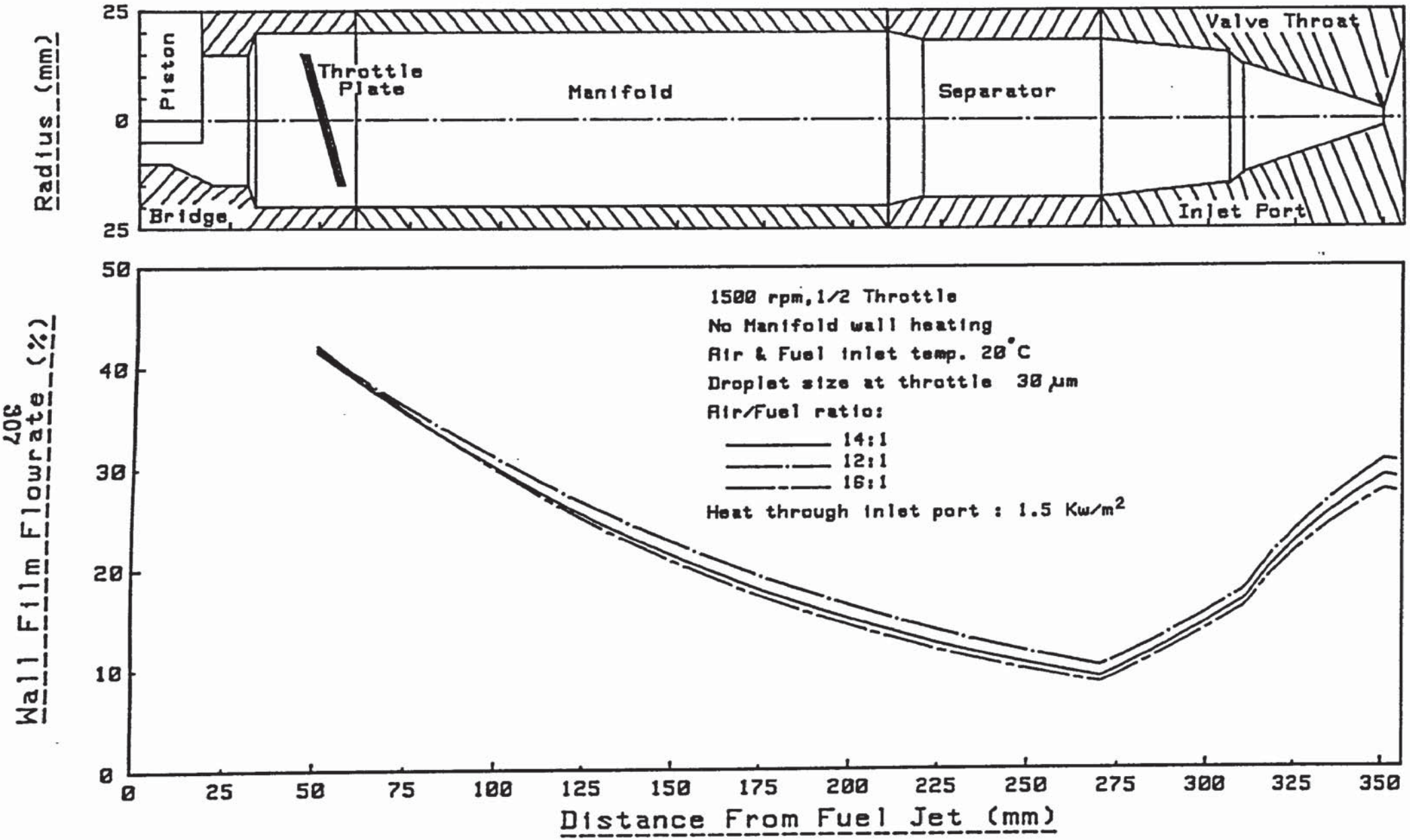

FIG. (7.31) Effect of Air/Fuel Mass Ratio on Wall Film Quantity

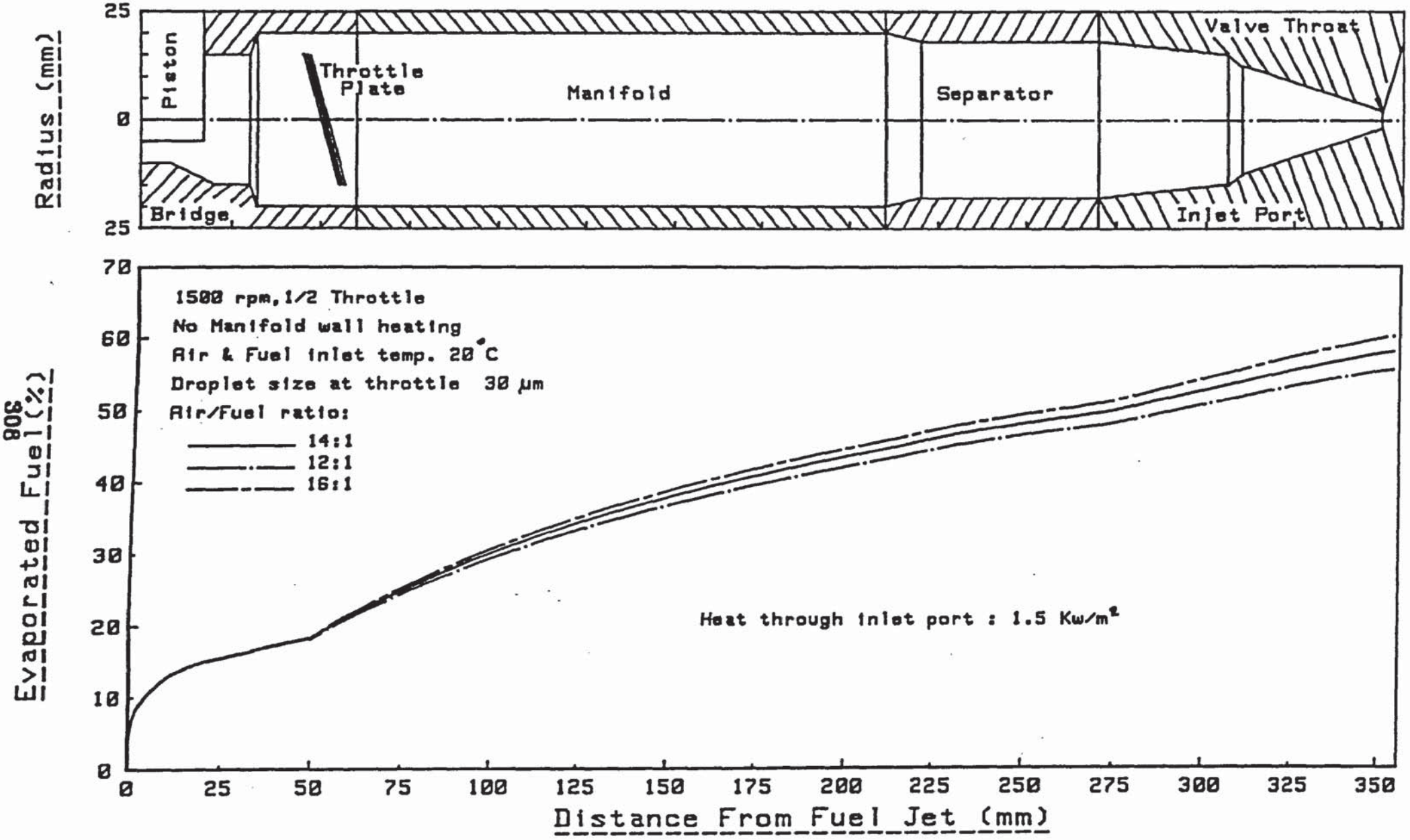

FIG. (7.32) Effect of Air/Fuel Mass Ratio on Fuel Evaporation

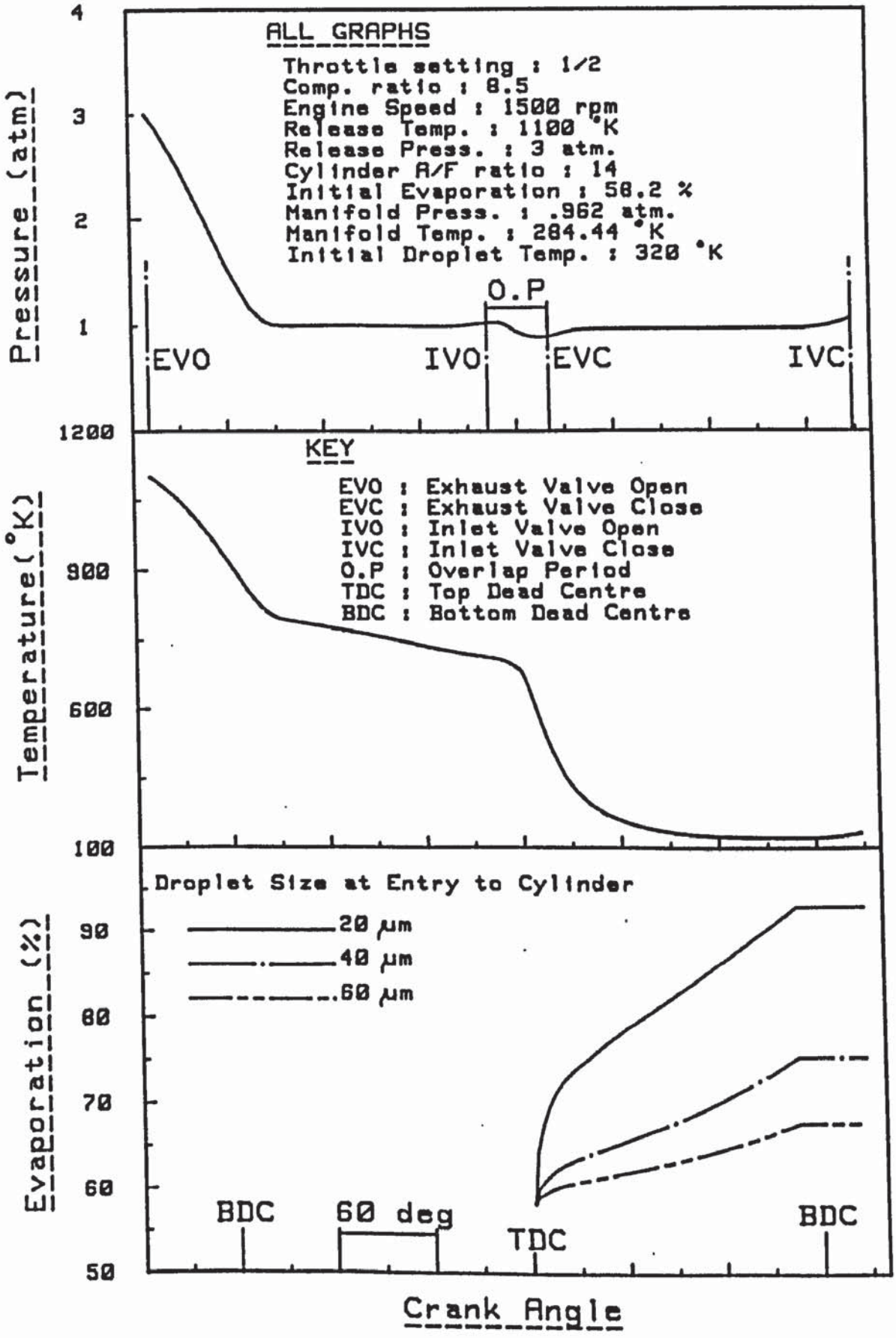

FIG. (7.33) Typical Variation of Cylinder Pressure, Temperature and Evaporation During The Gas Exchange Period

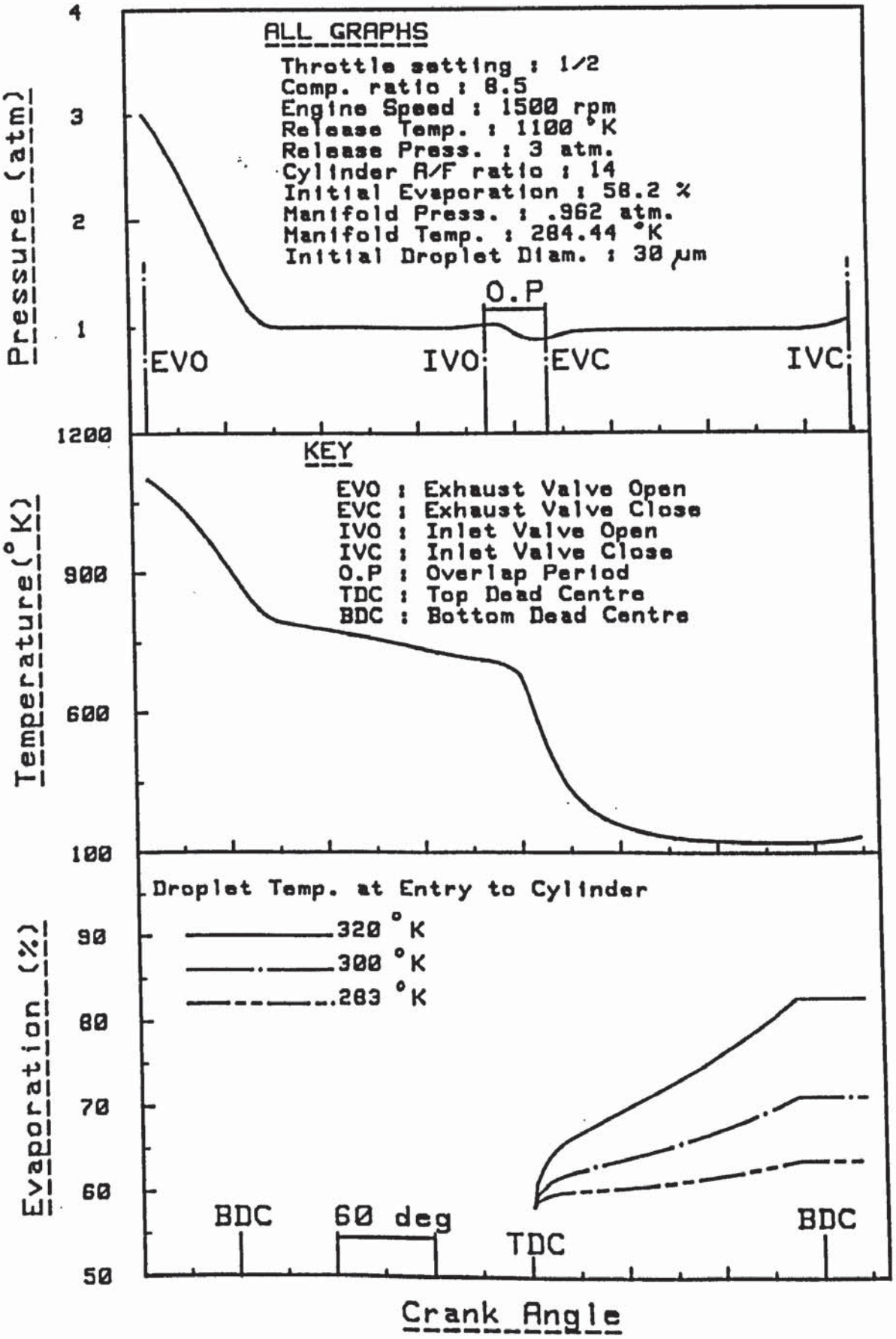

FIG. (7.34) Typical Variation of Cylinder Pressure, Temperature and Evaporation During The Gas Exchange Period

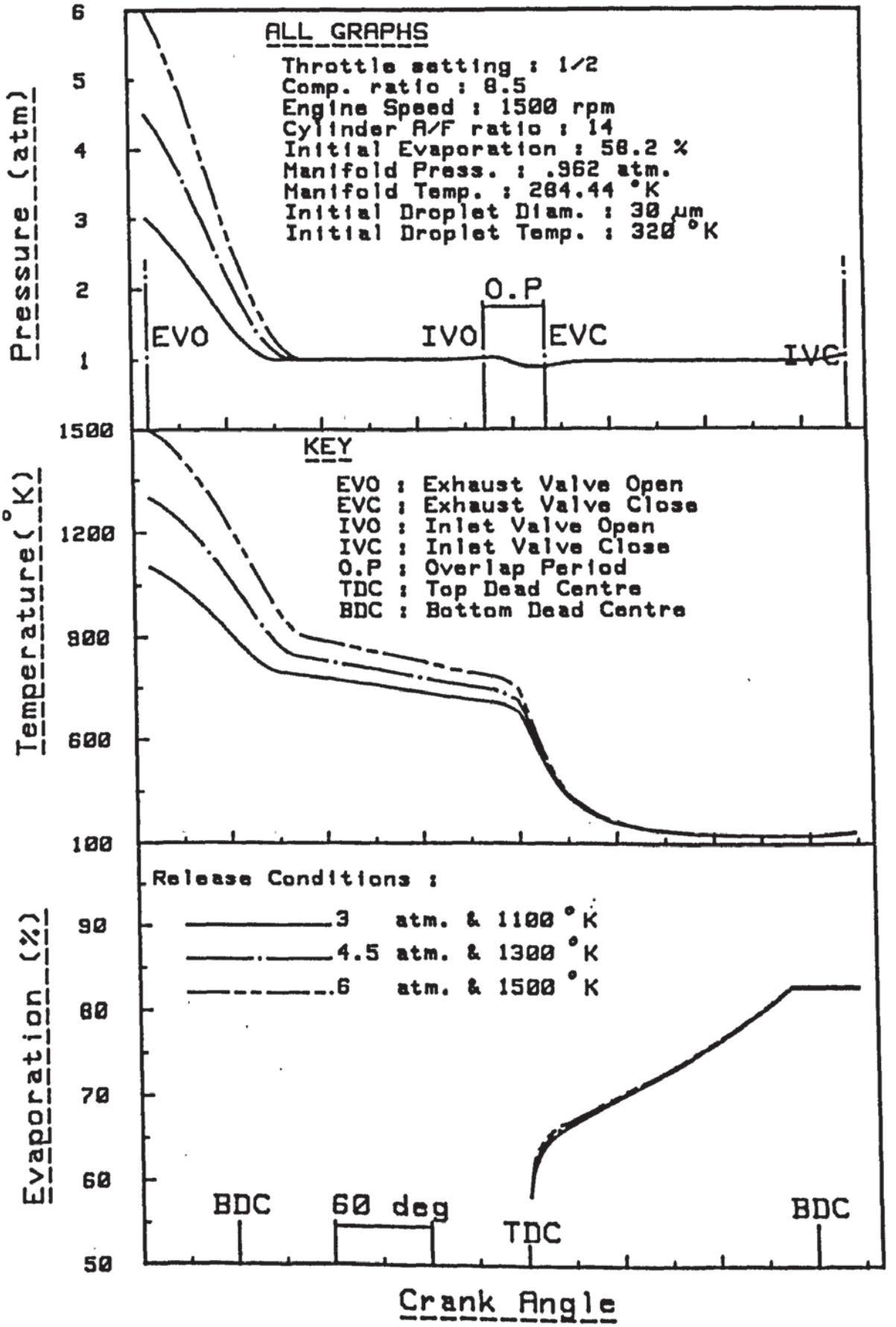

FIG. (7.35) Typical Variation of Cylinder Pressure, Temperature and Evaporation During The Gas Exchange Period

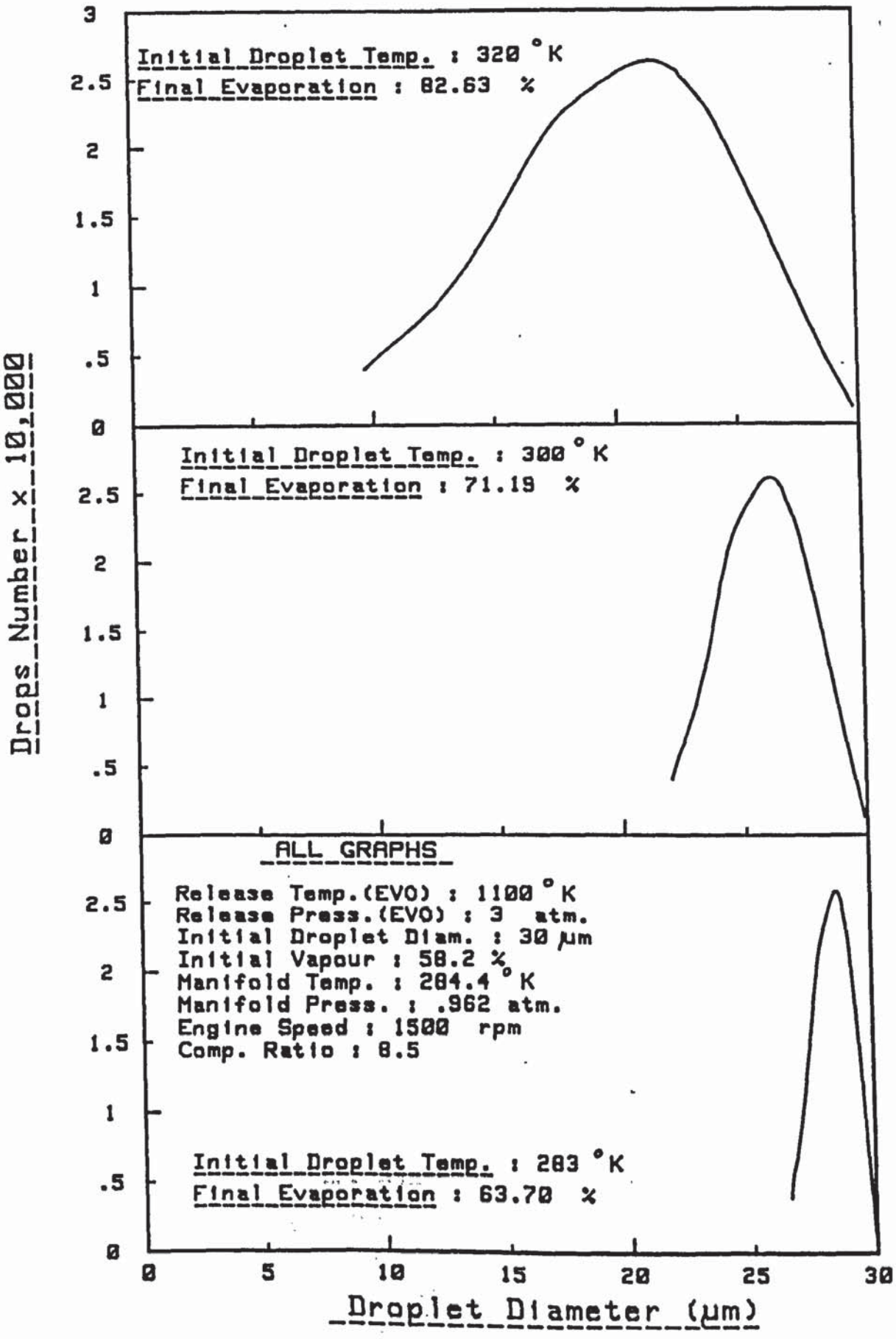

FIG. (7.36) Drops Number-Size Distribution at Trapped Point

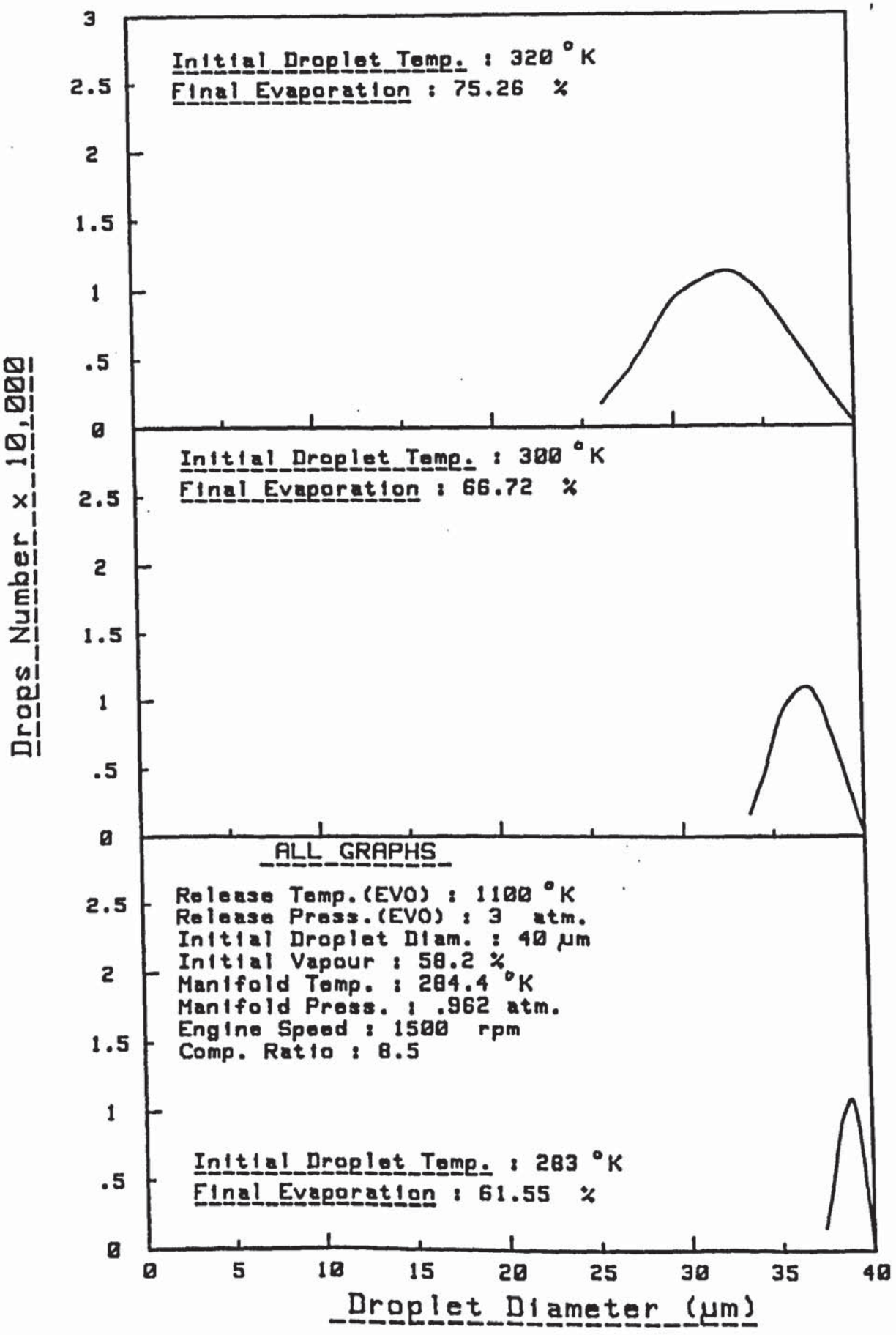

FIG. (7.37) Drops Number-Size Distribution at Trapped Point

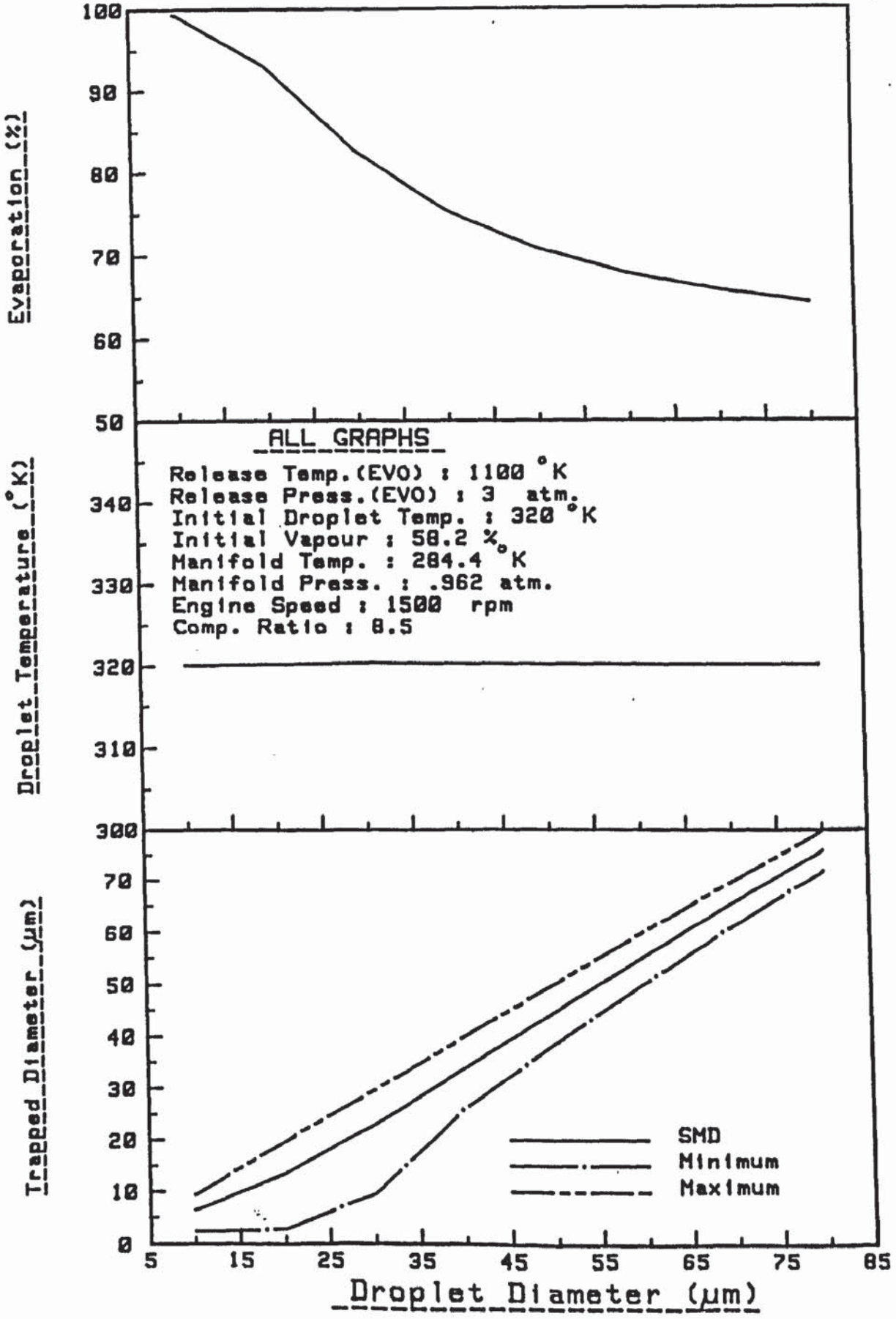

FIG. (7.38) Effect of Initial Droplet Size on Fuel Condition at the Trapped Point

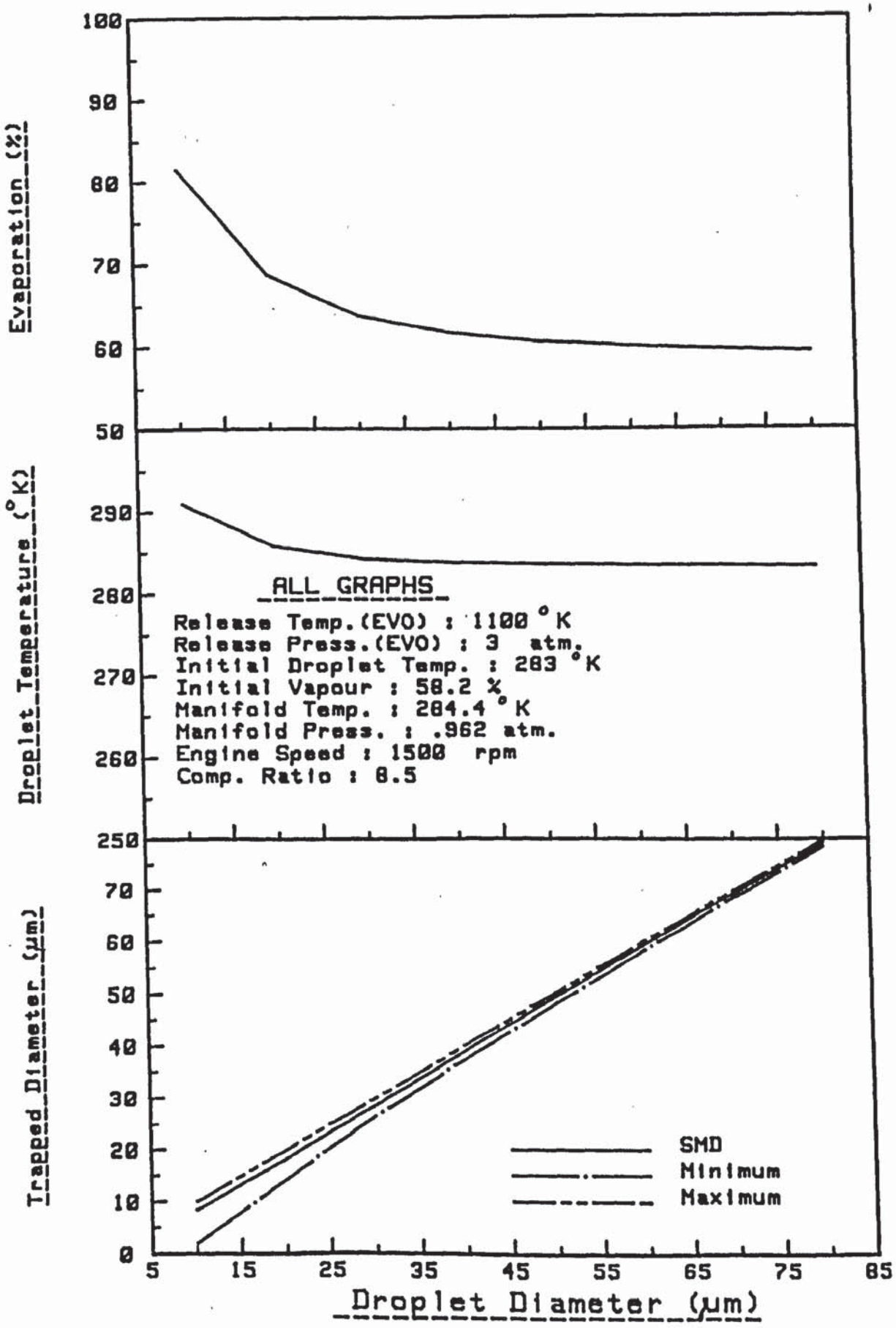

FIG. (7.39) Effect of Initial Droplet Size on Fuel Condition at the Trapped Point

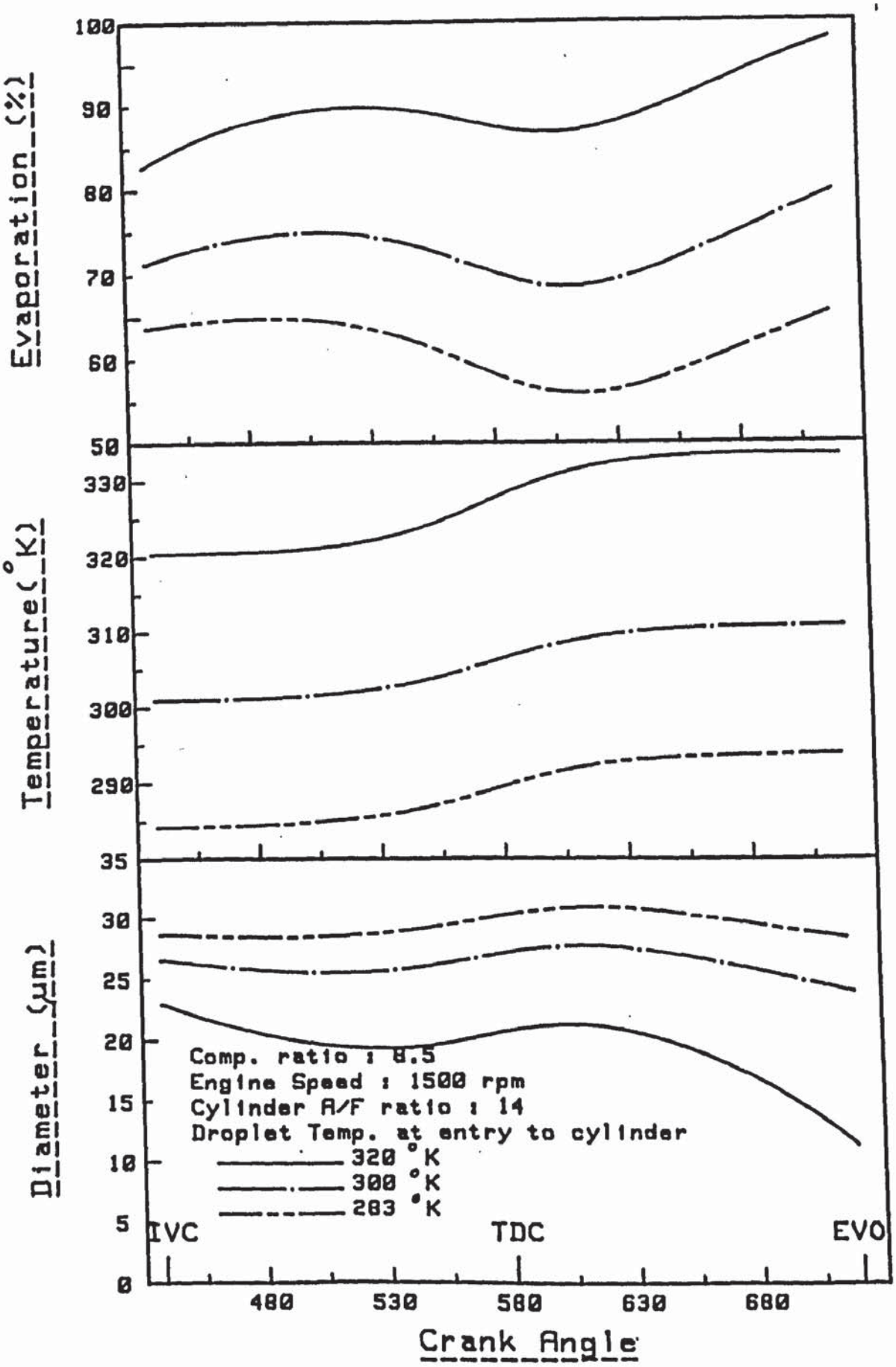

FIG. (7.40) Typical Variation of Droplet Parameters During Motoring

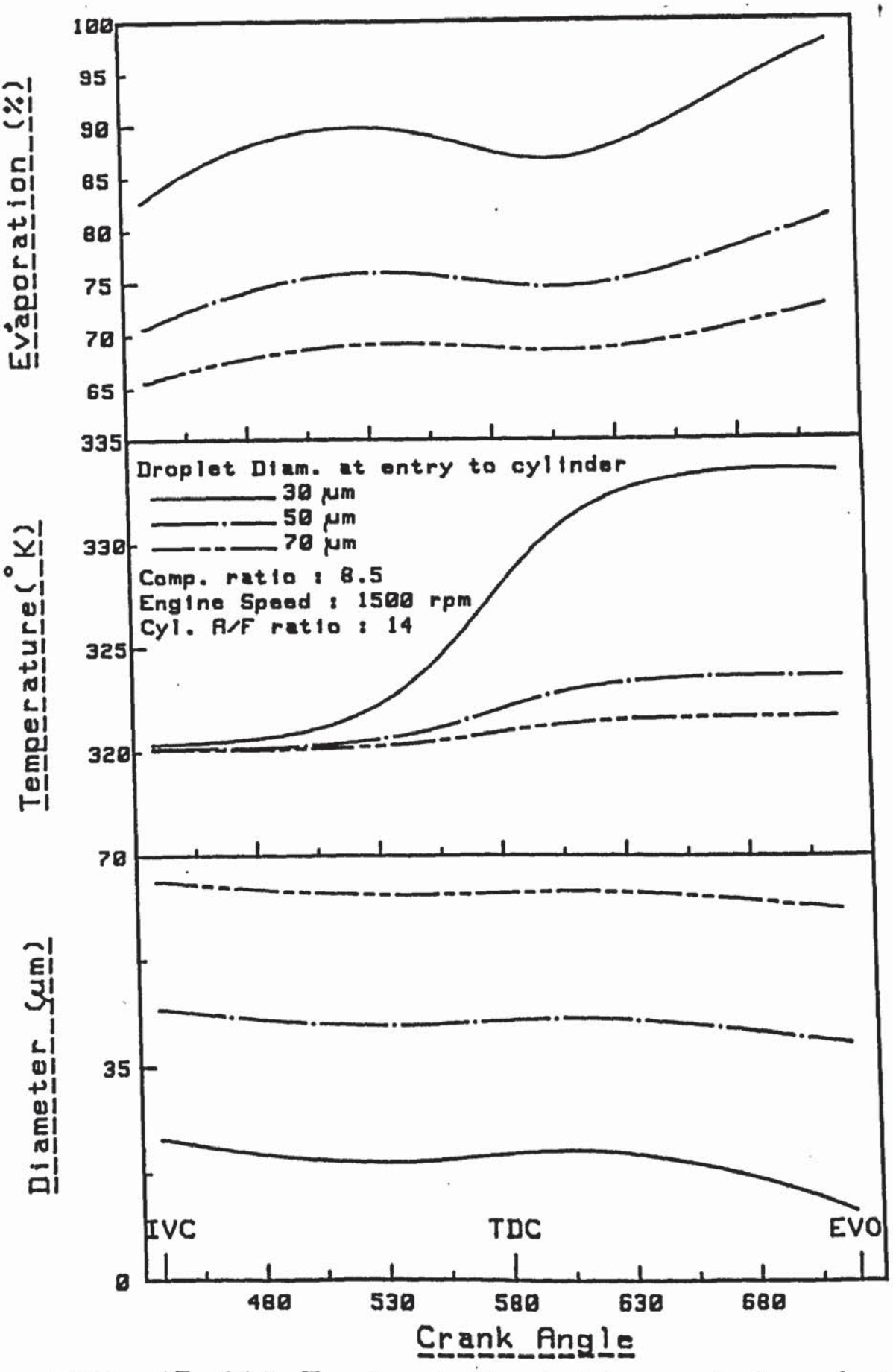

FIG. (7.41) Typical Variation of Droplet Parameters During Motoring

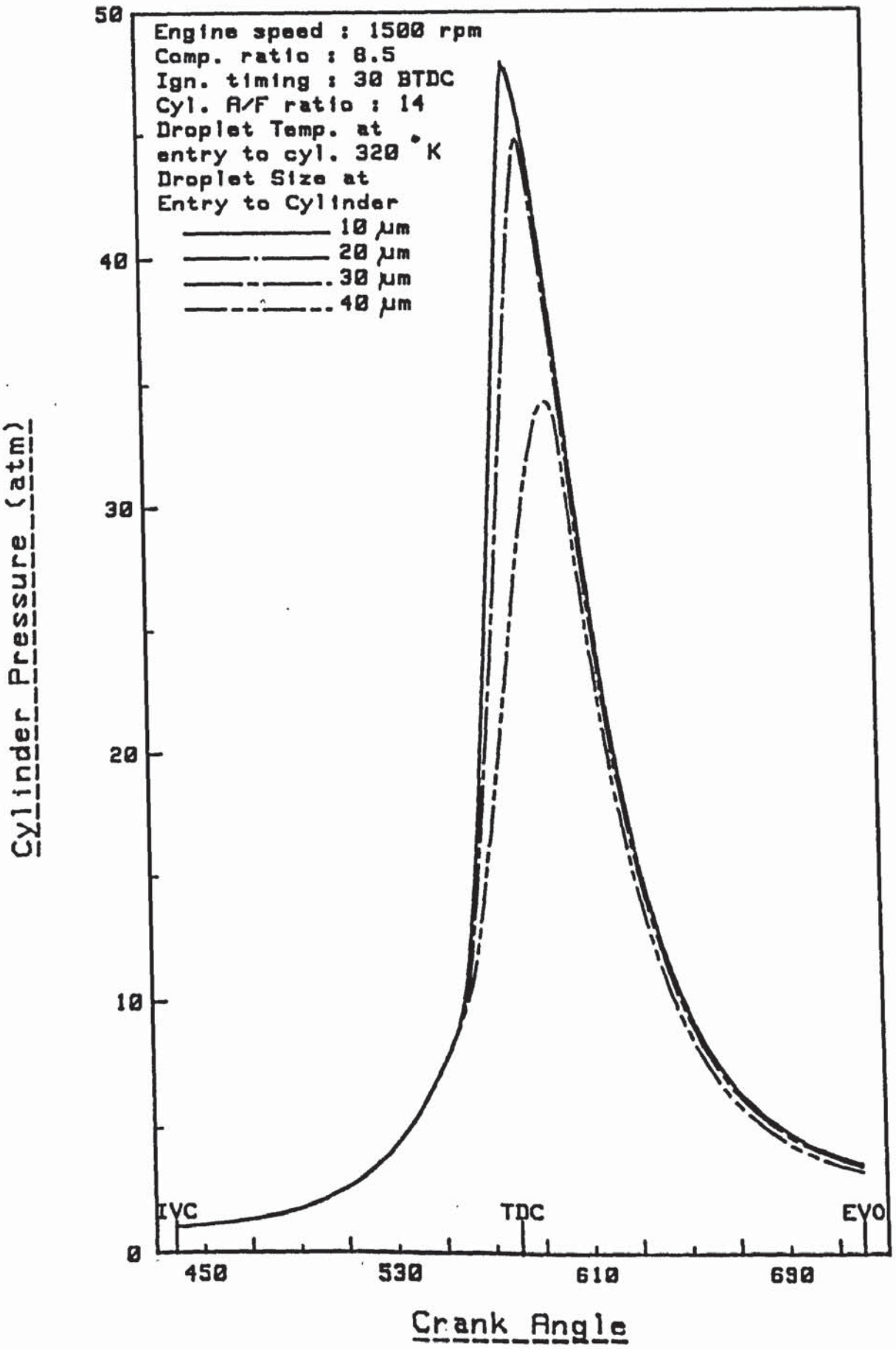

FIG. (7.42) Effect of Droplet Size on Cylinder Pressure

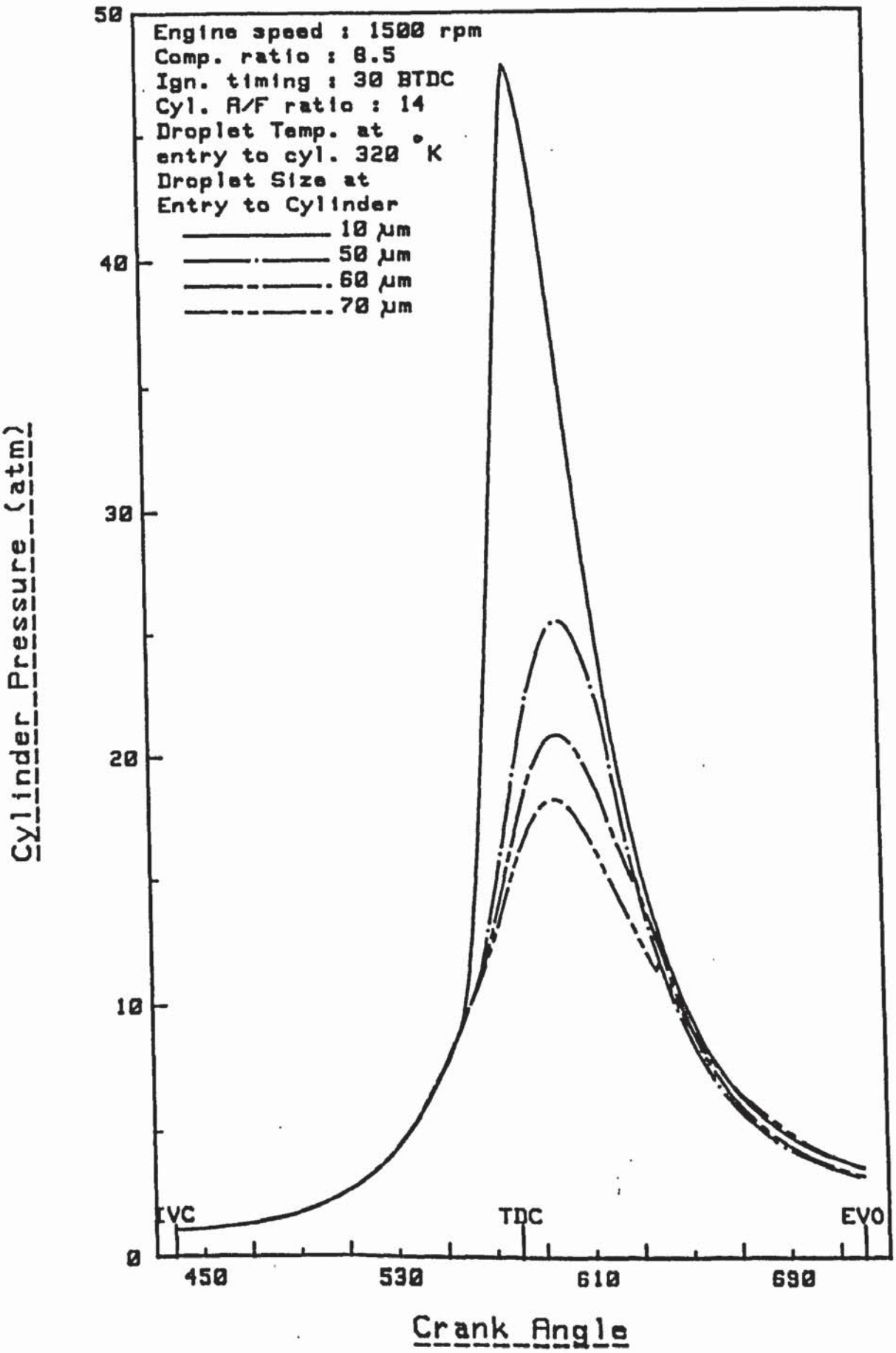

FIG. (7.43) Effect of Droplet Size on Cylinder Pressure

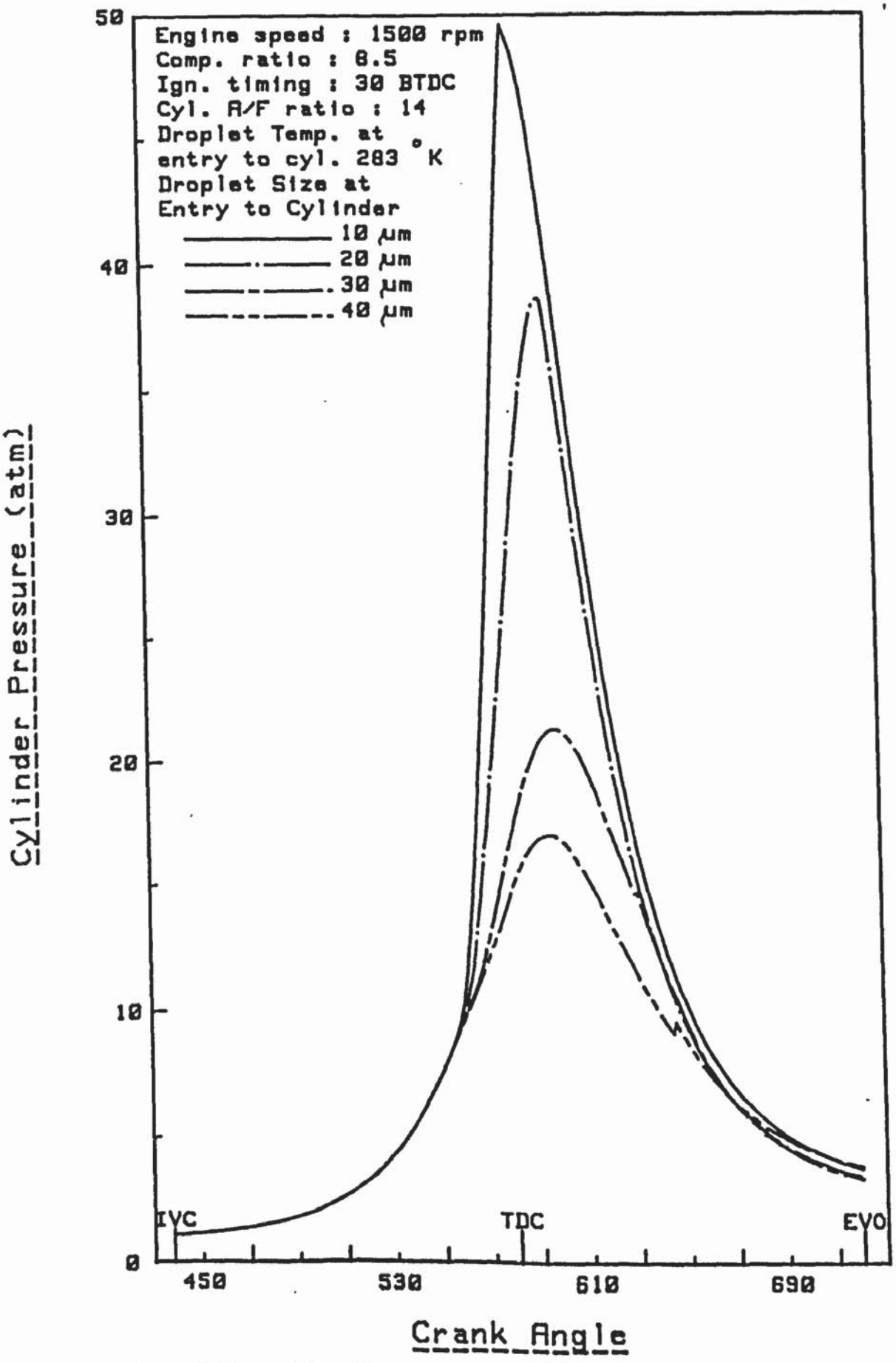

FIG. (7.44) Effect of Droplet Size on Cylinder Pressure

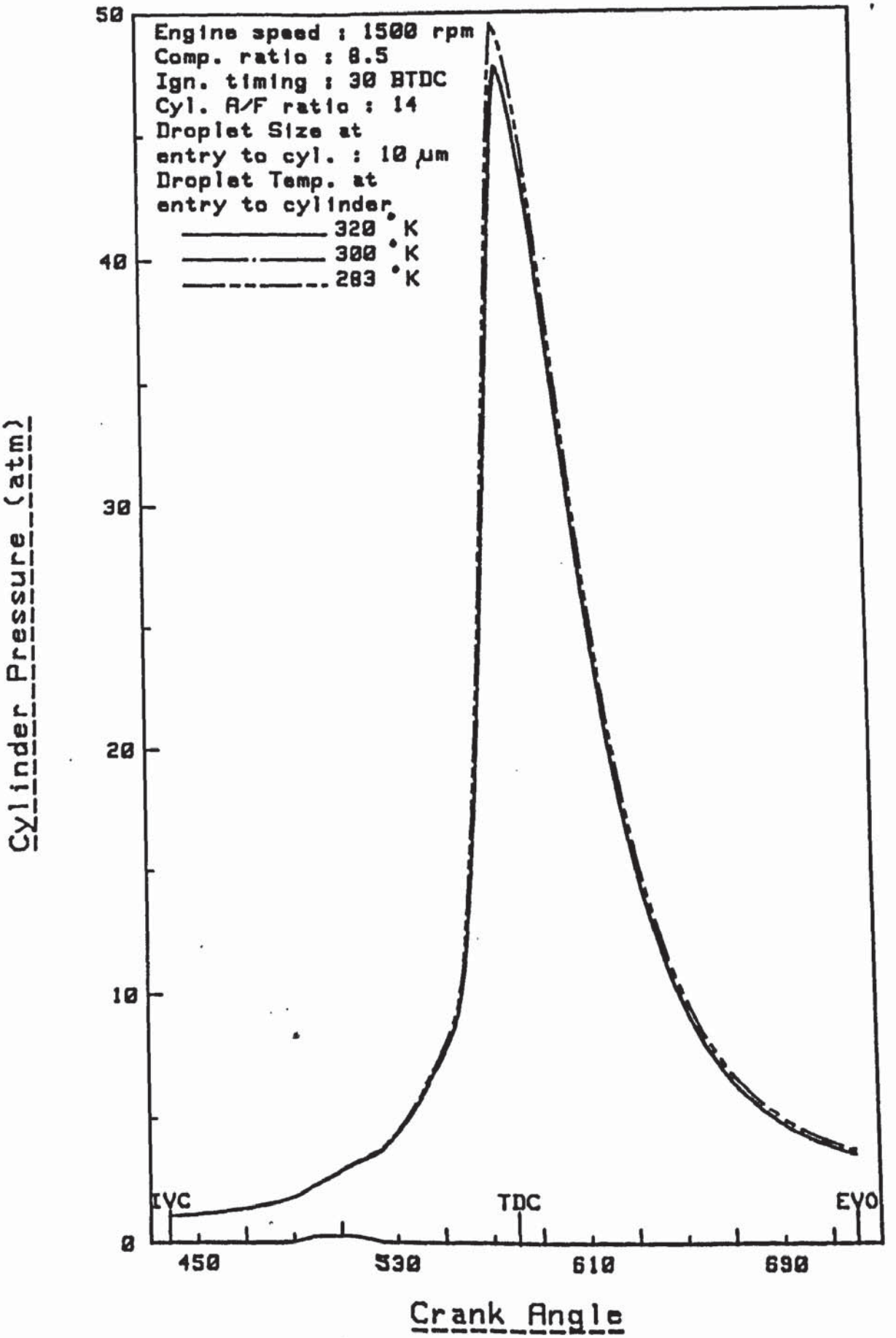

FIG. (7.45) Effect of Droplet Temp. on Cylinder Pressure

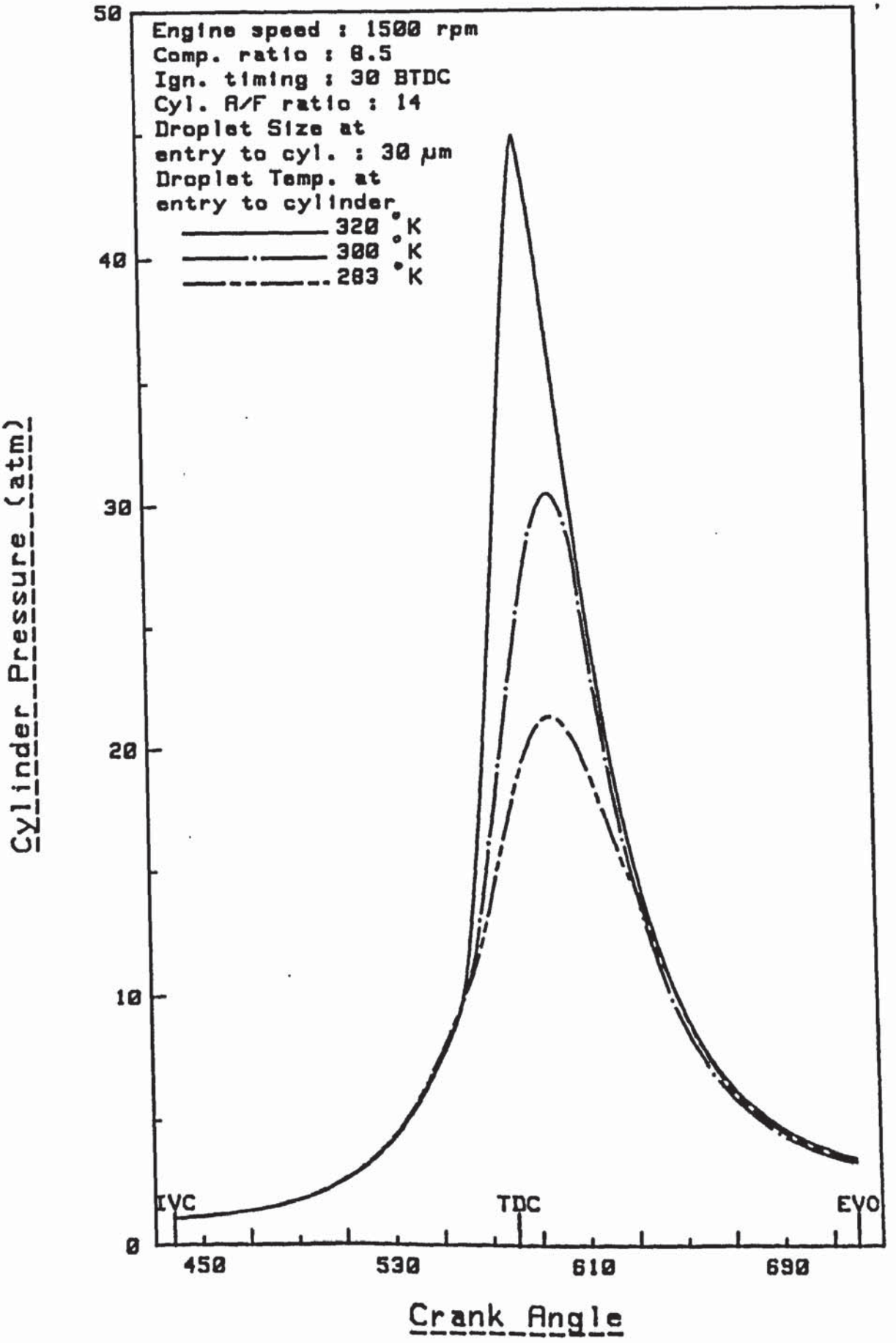

FIG. (7.46) Effect of Droplet Temp. on Cylinder Pressure

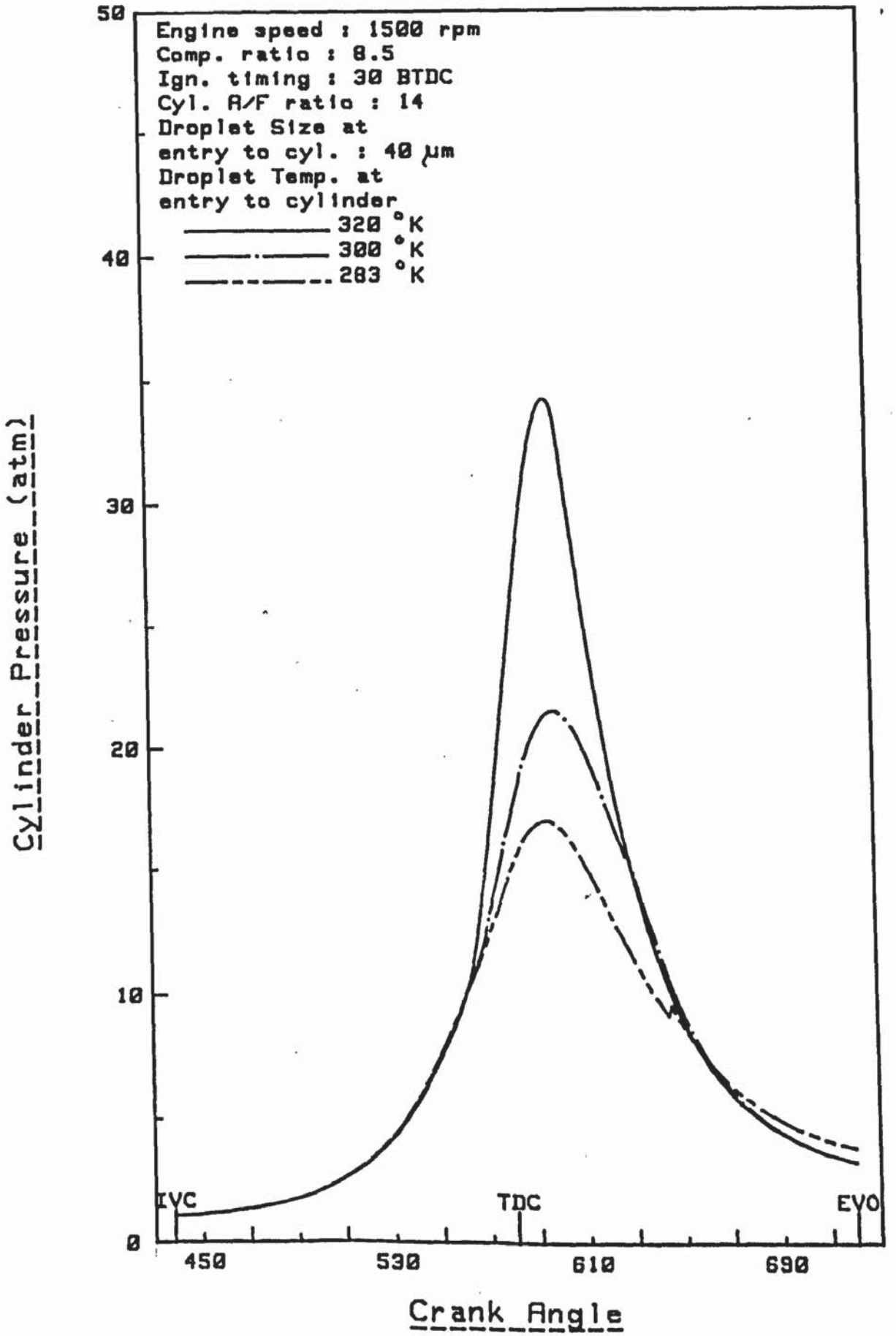

FIG. (7.47) Effect of Droplet Temp. on Cylinder Pressure

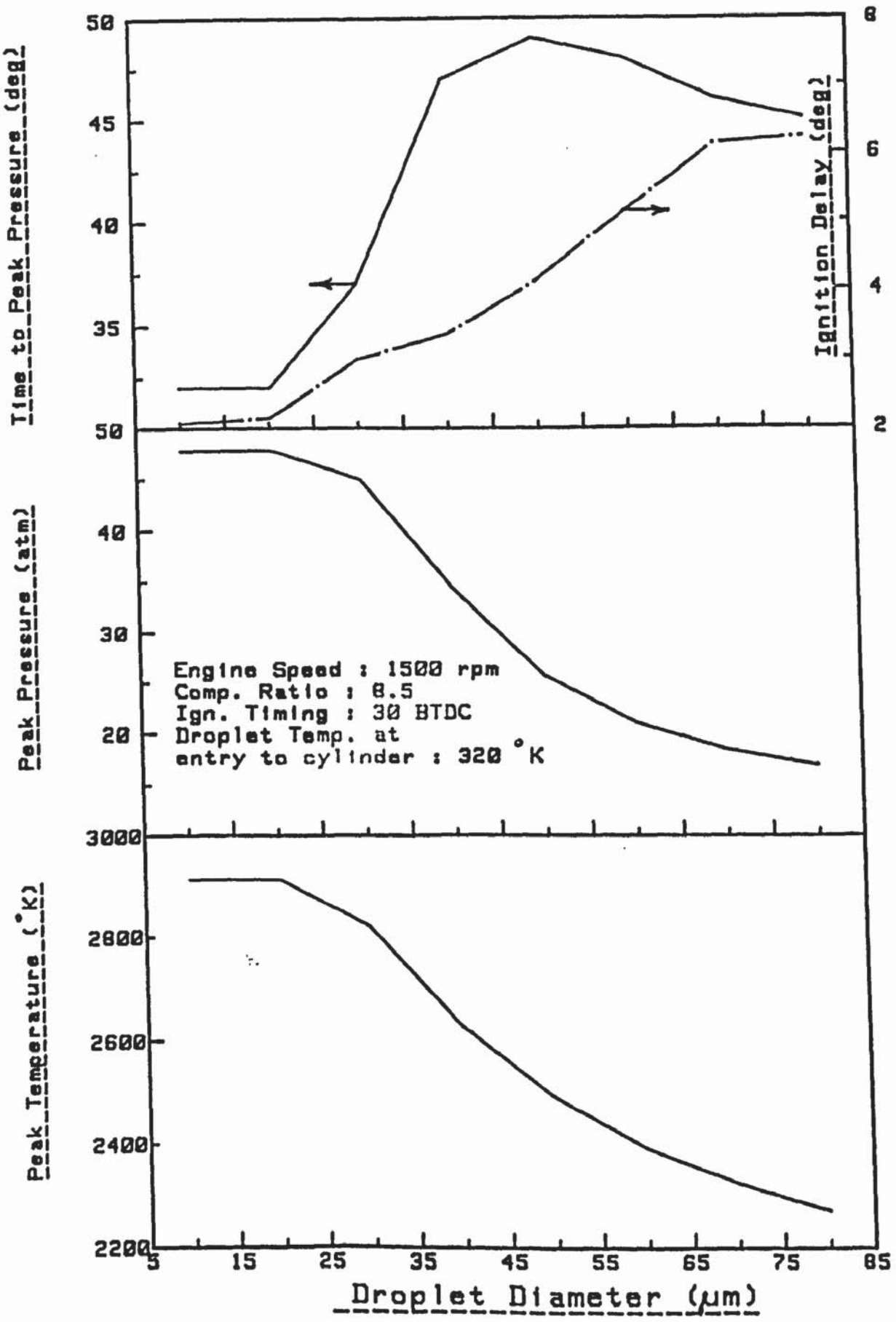

FIG. (7.48) Effect of Initial Droplet Size on Some Combustion Parameters

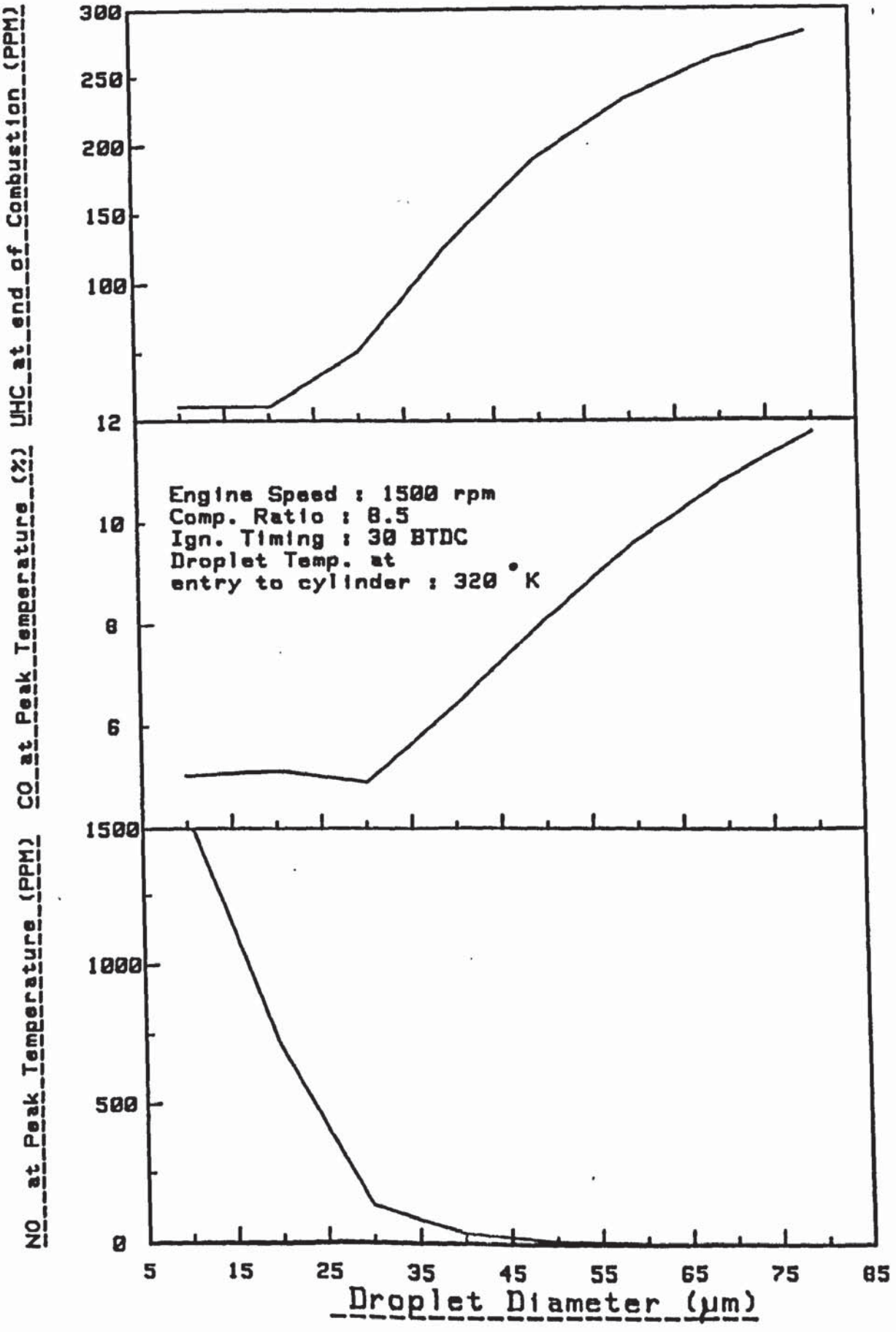

FIG. (7.49) Effect of Initial Droplet Size on Exhaust Emissions

CHAPTER EIGHT

CONCLUSIONS

8.1 General

The work identified at the outset of the project was to study the mixture preparation and combustion processes in a carburetted spark ignition engine through the combination of mathematical models and experimental data. The results of the experimental and theoretical investigations have been detailed and discussed in the relevant sections of this thesis. The problem was approached by means of a complete study of the liquid fuel life-cycle from the time of introduction to the air stream at the carburettor until this fuel is traversed by the flame front inside the engine cylinder.

An extensive literature survey revealed that:

(a) the composition of the liquid fuel has a powerful influence on both the mixture preparation and combustion processes. Many theoretical and experimental investigations have been carried out using single component fuels, the results of which cannot be extended and applied to the conventional fuels or engines. The conventional spark ignition engine fuel is a blend of a large number of chemical species with a wide range of boiling temperatures. The fuel model to be used in any realistic experimental or theoretical study should, therefore, represent this type of fuel.

(b) the combustible mixture is prepared in both the intake system and inside the engine cylinder. Within the intake system, the liquid fuel is present as droplets and liquid wall film. Many theoretical investigations on fuel evaporation and transportation in the intake system have neglected the presence of the liquid wall film despite its strong influence on the mixture preparation process.

(c) experimental investigations of the annular, two-phase, multicomponent flow found in the intake system of a running engine are greatly hindered by the difficulties arising in this type of flow. The measurements of the different phases in which the fuel is present in the intake system are strongly influenced by the high rate of fuel evaporation in addition to the highly pulsating and turbulent nature of the flow.

(d) previous theoretical analysis of the fuel evaporation and transportation in the intake system have failed to present an adequate model of liquid wall film formation and destruction. The rates of droplet deposition and entrainment are functions of may flow parameters and the difficulty in considering all these parameters leads to the use of empirical correlations of experimental data to calculate these rates. Such correlations are available in the literature for study

flows, but not for the flow found in the intake system.

(e) the gas exchange period of the engine cycle has been considered in many reported cycle simulations to serve as a period for the cylinder emptying and filling processes only. Liquid wall film disintigration at the inlet valve and fuel evaporation during the intake stroke have been ignored as the formulation of any model to include these processes is extremely difficult.

(f) previous modelling of the closed period of the cycle has been performed assuming that the working fluid is a homogeneous mixture of fuel vapour and air based on the belief that complete fuel evaporation is obtained during the carburation and intake processes. Experimental investigations have shown that fuel is not completely vaporised in the intake system. Different engine performance and exhaust emissions have been obtained when the liquid fuel is artificially evaporated in the inlet manifold.

Considering the points above, it was decided that the present research should include the following initiatives:

(a) using a multicomponent fuel through all stages of mixture preparation and combustion.

(b) fuel evaporation and transportation within the intake system to take into account the liquid wall film.

(c) a series of experimental investigations to study the effect on the liquid wall film quantity of different inlet manifold designs and engine operating conditions.

(d) the data may be used to derive a set of empirical equations to determine the quantity of the liquid wall film at the carburettor exit, the droplet deposition and entrainment rates and to define a bend factor.

(e) the experimental work to include a study of the liquid wall film effect on engine performance and emissions and to obtain a set of experimental data on engine performance and emissions to be used in testing the reliability of the models used in the theoretical study.

(f) to build a new theoretical model for the gas exchange period which takes into account fuel evaporation during the intake stroke and the liquid wall film disintigration at the inlet valve.

(g) to build new models for the compression, combustion and expansion phases of the cycle which includes fuel evaporation and the combustion of the liquid fuel droplets.

The points above have been completely fulfilled throughout the duration of the work leading to satisfactory experimental and theoretical results.

The experimental results indicated that:

(a) liquid wall film is mainly generated within the carburettor.

(b) at bends, droplet deposition is enhanced due to the high rate of impaction.

(c) liquid film flowrate decreases with the increase in air/fuel ratio and distance from the fuel jet (in a straight pipe manifold) and increases with the increase in engine speed.

(d) the throttle plate has a strong influence on liquid fuel distribution down stream of the plate. At sharp bends, however, the fuel is redistributed.

(e) at 1/4 throttle setting the liquid wall film is sheared off into the main stream in relatively large drops.

(f) the liquid wall film is mainly composed of heavier fuel fractions.

(g) the removal of the liquid wall film prior to entry to the cylinder reduces cycle to cycle variation and levels of exhaust emissions and improves engine power and specific fuel comsumption.

(h) the slit method used for liquid wall film flowrate measurement is a reliable method.

The comparison between the measured and predicted results indicated that:

(a) the rate of droplet deposition in the inlet port is very high due to the geometrical nature of the port.

(b) liquid wall film disintegration at the inlet valve occurs in relatively large droplets.

(c) there is a considerable effect of the total air/fuel ratio on the size of the droplets in the mixture.

(d) assuming that the emitted unburnt hydrocarbons as the sum of the fuel trapped in the quench layer of the combustion chamber and the liquid fuel droplets overtaken by the flame front is a valid assumption.

(e) the adopted mixture preparation and thermodynamic models are satisfactory

(f) the suggested wall film model is satisfactory.

(g) the prediction of CO and CO_2 is not satisfactory.

The results of the parametric study indicated that:

(a) droplet size has a considerable effect on mixture preparation processes in both the intake system and inside the engine cylinder.

(b) at normal operating conditions, droplets of sizes 20 μm or less at entry to the cylinder have no effect on engine performance and emissions (except NO emissions).

(c) the increasing cylinder pressure during compression reduces droplet evaporation and even causes fuel vapour condensation.

(d) there is an optimum droplet size for minimum CO emissions.

(e) to achieve the best overall results, the liquid film should be heated in the inlet port and atomized at the inlet valve to droplets with sizes 20 μm - 35 μm .

(f) droplets of sizes 15 μm or less can negotiate the geometry of the inlet port and produce less wall film.

(g) the programs which have been developed can be used to predict the effects of many operating conditions which would be very difficult to investigate on the test bed.

8.2 Conclusions

The complete life of a multicomponent liquid fuel has been studied in a carburetted spark ignition engine. A model of fuel evaporation and transportation in the intake system proposed by Boam and Finlay[42] has been extended to incorporate a new model of liquid wall film generation and destruction. The liquid wall film model is formulated from a set of empirical equations derived from experimental wall film flowrate measurements using different inlet manifold designs and engine operating conditions. Using these equations the liquid wall film quantity at the carburettor exit, the rates of droplet deposition and entrainment and a bend factor can be determined for any air/fuel ratio at any throttle plate setting.

A model for the gas exchange period of the cycle has been suggested. The model comprises two sub-models: a thermodynamic model based on the solution of the first law of thermodynamics for open systems and a droplet evaporation model adopted from Law[21]. In this model the cylinder is divided into numerous numbers of segments each of which is characterised by its own mass, number of droplets, droplet size and droplet temperature with a common cylinder pressure, temperature and fuel vapour concentration. The number of segments increases as the intake stroke proceeds and decreases if complete evaporation of the droplets in any segment occurs.

A number of models describing the different processes during the closed period of the cycle have been adopted and joined together to provide a complete model of the thermodynamic cycle based on the solution of the first law of thermodynamics for the closed system. The fuel evaporation model has been adopted from Law[21] and takes into account droplet heating and the effect of cylinder pressure on the evaporation rate.

Three computer programs have been developed and tested satisfactorily. It is concluded that:

1. The liquid wall film represents the major problem in the mixture preparation process due to its high quantity and low quality.

2. To reduce liquid wall film deposition at the bends and branch points, droplet sizes should be less than 15 μm .

3. Over-heating the liquid fuel prior to entry to the cylinder reduces the engine volumetric efficiency.

4. Smaller sized droplets produce higher cylinder pressures, higher cylinder temperatures and higher NO emissions, but they also lead to lower emissions of CO and unburnt hydrocarbons. The best overall results can be gained if droplet sizes at entry to the cylinder are in the range 20 μm - 35 μm .

5. At normal engine operating conditions the undesirable effects of the liquid wall film could be reduced considerably if the film was atomized into droplets of 20 μm or less.

8.3 Recommendations for Further Work

1. The present work was confined to a single cylinder engine operating at a maximum speed of 2000 rpm. As the air mass flowrate has a powerful influence on the mixture preparation processes it is recommended that the liquid wall film model be further tested using data obtained from a multi-cylinder engine.

2. The prediction of CO emissions was not satisfactory. It is recommended to change the rate constants used in the model or use a new set of rate equations.

3. The programs were written for a mini computer and consequently require long running times. They should be re-written to run on the University's main-frame computer.

APPENDICES

Appendix A: Thermodynamic Data and Properties of the Components Comprise the Working Fluid.

Appendix B: Liquid Fuel Film Thickness.

Appendix C: Geometry of Spherical Flame Propogation.

Appendix D: Determination of the Composition of Combustion Products.

Appendix E1: The 4th Order Runge-Kutta Method.

Appendix E2: Ignition and Initiation of Two Zones in the Combustion Chamber.

Appendix F: Program Listings.

Appendix A: Thermodynamic Data and Properties of the Components Comprise the Working Fluid

Since the analytical models for mixture preparation and spark ignition engine cycle presented in this study are designed to be simulated mathematically on a computer, it was desirable to estimate as many thermodynamic properties as possible from polynominal equations. Such a system would reduce the required computer storage capacity.

Ideal Gas Specific Heat

In consideration of the 12 species which are present in the combustion products (viz. N_2, O_2, CO_2, H_2O, CO, H_2, NO, OH, NH, O and Ar), the specific heat at constant pressure Cp, for each specie is approximated by a sixth-order polynomial over the temperature range 273-3000^{0}K and a forth order polynomial over the temperature range 3000-6000^{0}K. Thus,

$$Cp_K(T) = a_0 + a_1T + a_2T^2 + a_3T^3 + a_4T^4 + a_5T^5 + a_6T^6 \qquad (A.1)$$

for the temperature range 273-3000^{0}K, and

$$Cp_K(T) = b_0 + b_1T + b_2T^2 + b_3T^3 + b_4T^4 \qquad (A.2)$$

for the temperature range 3000-6000^{0}K

where:

$Cp_K(T)$ is the specific heat at temperature, T for the K^{th} specie (K = 1 to 12), (KJ/Kgmol^{0}K).

The coefficients are derived from polynomial fittings of tabulated data published in JANAF tables[175]. They are listed in tables A-1a and A-1b.

In addition, the Cp data for the 16 vapour fuel components are required. These are also expressed in polynomial form as follows:

$$Cp_i(T) = C_0 + C_1T + C_2T^2 + C_3T^3 \qquad (A.3)$$

The coefficients of this equation for each fuel component are given in Ref. (87), they are also shown in table A-2.

Enthalpy and Internal Energy

The enthalpy at a given temperature, h(T) is defined by

$$h(T) = \int Cp(T)d\,T \qquad (A.4)$$

The integration of eqns. A.1, A.2 and A.3 yields: (e.g. eqn. A.1)

$$h(T) = a_0T + a_1 + \frac{a_2}{2}T + \frac{a_3}{3}T^2 + \frac{a_4}{4}T^3 + \frac{a_5}{5}T^4 + \frac{a_6}{6}T^5 + A$$

or

$$h(T) = d_0 + d_1T + d_2T^2 + d_3T^3 + d_4T^4 + d_5T^5 + A \qquad (A.5)$$

The constant of integration, A is the sum of two parts, A_1 having a value for each gas to obtain h(298) = 0, and A_2 to include the enthalpy of formation. The values of A_1 and A_2 are given in table A-3a and A-3b for the 28 components of the working mixture.

The internal energy , u(T) is given by:

$$u(T) = h(T) - RT \qquad (A.6)$$

where R is the universal gas constant.

Thermal Conductivity and Viscosity

Unfortunately, thermal conductivity and viscosity data were not available for all the components of interest. The available data was only for N_2, O_2, CO_2, CO and H_2 which form the major components in the mixture. This data was fitted by third order polynomial equations, thus:

$$K = e_0 + e_1T + e_2T^2 + e_3T^3 \qquad (W/m^2{}^\circ K) \qquad (A.7)$$

and

$$\mu = f_0 + f_1T + f_2T^2 + f_3T^3 \qquad (Kg/m.s) \qquad (A.8)$$

The coefficients are given in tables A-4a and A-4b respectively.

Liquid Fuel Specific Heat

Many methods for estimating the specific heat of liquids have been reported in the literature. These are detailed in Ref. (87). The method used in the present work is that of Sternling and Brown, which relates the liquid specific heat of a component to it's gaseous specific heat, that is,

$$Cp_L = Cp_g + (4.155 = 18.28\omega)[3.67 + 11.64(1-T_r^4) + .634(1-T_r)^{-1}] \qquad (A.9)$$

where T_r is the reduced temperature

$$= \frac{T_L}{T_c}$$

T_c is the critical temperature,

T_L is the liquid temperature,

ω is the Pitzer acentric factor.

The values of T_c and ω for each fuel component are given in table A-5.

Liquid Fuel Density

Chueh and Prausnitz[133,134] correlated the liquid density with the system pressure, P, liquid temperature, T_L, critical-compressibility factor Z_c, critical pressure, P_c, critical temperature, T_c and the acentric factor, ω as:

$$w = \rho_s \left[1 + \frac{9 Z_c N (P-P_v)^{1/9}}{P_c}\right] \qquad (A.10)$$

where:

N is the function of the acentric factor and the reduced temperature, T_r:

$$N = (1-.89\omega)[\exp (6.9547 - 76.2853\ T_r + 191.306\ T_r^2$$

$$- 203.5472\ T_r^3 + 82.7631\ T_r^4)]$$

The term ρ_s refers to the saturated density at T_r and P_v. It is given by:

$$\frac{\rho_c}{\rho_s} = V_r^{(0)} + \omega V_r^{(1)} + \omega^2 V_r^{(2)}$$

The V_r, functions may be expressed as:

$$V_r^{(j)} = a_j + b_j T_r + C_j T_r^2 + d_j T_r^3 + e_j/T_r + f_j \ell n(1-T_r)$$

The coefficients are

j	a_j	b_j	c_j	d_j	e_j	f_j
0	.11917	.009513	.21091	-.06922	.0748	-.084476
1	.98465	-1.60378	1.82484	-.61432	-.34546	.087037
2	-.55314	-.15793	-1.01601	.34095	.46795	-.239938

The values for V_c (= $1/\rho_c$), Z_c and P_c for the 16 fuel components are given in table A-5.

The remaining fuel properties of interest are the heat of combustion and the latent heat of evaporation. These are shown in table 3.1.

Ideal Mixture Properties

Properties of ideal mixtures (liquids or gases) are estimated using the general formula:

$$X_{mix} = \sum_{i=1}^{n} X_i \, M_{fi} \qquad \text{(A.11)}$$

where:

X is any property

M_{fi} is the mole fraction of component i.

Species	a_0	a_1	a_2	a_3	a_4	a_5	a_6
N2	31.91925	−.02078772	4.95996E−5	−4.30281E−8	1.869462E−11	−4.07381E−15	3.54647E−19
O2	27.66771	−4.739E−5	2.68353E−5	−3.33812E−8	1.78445E−11	−4.47712E−15	4.31741E−19
CO2	19.2473	.0787683	−7.39649E−5	4.2335E−8	−1.46555E−11	2.80369E−15	−2.26187E−19
H2O	33.31431	−5.3853E−3	2.50642E−5	−1.53772E−8	4.0347E−12	−4.2893E−16	7.519E−21
CO	31.55638	−.01999556	5.20741E−5	−4.75709E−8	2.150682E−11	−4.83929E−15	4.32525E−19
H2	26.83824	.01296369	−2.8508E−5	3.15516E−8	−1.627073E−11	3.99155E−15	−3.78677E−19
NO	32.47533	−.02263879	6.04173E−5	−5.76354E−8	2.706673E−11	−6.28542E−15	5.76526E−19
OH	31.59991	−.01580704	3.21212E−5	−2.27245E−8	8.01282E−12	−1.40907E−15	9.8088E−20
N	20.784592	1.224E−5	−3.461E−8	4.45E−11	−2.69E−14	6.24E−18	−1.39E−22
H	20.786112	0	0	0	0	0	0
O	24.232911	−.01228471	1.877297E−5	−1.49806E−8	6.48949E−12	−1.4436E−15	1.29253E−19
Ar	20.786112	0	0	0	0	0	0

Cp (KJ/Kgmol.°K) & T =273−3000 (°K)

Table (A.1a) Specific Heat Polynomial Coefficients

Species	b_o	b_1	b_2	b_3	b_4	b_5	b_6
N2	31.778	3.4336E−3	−7.903E−7	.8755E−10	−3.474E−15	0	0
O2	32.2127	2.6186E−3	2.663E−7	−1.1847E−10	8.541E−15	0	0
CO2	52.4616	6.3563E−3	−14.649E−7	1.6187E−10	−6.044E−15	0	0
H2O	31.8323	15.391E−3	−34.66E−7	3.7375E−10	−15.262E−15	0	0
CO	32.7492	2.8562E−3	−6.503E−7	.7467E−10	−3.257E−15	0	0
H2	28.7557	3.3083E−3	−1.561E−7	−.1255E−10	1.539E−15	0	0
NO	33.5535	2.5399E−3	−5.969E−7	.7164E−10	−3.336E−15	0	0
OH	29.4424	5.2015E−3	−11.38E−7	1.3222E−10	−5.968E−15	0	0
N	22.1131	−.2143E−3	−4.9853E−7	1.903E−10	−14.25E−15	0	0
H	20.786112	0	0	0	0	0	0
O	22.8182	−1.9186E−3	5.8824E−7	−.581E−10	1.7956E−15	0	0
Ar	20.786112	0	0	0	0	0	0

Cp (KJ/Kgmol.°K) & T =3000−6000 (°K)

Table (A.1b) Specific Heat Polynomial Coefficients

No	Formula	Name	C_o	C_1	C_2	C_3
1	C_3H_8	Propane	-.241157	1.748E-2	-9.056E-6	1.835E-9
2	C_4H_{10}	Iso-Butane	-7.93E-2	2.196E-2	-1.053E-5	1.853E-9
3	C_4H_{10}	N-Butane	.541587	1.891E-2	-6.326E-6	-1.61E-10
4	C_5H_{12}	2-Methyl Butane	-9.5186	.506264	-27.27E-5	5.7195E-8
5	C_5H_{12}	N-Pentane	-3.62334	.487017	-25.78E-5	5.3011E-8
6	C_5H_{10}	2-Methyl-2 Butene	11.79469	.350661	-11.16E-5	-.5803E-8
7	C_6H_{14}	2-Methyl Pentane	-10.5604	.617976	-35.7E-5	8.0793E-8
8	C_6H_{14}	N-Hexane	-4.40993	.581576	-31.16E-5	6.4894E-8
9	C_6H_6	Benzene	-33.8948	.474047	-30.15E-5	7.1253E-8
10	C_7H_{16}	2,3-Dimethyl Pentane	-7.04167	.683247	-37.32E-5	7.8283E-8
11	C_7H_{16}	N-Heptane	-5.14213	.675716	-36.48E-5	7.6525E-8
12	C_7H_8	Toluene	-24.3383	.5121216	-27.63E-5	4.9078E-8
13	C_8H_{10}	M-Xylene	-29.1457	.6292736	-37.44E-5	8.4726E-8
14	C_9H_{12}	3-Ethyl Toluene	-28.9784	.7288528	-43.59E-5	9.9914E-8
15	C_9H_{12}	Pseudo Cumene	-4.86516	.623416	-32.6E-5	6.3722E-8
16	$C_{10}H_{14}$	N-Butyl Benzene	-22.9743	.792868	-43.93E-5	8.5645E-8

Cp (KJ/Kgmol.°K) & T=273-1750 (°K)

Table (A.2) Specific Heat Polynomial Coefficients

No	Species	A_1	A_2
1	N2	−8949.94	0
2	O2	−8421.66	0
3	CO2	−8657.60	−393172
4	H2O	−9881.17	−238919
5	CO	−8891.08	−113888
6	H2	−8376.94	0
7	NO	−8937.30	89872.32
8	OH	−8957.06	1316077
9	N	−6194.12	472792
10	H	−6194.26	216026.2
11	O	−6814.89	246809.9
12	Ar	−6194.26	0

Table (A.3a) The Constants of Integration of Eqn.(A.5).

No	Formula	Name	A_1	A_2
1	C_3H_8	Propane	-628.162	-81512.68
2	C_4H_{10}	Iso-Butane	-861.822	-102934.7
3	C_4H_{10}	N-Butane	-945.02	-97621.08
4	C_5H_{12}	2-Methyl Butane	-17349.32	-119913.4
5	C_5H_{12}	N-Pentane	-18374.65	-114097.6
6	C_5H_{10}	2-Methyl-2 Butene	-18089.09	-15384.56
7	C_6H_{14}	2-Methyl Pentane	-21302.34	-134222.7
8	C_6H_{14}	N-Hexane	-21887.65	-129620.3
9	C_6H_6	Benzene	-8428.954	100416
10	C_7H_{16}	2,3-Dimethyl Pentane	-25101.65	-158992
11	C_7H_{16}	N-Heptane	-25403.29	-144975.6
12	C_7H_8	Toluene	-13145.39	73220
13	C_8H_{10}	M-Xylene	-16119.36	45714.3
14	C_9H_{12}	3-Ethyl Toluene	-20078.14	31769.11
15	C_9H_{12}	Pseudo Cumene	-23540.09	18694.11
16	$C_{10}H_{14}$	N-Butyl Benzene	-24652.09	24643.76

Table (A.3b) The Constants of Integration of Eqn.(A.5).

No	Species	e_0	e_1	e_2	e_3
1	N2	7.273E-3	6.934E-5	-1.61E-8	2.1E-12
2	O2	3.731E-3	8.05E-5	-1.54E-8	2.43E-12
3	CO2	-1.14E-2	9.908E-5	-2.64E-8	5.63E-12
4	H2O	-6.92E-3	7.268E-5	3.475E-8	-1.2E-11
5	CO	.681E-3	9.032E-5	-3.39E-8	9.41E-12
6	H2	3.75E-2	5.385E-4	-2.3E-7	8.61E-11

K (W/m.°K) & T=273-1500 (°K)

Table (A.4a) Thermal Conductivity Polynomial Coefficients.

No	Species	f_0	f_1	f_2	f_3
1	N2	4.336E-6	5.2E-8	-1.95E-11	4.58E-15
2	O2	2.962E-6	6.077E-8	-2.88E-11	7.208E-15
3	CO2	-1.02E-6	6.077E-8	-2.37E-11	5.032E-15
4	H2O	-5.93E-6	5.122E-8	-1.13E-11	3.616E-15
5	CO	3.503E-6	5.473E-8	-2.21E-11	5.622E-15
6	H2	3.423E-6	1.974E-8	-3.34E-12	4.709E-15

u (Kg/m.s) & T=273-1500 (°K)

Table (A.4b) Dynamic Viscosity Polynomial Coefficients.

Tc = Critical temperature, °K
Pc = Critical pressure, atm
Vc = Critical volume, cm /gm.mol
Zc = Critical compressibility
$\acute{o}$ = Pitzer's acentric factor

No	Formula	Name	Tc	Pc	$\acute{o}$	Vc	Zc
1	C_3H_8	Propane	369.8	41.9	.152	203	.281
2	C_4H_{10}	Iso-Butane	408.1	36	.176	263	.283
3	C_4H_{10}	N-Butane	425.2	37.5	.193	255	.274
4	C_5H_{12}	2-Methyl Butane	460.2	33.4	.227	306	.262
5	C_5H_{12}	N-Pentane	469.6	33.3	.251	304	.262
6	C_5H_{10}	2-Methyl-2 Butene	470	34	.285	318	.28
7	C_6H_{14}	2-Methyl Pentane	479.5	29.7	.279	367	.267
8	C_6H_{14}	N-Hexane	507.4	29.3	.296	370	.26
9	C_6H_6	Benzene	562.1	48.3	.212	259	.271
10	C_7H_{16}	2,3-Dimethyl Pentane	537.3	28.7	.299	393	.256
11	C_7H_{16}	N-Heptane	540.2	27	.351	432	.263
12	C_7H_8	Toluene	591.7	40.6	.257	376	.264
13	C_8H_{10}	M-Xylene	617	35	.331	316	.26
14	C_9H_{12}	3-Ethyl Toluene	637	28	.36	490	.26
15	C_9H_{12}	Pseudo Cumene	649.1	31.9	.39	430	.258
16	$C_{10}H_{14}$	N-Butyl Benzene	660.5	28.5	.392	497	.261

Table (A.5) Critical Properties of Fuel Components

Appendix B: Liquid Fuel Film Thickness

It is assumed that the liquid fuel film is uniformly distributed around the manifold periphery, and that the velocity at the surface of the film flow is $2V_f$ [44] (V_f is the mean velocity of the film flow) then the film mass flowrate, $\dot{m}_{ff}$ is given by:

$$\dot{m}_{ff} = \pi D_m h \, V_f \rho_f \qquad \text{(B.1)}$$

where:

D_m is the manifold diameter

h is the thickness of the liquid film.

To find a relationship between V_f and h the following assumptions, which are similar to those used in reference (42), are made:

(i) the shear stresses at the main-stream and liquid film interface are equal.

(ii) the shear stress in the gas phase, τ_g, is related to its pressure drop, ΔP, as follows:

$$\tau = \frac{\Delta P}{L} \frac{H_g}{4} \qquad \text{(B.2)}$$

with

$$\frac{\Delta P}{L} = \frac{2 f_g \rho_g U_g^2}{H_g} \qquad (B.3)$$

where:

H_g is the hydraulic diameter of the gas phase

f_g is the gas phase friction factor.

Eqn. (B.2) thus becomes

$$\tau_g = \frac{f_g \rho_g U_g^2}{2} \qquad (B.4)$$

The shear stress of the film flow is given by:

$$\tau_f = \mu_f \frac{dV_f}{dy} \qquad (B.5)$$

where:

μ_f is the viscosity of the fuel in the film

dV_f / dy is the velocity gradient of the film flow.

since

$$\tau_f = \tau_g$$

eqns. B.4 and B.5 may be combined to yield:

$$\mu_f \frac{dV_f}{dy} = \frac{f_g \rho_g U_g^2}{2} \qquad (B.6)$$

The above equation can be integrated with the boundary conditions of $V_f(0) = 0$ and $V_f(h) = 2V_f$. One obtains:

$$V_f = \frac{f_g \rho_g U_g^2}{4\mu_f} h \qquad (B.7)$$

Substituting eqn. B.7 in eqn. B.1 the mass flowrate of the liquid film and the film velocity can be expressed as:

$$\dot{m}_{ff} = \pi D_m \rho_g \frac{f_g \rho_g U_g^2}{4\mu_f} h^2 \qquad (B.8)$$

or

$$V_f = \left(\frac{\dot{m}_{ff} f_g \rho_g U_g^2}{4\pi \mu_f D_m \rho_f}\right)^{.5} \qquad (B.9)$$

Appendix C: Geometry of Spherical Flame Propagation

In the simulation model of the engine cycle it is assumed that the flame front propogates spherically outwards from the ignition point. In order to estimate the rates of heat release and transfer, relationships are needed expressing the burnt zone volume, flame front area and wall surface area surrounding the burnt zone in terms of the flame radius.

The geometry of the combustion chamber of the Ricardo E6 engine is shown schematically in Fig. C.1. The chamber is a right circular cylinder of diameter,D and a variable height, h:

$$h = h_o = \frac{1}{2}s(1-\cos\theta) \qquad (C.1)$$

where:

h_o is the clearance height,

s is the engine stroke,

θ is the crank angle relative to TDC.

A spherical flame front of radius, r originates at a point on the upper flat surface of distance, a, from the edge will propagate through four different regions before traversing all the combustion chamber, that is:

$r \leq a$

$a < r \leq \sqrt{(a^2 + h^2)}$

$\sqrt{(a^2 + h^2)} < r \leq D-a$

$r > D-a$

For $r \leq a$ the required parameters are easily evaluated:

$$v = \pi x(r^2 - x^2) \qquad (C.2)$$

$$S = 2\pi r\, x \qquad (C.3)$$

$$C_1 = \pi r$$
$$C_2 = 0 \qquad (C.4)$$
$$C_3 = \pi(r^2 - x^2)$$

where:

v is the burnt volume,

S is the flame front area,

C_1, C_2 and C_3 are the areas of chamber surface in contact with the burnt zone at the upper flat surface, cylinder wall and lower flat surface, respectively.

x is a variable defined such as $x = r$ if $r < h$ otherwise $x = h$.

For $r > a$, Annand[120] suggested an approximate procedure which gives accuracy adequate for most purposes.

The basis of the approximation is to seek a representative plane at depth Y, at which the flame-enclosed area, B is such that

$$v = Bx \tag{C.5}$$

The intersection of the flame front and the curved chamber wall with a plane parallel to the flat faces, at distance y from the upper, is shown in Fig. C.2. Denoting the enclosed area, by, b, the "free" perimeter by p, the perimeter of wall contact by, q and the radius of the flame from in plane y, f ($f = \sqrt{r^2 - y^2}$), we have

$$\cos\alpha = [\frac{a}{D} - (\frac{a}{D})^2 - (\frac{f}{D})^2]/[(1 - \frac{2a}{D})\ f/D] \tag{C.6}$$

$$\cos\beta = 1 + [(a/D)^2 - (f/D)^2]/[1/2 - \frac{a}{D}] \tag{C.7}$$

$$b = [\pi-\alpha + 1/2\ \sin(2\alpha)]f^2 + [2\beta - \sin(2\beta)]D^2/8 \tag{C.8}$$

$$P = 2(\pi-\alpha)f \tag{C.9}$$

and

$$q = D\beta \tag{C.10}$$

(a) Range $\sqrt{(a^2 + h^2)} \angle r \leq D-a$

Evaluating Y for a wide range of a and h, Annand found that in almost all cases the result was $Y/x = .58 \pm .02$. Values of ν based on eqn. C.5, and of s and c based on eqns. C.11 and C.12 below, were therefore evaluated for $Y = .58x$.

$$s = (rP/F)x \qquad (C.11)$$

$$C_2 = Qx \qquad (C.12)$$

where F, P and Q are the values of f, p, and q at $y = Y$.

(b) Range $a \angle r \leqq \sqrt{(a^2 + h^2)}$

In this range, it is necessary to divide the burnt zone volume into two regions, above and below the intersection of the flame with the cylindrical wall, as indicated in Fig. C.3a. Writing

$$z = \sqrt{(r^2 - a^2)}$$

and defining a representative plane for the upper section as before, so that $Y' = .58z$, we obtain

$$\nu = B'z + \pi(x-z)[r^2 - (x^2 + xz + z^2)/3] \qquad (C.13)$$

$$C_2 = Q'z$$

$$S = rP'z/F' + 2\pi r\,(x-z)$$

where B', F', P' and Q' represent values of b, f, p and q calculated at plane Y'.

(c) Range $r \geq (D-a)$

In this case, the burnt zone volume must be divided as in Fig. C.3b. Using z now to represent the depth at which the flame just touches the most remote point on the cylindrical wall, we have:

$$z = \sqrt{[r^2 - (D - a)^2]} \qquad (C.14)$$

and obtain:

$$\begin{aligned} \nu &= 1/4\ \pi\ D^2 z + B'(x - z) \\ C_2 &= \pi D z + Q'(x - z) \\ s &= r(x - z)\ P'/F' \end{aligned} \qquad (C.15)$$

where B', F', P' and Q' are again evaluated at a new representative depth Y'. The best overall precision is obtained in this case by setting:

$$Y' = z + 1/2\ (x - z) \qquad (C.16)$$

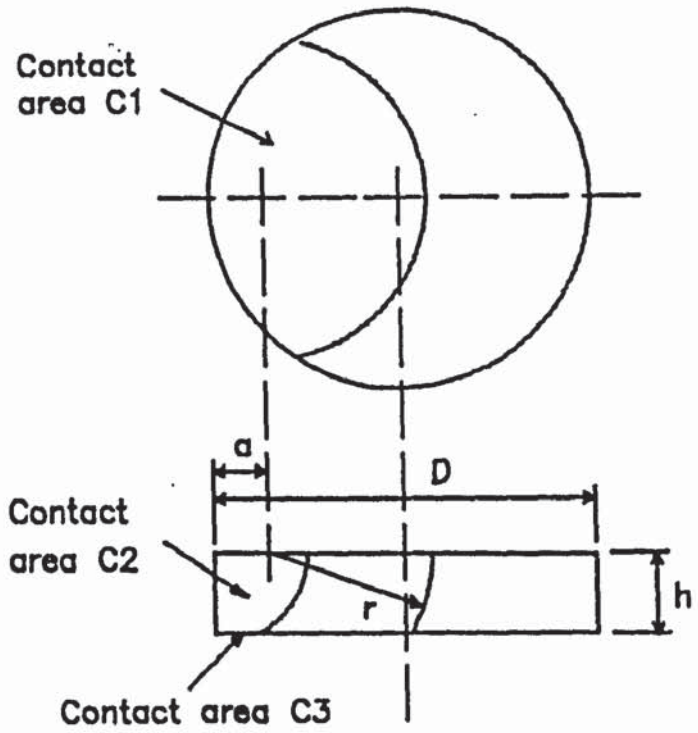

FIG. (C.1) Basic Geometry

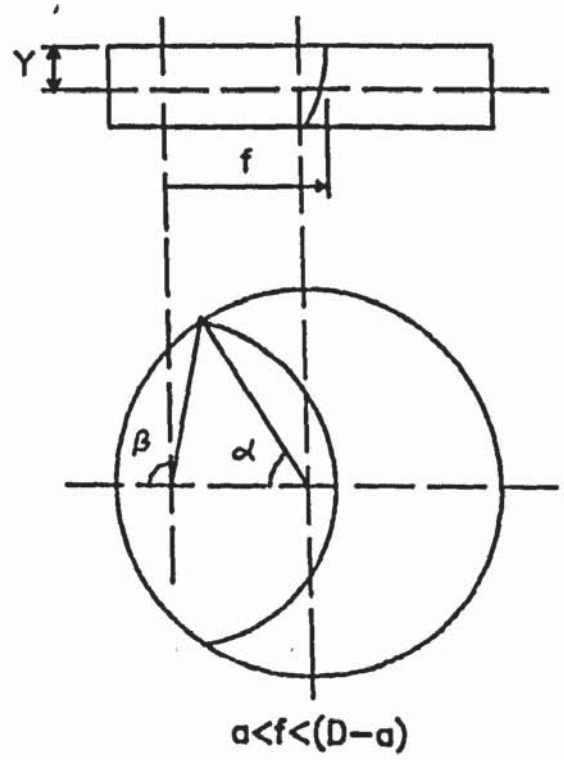

FIG. (C.2) Representative Plane

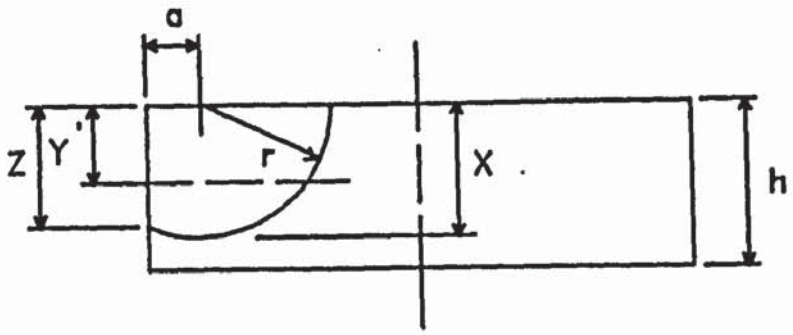

(a) $a < r < (a + h)$

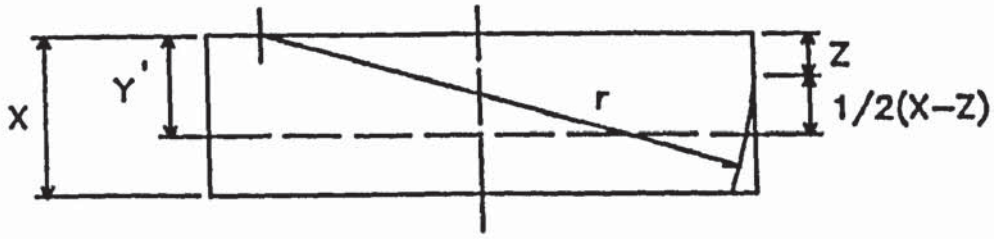

(b) $r > (D - a)$

FIG. (C.3) "Representative" Planes for Two Cases

Appendix D: Determination of the Composition of Combustion Products

As mentioned in chapter (4) the method used to calculate the composition of combustion products is based on the system suggested by Way[167], which uses a combination of chemical rate equations for slower reactions with partial equilibrium for faster reactions. The method has the advantage of requiring fewer parameters to be estimated (only O/O_2 ratio).

The chosen species are:

1. Nitrogen N_2
2. Oxygen O_2
3. Carbon Dioxide CO_2
4. Water vapour H_2O
5. Carbon Monoxide CO
6. Hydrogen H_2
7. Nitric Oxide NO
8. Hydroxyl OH
9. Atomic Nitrogen N
10. Atomic Hydrogen H
11. Atomic Oxygen O
12. Argon A

The complete list of reactions considered is:

$$CO + O_2 \rightleftharpoons CO_2 + O \qquad (D.1)$$

$$H_2 + O_2 \rightleftharpoons H_2O + O \qquad (D.2)$$

$$H + O_2 \rightleftharpoons OH + O \qquad (D.3)$$

$$2H + O_2 \rightleftharpoons H_2 + 2O \qquad (D.4)$$

$$H_2O + M \rightleftharpoons OH + H + M \qquad (D.5)$$

$$H_2 + M \rightleftharpoons H + H + M \qquad (D.6)$$

$$O_2 + M \rightleftharpoons O + O + M \qquad (D.7)$$

$$N + O_2 \rightleftharpoons NO + O \qquad (D.8)$$

$$N + NO \rightleftharpoons N_2 + O \qquad (D.9)$$

$$N + OH \rightleftharpoons NO + H \qquad (D.10)$$

The symbol M denotes any non-reacting molecule that is required to promote certain reactions. Reactions D.1 to D.4 are so fast that they continually equilibrated so that actual rate coefficients of these reactions are of no importance. A saving in computation time can be made if equilibrium equations are used instead of kinetic equations for these fast reactions. Together with three atom balance equations this is not sufficient to solve for the 8 gases in the C-H-O system so this system is in a state of partial equilibrium. The additional equation must be obtained from reactions D.5 - D.10 that are kinetically limited. The C-H-O system is very little affected by the nitric oxide forming reactions D.8 - D.10 since these are very much slower than reactions D.5 - D.8.

For weak to stoichiometric mixtures, C-H-O dissociation is indicated by the presence of the species Co, H_2, OH, H and O. The weighted sum of these gases given by:

$$D_1 = n_5 + n_6 + \frac{1}{2} n_8 + \frac{2}{3} n_{10} + n_{11} \qquad (D.11)$$

For stoichiometric to rich mixtures the presence of the species O_2, OH, H, O indicates dissociation so an alternative measure of C-H-O system dissociation is given by:

$$D_2 = 2n_2 + n_8 + n_{10}\ 2n_{11} \qquad (D.12)$$

For a given value of D (either D_1 or D_2) sufficient equations are available to solve for the 8 gases in the C-H-O system as follows.

Iterative solution for partial equilbrium system

The molal composition of dry air is taken from Ref. (161) to be:

Nitrogen N_2	.78084
Oxygen O_2	.20946
Carbon dioxide CO_2	.00033
Argon A	.00937

For a hydrocarbon fuel of carbon fraction CF, the chemical equation for complete combustion of unit mass of

fuel may be represented by:-

$$C_yH_{4x} + (y + x)\ O_2 \rightarrow y\ CO_2 + 2xH_2O \qquad (D.13)$$

where:

$$y = C_f/12.01,\ x = (1 - C_f)/4.032$$

The eight equations required to solve for the C-H-O species comprise four equilibrium equations, atom balance equations for carbon, hydrogen, oxygen and nitrogen and one net dissociation equation either for D_1 eqn. D.11 or for D_2 eqn. D.12.

From reactions D.1 to D.4, 4 equilibrium coefficients K_1 to K_4 are defined so that, for example:-

$$K_1 = n_3.n_{11}/(n_5.n_2) = n_3^{\alpha}/n_5 \qquad (D.14)$$

where $\alpha = n_{11}/n_2$

For a mass of fuel m_f burnt in n_a moles of air the four atom balance equations are:

$$\text{Nitrogen: } 2n_1 + n_7 + n_9 = 1.56168\ n_a$$
$$\text{Oxygen: } 2n_2 + 2n_3 + n_4 + n_7 + n_8 + n_{11} = .41958\ n_a$$
$$\text{Carbon: } n_3 + n_5 = y.m_f$$
$$\text{Hydrogen: } 2n_2 + 2n_6 + n_8 + n_{10} = 4xm_f \qquad (D.15)$$

The solution is carried out in terms of α, the ratio of the number of moles of O/O_2 . Only the solution for weak to stoichiometric mixtures - using D_1 - is given here. For rich mixtures, the same process may be used, using the relationship:-

$$D_1 = D_2 - .41892\, n_a + n_7 + 2(x + y)m_f \qquad (D.16)$$

For carbon gases substitution from equilibrium equation into the carbon atom balance equation gives:-

$$n_3 = (y.m_f + .00033.n_a)/(1 + \alpha/K_1)$$

$$n_5 = (y.m_f + .00033.n_a)/(1 + K_1/\alpha)$$

For hydrocarbon gases, rewriting the net dissociation equation (D.11)

$$4n_{11} = 4D_1 - 4n_6 - 2n_8 - 6n_{10}$$

Similarly, from the oxygen balance equation

$$4n_2 = .831916.n_a - 2n_7 - 4n_3 - 2n_8 - 2n_{11}$$

which becomes, by substituting for n_{11}

$$4n_2 = .83916.n_a - 2n_7 - 4n_3 + 2n_6 - 2n_8 + 3n_{10} - 2D_1$$

$$\alpha = \frac{4D_1 - 4n_5 - 4n_6 - 2n_8 - 6n_{10}}{.83916.n_a - 2n_7 - 4n_3 + 2n_6 - n_8 + 3n_{10} - 2D_1}$$

This re-arranges to:

$$(2\alpha + 4)n_6 - 2\alpha n_4 + (2 - \alpha)n_8 + (3\alpha + 6)n_{10} =$$

$$.83916.\alpha.n_a + 4\alpha.n_3 - 4n_5 + 2\alpha n_7$$

Using equilibrium equations to substitute for n_6 and n_{10}

$$((2\alpha + 4)\frac{\alpha}{K_2} - 2\alpha)n_4 + (2 - \alpha + (3\alpha + 6)\frac{\alpha}{K_3})\, n_8 = (2\alpha + 4)D_1 -$$

$$- .83916.\alpha.n_\alpha + 4\alpha.n_3.4n_5 + 2\alpha n_7$$

Similarly, substitution for n_6 and n_{10} in the hydrogen atom balance equations gives:

$$[\frac{2\alpha}{K_2} + 2]\, n_4 + [\frac{\alpha}{K_3} + 1]\, n_8 = 4x.m_f$$

These simultaneous linear equations are solved for n_4 and n_8. Values for n_6 and n_{10} are followed from equilibrium equations. For oxygen group n_2, n_{11} using the final equilibrium equation

$$n_{11} = n_{10}^2\, K_4/(n_6.\alpha)$$
$$n_2 = n_{11}/\alpha$$

Thus for any value of α, a complete solution for the 8 variable species is obtained. A simple iterative method is used to calculate the final composition from an initial estimate of α. The oxygen balance equation is written in the form:

$$\text{Error} = .41958\, n_a - 2n_2 - 2n_3 - n_4 - n_5 - n_7 - n_8 - n_{11}$$

where Error must be zero at the true solution. For any estimate of α a value of Error can be found; if Error is positive the correct value of α is greater than the estimate, and vice versa.

Appendix E1:

The 4th Order Runge-Kutta Method

A number of formulae has been developed whose use obviates calculating the derivatives in the Taylor's series method. The best known of these was devised by C. Runge and improved by W. Kutta. The following quantities are to be calculated:

$$K_1 = hf(x.,yo)$$

$$K_2 = hf(xo + 1/2h,\ yo + 1/2\ K_1)$$

$$K_3 = hf(xo + 1/2h,\ yo + 1/2\ K_2)$$

$$K_4 = hf(xo + h),\ yo + K_3)$$

$$K = \frac{1}{6}\ (K_1 + 2K_2 + 2K_3 + K_4)$$

Runge showed that the error in the value of K is of the order h^5 (where h is the step size) and can therefore be made arbitrarily small.

To find a solution of the equation

$$y' = f(x,y)$$

which reduces to y = yo when x = xo, we obtain a succession of pairs of values (x_n = xo + nh, yn)from Runge's formulae. The method is best explained in the following table:

x	y	f	hf	
xo	yo	f(xo,yo)	K_1	$1/2(K_1 + K_4)$
xo + 1/2h	yo + $1/2K_1$	f(xo + 1/2h,yo + $1/2K_1$)	K_2	$K_2 + K_3$
xo + 1/2h	yo + $1/2K_2$	f(xo + 1/2h,yo + $1/2K_2$)	K_3	sum
xo + h	yo + K_3	f(xo + h,yo + K_3)	K_4	
x_1	y_1			$K = \frac{1}{3}$ sum

Having found (x_1, y_1) the process is repeated with (x_1, y_1) as starting values, thus obtaining (x_2, y_2) and as many more values as may be desired. An estimate of the error δ when h is small can be made by repeating the above calculations with the double step size, 2h. The error in Y is approximately

$$\delta = \lambda h^5$$

where λ is a constant. If y_2 and $\bar{y}_2$ are the y values calculated for the single and double increments, respectively, it is known that the error in y_2 is given by[146].

$$\delta = \frac{1}{15} (\bar{y}_2 - y_2)$$

Appendix E2:

Ignition and Initiation of Two Zones in the Combustion Chamber

In the present work it is assumed that ignition of the fuel is said to take place when a finite volume of the burnt mixture exceeds .001 times the total cylinder volume[67]. The process is carried out in the following stages:

1. The unburnt mixture at T_1, P_1, V_1 and m_1 undergoes adiabatic compression to T_2, P_2 and V_2 as the crank shaft rotates through a small angle $d\theta$, i.e:

$$T_2 = T_1\left(\frac{V_1}{V_2}\right)^{\gamma_u - 1}$$

$$P_2 = P_1\left(\frac{V_1}{V_2}\right)^{\gamma_u} \frac{Ru_2}{Ru_1} \qquad \text{(E1)}$$

The volume V_2 is calculated from engine geometry and γ_u, R_u are the unburnt mixture specific heat ratio and gas constant respectively.

2. Heat is transfered, at constant cylinder volume, between the working mixture and chamber walls; accordingly, cylinder pressure and temperature are changed to:

$$T_3 = T_2 \frac{Q_u}{m_1 Cv_u}$$

$$P_3 = P_2 \frac{T_3}{T_2} \frac{Ru_3}{Ru_2} \qquad \text{(E2)}$$

where Q_u and Cv_u are the heat transferred and the specific heat at constant volume respectively.

3. At the nominal ignition timing a flame will propogate at a speed which depends on T_3, P_3 and the mixture vapour fuel-air equivalence ratio. The flame radius, r is calculated from:

$$r = U.dt \qquad \text{(E3)}$$

where U is the flame speed,

dt is the time increment = $^{d\theta}/_{6.N}$

N is the engine speed, rpm.

4. The burnt volume is then calculated using the flame radius and piston height (appendix C). The mass of the mixture in the burnt volume, m_b is given by:

$$m_b = V_b \cdot \rho_u \qquad \text{(E4)}$$

Where ρ_u is the unburnt mixture density. From the knowledge of m_b, the partial masses of air, vapour fuel, exhaust residuals and the number of fuel droplets are determined.

5. It is assumed that initiation of combustion occurs only in the vapour fuel only. Burning the available vapour fuel gives:

$$T_b = T_u + \frac{Q_c}{m_b . Cv_u}$$

$$P_b = P_u \frac{T_b}{T_u} \cdot \frac{R_b}{R_u} \qquad \text{(E5)}$$

where Q_c is the heat of combustion, R_b and R_u are the gas constants of the burnt and unburnt mixtures respectively.

6. Now the combustion chamber is divided into two zones, burnt and unburnt specified by their own pressure, temperature, mass and composition. The pressure in the combustion chamber should be uniform, the burnt and unburnt pressures are equalized by assuming isentropic change in temperature to an equalized pressure $P_c = P_{bf} = P_{uf}$ [67]. The basic relations are:

$$\text{Burnt Zone} = \frac{T_{bf}}{T_b} = \left(\frac{P_c}{P_b}\right)^{\frac{\gamma_b - 1}{\gamma_b}} \qquad \text{(E6)}$$

$$\text{Unburnt Zone} = \frac{T_{uf}}{T_u} = \left(\frac{P_c}{P_u}\right)^{\frac{\gamma_u - 1}{\gamma_u}} \qquad \text{(E7)}$$

A third relationship is required between the temperatures and this is the energy balance:

$$m_u \, Cv_u(T_{uf} - T_u) = m_b \, Cv_b(T_b - T_{bf}) \qquad \text{(E8)}$$

An iterative technique is used to calculate P_c, T_{uf} and T_{bf}.

7. The final burnt volume is calculated from:

$$V_{bf} = V_b \left(\frac{P_b}{P_{bf}}\right)^{1/\gamma_b} \qquad \text{(E9)}$$

If the final burnt volume, V_{bf} is $\geq .001 \times V_2$ the combustion is said to occur. If not, the compression process will continue.

APPENDIX F
Program Listings

```
10   !  RE-STORE "INTSYS:F8"
20    ! ************************************************
30    ! ***              THE PROGRM "INTSYS"             ***
40    ! *    This Program Deals with the Calculations    *
50    ! * Involved in the Intake System of a Carburetted *
60    ! *               SPARK IGNITION ENGINE            *
70    ! ************************************************
80    DIM Xx(8),F(8),Yi(8),Yj(8),Yk(8),Yl(8),Uu(8),Vr(2),Ar(2),Br(2)
,Cr(2),Dr(2),Er(2),Fr(2),Rc(15),Vc(15),Rs(15),Nr(15),Zc(15)
90    DIM Xx1(4,15),F1(4,15),Yi1(4,15),Yj1(4,15),Yk1(4,15),Yl1(4,15)
,Uu1(4,15),Pvr(15),Rl(15),Cvf(15),Uu2(4,15),Uu3(8)
100   DIM Pw(15),Mw(15),Bt(15),Tc(15),Pc(15),Ca(15),Cb(15),Cc(15),Cd
(15),Ha(15),Hb(15),Hc(15),Hd(15),Hv(15),Um(15),Cv(15),Cl(15),Gc(15),
Ps(15)
110   DIM Pv(15),D(15),Rv(15),Car(15),Hyd(15),Mf(15),Sc(15),Betd(15)
,Betf(15),Aw(15),Vapm(120),Win(15),Wout(15)
120   DIM Wat(15),Mff(15),Psf(15),Awf(15),Clf(15),Liqd(15),Liqf(15)
130   FOR J=0 TO 15
140   READ Pw(J),Mw(J),Bt(J),Tc(J),Pc(J),Rl(J),Ca(J),Cb(J),Cc(J),Cd(
J),Ha(J),Hb(J),Hc(J),Hd(J),Hv(J),Um(J),Car(J),Hyd(J),Vc(J),Zc(J)
150   NEXT J
160   FOR G=0 TO 2
170   READ Ar(G),Br(G),Cr(G),Dr(G),Er(G),Fr(G)
180   NEXT G
190   PRINT PAGE
200   PRINT "  INPUT The NAME of the File You Wish to Store Data in
  "
210   INPUT Filename$
220   CREATE ""&Filename$,120
230   ASSIGN #1 TO ""&Filename$
240   PRINTER IS 16
250   PRINT PAGE
260   PRINT "   INPUT Throttle Setting 4/4 for Full,3/4,1/2,1/4
"
270   INPUT Thr$
280   IF Thr$<>"1/4" THEN 310
290   Area1=1.36636E-4
300   GOTO 390
310   IF Thr$<>"1/2" THEN 340
320   Area1=1.47881E-4
330   GOTO 390
340   IF Thr$<>"3/4" THEN 370
350   Area1=1.54442E-4
360   GOTO 390
370   IF Thr$<>"4/4" THEN 390
380   Area1=1.59828E-4
390   IF (Thr$<>"1/4") AND (Thr$<>"1/2") AND (Thr$<>"3/4") AND (Thr$
<>"4/4") THEN 250
400   Areav=3.594E-4 ! Inlet valve Mean Throat area
410   PRINT PAGE
420   PRINT "     INPUT  Manifold Length  IN  mm   "
430   INPUT Mlenth
440   PRINT PAGE
450   PRINT "     INPUT  Manifold Shape    "
460   PRINT ""
470   PRINT ""
480   PRINT ""
490   PRINT "                                              "
500   PRINT "                                              "
510   PRINT "    S     for Straight Pipe Manifold    "
```

```
520   PRINT "    SMB   for Smooth Bended Manifold    "
530   PRINT "    SHB   for Sharp Bended Manifold     "
540   PRINT "                                        "
550   PRINT "                                        "
560   INPUT Mshape$
570   IF (Mshape$<>"S") AND (Mshape$<>"SMB") AND (Mshape$<>"SHB") TH
EN 440
580   PRINT PAGE
590   PRINT "     INPUT  AIR MASS FLOWRATE  IN  Kg/s    "
600   INPUT Wa
610   PRINT PAGE
620   PRINT "     INPUT AIR/FUEL RATIO   "
630   INPUT Afr
640   Wl=Wli=Wa/Afr
650   Mlenth=Lman=Mlenth/1000! Manifold Length (m) ( First part only
)
660   Dm=4.0E-2        ! Manifold diameter in meters
670   Lenth=(Lman+.12)*1000  !Total Manifold length(From Nozzle to V
alve (mm)
680   Rh=Dm/2          ! Hydraulic radius
690   Cpa=1004.6079    !J/Kg.K
700   Ka=2.5704775E-2 !W/m.K
710   Mue=1.8130754E-5!Kg/m.s
720   PRINT PAGE
730   PRINT "      INPUT INITIAL AIR VELOCITY IN  m/s    "
740   PRINT "       AT THE BRIDGE OF THE CARBURETTOR     "
750   INPUT Avelocity
760   Va=Avelocity
770   PRINT PAGE
780   PRINT "      INPUT INITIAL AIR TEMPERATURE  IN  DEG  C   "
790   INPUT Atemp
800   PRINT PAGE
810   PRINT "      INPUT INITIAN FUEL TEMPERATURE IN DEG C      "
820   INPUT Ftemp
830   PRINT PAGE
840   PRINT "     DO YOU WANT THE WALL FILM TO BE SEPARATED  Y OR N
  "
850   INPUT Fsep$
860   PRINT PAGE
870   PRINT "       INPUT TOTAL HEAT ADDED THROUGH THE MANIFOLD WAL
L  IN Kw/m2  "
880   INPUT H
890   PRINT PAGE
900   PRINT "        INPUT  MANIFOLD PRESSURE IN  mm Hg    "
910   INPUT Pman
920   Pman=Pman*1E-3*13595*9.81
930   IF Thr$<>"4/4" THEN 950
940   GOTO 1080
950   PRINT PAGE
960   PRINT "                          DEGREE OF SECONDARY ATOMIZATION
 "
970   PRINT ""
980   PRINT " SELECT ONE OF THE FOLLOWING DIAMETERS TO BE THE SECON
DARY ATOMIZATION ONE "
990   PRINT ""
1000  PRINT "  10 "
1010  PRINT "  20 "
1020  PRINT "  30 "
1030  PRINT "  40 "
1040  PRINT ""
```

```
1050  PRINT "            OR INPUT ANY DESIRED DIAMETER "
1060  PRINT "  IF NO Secondary Atomization is required INPUT  0  ze
ro "
1070  INPUT Dsecondary
1080  PRINT PAGE
1090  Tx=Ty=Atemp+273.15
1100  Ta=Atemp+273.15 !Deg. Kelvin
1110  Tl=Tlf=Ftemp+273.15 !Deg. Kelvin
1120  L=0
1130  Row=Wa/(.6*Avelocity*Area1)
1140  Press=Row*287*Ta
1150  P=Press/1.01325E5  !Total Pressure in Atm.
1160  Pss=Press/(1E-3*9.80665*13595.098)
1170  Liqdtot=0
1180  Liqftot=0
1190  FOR J=0 TO 15
1200  Liqd(J)=Pw(J)*Wli/100
1210  Liqf(J)=0
1220  Liqdtot=Liqdtot+Liqd(J)
1230  Liqftot=Liqftot+Liqf(J)
1240  NEXT J
1250  GOSUB Rowf
1260  Ddiam=3045/Va+30*(1000/(Afr*Lmd)*Row)^1.5
1270  IF Thr$<>"1/4" THEN 1300
1280  Bfsm=3.885+44.885*Wli*60-771.43*(Wli*60)^2
1290  Bfsh=4.345+52.25*Wli*60-917.14*(Wli*60)^2
1300  IF Thr$<>"1/2" THEN 1330
1310  Bfsm=1.865+55.677*Wli*60-1524.3*(Wli*60)^2
1320  Bfsh=.762+64.8*Wli*60-997.14*(Wli*60)^2
1330  IF Thr$<>"3/4" THEN 1360
1340  Bfsm=1.354+122.78*Wli*60-2620*(Wli*60)^2
1350  Bfsh=.228+149.4*Wli*60-2674.3*(Wli*60)^2
1360  IF Thr$<>"4/4" THEN 1390
1370  Bfsm=.632+149.43*Wli*60-2777.14*(Wli*60)^2
1380  Bfsh=-.623+185.8*Wli*60-3011.4*(Wli*60)^2
1390  PRINTER IS 0
1400  PRINT "INITIAL CONDITIONS"
1410  PRINT ""
1420  PRINT "Initial droplet diameter           ";Ddiam;"(um)"
1430  PRINT "Heat input through manifold wall   ";H;"(Kw/m2)"
1440  PRINT "Heat input through inlet port wall ";1.5;"(Kw/m2)"
1450  IF Dsecondary>0 THEN 1480
1460  PRINT "No Secondary Atomization"
1470  GOTO 1490
1480  PRINT "Secondary atomization to           ";Dsecondary;"(um)"
1490  PRINT "Air/Fuel ratio (total)             ";Afr
1500  PRINT "Manifold Press                     ";Pman/1.01325E5;"(b
ar)"
1510  PRINT "Air Temp.                          ";Atemp;"(C)"
1520  PRINT "Fuel Temp.                         ";Ftemp;"(C)"
1530  PRINT "Air Velocity at Bridge             ";Va;"(m/s)"
1540  PRINT "-------------------------------------------------"
1550  PRINTER IS 16
1560  H=H*1000
1570  GOSUB Segma1
1580  GOSUB Data1
1590  GOSUB Data2
1600  GOSUB Seg
1610  ! ************************
1620  ! *  INITIAL CONDITIONS *
```

```
1630  ! ************************
1640  FOR J=0 TO 15
1650  Xx1(0,J)=0          ! Massflow Rate of droplet evaporation of c
omponent J
1660  Xx1(1,J)=0          ! Massflow Rate of film evaporation of comp
onent J
1670  Xx1(2,J)=0          ! Vapour total massfiow rate of component J
 in Kg/s
1680  Xx1(3,J)=0          ! Vapour pressure of component J in N/m^2
1690  Xx1(4,J)=Rv(J)       ! Vapour density of component J in Kg/m^3
1700  NEXT J
1710  Xx(0)=.1            ! Droplet Velosity In m/s
1720  Xx(1)=Ddiam*1E-6    ! Droplet Diameter In m
1730  Xx(2)=T1            ! Droplet Temperature In Deg. K
1740  Xx(3)=273.15        ! Film Temperature in  Deg. K
1750  Xx(4)=Press         ! Total Pressure in N/m2
1760  Xx(5)=Press         ! Air Pressure in N/m2
1770  Xx(6)=Row            ! Air Density in Kg/m3
1780  Xx(7)=Avelocity     ! Air velosity in m/s
1790  Xx(8)=Ta            ! Air Temperature in Deg. K
1800  I=0
1810  L=0
1820  GOSUB Printout
1830  N=6*Liqdtot/(Lmd*PI*Xx(1)^3)
1840  Delta=1E-4          ! mm
1850  GOSUB Initials
1860  Lf2=.05
1870  FOR I=1 TO 3000
1880  IF L<Mlenth+.12 THEN 1900
1890  H=1500              ! HEAT Addition in the Inlet Port W/m2
1900  IF L>=Mlenth+.206 THEN 3320
1910  IF L>=2.0E-3 THEN Delta=2.0E-3
1920  IF L>=.048 THEN Delta=1E-4
1930  IF L>=.052 THEN Delta=2.0E-3
1940  IF L>=5.8E-2+Mlenth+6.0E-2 THEN Delta=1E-4
1950  IF L>=6.2E-2+Mlenth+6.0E-2 THEN Delta=2.0E-3
1960  IF L>=5.8E-2+Mlenth+.14 THEN Delta=1E-4
1970  IF L>=6.2E-2+Mlenth+.14 THEN Delta=2.0E-3
1980  GOSUB Area
1990  IF Fsep$<>"N" THEN 2020
2000  IF L>.05 THEN GOSUB Film
2010  GOTO 2030
2020  IF (L>=.05) AND (L<=Mlenth+6.0E-2) THEN GOSUB Film
2030  GOSUB Runge
2040  GOSUB Seg
2050  Vapm=Seg(1)
2060  Vapf1=Vapf2
2070  Lf1=Lf2
2080  Vapf=Vapf2=Seg(7)
2090  Lf2=L
2100  IF Thr$<>"4/4" THEN 2120
2110  GOTO 2430
2120  IF L<>.05-Delta THEN 2310
2130  Tex=Xx(8)
2140  Rex=Xx(6)
2150  Vex=Xx(7)
2160  Pex=Xx(5)
2170  M1=Vex/SQR(1.4*287*Tex)
2180  Rtot=Rex*(1+.2*M1^2)^2.5
2190  Ptot=Pex*(1+.2*M1^2)^3.5
```

```
2200  Pexx=Pman-Seg(0)
2210  Msqr1=.8
2220  Msqr2=.9763144/(1+.25*Msqr1)
2230  Error=ABS(Msqr2-Msqr1)
2240  IF Error<1E-11 THEN 2270
2250  Msqr1=Msqr2
2260  GOTO 2220
2270  Pexx=Pexx
2280  Texx=Tex
2290  Vexx=Msqr2*SQR(1.4*287*Tex)
2300  Rexx=Rtot/(1+.2*Msqr2)^2.5
2310  ! ***************************
2320  ! * Secondary Automization *
2330  ! ***************************
2340  IF L<>.05 THEN 2610
2350  IF Dsecondary>0 THEN 2370
2360  Dsecondary=Xx(1)/1E-6
2370  Xx(1)=Dsecondary*1E-6
2380  Xx(5)=Pexx
2390  Xx(4)=Xx(5)+Seg(0)
2400  Xx(8)=Texx
2410  Xx(6)=Rexx
2420  Xx(3)=Xx(2)
2430  IF L<>.05 THEN 2610
2440  IF Thr$<>"4/4" THEN 2470
2450  Liqftot=1.55647680848*EXP(55.9762062471*Wli*60)/(1000*60)
2460  GOTO 2540
2470  IF Thr$<>"3/4" THEN 2500
2480  Liqftot=3.1011770169*EXP(44.2236888443*Wli*60)/(1000*60)
2490  GOTO 2540
2500  IF Thr$<>"1/2" THEN 2530
2510  Liqftot=3.4279180064*EXP(44.524425927*Wli*60)/(1000*60)
2520  GOTO 2540
2530  Liqftot=.9027750421*EXP(63.5692687729*Wli*60)/(1000*60)
2540  FOR J=0 TO 15
2550  Liqf(J)=Liqd(J)*Liqftot/Liqdtot
2560  Liqd(J)=Liqd(J)-Liqf(J)
2570  NEXT J
2580  Liqdtot=Liqdtot-Liqftot
2590  Xx(3)=Xx(2)
2600  N=6*Liqdtot/(Lmd*PI*Xx(1)^3)
2610  ! ***************************
2620  IF Fsep$<>"Y" THEN 2710
2630  IF L<=Mlenth+6.0E-2 THEN 2710
2640  FOR J=0 TO 15
2650  Liqf(J)=0
2660  NEXT J
2670  Qd=Qe=0
2680  Wli=Wli-Liqftot
2690  Liqftot=0
2700  Xx(3)=273.15 ! Dummy Value actually there is no film
2710  IF Fsep$<>"Y" THEN 2740
2720  IF L<>Mlenth+6.0E-2 THEN 2740
2730  GOTO 2770
2740  IF L<>Mlenth+.206 THEN 2760
2750  GOTO 2770
2760  IF L<>.05 THEN 3210
2770  PRINTER IS 16
2780  PRINT ""
2790  PRINT "L=";L*1000;" mm"," % Evaporation=";Vaptot/Wli*100;"% Fil
m=";Liqftot/Wli*100
```

```
2800  PRINT "-----------------------------------------"
2810  PRINT ""
2820  FOR J=0 TO 15
2830  FIXED 0
2840  PRINT " Initial quantity of component   (";J+1;")  =";
2850  FLOAT 5
2860  PRINT Pw(J)*W1/100
2870  FIXED 0
2880  PRINT " Final quantity of component     (";J+1;")  =";
2890  FLOAT 5
2900  PRINT Liqd(J)+Liqf(J)
2910  FIXED 0
2920  PRINT " % Initial quantity of component (";J+1;")  =";
2930  FIXED 5
2940  PRINT Pw(J)
2950  FIXED 0
2960  PRINT " % Final quantity of component   (";J+1;")  =";
2970  FIXED 5
2980  PRINT (Liqd(J)+Liqf(J))/W1*100
2990  FIXED 0
3000  PRINT " % Evaporation of component      (";J+1;")  =";
3010  FIXED 5
3020  PRINT (Pw(J)*W1/100-(Liqd(J)+Liqf(J)))/W1*100
3030  FIXED 0
3040  PRINT " Drop content of component       (";J+1;")  =";
3050  FLOAT 5
3060  PRINT Liqd(J)
3070  FIXED 0
3080  PRINT " Film content of component       (";J+1;")  =";
3090  FLOAT 5
3100  PRINT Liqf(J)
3110  FIXED 0
3120  PRINT " % Film content of component     (";J+1;")  =";
3130  FIXED 5
3140  PRINT Liqf(J)/W1*100
3150  FIXED 0
3160  PRINT " % Drop content of component     (";J+1;")  =";
3170  FIXED 5
3180  PRINT Liqd(J)/W1*100
3190  PRINT "-------------------------------------------------
--------"
3200  NEXT J
3210  PRINTER IS 16
3220  Ta=Xx(8)
3230  T1=Xx(2)
3240  T1f=Xx(3)
3250  P=Xx(4)/1.01325E5
3260  IF Xx(1)>0 THEN 3280
3270  T1=T1f
3280  GOSUB Data2
3290  IF I MOD 1=0 THEN GOSUB Printout
3300  NEXT I
3310  END
3320  STOP
3330 Printout: !
3340  FIXED 1
3350  PRINTER IS 16
3360  PRINT "L=";L*1000;" mm"
3370  FIXED 3
3380  PRINT "  Vd=";Xx(0);
```

```
3390  PRINT "  Dd=";Xx(1)/1E-6;
3400  PRINT "  Td=";Xx(2)-273.15;
3410  PRINT "  Tf=";Xx(3)-273.15;
3420  PRINT "  Pt=";Xx(4)/1.01325E5;
3430  PRINT "  Pa=";Xx(5)/1.01325E5;
3440  PRINT "                Da=";Xx(6);
3450  PRINT "  Va=";Xx(7);
3460  PRINT "    Ta=";Xx(8)-273.15;
3470  PRINT " Vapm=";Vapm*100/W1;" %  "
3480  IF Fsep$="Y" THEN 3500
3490  GOTO 3520
3500  IF (L<.05) OR (L>Mlenth+6.0E-2) THEN 3590
3510  GOTO 3530
3520  IF L<.049 THEN 3590
3530  PRINT "% Film massflow =";Liqftot/W1*100,"Film flow gm/min=";L
iqftot*60*1000
3540  FIXED 3
3550  PRINT "% Film Evap=";Vapf/W1i*100,
3560  FLOAT 4
3570  PRINT "Film Evap.=";Vapf;"(Kg/s)";"Evap Rate=";Fvrate;"(Kg/m2.
s)"
3580  FIXED 3
3590  PRINT "-----------------------------------------------------
-----"
3600  PRINTER IS 16
3610  IF L<>Mlenth+.206 THEN 3710
3620  FOR J=0 TO 15
3630  PRINT #1;Liqd(J)/W1*100,Liqf(J)/W1*100
3640  NEXT J
3650  Fueltot=0
3660  FOR J=0 TO 15
3670  Fueltot=Liqd(J)+Liqf(J)+Fueltot
3680  NEXT J
3690  Fueltot=Fueltot+Vapm
3700  PRINT #1;Xx(8),Xx(4),Xx(2),Xx(1)/2,Xx(6),Wa/Fueltot
3710  GOSUB Disk
3720  RETURN
3730 Disk: !
3740  PRINT #1;L*1000,Xx(0),Xx(1)/1E-6,Xx(2)-273.15,Xx(3)-273.15,Xx(
7),Xx(8)-273.15,Vapm*100/W1,Vapf/W1i*100,Fvrate,Liqftot/W1*100,Liqft
ot*60*1000
3750  RETURN
3760  END
3770  ! **********************
3780  ! *  RUNGE SUBROUTINE *
3790  ! **********************
3800 Runge: !
3810  FOR Zz=0 TO 4
3820  FOR J=0 TO 15
3830  Uu1(Zz,J)=Xx1(Zz,J)
3840  NEXT J
3850  NEXT Zz
3860  Step=1
3870  GOSUB Functions1
3880  FOR Zz=0 TO 4
3890  FOR J=0 TO 15
3900  Yi1(Zz,J)=F1(Zz,J)*Delta
3910  Xx1(Zz,J)=Uu1(Zz,J)+Yi1(Zz,J)/2
3920  Uu2(Zz,J)=Xx1(Zz,J)
3930  NEXT J
```

```
3940  NEXT Zz
3950  Liqdtot=Liqftot=Vaptot=0
3960  FOR J=0 TO 15
3970  Liqd(J)=Liqd(J)-ABS(Yi1(0,J))/2
3980  Liqf(J)=Liqf(J)-ABS(Yi1(1,J))/2
3990  Pvr(J)=Xx1(3,J)
4000  Liqdtot=Liqdtot+Liqd(J)
4010  Liqftot=Liqftot+Liqf(J)
4020  Vaptot=Vaptot+Xx1(2,J)
4030  NEXT J
4040  GOSUB Update
4050  IF (Liqdtot>0) AND (Xx(1)<>0) THEN 4080
4060  N=0
4070  GOTO 4100
4080  N=6*Liqdtot/(Lmd*PI*Xx(1)^3)
4090  GOSUB Segma1
4100  GOSUB Segmaf
4110  GOSUB Seg
4120  GOSUB Segd
4130  GOSUB Runge1
4140  L=L+Delta/2
4150  GOSUB Functions1
4160  FOR Zz=0 TO 4
4170  FOR J=0 TO 15
4180  Yj1(Zz,J)=F1(Zz,J)*Delta
4190  Xx1(Zz,J)=Uu2(Zz,J)+Yj1(Zz,J)/2
4200  Uu2(Zz,J)=Xx1(Zz,J)
4210  NEXT J
4220  NEXT Zz
4230  Liqdtot=Liqftot=Vaptot=0
4240  FOR J=0 TO 15
4250  Liqd(J)=Liqd(J)-ABS(Yj1(0,J))/2
4260  Liqf(J)=Liqf(J)-ABS(Yj1(1,J))/2
4270  Pvr(J)=Xx1(3,J)
4280  Liqdtot=Liqdtot+Liqd(J)
4290  Liqftot=Liqftot+Liqf(J)
4300  Vaptot=Vaptot+Xx1(2,J)
4310  NEXT J
4320  GOSUB Update
4330  IF (Liqdtot>0) AND (Xx(1)<>0) THEN 4360
4340  N=0
4350  GOTO 4370
4360  N=6*Liqdtot/(Lmd*PI*Xx(1)^3)
4370  GOSUB Segma1
4380  GOSUB Segmaf
4390  GOSUB Seg
4400  GOSUB Segd
4410  GOSUB Runge2
4420  Step=2
4430  GOSUB Functions1
4440  FOR Zz=0 TO 4
4450  FOR J=0 TO 15
4460  Yk1(Zz,J)=F1(Zz,J)*Delta
4470  Xx1(Zz,J)=Uu2(Zz,J)+Yk1(Zz,J)
4480  NEXT J
4490  NEXT Zz
4500  Liqdtot=Liqftot=Vaptot=0
4510  FOR J=0 TO 15
4520  Liqd(J)=Liqd(J)-ABS(Yk1(0,J))
4530  Liqf(J)=Liqf(J)-ABS(Yk1(1,J))
```

```
4540  Pvr(J)=Xx1(3,J)
4550  Liqdtot=Liqdtot+Liqd(J)
4560  Liqftot=Liqftot+Liqf(J)
4570  Vaptot=Vaptot+Xx1(2,J)
4580  NEXT J
4590  GOSUB Update
4600  IF (Liqdtot>0) AND (Xx(1)<>0) THEN 4630
4610  N=0
4620  GOTO 4640
4630  N=6*Liqdtot/(Lmd*PI*Xx(1)^3)
4640  GOSUB Segma1
4650  GOSUB Segmaf
4660  GOSUB Seg
4670  GOSUB Segd
4680  GOSUB Runge3
4690  L=L+Delta/2
4700  GOSUB Functions1
4710  FOR Zz=0 TO 4
4720  FOR J=0 TO 15
4730  Yl1(Zz,J)=F1(Zz,J)*Delta
4740  Xx1(Zz,J)=Uu1(Zz,J)+(Yi1(Zz,J)+2*Yj1(Zz,J)+2*Yk1(Zz,J)+Yl1(Zz,
J))/6
4750  NEXT J
4760  NEXT Zz
4770  Liqdtot=Liqftot=Vaptot=0
4780  FOR J=0 TO 15
4790  Liqd(J)=Liqd(J)+ABS(Yi1(0,J)/2+Yj1(0,J)/2+Yk1(0,J))
4800  Liqf(J)=Liqf(J)+ABS(Yi1(1,J)/2+Yj1(1,J)/2+Yk1(1,J))
4810  Liqd(J)=Liqd(J)-ABS(Yi1(0,J)+2*Yj1(0,J)+2*Yk1(0,J)+Yl1(0,J))/6
4820  Liqf(J)=Liqf(J)-ABS(Yi1(1,J)+2*Yj1(1,J)+2*Yk1(1,J)+Yl1(1,J))/6
4830  Pvr(J)=Xx1(3,J)
4840  Liqdtot=Liqdtot+Liqd(J)
4850  Liqftot=Liqftot+Liqf(J)
4860  Vaptot=Vaptot+Xx1(2,J)
4870  NEXT J
4880  GOSUB Update
4890  IF (Liqdtot>0) AND (Xx(1)<>0) THEN 4920
4900  N=0
4910  GOTO 4930
4920  N=6*Liqdtot/(Lmd*PI*Xx(1)^3)
4930  GOSUB Segma1
4940  GOSUB Segmaf
4950  GOSUB Seg
4960  GOSUB Segd
4970  GOSUB Runge4
4980  RETURN
4990  END
5000 Update: !
5010  IF (Liqdtot+Liqftot+Vaptot)/Wli=1 THEN RETURN
5020  Sum=Wli-Liqftot-Liqdtot
5030  FOR J=0 TO 15
5040  Old=Xx1(2,J)
5050  Xx1(2,J)=Old*Sum/Vaptot
5060  Xx1(0,J)=Xx1(0,J)*Xx1(2,J)/Old
5070  Xx1(1,J)=Xx1(1,J)*Xx1(2,J)/Old
5080  NEXT J
5090  RETURN
5100  END
5110  !  ************************
5120  !  * RUNGE ONE SUBROUTINE *
```

```
5130  !  ************************
5140 Runge1:!
5150  FOR K=0 TO 8
5160  Uu(K)=Xx(K)
5170  NEXT K
5180  Tx=Xx(8)
5190  GOSUB Functions2
5200  FOR K=0 TO 8
5210  Yi(K)=F(K)*Delta
5220  Xx(K)=Uu(K)+Yi(K)/2
5230  Uu3(K)=Xx(K)
5240  NEXT K
5250  IF Liqftot>0 THEN 5280
5260  Xx(3)=273.15
5270  Yi(3)=0
5280  Ty=Xx(8)
5290  Ta=Xx(8)
5300  Tl=Xx(2)
5310  Tlf=Xx(3)
5320  P=Xx(4)/1.01325E5
5330  IF Xx(1)>0 THEN 5350
5340  Tl=Tlf
5350  GOSUB Data2
5360  GOSUB Initials
5370  RETURN
5380  END
5390  ! ************************
5400  ! *RUNGE TWO SUBROUTINE *
5410  ! ************************
5420 Runge2:!
5430  Tx=Xx(8)
5440  GOSUB Functions2
5450  FOR K=0 TO 8
5460  Yj(K)=F(K)*Delta
5470  Xx(K)=Uu3(K)+Yj(K)/2
5480  Uu3(K)=Xx(K)
5490  NEXT K
5500  IF Liqftot>0 THEN 5530
5510  Xx(3)=273.15
5520  Yj(3)=0
5530  Ty=Xx(8)
5540  Ta=Xx(8)
5550  Tl=Xx(2)
5560  Tlf=Xx(3)
5570  P=Xx(4)/1.01325E5
5580  IF Xx(1)>0 THEN 5600
5590  Tl=Tlf
5600  GOSUB Data2
5610  GOSUB Initials
5620  RETURN
5630  END
5640  ! ***************************
5650  ! * RUNGE TRHREE SUBROUTINE *
5660  ! ***************************
5670 Runge3:!
5680  Tx=Xx(8)
5690  GOSUB Functions2
5700  FOR K=0 TO 8
5710  Yk(K)=F(K)*Delta
5720  Xx(K)=Uu3(K)+Yk(K)
```

```
5730  NEXT K
5740  IF Liqftot>0 THEN 5770
5750  Xx(3)=273.15
5760  Yk(3)=0
5770  Ty=Xx(8)
5780  Ta=Xx(8)
5790  T1=Xx(2)
5800  T1f=Xx(3)
5810  P=Xx(4)/1.01325E5
5820  IF Xx(1)>0 THEN 5840
5830  T1=T1f
5840  GOSUB Data2
5850  GOSUB Initials
5860  RETURN
5870  END
5880  ! *************************
5890  ! * RUNGE FOUR SUBROUTINE *
5900  ! *************************
5910 Runge4:!
5920  Tx=Xx(8)
5930  GOSUB Functions2
5940  FOR K=0 TO 8
5950  Y1(K)=F(K)*Delta
5960  Xx(K)=Uu(K)+(Yi(K)+2*Yj(K)+2*Yk(K)+Y1(K))/6
5970  NEXT K
5980  IF Liqftot>0 THEN 6010
5990  Xx(3)=273.15
6000  Y1(3)=0
6010  Ty=Xx(8)
6020  Ta=Xx(8)
6030  T1=Xx(2)
6040  T1f=Xx(3)
6050  P=Xx(4)/1.01325E5
6060  IF Xx(1)>0 THEN 6080
6070  T1=T1f
6080  GOSUB Data2
6090  GOSUB Initials
6100  RETURN
6110  END
6120  ! *************************
6130  ! *  Initials Subroutine  *
6140  ! *************************
6150 Initials:!
6160  Pr=Cpa*Mue/Ka
6170  IF Xx(1)>0 THEN 6200
6180  Red=Alfd=Dcof=0
6190  GOTO 6230
6200  Red=Xx(6)*Xx(1)*ABS(Xx(7)-Xx(0))/Mue
6210  Alfd=Ka*(2+.6*Red^.5*Pr^.33)/Xx(1)
6220  Dcof=27*Red^(-.84)
6230  Rem=Xx(6)*Xx(7)*Dm/Mue
6240  IF Liqftot>0 THEN 6270
6250  Alff=0
6260  GOTO 6280
6270  Alff=Ka*.023*Rem^.8*Pr^.4/Dm
6280  IF Rem>2000 THEN 6310
6290  Fr=64/SQR(Rem)
6300  GOTO 6380
6310  Fr1=64/SQR(Rem)
6320  Fr2=(1/(-2*LGT(.00004572/(Dm*3.7)+2.51/(Rem*SQR(Fr1)))))^2
```

```
6330  Err=Fr2-Fr1
6340  IF ABS(Err)<=1E-6 THEN 6370
6350  Fr1=Fr2
6360  GOTO 6320
6370  Fr=Fr2
6380  FOR J=0 TO 15
6390  Sc(J)=Mue/(Xx(6)*D(J))
6400  IF Xx(1)>0 THEN 6430
6410  Betd(J)=0
6420  GOTO 6440
6430  Betd(J)=D(J)*(2+.6*Red^.5*Sc(J)^.33)/(Xx(1)*Gc(J)*Xx(2))
6440  Betf(J)=D(J)*.023*Rem^.8*Sc(J)^.4/(Dm*Gc(J)*Xx(3))
6450  NEXT J
6460  IF Liqdtot>0 THEN 6490
6470  Mixd=Xx(6)
6480  GOTO 6520
6490  GOSUB Rowf
6500  Mixq=Wa/(Wa+Wli-Liqftot)
6510  Mixd=1/(Mixq^1.5/Xx(6)+(1-Mixq^1.5)/Lmd)
6520  Macd=ABS(Xx(0)-Xx(7))/SQR(1.4*287*Xx(8))
6530  Macf=Xx(7)/SQR(1.4*287*Xx(8))
6540  IF Red>2000 THEN 6570
6550  Recfd=Pr^(1/2)
6560  GOTO 6580
6570  Recfd=Pr^(1/3)
6580  Tawd=Xx(8)*(1+Recfd*.2*Macd^2)     ! .2 is (Gam-1)/2
6590  IF Rem>2000 THEN 6620
6600  Recff=Pr^(1/2)
6610  GOTO 6630
6620  Recff=Pr^(1/3)
6630  Tawf=Xx(8)*(1+Recff*.2*Macf^2)     ! .2 is (Gam-1)/2
6640  RETURN
6650  END
6660  ! ****************************
6670  ! * FUNCTIONS ONE SUBROUTINE *
6680  ! ****************************
6690 Functions1:!
6700  FOR J=0 TO 15
6710  IF Xx(1)<>0 THEN 6750
6720  F1(0,J)=Xx(0)=0
6730  Xx(2)=273.15    ! Just A dummy Value Actually it is Zero
6740  GOTO 6930
6750  IF Xx(1)>3E-6 THEN 6830
6760  IF Step>1 THEN 6800
6770  F1(0,J)=2/Delta*Liqd(J)
6780  Xx(1)=0
6790  GOTO 6930
6800  F1(0,J)=-Liqd(J)/Delta
6810  Xx(1)=0
6820  GOTO 6930
6830  IF Liqd(J)>0 THEN 6860
6840  F1(0,J)=0
6850  GOTO 6930
6860  F1(0,J)=-PI*N*Xx(1)^2*Betd(J)*(Ps(J)-Xx1(3,J))/Xx(0)
6870  IF Step>1 THEN 6910
6880  IF ABS(F1(0,J))*Delta/2<=Liqd(J) THEN 6930
6890  F1(0,J)=-2/Delta*Liqd(J)
6900  GOTO 6930
6910  IF ABS(F1(0,J))*Delta<=Liqd(J) THEN 6930
6920  F1(0,J)=-Liqd(J)/Delta
```

```
6930  IF Liqf(J)>0 THEN 6960
6940  F1(1,J)=0
6950  GOTO 7030
6960  F1(1,J)=-PI*Dm*Betf(J)*(Psf(J)-Xx1(3,J))
6970  IF Step>1 THEN 7010
6980  IF ABS(F1(1,J))*Delta/2<=Liqf(J) THEN 7030
6990  F1(1,J)=-2/Delta*Liqf(J)
7000  GOTO 7030
7010  IF ABS(F1(1,J))*Delta<=Liqf(J) THEN 7030
7020  F1(1,J)=-Liqf(J)/Delta
7030  F1(2,J)=-(F1(0,J)+F1(1,J))
7040  F1(3,J)=Gc(J)*F1(2,J)*(Xx(4)-Seg(0))^2/((Xx(4)+Xx1(3,J)-Seg(0)
)*287*Wa)
7050  F1(4,J)=Xx1(4,J)*(F(4)/Xx(4)-F(8)/Xx(8))
7060  NEXT J
7070  RETURN
7080  END
7090  ! ****************************
7100  ! * FUNCTIONS TWO SUBROUTINE *
7110  ! ****************************
7120 Functions2:!
7130  IF Xx(1)>0 THEN 7170
7140  F(0)=0
7150  Xx(0)=0
7160  GOTO 7220
7170  IF Xx(7)-Xx(0)<0 THEN 7200
7180  F(0)=.75*Dcof*Xx(6)*(Xx(7)-Xx(0))^2/(Xx(1)*Xx(0)*Lmd)
7190  GOTO 7210
7200  F(0)=-(.75*Dcof*Xx(6)*(Xx(7)-Xx(0))^2/(Xx(1)*Xx(0)*Lmd))
7210  IF Xx(1)>0 THEN 7250
7220  F(1)=0
7230  Xx(1)=0
7240  GOTO 7350
7250  F(1)=2*Segd(0)/(PI*Xx(1)^2*Lmd*N)
7260  IF Step>1 THEN 7310
7270  IF ABS(F(1))*Delta/2<=Xx(1) THEN 7340
7280  F(1)=-Xx(1)*2/Delta
7290  Xx(1)=0
7300  GOTO 7340
7310  IF ABS(F(1))*Delta<=Xx(1) THEN 7340
7320  F(1)=-Xx(1)/Delta
7330  Xx(1)=0
7340  IF Xx(1)>0 THEN 7380
7350  F(2)=0
7360  Xx(2)=273.15
7370  GOTO 7390
7380  F(2)=(-Alfd*N*PI*Xx(1)^2*(Xx(2)-Tawd)/Xx(0)+Segd(4)+Qe*PI*Dm*L
msh*(Xx(3)-Xx(2)))/Seg(3)
7390  IF Liqftot>0 THEN 7430
7400  F(3)=0
7410  Xx(3)=Xx(2)
7420  GOTO 7440
7430  F(3)=(PI*Dm*(H-Alff*(Xx(3)-Tawf)+Qd*Lmsh*(Xx(2)-Xx(3)))+Segd(5
))/Seg(6)
7440  F(4)=(PI*Rh*Fr*Mixd*Xx(7)^2-(Wa+Seg(1))*F(7)-(Xx(7)-Xx(0))*Seg
d(0)+(Wi-Seg(4))*F(0)+Xx(7)*Segd(2)-PI*Dm*Xx(0)*(Qd-Qe))/Area
7450  F(5)=F(4)-Segd(1)
7460  F(6)=Xx(6)*(F(5)/Xx(5)-F(8)/Xx(8))
7470  F(7)=Xx(7)*(Segd(8)/(Area*Xx(7)*(Xx(6)+Seg(2)))-(F(6)+Segd(3))
/(Xx(6)+Seg(2))-Darea/Area)
```

```
7480  IF Xx(1)>0 THEN 7510
7490  F(8)=(PI*Dm*Alff*(Xx(3)-Tawf)-Segd(7)+.5*Segd(6)-Xx(7)*F(7)*(W
a+Seg(1))-Xx(0)*F(0)*Seg(8))/(Wa*Cpa+Seg(5))
7500  GOTO 7520
7510  F(8)=(Alfd*N*PI*Xx(1)^2*(Xx(2)-Tawd)/Xx(0)+PI*Dm*Alff*(Xx(3)-T
awf)-Segd(7)+.5*Segd(6)-Xx(7)*F(7)*(Wa+Seg(1))-Xx(0)*F(0)*Seg(8))/(W
a*Cpa+Seg(5))
7520  RETURN
7530  END
7540  ! ********************
7550  ! *  SEG SUBROUTINE *
7560  ! ********************
7570 Seg:!
7580  FOR Kk=0 TO 9
7590  Seg(Kk)=0
7600  NEXT Kk
7610  FOR J=0 TO 15
7620  Seg(0)=Seg(0)+Xx1(3,J)
7630  Seg(1)=Seg(1)+Xx1(2,J)
7640  Seg(2)=Seg(2)+Xx1(4,J)
7650  Seg(3)=Seg(3)+Liqd(J)*Cl(J)
7660  Seg(4)=Seg(4)+ABS(Xx1(0,J))
7670  Seg(5)=Seg(5)+Xx1(2,J)*Cv(J)
7680  Seg(6)=Seg(6)+Liqf(J)*Clf(J)
7690  Seg(7)=Seg(7)+ABS(Xx1(1,J))
7700  Seg(8)=Seg(8)+Liqd(J)
7710  Seg(9)=Seg(9)+Liqf(J)
7720  NEXT J
7730  RETURN
7740  END
7750  ! ********************
7760  ! * SEGD SUBROUTINE *
7770  ! ********************
7780 Segd:!
7790  FOR Kk=0 TO 8
7800  Segd(Kk)=0
7810  NEXT Kk
7820  FOR J=0 TO 15
7830  Segd(0)=Segd(0)+F1(0,J)
7840  Segd(1)=Segd(1)+F1(3,J)
7850  Segd(2)=Segd(2)+F1(1,J)
7860  Segd(3)=Segd(3)+F1(4,J)
7870  Segd(4)=Segd(4)+F1(0,J)*Hv(J)
7880  Segd(5)=Segd(5)+F1(1,J)*Hv(J)
7890  Segd(6)=Segd(6)+(F1(0,J)*(Xx(7)^2-Xx(0)^2)+F1(1,J)*Xx(7)^2)
7900  Segd(7)=Segd(7)+(Cv(J)*F1(0,J)*(Xx(2)-Xx(8))+Cvf(J)*F1(1,J)*(X
x(3)-Xx(8)))
7910  Segd(8)=Segd(8)+F1(2,J)
7920  NEXT J
7930  RETURN
7940  END
7950  ! *************************
7960  ! *  DATA ONE SUBROUTINE *
7970  ! *************************
7980 Data1:!
7990  FOR J=0 TO 15
8000  Gc(J)=8314.4/Mw(J)
8010  Rv(J)=P*1.01325E5/(Ta*Gc(J))/1000000
8020  ! ************************************************************
********
```

```
8030  Hv(J)=Hv(J)*4184/Mw(J)
8040  NEXT J
8050  RETURN
8060  END
8070  ! ************************
8080  ! * DATA TWO SUBROUTINE *
8090  ! ************************
8100 Data2:!
8110  Mue=Mue*(Ty/Tx)^.7791404
8120  Cpa=Cpa*(Ty/Tx)^.0125872
8130  Ka=Ka*(Ty/Tx)^.8922051
8140  FOR J=0 TO 15
8150  Tr=T1/Tc(J)
8160  Trf=T1f/Tc(J)
8170  FOR G=0 TO 2
8180  Vr(G)=Ar(G)+Br(G)*Tr+Cr(G)*Tr^2+Dr(G)*Tr^3+Er(G)/Tr+Fr(G)*LOG(
1-Tr)
8190  NEXT G
8200  Rc(J)=1/Vc(J)
8210  Rs(J)=Rc(J)/(Vr(0)+Um(J)*Vr(1)+Um(J)^2*Vr(2))
8220  Nr(J)=(1-.89*Um(J))*EXP(6.9547-76.2853*Tr+191.306*Tr^2-203.547
2*Tr^3+82.7631*Tr^4)
8230  R1(J)=Rs(J)*(1+9*Zc(J)*Nr(J)*(P-Pvr(J)/1.01325E5)/Pc(J))^(1/9)
8240  R1(J)=R1(J)*Mw(J)*1000
8250  ! ************************************************************
*******
8260  Cv(J)=Ca(J)+Cb(J)*T1+Cc(J)*T1^2+Cd(J)*T1^3
8270  C1(J)=(.5+2.2*Um(J))*(3.67+11.64*(1-Tr)^4+.634*(1-Tr)^(-1))
8280  C1(J)=(Cv(J)+C1(J)*1.98)*4184/Mw(J)
8290  Cv(J)=Cv(J)*4184/Mw(J)
8300  Cvf(J)=Ca(J)+Cb(J)*T1f+Cc(J)*T1f^2+Cd(J)*T1f^3
8310  C1f(J)=(.5+2.2*Um(J))*(3.67+11.64*(1-Trf)^4+.634*(1-Trf)^(-1))
8320  C1f(J)=(Cvf(J)+C1f(J)*1.98)*4184/Mw(J)
8330  ! ************************************************************
********
8340  D(J)=2.745E-4*SQR((Mw(J)+28.97)/(Mw(J)*28.97))*(Pc(J)*37.2)^(1
/3)*(Tc(J)*132.3)^(-.495)*Ta^1.823/P*1E-4
8350  ! ************************************************************
********
8360  Psf(J)=EXP(Hv(J)/Gc(J)*(1/Bt(J)-1/T1f))*Mff(J)*1.01325E5
8370  Ps(J)=EXP(Hv(J)/Gc(J)*(1/Bt(J)-1/T1))*Mf(J)*1.01325E5
8380  NEXT J
8390  RETURN
8400  END
8410  ! ************************
8420  ! *  SEGMA ONE SUBROUTIN  *
8430  ! ************************
8440 Segma1:!
8450  Segma=0
8460  FOR J=0 TO 15
8470  Segma=Segma+Liqd(J)/Mw(J)
8480  NEXT J
8490  FOR J=0 TO 15
8500  IF Liqd(J)>0 THEN 8540
8510  Mf(J)=0
8520  Liqd(J)=0
8530  GOTO 8550
8540  Mf(J)=Liqd(J)/Mw(J)/Segma
8550  NEXT J
8560  RETURN
```

```
8570  END
8580 Rowf: !
8590  IF Liqdtot=0 THEN RETURN
8600  Liqsum=0
8610  Liqmd=0
8620  Lmshtot=0
8630  FOR J=0 TO 15
8640  Liqmd=Liqmd+Liqd(J)/Mw(J)*Rl(J)
8650  Liqsum=Liqsum+Liqd(J)/Mw(J)
8660  Lmshtot=Lmshtot+Liqd(J)/Mw(J)*Cl(J)
8670  NEXT J
8680  Lmd=Liqmd/Liqsum
8690  Lmsh=Lmshtot/Liqsum
8700  RETURN
8710  END
8720 Segmaf: !
8730  Segmaf=0
8740  FOR J=0 TO 15
8750  Segmaf=Segmaf+Liqf(J)/Mw(J)
8760  NEXT J
8770  FOR J=0 TO 15
8780  IF Liqf(J)>0 THEN 8820
8790  Mff(J)=0
8800  Liqf(J)=0
8810  GOTO 8830
8820  Mff(J)=Liqf(J)/Mw(J)/Segmaf
8830  NEXT J
8840  RETURN
8850  END
8860  ! **********************
8870  ! *  Film Subroutine  *
8880  ! **********************
8890 Film:!
8900  Fvrate=(Vapf2-Vapf1)/((Lf2-Lf1)*PI*Dm)
8910  IF Mshape$<>"SMB" THEN 8940
8920  Bendf=Bfsm
8930  GOTO 9000
8940  IF Mshape$<>"SHB" THEN 8960
8950  Bendf=Bfsh
8960  IF L<Mlenth+.12 THEN 8990
8970  Bendf=Bfsm
8980  GOTO 9000
8990  Bendf=1
9000  Depf=1.5E-3*Xx(7)^2.34    ! m/s
9010  Dcons=N*(PI*Lmd*Xx(1)^3/6)/(Delta*PI*Dm^2/4)*Delta/Xx(0)    !Kg
/m3
9020  Deparea=Delta*PI*Dm      ! m2
9030  Qd=Dcons*Depf
9040  Filmin=Qd*Deparea*Bendf
9050  IF Filmin>Liqdtot THEN Filmin=Liqdtot
9060  FOR J=0 TO 15
9070  Win(J)=Filmin*Liqd(J)/Liqdtot
9080  IF Liqd(J)>Win(J) THEN 9120
9090  Liqf(J)=Liqf(J)+Liqd(J)
9100  Liqd(J)=0
9110  GOTO 9140
9120  Liqd(J)=Liqd(J)-Win(J)
9130  Liqf(J)=Liqf(J)+Win(J)
9140  NEXT J
9150  IF Filmin<Liqdtot THEN 9180
```

```
9160  Nd=N
9170  GOTO 9190
9180  Nd=Filmin/(Lmd*PI*Xx(1)^3/6)
9190  Liqftot=Liqftot+Filmin
9200  Liqdtot=Liqdtot-Filmin
9210  Fdiff1=2.653E-3*1.26*(-.08586+.33655*(Liqftot*60000)-.00855*(L
iqftot*60000)^2+.0001688*(Liqftot*60000)^3)
9220  Fdiff2=2.653E-3*1.04*(-.08586+.33655*(Liqftot*60000)-.00855*(L
iqftot*60000)^2+.0001688*(Liqftot*60000)^3)
9230  Fdiff3=2.653E-3/1.15*(-.08586+.33655*(Liqftot*60000)-.00855*(L
iqftot*60000)^2+.0001688*(Liqftot*60000)^3)
9240  Lftot=Liqftot+Liqdtot
9250  IF Wli<.03/60 THEN 9280
9260  Fdiff=Fdiff2+(Wli-.03/60)*(Fdiff3-Fdiff2)/((4.0E-2-.03)/60)
9270  GOTO 9320
9280  IF Wli=.03/60 THEN 9310
9290  Fdiff=Fdiff2+(Wli-.03/60)*(Fdiff1-Fdiff2)/((.020-.03)/60)
9300  GOTO 9320
9310  Fdiff=Fdiff2
9320  Qe=Qd/Bendf+Fdiff-Fvrate!The later is The Film Evap. Rate
9330  Filmout=Qe*Deparea
9340  IF Filmout>Liqftot THEN Filmout=Liqftot
9350  Ne=Filmout/(Lmd*PI*Xx(1)^3/6)
9360  N=N+Ne-Nd
9370  FOR J=0 TO 15
9380  Wout(J)=Filmout*Liqf(J)/Liqftot
9390  IF Liqf(J)>Wout(J) THEN 9430
9400  Liqd(J)=Liqd(J)+Liqf(J)
9410  Liqf(J)=0
9420  GOTO 9450
9430  Liqd(J)=Liqd(J)+Wout(J)
9440  Liqf(J)=Liqf(J)-Wout(J)
9450  NEXT J
9460  Liqdtot=Liqftot=0
9470  FOR J=0 TO 15
9480  Liqdtot=Liqdtot+Liqd(J)
9490  Liqftot=Liqftot+Liqf(J)
9500  NEXT J
9510  N=6*Liqdtot/(Lmd*PI*Xx(1)^3)
9520  RETURN
9530  END
9540 ! ************************
9550 ! *    Area Subroutine   *
9560 ! ************************
9570 Area: !
9580  IF L<=8E-3 THEN 9600
9590  GOTO 9630
9600  Darea=0
9610  Area=Area1
9620  RETURN
9630  IF (L>8E-3) AND (L<=.020) THEN 9650
9640  GOTO 9680
9650  Darea=(2.730437E-4-Area1)/1.2E-2
9660  Area=Area+Darea*Delta
9670  RETURN
9680  IF (L>.020) AND (L<=.03) THEN 9700
9690  GOTO 9730
9700  Darea=.09835863
9710  Area=Area+Darea*Delta
9720  RETURN
```

```
9730  IF Thr$<>"4/4" THEN 9750
9740  IF (L>.03) AND (L<=6.0E-2+Mlenth) THEN 9770
9750  IF (L>.03) AND (L<=4.0E-2) THEN 9770
9760  GOTO 9800
9770  Darea=0
9780  Area=Area
9790  RETURN
9800  IF (L>4.0E-2) AND (L<.05) THEN 9820
9810  GOTO 9910
9820  IF Thr$<>"1/4" THEN 9850
9830  Darea=-.07425
9840  GOTO 9890
9850  IF Thr$<>"1/2" THEN 9880
9860  Darea=-.045965
9870  GOTO 9890
9880  Darea=-.0218493
9890  Area=Area+Darea*Delta
9900  RETURN
9910  IF L=.05 THEN 9930
9920  GOTO 10080
9930  IF Thr$<>"1/4" THEN 9980
9940  Area=5.1413E-4
9950  Rec1=7.5E-2
9960  Dareath=.0297002824
9970  GOTO 10060
9980  IF Thr$<>"1/2" THEN 10030
9990  Area=7.96995E-4
10000 Rec1=6.6E-2
10010 Dareath=.0287276
10020 GOTO 10060
10030 Area=1.038137E-3
10040 Rec1=6.2E-2
10050 Dareath=1.820834E-2
10060 Darea=0
10070 RETURN
10080 IF (L>.05) AND (L<=Rec1) THEN 10100
10090 GOTO 10130
10100 Darea=Dareath
10110 Area=Area+Darea*Delta
10120 RETURN
10130 IF (L>Rec1) AND (L<=6.0E-2+Mlenth) THEN 10150
10140 GOTO 10180
10150 Darea=0
10160 Area=1.25663706E-3
10170 RETURN
10180 IF (L>6.0E-2+Mlenth) AND (L<=6.0E-2+Mlenth+1.0E-2) THEN 10200
10190 GOTO 10230
10200 Darea=-2.38761E-2
10210 Area=Area+Darea*Delta
10220 RETURN
10230 IF (L>6.0E-2+Mlenth+1.0E-2) AND (L<=6.0E-2+Mlenth+6.0E-2) THEN
 10250
10240 GOTO 10280
10250 Darea=0
10260 Area=1.017876E-3
10270 RETURN
10280 IF (L>6.0E-2+Mlenth+6.0E-2) AND (L<=6.0E-2+Mlenth+.096) THEN 1
0300
10290 GOTO 10330
10300 Darea=-8.63937979E-3
```

```
10310 Area=Area+Delta*Darea
10320 RETURN
10330 IF (L>6.0E-2+Mlenth+.096) AND (L<=6.0E-2+Mlenth+.1) THEN 10350
10340 GOTO 10380
10350 Darea=-4.3982297E-2
10360 Area=Area+Delta*Darea
10370 RETURN
10380 IF (L>6.0E-2+Mlenth+.1) AND (L<6.0E-2+Mlenth+.14) THEN 10400
10390 GOTO 10430
10400 Darea=(Areav-5.3092916E-4)/4.0E-2
10410 Area=Area+Delta*Darea
10420 RETURN
10430 IF L>6.0E-2+Mlenth+.14 THEN 10470
10440 Area=Areav
10450 Darea=0
10460 RETURN
10470 Darea=(1.9635E-3-Areav)/1.0E-2
10480 Area=Area+Darea*Delta
10490 RETURN
10500 END
```

```
10    ! RE-STORE"OPNSYS:F8"
20    ! ************************************************************
30    ! *                    THE PROGRAM "OPNSYS"                  *
40    ! *        This Program Deals with the Calculations          *
50    ! * Involved During the GAS EXCHANE PERIOD of the cycle of *
60    ! *                    SPARK IGNITION ENGINE                 *
70    ! ************************************************************
80    OPTION BASE 0
90    DIM Mdrop(220),Yc(16),Ys(16),R1(220),R2(220),Q(16),Nd(220),Ts1
(220),Ts2(220),Dmd(16)
100   DIM Mfvap(16),Vap(16),Segvap(220),Mfliq(220,16),Liq(16),Segliq
(220),Vaptot(220,16),Mfrac(220,16),Diff(16)
110   DIM Vr(3),Ar(3),Br(3),Cr(3),Dr(3),Er(3),Fr(3),Rc(16),Rs(16),Nr
(16),Rowv(16)
120   DIM Pv(16),Rl(16),Gc(16),Cv(16),Cl(16),Dts(16),Fliq(16),Fvap(1
6),Ps(16),Suml(16),Sumv(16),Xs(16)
130   DIM Mw(16),Bt(16),Tc(16),Pc(16),Ca(16),Cb(16),Cc(16),Cd(16),Ha
(16),Hb(16),Hc(16),Hd(16),Lh(16),Um(16),Car(16),Hyd(16),Vc(16),Zc(16
),Film(16),Pw(16)
140   PRINT PAGE
150   PRINT "  INPUT the NAME of the File to READ FROM  "
160   INPUT Filename$
170   ASSIGN #2 TO ""&Filename$
180   FOR I=1 TO 311
190   READ #2;X1,X2,X3,X4,X5,X6,X7,X8,X9,X10,X11,X12
200   NEXT I
210   FOR J=1 TO 16
220   READ Pw(J),Mw(J),Bt(J),Tc(J),Pc(J),Ca(J),Cb(J),Cc(J),Cd(J),Ha(
J),Hb(J),Hc(J),Hd(J),Lh(J),Um(J),Car(J),Hyd(J),Vc(J),Zc(J)
230   NEXT J
240   FOR G=1 TO 3
250   READ Ar(G),Br(G),Cr(G),Dr(G),Er(G),Fr(G)
260   NEXT G
270   FOR J=1 TO 16
280   READ #2;Liq(J),Film(J)
290   Vap(J)=Pw(J)-Liq(J)-Film(J)
300   NEXT J
310   Vaptot=Liqtot=0
320   FOR J=1 TO 16
330   Vaptot=Vaptot+Vap(J)
340   Liqtot=Liqtot+Liq(J)+Film(J)
350   NEXT J
360   ! **** ENGINE SPESIFICATIONS ****
370   Dc=.076          ! bore (m)
380   Crod=.23785        ! conn. rod length (m)
390   Crl=.0555      ! crank length (m)
400   !   ***** INPUT DATA *****
410   Compr=8.5            ! Compression Ratio
420   Dthe=2
430   N=1500          ! Engine Speed (rpm)
440   Pex=1.01325E5   ! Exh Press
450   ! **** Heat transfer Parameters *****
460   Ap=Ah=PI*Dc^2/4
470   Tp=520! P..Piston,h...Head & c... Linear
480   Th=420
490   Tcy=395
500   Ana=.4    ! Anand first coeff.
510   Anb=.7    ! Anand second coeff.
520   ! *** Initial Conditions ***
530   READ #2;Ta,Pa,Td,Rl,Row,Afr
```

```
540   PRINT PAGE
550   PRINT "  INPUT the NAME of the File to WRITE TO  "
560   INPUT Filename2$
570   CREATE ""&Filename2$,100
580   ASSIGN #1 TO ""&Filename2$
590   Vapinitial=Vaptot/(Vaptot+Liqtot)*100! Initail vapour quantity
  (%) from manifold calculations
600   Mwa=30.3!28.96   ! Mol. W.
610   Ra=287      ! Gas Const.  J/kgK
620   Pca=37.2    ! Critical Press.  atm
630   Tca=132.3   ! Critical Temp. K
640   Cpa=1005         ! J/kgK
650   Ga=1.4
660   Ka=2.57E-2
670   Mue=1.82E-5
680   Cpg=1100
690   Cvg=950
700   Gag=1.33
710   Rg=280
720   T1=Td
730   GOSUB Data1
740   Vst=PI*Dc^2/2*Cr1    ! Strok Vol.
750   Vc1=Vst/(Compr-1)
760   Dtime=Dthe/(N*6)
770   Vpis=2*2*Cr1*N/60
780   Ren=Row*Vpis*Dc/Mue
790   ! **** Cylinder Initial Conditions *****
800   P1=3*1.01325E5
810   T1=1100
820   V1=Vc1+(Crod+Cr1*(1-COS(PI*500/180))-(Crod^2-Cr1^2*SIN(PI*500/
180)^2)^.5)*PI*Dc^2/4
830   M1=P1*V1/(Rg*T1)
840   PRINTER IS 0
850   PRINT "Dtheta=";Dthe
860   PRINT "Release Temp.=";T1;"    (K)"
870   PRINT "Release Press.=";P1/1.01325E5;"    (Atm)"
880   PRINT "Initial Droplet Diam.=";R1*2E6;"(um)"
890   PRINT "Initial Droplet Temp.=";Td;"(K)"
900   PRINT "Initial Vapour =";Vapinitial;"(%)"
910   PRINT "Manifold Press. ";Pa/1.01325E5;"(bar)"
920   PRINT "Manifold Temp. ";Ta;"(K)"
930   PRINT "Engine Speed =";N;"(rpm)"
940   PRINT "Comp. Ratio =";Compr
950   PRINT ""
960   PRINTER IS 16
970   K=0   ! Counter
980   Mio=0
990   Change=0
1000  PRINT The,P1/1.01325E5;T1;Vapinitial
1010  PRINTER IS 16
1020  PRINT #1;The,P1/1.01325E5,T1,Vap1initial
1030  FOR J=1 TO 16
1040  Sum1(J)=Sumv(J)=0
1050  NEXT J
1060  ! **** A step Dthe has been applied *****
1070  FOR The=Dthe TO 438 STEP Dthe ! 438 is the angle at IVC
1080  GOSUB Thermo
1090  IF The<=210 THEN 2350
1100  IF Min>0 THEN 1130
1110  Mio=Mio+ABS(Min)
```

```
1120  GOTO 2350
1130  IF Change=1 THEN 1190
1140  Mio=Mio-Min
1150  IF Mio>=0 THEN 2350
1160  Change=1
1170  Min=-Mio
1180  Mc=M1
1190  K=K+Dthe
1200  Ts1(K)=Td
1210  R1(K)=R1
1220  Mfc=Min/(Afr+1)
1230  Ma=Afr*Mfc
1240  Segfilm=0
1250  FOR J=1 TO 16
1260  Segfilm=Segfilm+Film(J)
1270  NEXT J
1280  IF Segfilm=0 THEN 1310
1290  Mft=Mfc
1300  GOTO 1320
1310  Mft=Mfc/(1-Segfilm/100)
1320  Segliq(K)=0
1330  Segvap(K)=0
1340  FOR J=1 TO 16
1350  Mfvap(J)=Vap(J)/100*Mft
1360  Mfliq(K,J)=(Liq(J)+Film(J))/100*Mft
1370  Segliq(K)=Segliq(K)+Mfliq(K,J)
1380  Segvap(K)=Segvap(K)+Mfvap(J)
1390  Sumv(J)=Sumv(J)+Mfvap(J)
1400  Suml(J)=Suml(J)+Mfliq(K,J)
1410  NEXT J
1420  Mfliqtot=Mfliqtot+Segliq(K)
1430  Mfvaptot=Mfvaptot+Segvap(K)
1440  Matot=Matot+Ma
1450  T1=Ts1(K)
1460  Xx=K
1470  GOSUB Mfrac
1480  FOR J=1 TO 16
1490  Mfrac(K,J)=Mfrac(Xx,J)
1500  NEXT J
1510  Tx=Ts1(K)
1520  Ptot=(P1+P2)/(2*1.01325E5)
1530  Ttot=(T1+T2)/2
1540  GOSUB Vpress
1550  FOR J=1 TO 16
1560  Yc(J)=Sumv(J)/(Mc+Matot+Mfvaptot+Mfliqtot)
1570  NEXT J
1580  GOSUB Data2
1590  GOSUB Lmdf
1600  Mdrop(K)=4/3*PI*R1(K)^3*Rowf1
1610  Nd(K)=Segliq(K)/Mdrop(K)
1620  ! ***** Fuel Evaporation ******
1630  FOR J=1 TO 16
1640  Xs(J)=Mfrac(K,J)/Ptot*EXP(Lh(J)/Gc(J)*(1/Bt(J)-1/Ts1(K)))
1650  NEXT J
1660  Segxs=0
1670  Segxsmi=0
1680  FOR J=1 TO 16
1690  Segxs=Segxs+Xs(J)
1700  Segxsmi=Segxsmi+Xs(J)*Mw(J)/Mwa
1710  NEXT J
```

```
1720  FOR J=1 TO 16
1730  IF Mfrac(K,J)>0 THEN 1760
1740  Dmd(J)=Ys(J)=0
1750  GOTO 1830
1760  Ys(J)=Xs(J)*Mw(J)/(Mwa*(1-Segxs+Segxsmi))
1770  Diff(J)=2.745E-8/Ptot*((Mw(J)+Mwa)/(Mw(J)*Mwa))^.5*(Pc(J)*Pca)
^(1/3)*(Tc(J)*Tca)^(-.495)*Ttot^1.823
1780  Dmd(J)=4*PI*Rowv(J)*Diff(J)*R1(K)*LOG((1-Yc(J))/(1-Ys(J)))*Dti
me
1790  IF (Dmd(J)<=Mfliq(K,J)/Nd(K)) AND (Dmd(J)>0) THEN 1830
1800  IF Dmd(J)<0 THEN 1830
1810  Dmd(J)=Mfliq(K,J)/Nd(K)
1820  Ys(J)=1-(1-Yc(J))/EXP(Dmd(J)/(Dtime*4*PI*Rowv(J)*Diff(J)*R1(K)
)>
1830  Q(J)=C1(J)*(1-Ys(J))*((T1+T2)/2-Ts1(K))/(Ys(J)-Yc(J))
1840  NEXT J
1850  Segq=0
1860  Dtstot=0
1870  Dmdtot=0
1880  FOR J=1 TO 16
1890  Segq=Segq+Dmd(J)*(Q(J)+Cv(J)*(Ttot-Ts1(K)))
1900  Dmdtot=Dmdtot+Dmd(J)
1910  Mfliq(K,J)=Mfliq(K,J)-Dmd(J)*Nd(K)
1920  Sumv(J)=Sumv(J)+Dmd(J)*Nd(K)
1930  Suml(J)=Suml(J)-Dmd(J)*Nd(K)
1940  IF Suml(J)>1E-10 THEN 1970
1950  Sumv(J)=Sumv(J)+Suml(J)
1960  Suml(J)=0
1970  IF Suml(J)>=0 THEN 2000
1980  Sumv(J)=Sumv(J)+Suml(J)
1990  Suml(J)=0
2000  IF Mfliq(K,J)<0 THEN Mfliq(K,J)=0
2010  NEXT J
2020  Mfvaptot=Mfvaptot+Dmdtot*Nd(K)
2030  Mfliqtot=Mfliqtot-Dmdtot*Nd(K)
2040  FOR J=1 TO 16
2050  Yc(J)=Sumv(J)/(Mc+Matot+Mfvaptot+Mfliqtot)
2060  NEXT J
2070  Mdrop(K)=Mdrop(K)-Dmdtot
2080  IF Mdrop(K)<1E-15 THEN Mdrop(K)=0
2090  IF Mdrop(K)<0 THEN Mdrop(K)=0
2100  ! *** Update Cylinder Temp. & Press. Due to Evaporation ***
2110  T1=T2
2120  P1=P2
2130  T2=T1-Segq/(M2*Cpa)
2140  P2=P1*T2/T1
2150  IF Mdrop(K)>0 THEN 2180
2160  R2(K)=Ts2(K)=0
2170  GOTO 2270
2180  T1=Ts1(K)
2190  GOSUB Data2
2200  GOSUB Lmdf
2210  R2(K)=(Mdrop(K)/(4/3*PI*Rowfl))^(1/3)
2220  FOR J=1 TO 16
2230  Dts(J)=Dmd(J)*(Q(J)-Lh(J))/(4/3*PI*R2(K)^3*R1(J)*C1(J))*Dtime
2240  Dtstot=Dtstot+Dts(J)
2250  NEXT J
2260  Ts2(K)=Ts1(K)+Dtstot
2270  PRINT "D2(";K;")=";R2(K)*2E6
2280  R1(K)=R2(K)
```

```
2290  Ts1(K)=Ts2(K)
2300  IF (K=Dthe) OR (R2(K-Dthe)=0) THEN 2340
2310  FOR I=0 TO K-2*Dthe STEP Dthe
2320  GOSUB Evap
2330  NEXT I
2340  PRINT "**********************"
2350  P1=P2
2360  T1=T2
2370  M1=M2
2380  V1=V2
2390  IF Mfvaptot=0 THEN 2430
2400  PRINT The,P1/1.01325E5;T1;Mfvaptot/(Mfvaptot+Mfliqtot)*100
2410  PRINT #1;The,P1/1.01325E5,T1,Mfvaptot/(Mfvaptot+Mfliqtot)*100
2420  GOTO 2450
2430  PRINT The,P1/1.01325E5;T1
2440  PRINT #1;The,P1/1.01325E5,T1,0
2450  PRINTER IS 16
2460  NEXT The
2470  Enk=K
2480  PRINTER IS 0
2490  PRINT "Trapped Press. (bar) =";P1/1.01325E5
2500  PRINT "Trapped Temp.  (K)   =";T1
2510  PRINT "Trapped Mass   (Kg)  =";M1
2520  PRINT "Trapped Volume (m3)  =";V1
2530  PRINT "-------------------------------------------------------"
2540  FOR J=1 TO 16
2550  PRINT "Vapmass(";J;")=";Sumv(J);"(Kg)"
2560  PRINT "Liqmass(";J;")=";Suml(J);"(Kg)"
2570  PRINT #1;Sumv(J),Suml(J)
2580  NEXT J
2590  PRINT ""
2600  PRINT ""
2610  PRINTER IS 16
2620  PRINT "Diam. (um)","Number of droplets"
2630  PRINT "-----------------------------------"
2640  FOR K=Dthe TO Enk STEP Dthe
2650  IF R2(K)=0 THEN 2680
2660  PRINT R2(K)*2E6,Nd(K)
2670  PRINT #1;R2(K)*2E6,Nd(K)
2680  NEXT K
2690  PRINT ""
2700  PRINTER IS 0
2710  PRINT "Final Results"
2720  PRINT "Mc/M2 (%)";Mc/M1*100
2730  PRINT "Mg/M2 (%)";Mg/M1*100
2740  PRINT "Main=";Matot
2750  PRINT "Mvft=";Mfvaptot
2760  PRINT "(A/F)in=";Afr
2770  GOSUB Check
2780  GOSUB Diam
2790  PRINT #1;Afr,Mc/M1,Matot,D32*1E-6,T32,T1,P1,V1,M1
2800  PRINTER IS 16
2810  END
2820 Evap: !
2830  IF R2(K-I-Dthe)=0 THEN RETURN
2840  T1=Ts1(K-I-Dthe)
2850  Tx=Ts1(K-I-Dthe)
2860  Xx=K-I-Dthe
2870  GOSUB Data2
2880  GOSUB Mfrac
```

```
2890  FOR J=1 TO 16
2900  Mfrac(K-I-Dthe,J)=Mfrac(Xx,J)
2910  NEXT J
2920  Ptot=(P1+P2)/(2*1.01325E5)
2930  Ttot=(T1+T2)/2
2940  GOSUB Vpress
2950  FOR J=1 TO 16
2960  Xs(J)=Mfrac(K-I-Dthe,J)/Ptot*EXP(Lh(J)/Gc(J)*(1/Bt(J)-1/Ts1(K-
I-Dthe)))
2970  NEXT J
2980  Segxs=0
2990  Segxsmi=0
3000  FOR J=1 TO 16
3010  Segxs=Segxs+Xs(J)
3020  Segxsmi=Segxsmi+Xs(J)*Mw(J)/Mwa
3030  NEXT J
3040  FOR J=1 TO 16
3050  IF Mfrac(K-I-Dthe,J)>0 THEN 3080
3060  Dmd(J)=Ys(J)=Q(J)=0
3070  GOTO 3190
3080  Ys(J)=Xs(J)*Mw(J)/(Mwa*(1-Segxs+Segxsmi))
3090  IF Ys(J)<>Yc(J) THEN 3120
3100  Dmd(J)=Q(J)=0
3110  GOTO 3190
3120  Diff(J)=2.745E-8/Ptot*((Mw(J)+Mwa)/(Mw(J)*Mwa))^.5*(Pc(J)*Pca)
^(1/3)*(Tc(J)*Tca)^(-.495)*Ttot^1.823
3130  Dmd(J)=4*PI*Rowv(J)*Diff(J)*R1(K-I-Dthe)*LOG((1-Yc(J))/(1-Ys(J
)))*Dtime
3140  IF (Dmd(J)<=Mfliq(K-I-Dthe,J)/Nd(K-I-Dthe)) AND (Dmd(J)>0) THE
N 3180
3150  IF Dmd(J)<0 THEN 3180
3160  Dmd(J)=Mfliq(K-I-Dthe,J)/Nd(K-I-Dthe)
3170  Ys(J)=1-(1-Yc(J))/EXP(Dmd(J)/(Dtime*4*PI*Rowv(J)*Diff(J)*R1(K-
I-Dthe)))
3180  Q(J)=C1(J)*(1-Ys(J))*(Ttot-Ts1(K-I-Dthe))/(Ys(J)-Yc(J))
3190  NEXT J
3200  Segq=0
3210  Dtstot=0
3220  Dmdtot=0
3230  FOR J=1 TO 16
3240  Segq=Segq+Dmd(J)*(Q(J)+Cv(J)*(Ttot-Ts1(K-I-Dthe)))
3250  Dmdtot=Dmdtot+Dmd(J)
3260  Mfliq(K-I-Dthe,J)=Mfliq(K-I-Dthe,J)-Dmd(J)*Nd(K-I-Dthe)
3270  Sumv(J)=Sumv(J)+Dmd(J)*Nd(K-I-Dthe)
3280  Suml(J)=Suml(J)-Dmd(J)*Nd(K-I-Dthe)
3290  IF (Suml(J)>1E-10) OR (Suml(J)=0) THEN 3320
3300  Sumv(J)=Sumv(J)+Suml(J)
3310  Suml(J)=0
3320  IF Suml(J)>=0 THEN 3350
3330  Sumv(J)=Sumv(J)+Suml(J)
3340  Suml(J)=0
3350  IF Mfliq(K-I-Dthe,J)<0 THEN Mfliq(K-I-Dthe,J)=0
3360  NEXT J
3370  Mfvaptot=Mfvaptot+Dmdtot*Nd(K-I-Dthe)
3380  Mfliqtot=Mfliqtot-Dmdtot*Nd(K-I-Dthe)
3390  FOR J=1 TO 16
3400  Yc(J)=Sumv(J)/(Mc+Matot+Mfvaptot+Mfliqtot)
3410  NEXT J
3420  Mdrop(K-I-Dthe)=Mdrop(K-I-Dthe)-Dmdtot
3430  IF Mdrop(K-I-Dthe)<0 THEN Mdrop(K-I-Dthe)=0
```

```
3440  IF Mdrop(K-I-Dthe)<1E-15 THEN Mdrop(K-I-Dthe)=0
3450  ! *** Update Cylinder Temp. & Press. Due to Evaporation ***
3460  T1=T2
3470  P1=P2
3480  T2=T1-Segq/(M2*Cpa)
3490  P2=P1*T2/T1
3500  IF Mdrop(K-I-Dthe)>0 THEN 3530
3510  R2(K-I-Dthe)=Ts2(K-I-Dthe)=0
3520  GOTO 3620
3530  T1=Ts1(K-I-Dthe)
3540  GOSUB Data2
3550  GOSUB Lmdf
3560  R2(K-I-Dthe)=(Mdrop(K-I-Dthe)/(4/3*PI*Rowf1))^(1/3)
3570  FOR J=1 TO 16
3580  Dts(J)=Dmd(J)*(Q(J)-Lh(J))/(4/3*PI*R2(K-I-Dthe)^3*R1(J)*C1(J))
*Dtime
3590  Dtstot=Dtstot+Dts(J)
3600  NEXT J
3610  Ts2(K-I-Dthe)=Ts1(K-I-Dthe)+Dtstot
3620  PRINT "D2(";K-I-Dthe;")=";R2(K-I-Dthe)*2E6
3630  R1(K-I-Dthe)=R2(K-I-Dthe)
3640  Ts1(K-I-Dthe)=Ts2(K-I-Dthe)
3650  RETURN
3660  END
3670 Check: !
3680  FOR I=Dthe TO Enk STEP Dthe
3690  Mdrop(I)=4/3*PI*R2(I)^3*Rowf1*Nd(I)
3700  NEXT I
3710  Mltot=0
3720  FOR I=Dthe TO Enk STEP Dthe
3730  Mltot=Mltot+Mdrop(I)
3740  NEXT I
3750  PRINT "Mlfresd=";Mltot/Mfliqtot
3760  Afr2=Matot/(Mfvaptot+Mfliqtot)
3770  PRINT "% Evap Initial          =";Vapinitial
3780  PRINT "% Evap final            =";Mfvaptot/(Mfliqtot+Mfvaptot)
*100
3790  PRINT "(A/F)new=";Afr2
3800  RETURN
3810  END
3820 Diam: !
3830  D10=D20=D30=Na=Max=T20=T30=0
3840  Mmin=100
3850  FOR K=Dthe TO Enk STEP Dthe
3860  IF R2(K)=0 THEN 3950
3870  IF R2(K)*2E6>Mmax THEN Mmax=R2(K)*2E6
3880  IF R2(K)*2E6<Mmin THEN Mmin=R2(K)*2E6
3890  Na=Na+Nd(K)
3900  D10=D10+R2(K)*2E6*Nd(K)
3910  D20=D20+(R2(K)*2E6)^2*Nd(K)
3920  D30=D30+(R2(K)*2E6)^3*Nd(K)
3930  T20=T20+Ts2(K)^2*Nd(K)
3940  T30=T30+Ts2(K)^3*Nd(K)
3950  NEXT K
3960  D32=D30/D20
3970  T32=T30/T20
3980  D10=D10/Na
3990  D20=(D20/Na)^.5
4000  D30=(D30/Na)^(1/3)
4010  PRINT "Volume-Surfase Diam. (Sauter)  (D32) =";D32;"    (um)"
```

```
4020  PRINT "Volume-Surfase Temp. (Sauter)  (T32) =";T32;"   (K)"
4030  PRINT "Linear Mean Diam.               (D10) =";D10;"   (um)"
4040  PRINT "Surface Mean Diam.              (D20) =";D20;"   (um)"
4050  PRINT "Volume Mean Diam.               (D30) =";D30;"   (um)"
4060  PRINT "Maximum Diam.                         =";Mmax;"   (um)"
4070  PRINT "Minimum Diam.                         =";Mmin;"   (um)"
4080  PRINT "C1    (D20/D32) =                     =";D20/D32
4090  PRINT "C3    (D30/D32) =                     =";D30/D32
4100  RETURN
4110  END
4120  REM *************************
4130  REM *  DATA ONE SUBROUTINE *
4140  REM *************************
4150 Data1:!
4160  FOR J=1 TO 16
4170  Gc(J)=8314.4/Mw(J)
4180  Lh(J)=Lh(J)*4184/Mw(J)
4190  NEXT J
4200  RETURN
4210  END
4220  REM ************************
4230  REM * DATA TWO SUBROUTINE *
4240  REM ************************
4250 Data2:!
4260  FOR J=1 TO 16
4270  IF Mfliq(Xx,J)=0 THEN 4420
4280  Tr=T1/Tc(J)
4290  FOR G=1 TO 3
4300  Vr(G)=Ar(G)+Br(G)*Tr+Cr(G)*Tr^2+Dr(G)*Tr^3+Er(G)/Tr+Fr(G)*LOG(
1-Tr)
4310  NEXT G
4320  Rc(J)=1/Vc(J)
4330  Rs(J)=Rc(J)/(Vr(1)+Um(J)*Vr(2)+Um(J)^2*Vr(3))
4340  Nr(J)=(1-.89*Um(J))*EXP(6.9547-76.2853*Tr+191.306*Tr^2-203.547
2*Tr^3+82.7631*Tr^4)
4350  R1(J)=Rs(J)*(1+9*Zc(J)*Nr(J)*(Ptot-Pv(J))/Pc(J))^(1/9)
4360  R1(J)=R1(J)*Mw(J)*1000
4370  ! ***************************************************************
*******
4380  Cv(J)=Ca(J)+Cb(J)*T1+Cc(J)*T1^2+Cd(J)*T1^3
4390  C1(J)=(.5+2.2*Um(J))*(3.67+11.64*(1-Tr)^4+.634*(1-Tr)^(-1))
4400  C1(J)=(Cv(J)+C1(J)*1.98)*4184/Mw(J)
4410  Cv(J)=Cv(J)*4184/Mw(J)
4420  NEXT J
4430  RETURN
4440  END
4450  REM ******************************
4460  REM *  MASS FRACTION SUBROUTINE *
4470  REM ******************************
4480 Mfrac: !
4490  Segmas=0
4500  FOR J=1 TO 16
4510  IF Mfliq(Xx,J)=0 THEN 4530
4520  Segmas=Segmas+Mfliq(Xx,J)/Mw(J)
4530  NEXT J
4540  FOR J=1 TO 16
4550  IF Mfliq(Xx,J)=0 THEN 4580
4560  Mfrac(Xx,J)=Mfliq(Xx,J)/Mw(J)/Segmas
4570  GOTO 4590
4580  Mfrac(Xx,J)=0
```

```
4590  NEXT J
4600  RETURN
4610  END
4620 Lmdf: !
4630  Liqsum=0
4640  Lmd=0
4650  FOR J=1 TO 16
4660  IF Mfliq(Xx,J)=0 THEN 4690
4670  Lmd=Lmd+Mfliq(Xx,J)*Rl(J)
4680  Liqsum=Liqsum+Mfliq(Xx,J)
4690  NEXT J
4700  Rowfl=Lmd/Liqsum
4710  RETURN
4720  END
4730 Vpress:!
4740  FOR J=1 TO 16
4750  Pv(J)=Mfrac(Xx,J)*EXP(Lh(J)/Gc(J)*(1/Bt(J)-1/Ts1(Xx)))
4760  Rowv(J)=Ptot*1.01325E5/((Tx+Ttot)/2*Gc(J))
4770  NEXT J
4780  RETURN
4790  END
4800 Thermo: !
4810  Deg=The+500
4820  V2=Vc1+(Crod+Cr1*(1-COS(PI*Deg/180))-(Crod^2-Cr1^2*SIN(PI*Deg/
180)^2)^.5)*PI*Dc^2/4
4830  IF Deg<>720 THEN 4850
4840  Mg=M1
4850  IF The>230 THEN 4890
4860  P2=P1*(V1/V2)^Gag
4870  T2=T1*(P2/P1)^((Gag-1)/Gag)
4880  GOTO 4910
4890  P2=P1*(V1/V2)^Ga
4900  T2=T1*(P2/P1)^((Ga-1)/Ga)
4910  Acy=4*V2/Dc
4920  Twall=(Acy*Tcy+Ap*Tp+Ah*Th)/(Acy+Ap+Ah)
4930  Qa=-Ana*Ka/Dc*Ren^Anb*(T2-Twall)*(Acy+Ah+Ap)*Dtime
4940  IF The>230 THEN 4970
4950  T3=T2+Qa/(M1*Cpg)
4960  GOTO 4980
4970  T3=T2+Qa/(M1*Cpa)
4980  P3=P2*T3/T2
4990  IF The>230 THEN 5380
5000  IF The>120 THEN 5070
5010  IF The<110 THEN 5040
5020  Vlex=42.6
5030  GOTO 5090
5040  Ex=The+80
5050  Vlex=-329.168+13.83918*Ex-.2291995*Ex^2+.001838575*Ex^3-.00000
695922*Ex^4+9.99614E-9*Ex^5
5060  GOTO 5090
5070  Ex=The+80
5080  Vlex=-1234.434+17.06911*Ex-.0776783*Ex^2+.000133807*Ex^3-.0000
00062606*Ex^4
5090  IF Vlex<0 THEN Vlex=-Vlex
5100  Dcofex=1-.10652681*Vlex/42.6-2.3282347*(Vlex/42.6)^2+3.7092078
*(Vlex/42.6)^3-1.7628208*(Vlex/42.6)^4
5110  Vlex=Vlex/100*25.4*.001*SIN(45*PI/180)
5120  Vareaex=PI*(30+27)/2*.001*Vlex
5130  IF The>212 THEN 5370
5140  IF P3<Pex THEN 5250
```

```
5150  Px=Pex
5160  Py=P3
5170  Aa=Gag
5180  T=T3
5190  R=Rg
5200  A=Vareaex
5210  Cd=Dcofex
5220  GOSUB Mflow1
5230  Mout=Mass
5240  GOTO 5340
5250  Px=P3
5260  Py=Pex
5270  Aa=Gag
5280  T=T3
5290  R=Rg
5300  A=Vareaex
5310  Cd=Dcofex
5320  GOSUB Mflow1
5330  Mout=-Mass
5340  T4=T3*(M1-Gag*Mout)/(M1-Mout)
5350  P4=P3*T4/T3*(M1-Mout)/M1
5360  M2=M1-Mout
5370  IF The<=212 THEN 5790
5380  IF The>330 THEN 5470
5390  IF The<312 THEN 5420
5400  Vlin=42.1
5410  GOTO 5490
5420  In=The-160
5430  Vlin=-171.4146+10.1151*In-.2299964*In^2+.002480404*In^3-.00001
232942*In^4+2.29299E-8*In^5
5440  IF The<>212 THEN 5460
5450  Vlin=-Vlin
5460  GOTO 5490
5470  In=The-160
5480  Vlin=-1434.824+25.90649*In-.1633788*In^2+.0004376704*In^3-.000
000425936*In^4
5490  IF Vlin<0 THEN Vlin=-Vlin
5500  Dcofin=.8725-.207684*Vlin/42.1+.9026805*(Vlin/42.1)^2-2.041569
5*(Vlin/42.1)^3+1.1363634*(Vlin/42.1)^4
5510  Vlin=Vlin/100*25.4*.001*SIN(48*PI/180)
5520  Vareain=PI*(34.9+31.5)/2*.001*Vlin
5530  IF (The>212) AND (The<=230) THEN GOSUB Overlap
5540  IF The>230 THEN 5560
5550  GOTO 5790
5560  IF P3>Pa THEN 5670
5570  Px=P3
5580  Py=Pa
5590  Aa=Ga
5600  R=Ra
5610  A=Vareain
5620  Cd=Dcofin
5630  T=Ta
5640  GOSUB Mflow2
5650  Min=Mass
5660  GOTO 5760
5670  Px=Pa
5680  Py=P3
5690  Aa=Ga
5700  R=Ra
5710  A=Vareain
```

```
5720  Cd=Dcofin
5730  T=T3
5740  GOSUB Mflow2
5750  Min=-Mass
5760  T4=T3+Min/(M1+Min)*(Ga*Ta-T3)
5770  P4=P3*T4/T3*(M1+Min)/M1
5780  M2=M1+Min
5790  T2=T4
5800  P2=P4
5810  M2=M2
5820  V2=V2
5830  RETURN
5840  END
5850 Mflow1: !
5860  IF Px/Py<=(2/(Aa+1))^(Aa/(Aa-1)) THEN 5890
5870  Mass=Cd*A*Py/SQR(R*T)*SQR(2*Aa/(Aa-1)*((Px/Py)^(2/Aa)-(Px/Py)^
((Aa+1)/Aa)))*Dtime
5880  GOTO 5900
5890  Mass=Cd*A*Py/SQR(R*T)*SQR(Aa*(2/(Aa+1))^((Aa+1)/(Aa-1)))*Dtime
5900  RETURN
5910  END
5920 Mflow2: !
5930  IF Px/Py<=(2/(Aa+1))^(Aa/(Aa-1)) THEN 5960
5940  Mass=Cd*A*Py/SQR(R*T)*SQR(2*Aa/(Aa-1)*((Px/Py)^(2/Aa)-(Px/Py)^
((Aa+1)/Aa)))*Dtime
5950  GOTO 5970
5960  Mass=Cd*A*Py/SQR(R*T)*SQR(Aa*(2/(Aa+1))^((Aa+1)/(Aa-1)))*Dtime
5970  RETURN
5980  END
5990 Overlap: !
6000  IF P3<Pex THEN 6110
6010  Px=Pex
6020  Py=P3
6030  Aa=Gag
6040  T=T3
6050  R=Rg
6060  A=Vareaex
6070  Cd=Dcofex
6080  GOSUB Mflow1
6090  Mout=Mass
6100  GOTO 6200
6110  Px=P3
6120  Py=Pex
6130  Aa=Gag
6140  T=T3
6150  R=Rg
6160  A=Vareaex
6170  Cd=Dcofex
6180  GOSUB Mflow1
6190  Mout=-Mass
6200  T4=T3*(M1-Gag*Mout)/(M1-Mout)
6210  P4=P3*T4/T3*(M1-Mout)/M1
6220  M2=M1-Mout
6230  IF P4>Pa THEN 6340
6240  Px=P4
6250  Py=Pa
6260  Aa=Ga
6270  R=Ra
6280  A=Vareain
6290  Cd=Dcofin
```

```
6300  T=Ta
6310  GOSUB Mflow2
6320  Min=Mass
6330  GOTO 6430
6340  Px=Pa
6350  Py=P4
6360  Aa=Ga
6370  R=Ra
6380  A=Vareain
6390  Cd=Dcofin
6400  T=T4
6410  GOSUB Mflow2
6420  Min=-Mass
6430  T5=T4+Min/(Min+M2)*(Ga*Ta-T4)
6440  P5=P4*(M2+Min)/M2*T5/T4
6450  M2=M2+Min
6460  T1=T5
6470  P1=P5
6480  V1=V2
6490  M1=M2
6500  RETURN
6510  END
```

```
10    ! RE-STORE"CLSYS:F"
20    ! ******************************************************
30    ! *                THE PROGRAM "CLSYS"                 *
40    ! *      This Program Deals with the Calculations      *
50    ! * Involved during the CLOSED PERIOD of the cycle of *
60    ! *                SPARK IGNITION ENGINE               *
70    ! ******************************************************
80    OPTION BASE 1
90    DIM A(28,9),B(28,7),Mw(28),Vap(28),Liq(28),Ar(3),Br(3),Cr(3),D
r(3),Er(3),Fr(3),Pv(28),Rowv(28),Bt(28),Tc(28),Pc(28),Gc(28),Cpg(28)
,Cpl(28),Cvg(28)
100   DIM Um(28),Lh(28),Car(28),Hyd(28),Vc(28),Zc(28),Qvs(28),Fars(2
8),Massfv(28),Nm(28),Thc(6,4),Vis(6,4),Us(28),Molf(28),Rowl(28),Vr(3
),Kgas(6),Muegas(6)
110   DIM Dmd(28),Qevp(28),Xs(28),Fors(28),Bvap(28),Deltime(28),Aaut
(28),Baut(28),Daut(28),Cpv(28),Massfl(28),Diff(28),Pw(28)
120   DIM Gn(12),Gne(12),Dno(3),Ddis(3),Ak(7),Molfg(28),Vapb(28)
130   DIM Xeq(12),Xc(12),Rate(10),Nmb(28),Molfv(28),Rliq(28)
140   DIM Af(6),Bf(6),Cf(6),Ae(6),Be(6),Xkf(6),Xkb(6),Akc(6)
150   DIM Aa(7),Bb(7),Akp(7)
160   DIM S0(300),S1(300),S2(300),S3(300),S4(300),S5(300),S6(300),S7
(300),S8(300),S9(300),S10(300),S11(300),S12(300),S13(300),S14(300),S
15(300)
170   FOR I=1 TO 28
180   FOR K=1 TO 9
190   READ A(I,K)
200   NEXT K
210   NEXT I
220   FOR I=1 TO 12
230   FOR K=1 TO 7
240   READ B(I,K)
250   NEXT K
260   NEXT I
270   FOR I=13 TO 28
280   FOR K=1 TO 7
290   B(I,K)=A(I,K)
300   NEXT K
310   NEXT I
320   FOR I=1 TO 28
330   READ Mw(I)
340   NEXT I
350   FOR I=13 TO 28
360   READ Pw(I),Bt(I),Tc(I),Pc(I),Lh(I),Um(I),Car(I),Hyd(I),Vc(I),Z
c(I),Qvs(I)
370   NEXT I
380   FOR I=1 TO 3
390   READ Ar(I),Br(I),Cr(I),Dr(I),Er(I),Fr(I)
400   NEXT I
410   FOR I=1 TO 6
420   FOR K=1 TO 4
430   READ Thc(I,K)
440   NEXT K
450   NEXT I
460   FOR I=1 TO 6
470   FOR K=1 TO 4
480   READ Vis(I,K)
490   NEXT K
500   NEXT I
510   Dc=.076          ! bore (m)
520   Crod=.23785      ! Conn rod length (m)
```

```
530   Crl=.0555          ! Crank Length (m)
540   Compr=8.5          ! Comp Ratio
550   Anna=.4            ! Annand 1st Co-efficient
560   Annb=.7            ! Annand 2nd Co-efficient
570   Annc=0             ! Annand 3rd Co-efficient ,This will be=.075 du
ring Comb.
580   Sbc=5.68E-8        ! Stefan-Boltzman constant ( J/m2.S.K4)
590   Tpis=520           ! Piston Temp. (K)
600   Thead=420          ! Head Temp. (K)
610   Tcyl=395           ! Linear Temp. (K)
620   Cfn1=Cfn2=Cfn3=0     ! Flame contact areas
630   Pca=37.2           ! Critical press. (atm)
640   Tca=132.3          ! Critical temp. (K)
650   Mwa=28.964
660   Rmol=8.314         ! Universal gas constant (KJ/Kgmol.K)
670   Pref=1.01325E5 ! Ref Press for flame quinching ( bar )
680   Tref=300           ! Ref Temp for flame quinching ( K )
690   Dthe=1             ! Crank Angle STEP
700   N=1500             ! Engine speed rpm
710   Theadv=30          ! Advance Angle  BTDC
720   PRINT PAGE
730   PRINT "  INPUT the NAME of the FILE to READ from  "
740   INPUT Filename$
750   PRINT PAGE
760   PRINT "  INPUT the NAME of the FILE to WRITE to  "
770   INPUT Filename2$
780   PRINT PAGE
790   ASSIGN #1 TO ""&Filename$
800   FOR I=1 TO 220
810   READ #1;Xx1,Xx2,Xx3,Xx4
820   NEXT I
830   FOR J=13 TO 28
840   READ #1;Vap(J),Liq(J)
850   NEXT J
860   FOR I=1 TO 59
870   READ #1;Xx1,Xx2
880   NEXT I
890   READ #1;Afr,Resfrac,Airmass,D32,T32,Ttrap,Ptrap,Vtrap,Masst
900   Fuelmass=0
910   FOR J=13 TO 28
920   Fuelmass=Fuelmass+Vap(J)+Liq(J)
930   NEXT J
940   Airmass=Masst*(1-Resfrac)/(1+1/Afr)
950   Nma=Airmass/Mwa
960   Ffm=1-Resfrac
970   Resmass=Resfrac*Masst
980   Mubn1=Masst
990   Tubn1=Ttrap
1000  Pubn1=Ptrap
1010  Vtot1=Vtrap            ! Volume at IVC (438 Deg CR Angl)
1020  Td1=T32                ! Droplet Temp. (K)
1030  Rd1=D32/2              ! Droplet radius ( m)
1040  Tbn1=Mbn1=Vbn1=Rfn1=0
1050  Mubn2=Mubn1
1060  Vap1=Liq1=0
1070  FOR J=13 TO 28
1080  Vap1=Vap1+Vap(J)
1090  Liq1=Liq1+Liq(J)
1100  NEXT J
1110  Liq1=Liq1/(Vap1+Liq1)*100
```

```
1120  Assliq=Liq1+0
1130  Ffactor=.002337
1140  FOR J=13 TO 28
1150  Liq(J)=Assliq*Liq(J)/Liq1
1160  Vap(J)=(100-Assliq)*Vap(J)/(100-Liq1)
1170  NEXT J
1180  Theign=438+(180-38-Theadv)
1190  FOR J=13 TO 28
1200  Gc(J)=Rmol*1000/Mw(J)
1210  Lh(J)=Lh(J)*4184/Mw(J)
1220  NEXT J
1230  Vst=PI*Dc^2/2*Crl            ! Stroke volume (m3)
1240  Vcl=Vst/(Compr-1)            ! Clearance volume (m3)
1250  Vtot=Vst+Vcl
1260  Hcl=Vcl*4/(PI*Dc^2)          ! Clearance Height (m)
1270  Dtime=Dthe/(N*6)             ! Time equivalent of Dthe (sec)
1280  Vpis=2*2*Crl*N/60            ! Mean piston velocity (m/s)
1290  IF Assliq>0 THEN 1340
1300  Nd=0
1310  Mdrop1=0
1320  Rd1=0
1330  GOTO 1530
1340  Tliq=Td1
1350  GOSUB Molfrac
1360  GOSUB Density
1370  Mdrop1=4/3*PI*Rd1^3*Lmd
1380  Nd=Liqtot/Mdrop1
1390  GOSUB Equivalence
1400  T=Tubn1
1410  Unburnt=1
1420  GOSUB Nmols
1430  GOSUB Energy
1440  Uubn1=Umix
1450  Combustion=Bypass=Expansion=Del=0
1460  Initiation=Firststep=1
1470  S0(1)=438
1480  S1(1)=Tubn1
1490  S2(1)=S4(1)=S6(1)=S7(1)=S8(1)=S9(1)=S10(1)=S11(1)=S12(1)=0
1500  S3(1)=Pubn1/1.01325E5
1510  S5(1)=100-Assliq
1520  S13(1)=Phimix
1530  S14(1)=D32*1E6
1540  S15(1)=Td1
1550  FOR The=438+Dthe TO 720 STEP Dthe
1560  W=(The-438)/Dthe+1
1570  IF (Expansion=1) AND (Exstart=0) THEN 1630
1580  T=Tbn1
1590  Unburnt=0
1600  GOSUB Nmols
1610  GOSUB Energy
1620  Ubn1=Umix
1630  Deg=The+500
1640  Hpis=Crod+Crl*(1-COS(PI*Deg/180))-(Crod^2-Crl^2*SIN(PI*Deg/180
)^2)^.5
1650  Vtot2=Vcl+Hpis*PI*Dc^2/4
1660  IF Expansion=0 THEN 1690
1670  GOSUB Expansion
1680  GOTO 3310
1690  IF Combustion=0 THEN 2190
1700  Vubn1=Vubn1*Vtot2/Vtot1
```

```
1710  Vbn1=Vtot2-Vubn1
1720  IF Vbn1<=2/3*PI*Afn^3 THEN 2200
1730  Hfn=Hpis+Hcl
1740  Rfactor=1E-2
1750  Rad1=Rfn1
1760  Passall=1
1770  GOSUB Flame
1780  Err1=(Vbn1-Vfn)*1E6
1790  IF Err1<0 THEN 1990
1800  Rfn=Rad2=Rfn1+Rfn1*Rfactor
1810  IF Rfn>SQR((Dfn-Afn)^2+Hfn^2) THEN Rfn=SQR((Dfn-Afn)^2+Hfn^2)
1820  GOSUB Flame
1830  Err2=(Vbn1-Vfn)*1E6
1840  IF Err2<0 THEN 1870
1850  Rfactor=Rfactor+1E-2
1860  GOTO 1800
1870  Rfn=Radx=(Rad1*ABS(Err2)+Rad2*Err1)/(ABS(Err2)+Err1)
1880  IF Rfn>SQR((Dfn-Afn)^2+Hfn^2) THEN Rfn=SQR((Dfn-Afn)^2+Hfn^2)
1890  GOSUB Flame
1900  Errx=(Vbn1-Vfn)*1E6
1910  IF Errx<=1E-6 THEN 2180
1920  IF Errx>0 THEN 1960
1930  Err2=Errx
1940  Rad2=Radx
1950  GOTO 1870
1960  Err1=Errx
1970  Rad1=Radx
1980  GOTO 1870
1990  Rfn=Rad2=Rfn1-Rfactor*Rfn1
2000  IF Rfn>SQR((Dfn-Afn)^2+Hfn^2) THEN Rfn=SQR((Dfn-Afn)^2+Hfn^2)
2010  GOSUB Flame
2020  Err2=(Vbn1-Vfn)*1E6
2030  IF Err2>0 THEN 2060
2040  Rfactor=Rfactor+1E-2
2050  GOTO 1990
2060  Rfn=Radx=(Rad1*Err2+Rad2*ABS(Err1))/(Err2+ABS(Err1))
2070  IF Rfn>SQR((Dfn-Afn)^2+Hfn^2) THEN Rfn=SQR((Dfn-Afn)^2+Hfn^2)
2080  GOSUB Flame
2090  Errx=(Vbn1-Vfn)*1E6
2100  IF ABS(Errx)<=1E-6 THEN 2180
2110  IF Errx>0 THEN 2150
2120  Err1=Errx
2130  Rad1=Radx
2140  GOTO 2060
2150  Err2=Errx
2160  Rad2=Radx
2170  GOTO 2060
2180  Rfn1=Rfn
2190  GOTO 2210
2200  Rfn1=(3*Vbn1/(2*PI))^(1/3)
2210  IF The<=Theign THEN 2330
2220  IF (The>Theign) AND (Combustion=0) THEN 2330
2230  T=T1=Tbn1
2240  P1=Pbn1
2250  Unburnt=0
2260  GOSUB Adcomp
2270  Tbn2=T2
2280  Pbn2=P2
2290  V=Vbn1
2300  T=Tbn2
```

```
2310  Yesj=1
2320  GOSUB Diss
2330  T=T1=Tubn1
2340  P1=Pubn1
2350  Unburnt=1
2360  GOSUB Adcomp
2370  Tubn2=T2
2380  Pubn2=P2
2390  GOTO 2480
2400  Unburnt=1
2410  T=Tubn1
2420  GOSUB Specificheatgas
2430  Rmix1=Cpmix-Cvmix
2440  T=Tubn2
2450  GOSUB Specificheatgas
2460  Rmix2=Cpmix-Cvmix
2470  Pubn2=P1*Vtot1/Vtot2*Tubn2/Tubn1*Rmix2/Rmix1
2480  ! ----- Heat Transfer --------
2490  IF Combustion=0 THEN 2560
2500  Rfn=Rfn1
2510  Hfn=Hpis+Hcl
2520  Passall=0
2530  GOSUB Flame
2540  Aquinch=4*Vtot2/Dc+PI*Dc^2/2-Cfn+Sfn
2550  Vquinch=Vtot2-Vfn
2560  T=T2=Tubn2
2570  P2=Pubn2
2580  Unburnt=1
2590  Annc=0
2600  Anna=.4
2610  GOSUB Htransfer
2620  Qubn=Qtran
2630  Cvubn=Cvmix
2640  Cpubn=Cpmix
2650  IF The<=Theign THEN 2930
2660  IF (The>Theign) AND (Combustion=0) THEN 2930
2670  T=T2=Tbn2
2680  P2=Pbn2
2690  Unburnt=0
2700  IF Del=1 THEN 2730
2710  Annc=.075
2720  GOTO 2750
2730  Annc=.075
2740  Anna=.4
2750  GOSUB Htransfer
2760  Qbn=Qtran
2770  Cvbn=Cvmix
2780  Cpbn=Cpmix
2790  ! ----- Re-Calculate P & T for a constant vol process ------
2800  Tbn3=Tbn2+Qbn/(Mbn1*Cvbn)
2810  Unburnt=0
2820  T=Tbn2
2830  GOSUB Specificheatgas
2840  Rmix2=Cpmix-Cvmix
2850  T=Tbn3
2860  GOSUB Specificheatgas
2870  Rmix3=Cpmix-Cvmix
2880  Pbn3=Pbn2*Tbn3/Tbn2*Rmix3/Rmix2
2890  V=Vbn1
2900  T=Tbn3
```

```
2910  Yesj=1
2920  GOSUB Diss
2930  Tubn3=Tubn2+Qubn/(Mubn1*Cvubn)
2940  Unburnt=1
2950  T=Tubn2
2960  GOSUB Specificheatgas
2970  Rmix2=Cpmix-Cvmix
2980  T=Tubn3
2990  GOSUB Specificheatgas
3000  Rmix3=Cpmix-Cvmix
3010  Pubn3=Pubn2*Tubn3/Tubn2*Rmix3/Rmix2
3020  IF The<Theign THEN 3050
3030  IF (The>=Theign) AND (Initiation=0) THEN 3050
3040  GOSUB Initiation
3050  IF Combustion=0 THEN 3150
3060  Tdel=Tubn3
3070  Pdel=Pubn3
3080  GOSUB Ignitiondelay
3090  IF Knock<>1 THEN 3110
3100  GOTO 5520
3110  GOSUB Combustion
3120  IF Bypass=1 THEN 3310
3130  GOSUB Update
3140  GOTO 3310
3150  ! ------ Calculate Evaporation -------
3160  GOSUB Evaporation
3170  ! ------- Calculate Work -------
3180  Dwork=(Pubn1+Pubn4)/2*(Vtot2-Vtot1)
3190  ! ----- At Temp.=T4 AND the new mix composition CALCULATE U2 -
----
3200  T=Tubn4
3210  GOSUB Nummols
3220  GOSUB Energy
3230  Uubn2=Umix
3240  Diff=Uubn2-Uubn1-Qubn+Dwork+Segq
3250  IF ABS(Diff)>.1 THEN 3730
3260  Initiation=1
3270  GOSUB Update
3280  Tdel=Tubn1
3290  Pdel=Pubn1
3300  GOSUB Ignitiondelay
3310  PRINTER IS 16
3320  IF Combustion=1 THEN 3350
3330  PRINT The;Tubn1;Pubn1/1.01325E5;Vap1
3340  GOTO 3360
3350  PRINT The;Tubn1;Tbn1;Pbn1/1.01325E5;Vap1;Phyd
3360  PRINTER IS 16
3370  S0(W)=The
3380  S1(W)=Tubn1
3390  S2(W)=Tbn1
3400  S3(W)=Pubn1/1.01325E5
3410  S4(W)=Pbn1/1.01325E5
3420  S5(W)=Vap1
3430  S6(W)=Mbn1/Masst
3440  S7(W)=Utflame
3450  S8(W)=Rfn1
3460  S9(W)=Gn(7)*1E6
3470  S10(W)=Gn(5)
3480  S11(W)=Phyd
3490  S12(W)=Gn(3)
```

```
3500  S13(W)=Phimix
3510  S14(W)=Rd1*2E6
3520  S15(W)=Td1
3530  IF The<>720 THEN 3710
3540  PRINTER IS 0
3550  PRINT Filename2$
3560  PRINT "Evaporation=";100-Assliq;"%"
3570  PRINT "Droplet Diam.=";D32*1E6;"um"
3580  PRINT "Ignition Timing=";580-Theign;"BTDC"
3590  PRINT "Trapped Press=";Ptrap/1.01325E5;"bar"
3600  PRINT "Trapped Temp =";Ttrap;"K"
3610  PRINT "Cylinder A/F Ratio=";Afr
3620  PRINT "Release Press. =";Pbn1/1.01325E5
3630  PRINT "Release Temp. =";Tbn1
3640  PRINT "----------------------------"
3650  PRINTER IS 16
3660  CREATE ""&Filename2$,150
3670  ASSIGN #1 TO ""&Filename2$
3680  FOR I=1 TO W+1
3690  PRINT #1;S0(I),S1(I),S2(I),S3(I),S4(I),S5(I),S6(I),S7(I),S8(I)
,S9(I),S10(I),S11(I),S12(I),S13(I),S14(I),S15(I)
3700  NEXT I
3710  NEXT The
3720  GOTO 3810
3730  FOR J=13 TO 28
3740  Dmd(J)=0
3750  NEXT J
3760  GOSUB Nummols
3770  T=Tubn2
3780  GOSUB Specificheatgas
3790  Tubn2=Tubn2-Diff/(Mubn1*Cvmix)
3800  GOTO 2400
3810  END
3820 Adcomp: !
3830  GOSUB Specificheatgas
3840  Gama=Cpmix/Cvmix
3850  Rmix1=Cpmix-Cvmix
3860  T2=T1*(Vtot1/Vtot2)^(Gama-1)
3870  T=T2
3880  GOSUB Specificheatgas
3890  Rmix2=Cpmix-Cvmix
3900  P2=P1*Vtot1/Vtot2*T2/T1*Rmix2/Rmix1
3910  RETURN
3920  END
3930 Htransfer: !
3940  IF Unburnt=1 THEN 4010
3950  IF Expansion=1 THEN 4000
3960  Acyl=Cfn2
3970  Apis=Cfn3
3980  Ahead=Cfn1
3990  GOTO 4040
4000  Cfn1=Cfn2=Cfn3=0
4010  Acyl=4*Vtot2/Dc-Cfn2
4020  Apis=PI*Dc^2/4-Cfn3
4030  Ahead=PI*Dc^2/4-Cfn1
4040  GOSUB Specificheatgas
4050  GOSUB Viscosity
4060  GOSUB Thermalcond
4070  Rmix=Cpmix-Cvmix
4080  Denmix=P2/(Rmix*T2)
```

```
4090  Remix=Denmix*Vpis*Dc/Vismix
4100  Twall=(Acyl*Tcyl+Apis*Tpis+Ahead*Thead)/(Acyl+Apis+Ahead)
4110  Qtran=-(Anna*Kmix/Dc*Remix^Annb*(T2-Twall)+Annc*Sbc*(T2^4-Twal
l^4))*(Acyl+Ahead+Apis)*Dtime
4120  RETURN
4130  END
4140 Initiation: !
4150  Denubn=Mubn1/Vtot2
4160  GOSUB Equivalence
4170  Slr=27.58-78.34*(Phimix-1.13)^2
4180  Alfa=2.18-.8*(Phimix-1)
4190  Beta=-.16+.22*(Phimix-1)
4200  Ulflame=Slr*(Tubn3/298)^Alfa*(Pubn3/1.01325E5)^Beta*(1-2.1*Res
frac)/100
4210  Rfn=Ulflame*Dtime*(1+N*Ffactor)
4220  Hfn=Hpis+Hcl
4230  GOSUB Flame
4240  Vbn2=Vfn
4250  Vubn2=Vtot2-Vbn2
4260  Vf1=Vbn2-Vbn1
4270  Min=Denubn*Vf1
4280  Mbn2=Mbn1+Min
4290  Mubn2=Masst-Mbn2
4300  Fmass=Min*Vaptot/Mubn1
4310  Segheat=0
4320  FOR J=13 TO 28
4330  Segheat=Segheat+Fmass*Massfv(J)*(-Qvs(J)*1000/Mw(J))
4340  NEXT J
4350  T=Tubn3
4360  Unburnt=1
4370  GOSUB Specificheatgas
4380  Rubn1=Cpmix-Cvmix
4390  Tf1=Tubn3+Segheat/(Min*Cpmix)
4400  Amols=Min*Nma/Mubn1
4410  Ana=Airtot=Amols
4420  Amf=Fueltot=Fmass
4430  Nma=Nma-Amols
4440  FOR J=13 TO 28
4450  Vap(J)=Vap(J)-Fmass*Massfv(J)
4460  NEXT J
4470  T=Tf1
4480  V=Vf1
4490  GOSUB Diss
4500  Unburnt=0
4510  GOSUB Specificheatgas
4520  Rf1=Cpmix-Cvmix
4530  Pf1=Min*Rf1*Tf1/Vf1
4540  Gamf=Cpmix/Cvmix
4550  Kf=(Gamf-1)/Gamf
4560  T=Tubn3
4570  Unburnt=1
4580  Pass=0
4590  GOSUB Specificheatgas
4600  Gamubn=Cpmix/Cvmix
4610  Kubn=(Gamubn-1)/Gamubn
4620  Pr1=Pubn3
4630  Pr2=Pf1
4640  Pc2=(Pr2*Vf1*(Pr1/Pr2)^Kf+Pr1*Vubn2*(Pr1/Pr1)^Kubn)/Vtot2
4650  Err1=(Pc2-Pr1)/1.01325E5
4660  Pc2=(Pr2*Vf1*(Pr2/Pr2)^Kf+Pr1*Vubn2*(Pr2/Pr1)^Kubn)/Vtot2
```

```
4670  Err2=(Pc2-Pr2)/1.01325E5
4680  Px=(Pr1*ABS(Err2)+Pr2*ABS(Err1))/(ABS(Err1)+ABS(Err2))
4690  Pc2=(Pr2*Vf1*(Px/Pr2)^Kf+Pr1*Vubn2*(Px/Pr1)^Kubn)/Vtot2
4700  Errx=(Pc2-Px)/1.01325E5
4710  IF ABS(Errx)<=1E-2 THEN 4740
4720  Px=(Pc2+Px)/2
4730  GOTO 4690
4740  Tubnx=Tubn3*(Pc2/Pubn3)^Kubn
4750  Tbnx=Tf1*(Pc2/Pf1)^Kf
4760  Vbnx1=Vf1*(Pf1/Pc2)^(1/Gamf)
4770  Vbnx2=Vubn2*(Pubn3/Pc2)^(1/Gamubn)
4780  Vmean=(Vbnx1-Vf1+(Vubn2-Vbnx2))/2
4790  Vbn2=Vbn2+Vmean
4800  Rfn2=(3*Vbn2/(2*PI))^(1/3)
4810  Rfn1=Rfn2
4820  Vbn1=Vbn2
4830  Vubn2=Vtot2-Vbn2
4840  Initiation=0
4850  Combustion=1
4860  Pubn3=Pbn3=Pbn4=Pc2
4870  Tubn3=Tubnx
4880  Tbn3=Tbn4=Tbnx
4890  Vubn2=Vtot2-Vbn2
4900  Rfn=Rfn2
4910  Hfn=Hpis+Hcl
4920  GOSUB Flame
4930  V=Vbn2
4940  T=Tbnx
4950  GOSUB Diss
4960  Mubn1=Mubn2
4970  GOSUB Evaporation
4980  Annc=.075
4990  RETURN
5000  END
5010 Flamespeed: !
5020  Ulflame=1.087*1E4*Pcyl^(-.09876)/(1E4/Tprod+900/Tfresh)^4.938
5030  Utflame=Ulflame*(1+Ffactor*N)
5040  RETURN
5050  END
5060 Combustion: !
5070  IF Firststep=1 THEN RETURN
5080  Liqtot=0
5090  Vaptot=0
5100  FOR J=13 TO 28
5110  IF Liq(J)<0 THEN Liq(J)=0
5120  Liqtot=Liqtot+Liq(J)
5130  Vaptot=Vaptot+Vap(J)
5140  NEXT J
5150  FOR J=13 TO 28
5160  Massfv(J)=Vap(J)/Vaptot
5170  IF Liqtot=0 THEN 5190
5180  Massfl(J)=Liq(J)/Liqtot
5190  NEXT J
5200  IF (Liqtot=0) OR (Vap1>99) THEN 5250
5210  Tliq=Td1
5220  GOSUB Molfrac
5230  GOSUB Density
5240  Nd=Liqtot/(4/3*PI*Rd1^3*Lmd)
5250  IF Nd<0 THEN Nd=0
5260  Mfvap=Vaptot/Mubn1
```

```
5270  Mfair=Nma*Mwa/Mubn1
5280  Mfdrop=Nd/Mubn1
5290  Dropcon=Nd/Vubn1
5300  Unburnt=1
5310  T=Tubn3
5320  GOSUB Specificheatgas
5330  Rmix=Cpmix-Cvmix
5340  Denubn=Pubn3/(Rmix*Tubn3)!Mubn1/Vubn1
5350  Pcyl=(Pbn3+Pubn3)/2/(13595.098*9.80665)*3.281*12
5360  Tfresh=Tubn3
5370  Tprod=Tbn3
5380  GOSUB Flamespeed
5390  Rfn2=Rfn1+Utflame*Dtime
5400  Rfn=Rfn2
5410  Hfn=Hpis+Hcl
5420  IF Rfn>SQR((Dfn-Afn)^2+Hfn^2) THEN Rfn=SQR((Dfn-Afn)^2+Hfn^2)
5430  Passall=1
5440  GOSUB Flame
5450  Vbn2=Vfn
5460  IF (Vbn2/Vtot2<1E-3) OR (Del=1) THEN 5510
5470  Thedel=The
5480  Vdel=Vbn2/Vtot2
5490  Del=1
5500  Ffactor=2E-3
5510  IF Mbn2<.99*Masst THEN 5620
5520  Vbn2=Vtot2
5530  Min=Mubn1
5540  Mbn2=Masst
5550  Ndlost=Nd
5560  Vf1=Vbn2-Vbn1
5570  Vubn2=0
5580  Mubn2=0
5590  Amols=Nma
5600  Fmass=Vaptot
5610  GOTO 5920
5620  Vf1=Vbn2-Vbn1
5630  Vubn2=Vtot2-Vbn2
5640  Ndlost=Dropcon*(Vbn2-Vbn1)
5650  IF Ndlost<Nd THEN 5700
5660  Ndlost=Nd
5670  Nd=0
5680  Liqtot=0
5690  GOTO 5530
5700  Nd=Nd-Ndlost
5710  Min=Denubn*(Vbn2-Vbn1)
5720  IF Min>Mubn1 THEN Min=Mubn1
5730  Mbn2=Mbn1+Min
5740  Mubn2=Masst-Mbn2
5750  Amols=Min*Nma/Mubn1
5760  Fmass=Min*Vaptot/Mubn1
5770  Nma=Nma-Amols
5780  Resmass=Resmass-Min*Resmass/Mubn1
5790  IF Liqtot>0 THEN 5840
5800  FOR J=13 TO 28
5810  Vap(J)=Vap(J)-Fmass*Massfv(J)
5820  NEXT J
5830  GOTO 5930
5840  Tliq=Td1
5850  GOSUB Molfrac
5860  GOSUB Density
```

```
5870  FOR J=13 TO 28
5880  Vap(J)=Vap(J)-Fmass*Massfv(J)
5890  Liq(J)=Liq(J)-4/3*PI*Rd1^3*Lmd*Ndlost*Massfl(J)
5900  IF Liq(J)<0 THEN Liq(J)=0
5910  NEXT J
5920  IF Liqtot<>0 THEN 5960
5930  FOR J=13 TO 28
5940  Bvap(J)=0
5950  NEXT J
5960  GOSUB Flamequinching
5970  Ndlost=Ndlost-Ndquinch
5980  IF (Liqtot=0) OR (Vap1>99) THEN 6000
5990  GOSUB Evapcomb
6000  Segheat=0
6010  FOR J=13 TO 28
6020  Segheat=Segheat+((Fmass-Vapquinch)*Massfv(J)+Bvap(J))*(-Qvs(J)
*1000/Mw(J))
6030  NEXT J
6040  T=Tubn3
6050  Unburnt=1
6060  GOSUB Specificheatgas
6070  Rubn1=Cpmix-Cvmix
6080  Tf1=Tubn3+Segheat/(Min*Cpmix)
6090  T=Tf1
6100  Unburnt=0
6110  GOSUB Specificheatgas
6120  Rf1=Cpmix-Cvmix
6130  Gamf=Cpmix/Cvmix
6140  Kf=(Gamf-1)/Gamf
6150  Pf1=Min*Rf1*Tf1/Vf1
6160  T=Tbn3
6170  V=Vbn1
6180  Ana=Airtot
6190  Amf=Fueltot
6200  GOSUB Diss
6210  Unburnt=0
6220  GOSUB Specificheatgas
6230  Gambn=Cpmix/Cvmix
6240  Kbn=(Gambn-1)/Gambn
6250  Pr1=Pbn3
6260  Pr2=Pf1
6270  Pc2=(Pr2*Vf1*(Pr1/Pr2)^Kf+Pr1*Vbn1*(Pr1/Pr1)^Kbn)/Vbn2
6280  Err1=(Pc2-Pr1)/1.01325E5
6290  Pc2=(Pr2*Vf1*(Pr2/Pr2)^Kf+Pr1*Vbn1*(Pr2/Pr1)^Kbn)/Vbn2
6300  Err2=(Pc2-Pr2)/1.01325E5
6310  Px=(Pr1*ABS(Err2)+Pr2*ABS(Err1))/(ABS(Err1)+ABS(Err2))
6320  Pc2=(Pr2*Vf1*(Px/Pr2)^Kf+Pr1*Vbn1*(Px/Pr1)^Kbn)/Vbn2
6330  Errx=(Pc2-Px)/1.01325E5
6340  IF ABS(Errx)<=1E-3 THEN 6370
6350  Px=(Pc2+Px)/2
6360  GOTO 6320
6370  Tbn31=Tbn3*(Pc2/Pbn3)^Kbn
6380  Tf2=Tf1*(Pc2/Pf1)^Kf
6390  Pbn31=Pf2=Pc2
6400  Vbnx1=Vf1*(Pf1/Pf2)^(1/Gamf)
6410  Vbnx2=Vbn1*(Pbn3/Pbn31)^(1/Gambn)
6420  IF Vbnx1<Vbn2 THEN 6470
6430  Vbn2=Vbnx
6440  PRINT PAGE
6450  PRINT " Vbnx>Vbn2 "
```

```
6460  PAUSE
6470  T=Tbn31
6480  V=Vbnx2
6490  GOSUB Diss
6500  Unburnt=0
6510  GOSUB Specificheatgas
6520  Cpbn=Cpmix
6530  T=Tf2
6540  Unburnt=0
6550  GOSUB Specificheatgas
6560  Cpin=Cpmix
6570  Tfn=(Min*Cpin*Tf2+Mbn1*Cpbn*Tbn31)/(Mbn1*Cpbn+Min*Cpin)
6580  T=Tbn31=Tfn
6590  V=Vbn2
6600  Ana=Airtot=Airtot+Amols-Airquinch
6610  Amf=Fueltot=Fueltot+Fmass+Bvtot-Vapquinch
6620  Yesj=1
6630  GOSUB Diss
6640  Mwmean=Tothyd=0
6650  FOR J=13 TO 28
6660  Nmb(J)=Nmb(J)+Vapquinch*Massfv(J)/Mw(J)+Rliq(J)/Mw(J)
6670  Tothyd=Tothyd+Nmb(J)
6680  NEXT J
6690  FOR J=13 TO 28
6700  Mwmean=Mwmean+Nmb(J)/Tothyd*Mw(J)
6710  NEXT J
6720  IF Vubn2<>0 THEN 6760
6730  Tbn32=Tfn
6740  Tubn32=0
6750  GOTO 7140
6760  T=Tbn31
6770  Unburnt=0
6780  GOSUB Specificheatgas
6790  Kbn=(Cpmix/Cvmix-1)/(Cpmix/Cvmix)
6800  Gambn=Cpmix/Cvmix
6810  T=Tubn3
6820  Unburnt=1
6830  GOSUB Specificheatgas
6840  Kubn=(Cpmix/Cvmix-1)/(Cpmix/Cvmix)
6850  Gamubn=Cpmix/Cvmix
6860  Pr1=Pubn3
6870  Pr2=Pbn31
6880  Pc2=(Pr2*Vbn2*(Pr1/Pr2)^Kbn+Pr1*Vubn2*(Pr1/Pr1)^Kubn)/Vtot2
6890  Err1=(Pc2-Pr1)/1.01325E5
6900  Pc2=(Pr2*Vbn2*(Pr2/Pr2)^Kbn+Pr1*Vubn2*(Pr2/Pr1)^Kubn)/Vtot2
6910  Err2=(Pc2-Pr2)/1.01325E5
6920  Px=(Pr1*ABS(Err2)+Pr2*ABS(Err1))/(ABS(Err1)+ABS(Err2))
6930  Pc2=(Pr2*Vbn2*(Px/Pr2)^Kbn+Pr1*Vubn2*(Px/Pr1)^Kubn)/Vtot2
6940  Errx=(Pc2-Px)/1.01325E5
6950  IF ABS(Errx)<=1E-2 THEN 6980
6960  Px=(Pc2+Px)/2
6970  GOTO 6930
6980  Vbnx1=Vbn2*(Pbn31/Pc2)^(1/Gambn)
6990  Vbnx2=Vubn2*(Pubn3/Pc2)^(1/Gamubn)
7000  Vmean=(Vbnx1-Vbn2+(Vubn2-Vbnx2))/2
7010  Tbn32=Tbn31*(Pc2/Pbn31)^Kbn
7020  Tubn32=Tubn3*(Pc2/Pubn3)^Kubn
7030  Vbn2=Vbn2+Vmean
7040  T=Tbn32
7050  V=Vbn2
```

```
7060  Yesj=0
7070  GOSUB Diss
7080  Unburnt=0
7090  GOSUB Specificheatgas
7100  Phyd=Tothyd/(Mbn2/Mwmix)*1E6
7110  Phyd=Phyd*86.1624/(Mwmean*12)! 86.1624 is the Mw of C6H14
7120  IF Mbn2<.99*Masst THEN 7300
7130  PRINT PAGE
7140  PRINT " End of combustion "
7150  Hk=1
7160  Annc=.075
7170  Tbn1=Tbn32
7180  Pbn1=Pc2
7190  T=Tbn1
7200  V=Vtot2
7210  GOSUB Diss
7220  Mbn1=Masst
7230  Mubn1=Vap1=Tubn1=Pubn1=Utflame=Rfn2=Cfn1=Cfn2=Cfn3=0
7240  Vbn1=Vtot1=Vtot2
7250  Bypass=1
7260  Expansion=1
7270  IF Knock<>1 THEN 7290
7280  GOTO 3120
7290  GOTO 7630
7300  Vubn2=Vtot2-Vbn2
7310  IF Vbn2>2/3*PI*Afn^3 THEN 7340
7320  Rfn2=(3*Vbn2/(2*PI))^(1/3)
7330  GOTO 7580
7340  Hfn=Hpis+Hc1
7350  Rfactor=1E-2
7360  Rad1=Rfn2
7370  Err1=(Vbn2-Vfn)*1E6
7380  Rfn=Rad2=Rfn2+Rfn2*Rfactor
7390  IF Rfn>SQR((Dfn-Afn)^2+Hfn^2) THEN Rfn=SQR((Dfn-Afn)^2+Hfn^2)
7400  GOSUB Flame
7410  Err2=(Vbn2-Vfn)*1E6
7420  IF Err2<0 THEN 7450
7430  Rfactor=Rfactor+1E-2
7440  GOTO 7380
7450  Rfn=Radx=(Rad1*ABS(Err2)+Rad2*Err1)/(ABS(Err2)+Err1)
7460  IF Rfn>SQR((Dfn-Afn)^2+Hfn^2) THEN Rfn=SQR((Dfn-Afn)^2+Hfn^2)
7470  GOSUB Flame
7480  Errx=(Vbn2-Vfn)*1E6
7490  IF ABS(Errx)<=1E-6 THEN 7570
7500  IF Errx>0 THEN 7540
7510  Err2=Errx
7520  Rad2=Radx
7530  GOTO 7450
7540  Err1=Errx
7550  Rad1=Radx
7560  GOTO 7450
7570  Rfn2=Rfn
7580  Pubn3=Pbn4=Pc2
7590  Tbn4=Tbn32
7600  Tubn3=Tubn32
7610  Mubn1=Mubn2
7620  GOSUB Evaporation
7630  RETURN
7640  END
7650 Expansion: !
```

```
7660  Anna=.4
7670  Annc=.075
7680  T=Tbn1
7690  Unburnt=0
7700  GOSUB Specificheatgas
7710  Rmix1=Cpmix-Cvmix
7720  Exstart=1
7730  Unburnt=0
7740  T=T1=Tbn1
7750  P1=Pbn1
7760  GOSUB Adcomp
7770  Tbn2=T2
7780  Unburnt=0
7790  T=Tbn2
7800  GOSUB Specificheatgas
7810  Rmix2=Rmix
7820  IF Tbn2>1800 THEN 7840
7830  GOTO 7880
7840  T=Tbn2
7850  V=Vtot2
7860  Yesj=1
7870  GOSUB Diss
7880  Pbn2=P2*Rmix2/Rmix1
7890  IF Iter=0 THEN 7910
7900  Pbn2=Pbn1*Vtot1/Vtot2*Tbn2/Tbn1*Rmix2/Rmix1
7910  T=T2=Tbn2
7920  P2=Pbn2
7930  GOSUB Htransfer
7940  Tbn3=Tbn2+Qtran/(Masst*Cvmix)
7950  T=Tbn3
7960  GOSUB Specificheatgas
7970  Rmix3=Rmix
7980  IF Tbn3>1800 THEN 8000
7990  GOTO 8040
8000  T=Tbn3
8010  V=Vtot2
8020  Yesj=0
8030  GOSUB Diss
8040  Pbn3=Pbn2*Tbn3/Tbn2*Rmix3/Rmix2
8050  Dwork=(Pbn1+Pbn3)/2*(Vtot2-Vtot1)
8060  T=Tbn3
8070  Unburnt=0
8080  GOSUB Nmols
8090  GOSUB Energy
8100  Ubn2=Umix
8110  Diff=Ubn2-Ubn1-Qtran+Dwork
8120  IF ABS(Diff)<=.1 THEN 8190
8130  T=Tbn3
8140  Unburnt=0
8150  GOSUB Specificheatgas
8160  Tbn2=Tbn2-Diff/(Masst*Cvmix)
8170  Iter=1
8180  GOTO 7790
8190  Tbn1=Tbn3
8200  Pbn1=Pbn3
8210  Ubn1=Ubn2
8220  Vtot1=Vtot2
8230  Iter=0
8240  RETURN
8250  END
```

```
8260 Flamequinching: !
8270  GOSUB Equivalence
8280  Hydr=0
8290  Carb=0
8300  FOR J=13 TO 28
8310  Hydr=Hydr+Hyd(J)*Massfv(J)
8320  Carb=Carb+Car(J)*Massfv(J)
8330  NEXT J
8340  Hcrmix=Hydr/Carb
8350  Psy=1.25*(Hcrmix-3.26)^2+.563
8360  IF Phimix>1 THEN 8400
8370  Qdref=.92-.7*Phimix
8380  Beta=6.122-5.522*SQR(Phimix)
8390  GOTO 8420
8400  Qdref=.187+.033*Phimix
8410  Beta=1.386-.786*SQR(Phimix)
8420  Alfa=.63+.267*Phimix
8430  Qdis=Psy*Qdref*(Pref/Pubn3)^Alfa*(Tref/Tubn3)^Beta*1E-3
8440  Mquinch=Denubn*Aquinch/Vquinch*Vf1*Qdis
8450  Ndquinch=Mquinch*Mfdrop
8460  Vapquinch=Mquinch*Mfvap
8470  Airquinch=Mfair*Mquinch
8480  RETURN
8490  END
8500 Energy: !
8510  FOR J=1 TO 28
8520  Hs=0
8530  Us(J)=0
8540  FOR K=1 TO 7
8550  IF T>=3000 THEN 8580
8560  Coeff=A(J,K)
8570  GOTO 8590
8580  Coeff=B(J,K)
8590  Hs=Coeff/K*T^K+Hs
8600  NEXT K
8610  Hs=Hs+A(J,8)+A(J,9)
8620  Us(J)=Hs-Rmol*T
8630  NEXT J
8640  Umix=0
8650  FOR J=1 TO 28
8660  Umix=Umix+Us(J)*Nm(J)
8670  NEXT J
8680  Umix=Umix*1000       ! In Jouls
8690  RETURN
8700  END
8710 Vpress: !
8720  FOR J=13 TO 28
8730  Pv(J)=Molf(J)*EXP(Lh(J)/Gc(J)*(1/Bt(J)-1/Tliq))
8740  Rowv(J)=Ptot*1.01325E5/((Ttot+Tliq)/2*Gc(J))
8750  NEXT J
8760  RETURN
8770  END
8780 Lmd: !
8790  Liqsum=0
8800  Lmd=0
8810  Cplm=0
8820  FOR J=13 TO 28
8830  IF Liq(J)=0 THEN 8860
8840  Lmd=Lmd+Molf(J)*Rowl(J)
8850  Cplm=Cplm+Molf(J)*Cpl(J)
```

```
8860  NEXT J
8870  RETURN
8880  END
8890 Density: !
8900  FOR J=13 TO 28
8910  IF Liq(J)=0 THEN 9000
8920  Tr=Tliq/Tc(J)
8930  FOR G=1 TO 3
8940  Vr(G)=Ar(G)+Br(G)*Tr+Cr(G)*Tr^2+Dr(G)*Tr^3+Er(G)/Tr+Fr(G)*LOG(
1-Tr)
8950  NEXT G
8960  Rc=1/Vc(J)
8970  Rs=Rc/(Vr(1)+Um(J)*Vr(2)+Um(J)^2*Vr(3))
8980  Nr=(1-.89*Um(J))*EXP(6.9547-76.2853*Tr+191.306*Tr^2-203.5472*T
r^3+82.7631*Tr^4)
8990  Rowl(J)=Rs*(1+9*Zc(J)*Nr*(Ptot-Pv(J))/Pc(J))^(1/9)*Mw(J)*1000
9000  NEXT J
9010  GOSUB Lmd
9020  RETURN
9030  END
9040 Molfrac: !
9050  Segmol=0
9060  Liqtot=0
9070  FOR J=13 TO 28
9080  IF Liq(J)=0 THEN 9110
9090  Segmol=Segmol+Liq(J)/Mw(J)
9100  Liqtot=Liqtot+Liq(J)
9110  NEXT J
9120  FOR J=13 TO 28
9130  IF Liq(J)=0 THEN 9160
9140  Molf(J)=Liq(J)/Mw(J)/Segmol
9150  GOTO 9170
9160  Molf(J)=0
9170  NEXT J
9180  RETURN
9190  END
9200 Nmols:!
9210  IF Unburnt=1 THEN 9270
9220  FOR I=1 TO 12!28
9230  IF Nm(I)<0 THEN Nm(I)=0
9240  Nm(I)=Nmb(I)
9250  NEXT I
9260  GOTO 9380
9270  Nm(1)=.78984*Nma
9280  Nm(2)=.20946*Nma
9290  Nm(3)=.00033*Nma
9300  Nm(12)=.00937*Nma
9310  FOR I=4 TO 11
9320  Nm(I)=0
9330  NEXT I
9340  IF Pass=1 THEN 9380
9350  FOR I=13 TO 28
9360  Nm(I)=Vap(I)/Mw(I)
9370  NEXT I
9380  RETURN
9390  END
9400 Specificheatgas:! At temp=Tcyl
9410  GOSUB Nmols
9420  FOR J=1 TO 28
9430  Cpg(J)=A(J,1)
```

```
9440  FOR K=2 TO 7
9450  IF T>=3000 THEN 9480
9460  Coeff=A(J,K)
9470  GOTO 9490
9480  Coeff=B(J,K)
9490  Cpg(J)=Cpg(J)+Coeff*T^(K-1)
9500  NEXT K
9510  Cvg(J)=Cpg(J)-Rmol
9520  NEXT J
9530  Cpmix=Cvmix=Nmmix=Mwmix=0
9540  FOR J=1 TO 28
9550  Cpmix=Cpmix+Cpg(J)*Nm(J)
9560  Cvmix=Cvmix+Cvg(J)*Nm(J)
9570  Nmmix=Nmmix+Nm(J)
9580  Mwmix=Mwmix+Mw(J)*Nm(J)
9590  NEXT J
9600  Mwmix=Mwmix/Nmmix
9610  Cpmix=Cpmix/(Nmmix*Mwmix)*1000 ! J/Kg.K
9620  Cvmix=Cvmix/(Nmmix*Mwmix)*1000
9630  Rmix=Cpmix-Cvmix
9640  FOR J=1 TO 28
9650  Cpg(J)=Cpg(J)/Mw(J)*1000        ! J/Kg.K
9660  Cvg(J)=Cvg(J)/Mw(J)*1000
9670  NEXT J
9680  RETURN
9690  END
9700 Specificheatliq: ! At Temp=Tfuel
9710  T=Ttot
9720  FOR J=13 TO 28
9730  Tr=Tliq/Tc(J)
9740  Cpv(J)=A(J,1)
9750  FOR K=2 TO 7
9760  Cpv(J)=Cpv(J)+A(J,K)*T^(K-1)
9770  NEXT K
9780  Dcp=(.5+2.2*Um(J))*(3.67+11.64*(1-Tr)^4+.634*(1-Tr)^(-1))*1.98
*4.184
9790  Cpl(J)=(Cpv(J)+Dcp)/Mw(J)*1000     ! J/Kg.K
9800  Cpv(J)=Cpv(J)/Mw(J)*1000
9810  NEXT J
9820  RETURN
9830  END
9840 Nummols: !
9850  FOR J=13 TO 28
9860  Nm(J)=(Vap(J)+Dmd(J)*Nd)/Mw(J)
9870  NEXT J
9880  RETURN
9890  END
9900 Viscosity: !
9910  FOR I=1 TO 5
9920  Muegas(I)=Vis(I,1)
9930  FOR K=2 TO 4
9940  Muegas(I)=Muegas(I)+Vis(I,K)*T^(K-1)
9950  NEXT K
9960  NEXT I
9970  Vismix=0
9980  Ntot=0
9990  FOR I=1 TO 5
10000 Vismix=Vismix+Muegas(I)*Nm(I)
10010 Ntot=Ntot+Nm(I)
10020 NEXT I
```

```
10030 Vismix=Vismix/Ntot
10040 RETURN
10050 END
10060 Thermalcond:!
10070 FOR I=1 TO 6
10080 Kgas(I)=Thc(I,1)
10090 FOR K=2 TO 4
10100 Kgas(I)=Kgas(I)+Thc(I,K)*T^(K-1)
10110 NEXT K
10120 NEXT I
10130 Kmix=0
10140 Ntot=0
10150 FOR I=1 TO 6
10160 Kmix=Kmix+Kgas(I)*Nm(I)
10170 Ntot=Ntot+Nm(I)
10180 NEXT I
10190 Kmix=Kmix/Ntot
10200 RETURN
10210 END
10220 Evapcomb:!
10230 Ptot=Pbn3/1.01325E5
10240 Ttot=Tbn3
10250 GOSUB Molfrac
10260 Tliq=Td1
10270 GOSUB Vpress
10280 GOSUB Specificheatliq
10290 GOSUB Density
10300 T=Ttot
10310 Unburnt=0
10320 GOSUB Specificheatgas
10330 GOSUB Thermalcond
10340 FOR J=13 TO 28
10350 Xs(J)=Molf(J)/Ptot*EXP(Lh(J)/Gc(J)*(1/Bt(J)-1/Td1))
10360 NEXT J
10370 Segxs=0
10380 Segxsmi=0
10390 FOR J=13 TO 28
10400 Segxs=Segxs+Xs(J)
10410 Segxsmi=Segxsmi+Xs(J)*Mw(J)/Mwa
10420 NEXT J
10430 Unburnt=1
10440 GOSUB Nmols
10450 Segmol=0
10460 FOR J=1 TO 28
10470 Segmol=Segmol+Nm(J)*Mw(J)
10480 NEXT J
10490 Yo2cy=Nm(2)*Mw(2)/Segmol
10500 Bvtot=0
10510 Rltot=0
10520 Bliq=4/3*PI*Rd1^3*Lmd*Ndlost
10530 FOR J=13 TO 28
10540 IF Liq(J)>0 THEN 10570
10550 Bvap(J)=0
10560 GOTO 10640
10570 Ys=Xs(J)*Mw(J)/(Mwa*(1-Segxs+Segxsmi))
10580 Diff(J)=2.745E-8/Ptot*((Mw(J)+Mwa)/(Mw(J)*Mwa))^.5*(Pc(J)*Pca)
^(1/3)*(Tc(J)*Tca)^(-.495)*Ttot^1.823
10590 Bvap(J)=Ndlost*4*PI*Rowv(J)*Diff(J)*Rd1*LOG((1+Fors(J)*Yo2cy)/
(1-Ys))*Dtime
10600 IF Bvap(J)>Bliq*Massfl(J) THEN Bvap(J)=Bliq*Massfl(J)
```

```
10610 Rliq(J)=Bliq*Massfl(J)-Bvap(J)
10620 Rltot=Rltot+Rliq(J)
10630 Bvtot=Bvtot+Bvap(J)
10640 NEXT J
10650 RETURN
10660 END
10670 Evaporation:!
10680 IF Mubn1>0 THEN 10700
10690 GOTO 10790
10700 IF Vaptot/(Vaptot+Liqtot)*100<99.9 THEN 10830
10710 Vaptot=Vaptot+Liqtot
10720 Liqtot=0
10730 FOR J=13 TO 28
10740 IF Liq(J)<0 THEN Liq(J)=0
10750 Vap(J)=Vap(J)+Liq(J)
10760 Liq(J)=Dmd(J)=0
10770 NEXT J
10780 Rd1=Rd2=Td1=Td2=Mdrop1=Liqtot=0
10790 Pubn4=Pubn3
10800 Tubn4=Tubn3
10810 Rd1=Td1=Mdrop1=Liqtot=0
10820 RETURN
10830 Ptot=(Pubn1+Pubn3)/(2*1.01325E5)
10840 Ttot=(Tubn1+Tubn3)/2
10850 GOSUB Molfrac
10860 Tliq=Td1
10870 GOSUB Vpress
10880 GOSUB Specificheatliq
10890 GOSUB Density
10900 T=Ttot
10910 Unburnt=1
10920 GOSUB Specificheatgas
10930 Rmix3=Cpmix-Cvmix
10940 GOSUB Thermalcond
10950 FOR J=13 TO 28
10960 Xs(J)=Molf(J)/Ptot*EXP(Lh(J)/Gc(J)*(1/Bt(J)-1/Td1))
10970 NEXT J
10980 Segxs=0
10990 Segxsmi=0
11000 FOR J=13 TO 28
11010 Segxs=Segxs+Xs(J)
11020 Segxsmi=Segxsmi+Xs(J)*Mw(J)/Mwa
11030 NEXT J
11040 FOR J=13 TO 28
11050 IF Molf(J)>0 THEN 11080
11060 Dmd(J)=Ys=0
11070 GOTO 11170
11080 Yc=Vap(J)/Mubn1
11090 Ys=Xs(J)*Mw(J)/(Mwa*(1-Segxs+Segxsmi))
11100 Diff(J)=2.745E-8/Ptot*((Mw(J)+Mwa)/(Mw(J)*Mwa))^.5*(Pc(J)*Pca)
^(1/3)*(Tc(J)*Tca)^(-.495)*Ttot^1.823
11110 Dmd(J)=4*PI*Rowv(J)*Diff(J)*Rd1*LOG((1-Yc)/(1-Ys))*Dtime
11120 IF (Dmd(J)<=Liq(J)/Nd) AND (Dmd(J)>0) THEN 11160
11130 IF Dmd(J)<0 THEN 11160
11140 Dmd(J)=Liq(J)/Nd
11150 Ys=1-(1-Yc)/EXP(Dmd(J)/(Dtime*4*PI*Kmix/Cpmix*Rd1))
11160 Qevp(J)=Cpl(J)*(1-Ys)*(Ttot-Td1)/(Ys-Yc)
11170 NEXT J
11180 Dmdtot=0
11190 FOR J=13 TO 28
```

```
11200 Dmdtot=Dmdtot+Dmd(J)
11210 NEXT J
11220 Mdrop2=Mdrop1-Dmdtot
11230 Rd2=(Mdrop2/(4/3*PI*Lmd))^(1/3)
11240 Dtstot=0
11250 FOR J=13 TO 28
11260 IF Molf(J)>0 THEN 11290
11270 Dts=0
11280 GOTO 11310
11290 Dts=Dmd(J)*(Qevp(J)-Lh(J))/(4/3*PI*Rd2^3*Rowl(J)*Cpl(J))*Dtime
11300 Dtstot=Dtstot+Dts
11310 NEXT J
11320 Td2=Td1+Dtstot
11330 Segq=0
11340 FOR J=13 TO 28
11350 Segq=Segq+Nd*Dmd(J)*(Lh(J)+Cpv(J)*(Ttot-Td1))
11360 NEXT J
11370 Segq=Segq+(Mdrop1+Mdrop2)/2*Cplm*(Td2-Td1)*Nd
11380 ! *** Update Cylinder Temp. & Press. Due to Evaporation ***
11390  Tubn4=Tubn3-Segq/(Mubn2*Cvmix)
11400 T=Tubn4
11410 GOSUB Nummols
11420 Pass=1
11430 GOSUB Specificheatgas
11440 Rmix4=Cpmix-Cvmix
11450 Pubn4=Pubn3*Tubn4*Rmix4/(Tubn3*Rmix3)
11460 Pass=0
11470 IF Combustuion=0 THEN 11580
11480 Vaptot=0
11490 Liqtot=0
11500 FOR J=13 TO 28
11510 Vap(J)=Vap(J)+Dmd(J)*Nd
11520 Liq(J)=Liq(J)-Dmd(J)*Nd
11530 Vaptot=Vaptot+Vap(J)
11540 Liqtot=Liqtot+Liq(J)
11550 NEXT J
11560 Mdrop2=Liqtot/Nd!Nd=Liqtot/Mdrop2
11570 Rd2=(Mdrop2/(4/3*PI*Lmd))^(1/3)
11580 RETURN
11590 END
11600 Equivalence:!
11610 IF Mbn2/Masst=1 THEN RETURN
11620 Vaptot=0
11630 Liqtot=0
11640 Farsmix=0
11650 FOR J=13 TO 28
11660 Vaptot=Vaptot+Vap(J)
11670 IF Liq(J)<0 THEN Liq(J)=0
11680 Liqtot=Liqtot+Liq(J)
11690 NEXT J
11700 FOR J=13 TO 28
11710 Massfv(J)=Vap(J)/Vaptot
11720 IF Liq(J)<>0 THEN 11750
11730 Massfl(J)=0
11740 GOTO 11760
11750 Massfl(J)=Liq(J)/Liqtot
11760 Fars(J)=(12.011*Car(J)+1.0079*Hyd(J))/(138.28287*(Car(J)+Hyd(J
)/4))
11770 Fors(J)=Fars(J)/.2314
11780 Farsmix=Farsmix+Fars(J)*Massfv(J)
```

```
11790 NEXT J
11800 IF Combustion=0 THEN 11830
11810 Phimix=1/(Ana*Mwa/Amf)/Farsmix
11820 GOTO 11840
11830 Phimix=1/(Nma*Mwa/Vaptot)/Farsmix
11840 ! ****** TO CALCULATE CARBON FRACTION OF VAPOUR FUEL MIXTURE *
***
11850 Tot=0
11860 FOR I=13 TO 28
11870 Nm(I)=Vap(I)/Mw(I)
11880 Tot=Tot+Nm(I)
11890 NEXT I
11900 Cf=0
11910 FOR I=13 TO 28
11920 Molfv(I)=Nm(I)/Tot
11930 Cf=Cf+Car(I)*12.011/(Car(I)*12.011+Hyd(I)*1.0079)*Molfv(I)
11940 NEXT I
11950 Yf=Cf/12.011
11960 Xf=(1-Cf)/4.032
11970 RETURN
11980 END
11990 Carbfrac:!
12000 Tot=0
12010 Cf=0
12020 FOR J=13 TO 28
12030 Vapb(J)=(Amf*Massfv(J)+Bvap(J))/Mw(J)
12040 Tot=Tot+Vapb(J)
12050 NEXT J
12060 FOR J=13 TO 28
12070 Vapb(J)=Vapb(J)/Tot
12080 Cf=Cf+Car(J)*12.011/(Car(J)*12.011+Hyd(J)*1.0079)*Vapb(J)
12090 NEXT J
12100 Yf=Cf/12.011
12110 Xf=(1-Cf)/4.032
12120 RETURN
12130 END
12140 Update:!
12150 IF Combustion=0 THEN 12240
12160 Firststep=0
12170 Pbn1=Pbn4
12180 Tbn1=Tbn4
12190 Vbn1=Vbn2
12200 Mbn1=Mbn2
12210 Rfn1=Rfn2
12220 Pubn1=Pubn4
12230 IF Combustion=1 THEN 12350
12240 Vaptot=0
12250 Liqtot=0
12260 FOR J=13 TO 28
12270 Vap(J)=Vap(J)+Dmd(J)*Nd
12280 Liq(J)=Liq(J)-Dmd(J)*Nd
12290 Vaptot=Vaptot+Vap(J)
12300 Liqtot=Liqtot+Liq(J)
12310 NEXT J
12320 IF Vaptot/(Vaptot+Liqtot)*100>99.9 THEN 12350
12330 Mdrop2=Liqtot/Nd!Nd=Liqtot/Mdrop2
12340 Rd2=(Mdrop2/(4/3*PI*Lmd))^(1/3)
12350 Vap2=Vaptot/(Vaptot+Liqtot)*100
12360 Work=Work+Dwork
12370 Qtrantot=Qtrantot+Qubn+Qbn
```

```
12380 GOSUB Equivalence
12390 Uubn1=Uubn2
12400 Tubn1=Tubn4
12410 Tbn1=Tbn4
12420 IF Combustion=1 THEN 12440
12430 Pubn1=Pubn4
12440 Tubn1=Tubn4
12450 Vubn1=Vubn2
12460 Mubn1=Mubn2
12470 Vtot1=Vtot2
12480 Rd1=Rd2
12490 Td1=Td2
12500 Mdrop1=Mdrop2
12510 Vap1=Vap2
12520 RETURN
12530 END
12540 Ignitiondelay:!
12550 Adel=7.29E-3*(1+.9625*(Phimix/1.1-1)+5.445*(Phimix/1.1-1)^2+8.
32*(Phimix/1.1-1)^3)
12560 Deltime=Adel*(Pdel/1.01325E5)^(-1.685)*EXP(4341/Tdel)
12570 Autdelay=Autdelay+Dtime/Deltime
12580 PRINT "Delay=";Autdelay
12590 IF Autdelay<1 THEN 12640
12600 PRINT PAGE
12610 PRINT "KNOCK",The
12620 PAUSE
12630 Knock=1
12640 RETURN
12650 END
12660 Flame:!
12670 Dfn=Dc
12680 Afn=.15*Dfn      ! Spark Plug Position (m)
12690 IF Rfn<=SQR((Dfn-Afn)^2+Hfn^2) THEN 12730
12700 PRINT PAGE
12710 PRINT "      Flame Radius is More than the maximum possible
   "
12720 PAUSE
12730 IF Rfn>Afn THEN 12860
12740 IF Rfn>Hfn THEN 12770
12750 Xfn=Rfn
12760 GOTO 12780
12770 Xfn=Hfn
12780 Vfn=PI*Xfn*(Rfn^2-Xfn^2/3)
12790 IF Passall=0 THEN 12810
12800 GOTO 13370
12810 Sfn=2*PI*Rfn*Xfn
12820 Cfn1=PI*Rfn^2
12830 Cfn2=0
12840 Cfn3=PI*(Rfn^2-Xfn^2)
12850 GOTO 13360
12860 IF Rfn>Hfn THEN 12890
12870 Xfn=Rfn
12880 GOTO 12900
12890 Xfn=Hfn
12900 IF Rfn>=SQR(Afn^2+Hfn^2) THEN 13040
12910 Zfn=SQR(Rfn^2-Afn^2)
12920 Yfn=.58*Zfn
12930 GOSUB Alfa
12940 Vfn=Bfn*Zfn+PI*(Xfn-Zfn)*(Rfn^2-(Xfn^2+Xfn*Zfn+Zfn^2)/3)
12950 IF Passall=0 THEN 12970
```

```
12960 GOTO 13370
12970 Cfn2=Qfn*Zfn
12980 Sfn=Rfn*Pfn*Zfn/Ffn+2*PI*Rfn*(Xfn-Zfn)
12990 Cfn3=0
13000 Yfn=0
13010 GOSUB Alfa
13020 Cfn1=Bfn
13030 GOTO 13360
13040 IF Rfn>Dfn-Afn THEN 13230
13050 Xfn=Hfn
13060 Yfn=.58*Xfn
13070 GOSUB Alfa
13080 Vfn=Bfn*Xfn
13090 IF Passall=0 THEN 13110
13100 GOTO 13370
13110 Cfn2=Qfn*Xfn
13120 Sfn=Rfn*Pfn*Xfn/Ffn
13130 IF Rfn>SQR(Afn^2+Hfn^2) THEN 13160
13140 Cfn3=0
13150 GOTO 13190
13160 Yfn=Hfn
13170 GOSUB Alfa
13180 Cfn3=Bfn
13190 Yfn=0
13200 GOSUB Alfa
13210 Cfn1=Bfn
13220 GOTO 13360
13230 Zfn=SQR(Rfn^2-(Dfn-Afn)^2)
13240 Xfn=Hfn
13250 Yfn=Zfn+1/2*(Xfn-Zfn)
13260 GOSUB Alfa
13270 Vfn=.25*PI*Dfn^2*Zfn+Bfn*(Xfn-Zfn)
13280 IF Passall=0 THEN 13300
13290 GOTO 13370
13300 Cfn2=PI*Dfn*Zfn+Qfn*(Xfn-Zfn)
13310 Sfn=Rfn*(Xfn-Zfn)*Pfn/Ffn
13320 Cfn1=PI*Dfn^2/4
13330 Yfn=Hfn
13340 GOSUB Alfa
13350 Cfn3=Bfn
13360 Cfn=Cfn1+Cfn2+Cfn3
13370 RETURN
13380 END
13390 Alfa:!
13400 Ffn=SQR(Rfn^2-Yfn^2)
13410 Alfan=ACS((Afn/Dfn-(Afn/Dfn)^2-(Ffn/Dfn)^2)/((1-2*Afn/Dfn)*Ffn
/Dfn))
13420 Betan=ACS(1+((Afn/Dfn)^2-(Ffn/Dfn)^2)/(.5-Afn/Dfn))
13430 Bfn=(PI-Alfan+.5*SIN(2*Alfan))*Ffn^2+(2*Betan-SIN(2*Betan))*Df
n^2/8
13440 Pfn=2*(PI-Alfan)*Ffn
13450 Qfn=Dfn*Betan
13460 RETURN
13470 END
13480 Molfgas:!
13490 Segmolg=Nma
13500 FOR J=13 TO 28
13510 Segmolg=Segmolg+Nm(J)
13520 NEXT J
13530 FOR J=13 TO 28
```

```
13540 Molfg(J)=Nm(J)/Segmolg
13550 NEXT J
13560 Molfair=Nma/Segmolg
13570 RETURN
13580 END
13590 Diss:!
13600 GOSUB Equivalence
13610 Y=Yf
13620 X=Xf
13630 R=Rmol
13640 Xj=1E-2
13650 Pa=1.01325
13660 Dt=Dtime
13670 FOR I=1 TO 12
13680 Gn(I)=0
13690 NEXT I
13700 FOR I=1 TO 3
13710 Dno(I)=0
13720 Ddis(I)=0
13730 NEXT I
13740 Gn(1)=.78084*Ana
13750 Gn(2)=.20946*Ana-(X+Y)*Amf
13760 Gn(3)=Y*Amf
13770 Gn(4)=2*X*Amf
13780 Gn(12)=.00937*Ana
13790 An=Ana+X*Amf
13800 CALL Kinet(Ana,Amf,V,T,An,Gn(*),Dno(*),Ddis(*),Dis,Dt,Timcon,R
,Xj,X,Y,Cf,Pa)
13810 Alpha=Timcon/Dt
13820 IF Fzone=1 THEN 13970
13830 Tot=0
13840 FOR I=1 TO 12
13850 IF Gn(I)<0 THEN Gn(I)=0
13860 Nmb(I)=Gn(I)
13870 Tot=Tot+Gn(I)
13880 NEXT I
13890 FOR I=1 TO 12
13900 Gn(I)=Gn(I)/Tot
13910 NEXT I
13920 IF Yesj=1 THEN 13970
13930 PRINT "Temp(K)=";T,"Theta=";The
13940 PRINT "N2=";Gn(1);" O2=";Gn(2);" CO2=";Gn(3);" H2O=";Gn(4);" C
O=";Gn(5);" H2=";Gn(6);" NO=";Gn(7);" OH=";Gn(8);" N=";Gn(9);" H=";G
n(10);
13950 PRINT " O=";Gn(11);" Ar=";Gn(12)
13960 PRINT "-----------------------------------------------------"
13970 RETURN
13980 END
13990 ! ---------------------------------------------------------
-------
14000 SUB Kinet(Ana,Amf,V,T,An,Gn(*),Dno(*),Ddis(*),Dis,Dt,Timcon,R,
Xj,X,Y,Cf,Pa)
14010 Af(1)=7.1E14
14020 Af(2)=3.1E12
14030 Af(3)=3.4E15
14040 Af(4)=6.4E6
14050 Af(5)=3.1E10
14060 Af(6)=4.2E10
14070 Bf(1)=0
14080 Bf(2)=0
```

```
14090 Bf(3)=-1
14100 Bf(4)=1
14110 Bf(5)=0
14120 Bf(6)=0
14130 Cf(1)=-61200
14140 Cf(2)=-55000
14150 Cf(3)=-59000
14160 Cf(4)=-3125
14170 Cf(5)=-160
14180 Cf(6)=0
14190 Ae(1)=15.850275
14200 Ae(2)=14.4464
14210 Ae(3)=16.0737
14220 Ae(4)=1.3966
14230 Ae(5)=-1.6533
14240 Ae(6)=-1.064225
14250 Be(1)=-61962.825
14260 Be(2)=-54495.3
14270 Be(3)=-61366.3
14280 Be(4)=16447.55
14290 Be(5)=38203.15
14300 Be(6)=24362.1
14310 !   Calculation of Rate & Equilibrium coefficients
14320 FOR I=1 TO 6
14330 Xkf(I)=Af(I)*T^Bf(I)*EXP(Cf(I)/T)
14340 Akp(I)=EXP(Ae(I)+Be(I)/T)
14350 Akc(I)=Akp(I)
14360 IF I>=4 THEN 14380
14370 Akc(I)=Akp(I)*Pa/(Xj*R*T)
14380 Xkb(I)=Xkf(I)/Akc(I)
14390 NEXT I
14400 Gn(12)=.00937*Ana
14410 A=2*Dno(3)-Dno(2)
14420 Dno(1)=Dno(2)
14430 Dno(2)=Dno(3)
14440 Dno(3)=A
14450 A=2*Ddis(3)-Ddis(2)
14460 Ddis(1)=Ddis(2)
14470 Ddis(2)=Ddis(3)
14480 Ddis(3)=A
14490 Gno=Gn(7)
14500 Dis1=Dis
14510 FOR I=1 TO 2
14520 Gn(7)=Gno+Dt*(5*Dno(3)+8*Dno(2)-Dno(1))/12
14530 Dis=Dis1+Dt*(5*Ddis(3)+8*Ddis(2)-Ddis(1))/12
14540 IF Dis<=0 THEN 14560
14550 CALL Equilp(Ana,Amf,Dis,T,An,Gn(*),R,X,Y,Xj,Cf,Pa)
14560 Gn(9)=(Xkb(4)*Gn(7)*Gn(11)+Xkb(5)*Gn(1)*Gn(11)+Xkb(6)*Gn(7)*Gn
(10))/(Xkf(4)*Gn(2)+Xkf(5)*Gn(7)+Xkf(6)*Gn(8))
14570 Gn(1)=.78084*Ana-.5*(Gn(7)+Gn(9))
14580 An=0
14590 FOR J=1 TO 12
14600 An=An+Gn(J)
14610 NEXT J
14620 Dno(3)=2/V*(Xkb(5)*Gn(1)*Gn(11)-Xkf(5)*Gn(9)*Gn(7))
14630 Ddis(3)=2*An/V*(Xkf(1)*Gn(4)+Xkf(2)*Gn(6)+Xkf(3)*Gn(2)-(Xkb(1)
*Gn(8)*Gn(10)+Xkb(2)*Gn(10)^2+Xkb(3)*Gn(11)^2)/V)
14640 IF 2*Amf>(.41892*Ana-Gn(7))/(X+Y) THEN Ddis(3)=Ddis(3)-Dno(3)
14650 IF Gn(8)*Gn(11)<=0 THEN 14680
14660 Timcon=Dis*V^2/(4*Xkb(1)*An*Gn(8)*Gn(10))
```

```
14670 IF Timcon<Dt THEN Ddis(3)=Ddis(3)*Timcon/Dt
14680 NEXT I
14690 SUBEND
14700 ! ------------------------------------------------------------
-
14710 SUB Equilp(Ana,Amf,Dis,T,An,Gn(*),R,X,Y,Xj,Cf,Pa)
14720 !  Partial Equilibrium Calculation for Combustion Products
14730 ! The subroutine calculates the equilibrium composition of the
 C-H-O                system ,given a value for net dissociation obtai
ned from rate
14740 ! equations. The values for the Nitrogen based spicies,N2,NO,N
 are not             included as these are rate determined. Net disso
ciation is defined as:
14750 ! Dis=O+CO+H2+OH/2+3/2H        for weak to stoich mixtures  a
nd
14760 ! Dis=2+2*O2+OH+H              for rich mixtures
14770 ! Equilibrium values for 8 gases are obtained. These are numbe
red in the           arry as:
14780 ! (2)-O2,(3)-CO2,(4)-H2O,(5)-CO,(6)-H2,(8)-OH,(10)-H,(11)-O  .
 The actual        mathematical model used depends on defining Xx=O/O
2 . An initial value is
14790 ! guessed for Xx,then for this value the values for the other
gases are            found. The value of Xx is then corrected by ITER
ATION
14800 !  Units  : Temp. in Kelven;gas composition in moles
14810 Aa(1)=-2.01165
14820 Aa(2)=1.05695
14830 Aa(3)=2.460825
14840 Aa(4)=1.6273
14850 Bb(1)=2773.7
14860 Bb(2)=-446.95
14870 Bb(3)=-7914.55
14880 Bb(4)=-6871
14890 ! Equilibrium coefficients first calculated
14900 FOR I=1 TO 4
14910 Ak(I)=Aa(I)+Bb(I)/T
14920 IF ABS(Ak(I)>150) THEN Ak(I)=150*Ak(I)/ABS(Ak(I))
14930 Ak(I)=EXP(Ak(I))
14940 NEXT I
14950 Er1=0
14960 Er2=0
14970 J=0
14980 L=0
14990 ! Test to check if mixture is weak or rich
15000 IF .41892*Ana-Gn(7)<=2*(X+Y)*Amf THEN 15460
15010 ! Weak mixture . First set initial guess for O/O2
15020 Jn=1
15030 K=9
15040 Gn(5)=.5*Dis
15050 Gn(3)=Y*Amf-Gn(5)
15060 IF Gn(3)<Gn(5) THEN Gn(3)=Gn(5)
15070 Xx=Ak(1)*Gn(5)/Gn(3)
15080 Gn(2)=.20946*Ana-.5*Gn(7)-(X+Y)*Amf
15090 IF Gn(2)<1E-6*Ana THEN Gn(2)=1E-6*Ana
15100 Gn(6)=4*Dis^2*Ak(4)/(Gn(2)*Ak(3)^2)
15110 Gn(4)=2*X*Amf-Gn(6)
15120 IF Gn(4)<Gn(6) THEN Gn(4)=Gn(6)
15130 Xx2=Ak(2)*Gn(6)/Gn(4)
15140 IF Xx2<Xx THEN Xx=Xx2
15150 ! First guess for Xx
```

```
15160 Gn(3)=(Y*Amf+.00033*Ana)/(1+Xx/Ak(1))
15170 Gn(5)=(Y*Amf+.00033*Ana)/(1+Ak(1)/Xx)
15180 !  Solution for Carbon based gases CO2 & CO
15190 A1=(2*Xx+4)*Xx/Ak(2)-2*Xx
15200 B1=2-Xx+(3*Xx+6)*Xx/Ak(3)
15210 C1=(2*Xx+4)*Dis-.83916*Ana*Xx+4*Xx*Gn(3)-4*Gn(5)+2*Xx*Gn(7)
15220 A2=2*Xx/Ak(2)+2
15230 B2=Xx/Ak(3)+1
15240 C2=4*X*Amf
15250 Gn(4)=(C1*B2-B1*C2)/(A1*B2-B1*A2)
15260 Gn(8)=(C1*A2-A1*C2)/(B1*A2-B2*A1)
15270 Gn(6)=Gn(4)*Xx/Ak(2)
15280 Gn(10)=Gn(8)*Xx/Ak(3)
15290 !  Solution for Hydrogen based gases H2O,H2,OH & H
15300 IF Gn(6)>0 THEN 15330
15310 Gn(11)=0
15320 GOTO 15340
15330 Gn(11)=Gn(10)*ABS(Gn(10))*Ak(4)/(Gn(6)*Xx)
15340 Gn(2)=Gn(11)/Xx
15350 ! Solution for Oxygen based gases O2,O
15360 Error=.41958*Ana-Gn(7)-2*Gn(2)-2*Gn(3)-Gn(4)-Gn(5)-Gn(8)-Gn(11
)
15370 Error=-Error
15380 !    Error in total number of Oxygen atoms
15390 IF ABS(Error/Ana)<1E-6 THEN 15860
15400 IF K>13 THEN 15860
15410 CALL Simpit(K,1.4,Xx,Error,X1,Er1,X2,Er2)
15420 GOTO 15150
15430 !  Obtains next value of Xx
15440 !   End of calculation inside iteration loop WEAK
15450 ! Rich mixture . Check if mixture too rich for a solution to
 be possibile
15460 IF 1.01*Amf*Y>.41925*Ana-Gn(7) THEN Amf=.99*(.41925*Ana-Gn(7))
/Y
15470 Jn=2
15480 K=7
15490 IF Dis<1E-6*Ana THEN Dis=1E-6*Ana
15500 !   Set initial guess for Xx = O/O2
15510 Gn(5)=2*(X+Y)*Amf-.41892*Ana+Gn(7)+.5*Dis
15520 Gn(3)=.41892*Ana-(Y+2*X)*Amf-Gn(7)-.5*Dis
15530 IF Gn(3)<=0 THEN Gn(3)=Gn(3)+.5*Dis
15540 Xx=Ak(1)*Gn(5)/Gn(3)
15550 IF Xx<=0 THEN Xx=.15
15560 Dis=Dis-.41892*Ana+Gn(7)+2*(X+Y)*Amf
15570 GOTO 15150
15580 ! First guess for Xx
15590 Gn(3)=(Y*Amf+.00033*Ana)/(1+Xx/Ak(1))
15600 Gn(5)=(Y*Amf+.00033*Ana)/(1+Ak(1)/Xx)
15610 !  Solution for Carbon based gases CO2 & CO
15620 A1=-2*(Xx+1)
15630 B1=(Xx+2)*Xx/Ak(3)-Xx
15640 C1=(Xx+2)*Dis-.83916*(Xx+1)*Ana+4*(Xx+1)*Gn(3)+2*(Xx+1)*Gn(5)+
2*(Xx+1)*Gn(7)
15650 A2=2*Xx/Ak(2)+2
15660 B2=Xx/Ak(3)+1
15670 C2=4*X*Amf
15680 Gn(4)=(C1*B2-B1*C2)/(A1*B2-B1*A2)
15690 Gn(8)=(C1*A2-A1*C2)/(B1*A2-A1*B2)
15700 Gn(6)=Gn(4)*Xx/Ak(2)
15710 Gn(10)=Gn(8)*Xx/Ak(3)
```

```
15720 ! Solution for Hydrogen based gases H2O, H2, OH & H
15730 Gn(11)=Gn(10)*ABS(Gn(10))*Ak(4)/(Gn(6)*Xx)
15740 Gn(2)=Gn(11)/Xx
15750 ! Solution for Oxygen based gases O2 & O
15760 Error=Dis-2*Gn(2)-Gn(8)-Gn(10)-2*Gn(11)
15770 Erroe=-Error
15780 ! Error in total number Oxygen atoms
15790 L=L+1
15800 IF L>12 THEN 15860
15810 IF ABS(Error)<.001*Dis THEN 15860
15820 CALL Simpit(K,1.1,Xx,Error,X1,Er1,X2,Er2)
15830 GOTO 15580
15840 ! Obtains next value of Xx
15850 ! End of calculation inside iteration loop RICH
15860 An=0
15870 FOR I=1 TO 12
15880 IF Gn(I)<0 THEN Gn(I)=0
15890 An=An+Gn(I)
15900 NEXT I
15910 IF Jn=1 THEN 15930
15920 Dis=Dis+.41892*Ana-Gn(7)-2*(X+Y)*Amf
15930 SUBEND
15940 ! ------------------------------------------------------------

15950 SUB Simpit(N,Xk,Xx,Error,X1,Er1,X2,Er2)
15960 ! Simple iteration to find a value of Xx which reduces error-
F(Xx) to 0
15970 ! Parameters : N controls iteration technique. On first call N
 should be          set to 10.
15980 !              : Xk multiplier defining second guess for Xx. Xk
must be            greater than 1 if the curve of error vs. Xx has a
negative slope or less
15990 ! than 1 for a positive slope.
16000 !              : Xx subject of iteration.
                                 : Error error associated with the gue
ss Xx.
16010 !              : X1,X2 previous values of Xx.
                                 : Er1,Er2 previous error terms associ
ated with X1 & X2.
16020 ! Input on first call : Xx contains initial guess.
                                                 : Error contiane error assoc
iated with this guess.
16030 !                          : Xk contains a sutable multiplier.
                                                 : Er1,Er2 should be initiali
sed to zero.
16040 ! Input on further calls : Error new error associated with the
 value of Xx                                          found by last call to S
impit.
16050 ! Output on all calls : Xx new estimate of Xx.
16060 ! N.B. The variables X1,X2,Er1,Er2, should not be altered outs
ide of                     Simpit.
16070 OPTION BASE 1
16080 IF N>10 THEN 16230
16090 IF Error<0 THEN 16150
16100 Er1=Error
16110 X1=Xx
16120 IF Er2<0 THEN 16200
16130 Xx=Xx*Xk
16140 SUBEXIT
16150 Er2=Error
```

```
16160 X2=Xx
16170 IF Er1>0 THEN 16200
16180 Xx=Xx/Xk
16190 SUBEXIT
16200 N=N+1
16210 Xx=.5*(X1+X2)
16220 SUBEXIT
16230 IF (Error>Er1) OR (Error<Er2) THEN 16090
16240 IF (Er1-Error<.05*Er1) OR (Error-Er2<.05*ABS(Er2)) THEN 16090
16250 N=N+1
16260 Yk=Er1*X2*Er2+Er2*Xx*Error+Error*X1*Er1-Er2*X1*Er1-Error*X2*Er
2-Er1*Xx*Error
16270 Xz=Xx-Error*(X2-Xx)*(Xx-X1)*(Er1-Er2)/Yk
16280 IF Error<0 THEN 16320
16290 Er1=Error
16300 X1=Xx
16310 GOTO 16340
16320 Er2=Error
16330 X2=Xx
16340 Xx=Xz
16350 SUBEND
```

LIST OF REFERENCES

1. **Peters, B.D.**
"Fuel Droplets Inside the Cylinder of a Spark Ignition Engine with Axial Stratification".
SAE Paper No. 820132.

2. **Liu, X.Q., Wang, C.H. and Law, C.K.**
"Simulation of Fuel Droplet Gasification in SI Engines".
J. Engnr., Gas Turbine & Power, Vol. 106, P. 849, 1984.

3. **Hughes, D.W. and Goulburn, J.R.**
"Fuel Vaporization-Economy With Reduced Exhaust Emissions".
Proc. Instn. Mech. Engrs., Vol. 190,1976.

4. **Trayser, Creswick, et al.**
"A Study of the Influence of Fuel Atomization, Vaporization, and Mixing Processes on Pollutant Emissions from Motor Vehicle Power Plants".
Battelle Memorial Inst., Research report PB 185886, 1969.

5. **Lindsay, R., Thomas, A., Woodworth, J.A. and Zeschmann, E. G.**
"Influence of Homogenous Charge on the Exhaust Emissions of Hydrocarbons, Carbon Monoxide and Nitric Oxide from a Multicylinder Engine".
SAE Paper No. 710588.

6. **Dodd, A.E. and Wisdom, J.W.**
"Effect of Mixture Quality on Exhaust Emissions from Single-Cylinder Engines".
Proc. Instn. Mech. Engnrs., Vol. 183, Pt. 3E, 1968.

7. **Beale, N.R. and Hodgetts, D.**
"The Effect of Mixture Quality on the Exhaust Gas Emissions of a Petrol Engine".
Cranfield Report A.S.A.E. No. 1, Cranfield Inst. of Tech., Bedford, England, Jul. 1970.

8. **Yu, H.T.C.**
"Fuel Distribution Studies- A New Look to an Old Problem".
SAE Trans. Vol. 71, 1963.

9. **Matthes, W.R. and McGill, R.N.**
"Effects of the Degree of Fuel Atomization on Single-Cylinder Engine Performance".
SAE Trans. Vol. 85, 1976.

10. **Peters, B.D. and Quader, A.A.**
""Wetting" the Appetite of Spark Ignition Engines for Lean Combustion".
SAE Paper No. 780234.

11. **Godsave, G.A.E.**
"The Burning of Single Drops of Fuel".
4th Symp.(Int) on Combustion, PP. 818-30, 1953.

12. **Frössling, N.**
"Uber die Verdunstung Fallender Topfer".
Gerlands Beitr. Geophys. 52, PP. 170-216, 1938.

13. **Spalding, D.B.**
"The Construction of Liquid Fuels".
Ph. D. Thesis, Dept. Mech. Eng. , Cambridge University, 1951.

14. **Spalding, D.B.**
"Theory of Particle Combustion at High Pressure".
A.R.S. J., Nov. 1959.

15. **Law, C.K.**
"A Theory of Monodisperse Spray Vaporization in Adiabatic and Isothermal Systems".
Int. J. Heat & Mass Transfer, Vol. 18, PP. 1285-92, 1975.

16. **Kadota, T. and Hiroyasu, H.**
"Evaporation of a Single Droplet at Elevated Pressures and Temperatures".
1st Report : Experimental Study.
Trans. JSME Vol. 40, No. 339, 1974.

17. **Kadota, T. and Hiroyasu, H.**
"Evaporation of a Single Droplet at Elevated Pressures and Temperatures".
2nd Report : Theoretical Study.
Bull. JSME Vol. 19, No. 138, 1976.

18. **Law, C.K.**
"Unsteady Droplet Combustion with Droplet Heating".
Comb. & Flame 26, 17-22, 1976.

19. **Law, C.K. and Sirignano, W.A.**
"Unsteady Droplet Combustion with Droplet Heating-II: Combustion Limit".
Comb. & Flame 28, 175-86, 1977.

20. **Law, C.K., Prakash, S. and Sirignano, W.A.**
"Theory of Convective, Transient, Multicomponenet Droplet Vaporization".
16th Symp.(Int) on Combustion, PP. 605-15, 1976.

21. **Law, C.K.**
"Multicomponent Droplet Combustion with Rapid Internal Mixing".
Comb. & Flame 26, 219-33, 1976.

22. **Krasiakova, L.I.**
"Some Characteristics Flows of a Two-Phase Mixture in Horizontal Pipe".
Zhurnal Technicheskoi Fiziki, Vol. 22, No. 4, P. 656, 1952.

23. **McManus, H.N.**
"An Experimental Investigation of Film Characteristics in Horizontal Annular Two-Phase Flow".
ASME Paper 57-A-144, 1957,

24. **McManus, H.N.**
"Local Liquid Distribution and Pressure Drop in Annular Two-Phase Flow".
ASME Paper 61-hyd-20, 1961.

25. **Gill, L.E., Hewitt, G.F., Hitchon, J.W. and Lacey, P.M.**
"Sampling Probe Studies of the Gas Core in Annular Two-Phase Flow-I".
Chem. Engng. Sci., Vol. 18, PP. 525-35, 1963.

26. **Gill, L.E., Hewitt, G.F., Hitchon, J.W. and Lacey, P.M.**
"Sampling Probe Studies of the Gas Core in Annular Two-Phase Flow-II".
Chem. Engng. Sci., Vol. 19, PP. 665-82, 1964.

27. **Alexander, L.G. and Coldren, C.L.**
"Droplet Transfer from Suspending Air to Duct Walls".
Ind. & Eng. Chem. Vol. 43, No. 6, PP. 1325-31, 1951.

28. **Akagawa, K., Fuji, T., Ito, J., Hamano, Y. and Horiuchi, T.**
"Horizontal Liquid Film-Mist Two-Phase Flow".
Bull. JSME Vol. 28, No. 236, 1985.

29. **Collins, M.H.**
"A technique to Characterize Quantitatively the Air/Fuel Ratio in the Inlet Manifold of a Gasoline Engine".
SAE Paper No. 690515.

30. **Pao, H.C.**
"The Measurement of Fuel Evaporation in the Induction System Dring Warm-up".
SAE Paper No. 820409.

31. **Finlay, I.C. and Welsh, N.**
"Photographic Study of Fuel Atomization and Distribution in Air-Valve Carburettors".
Automotive Engineer Vol. 3, No. 2, PP. 30-33, 1978.

32. **Nightingale, C.J.K. and Tsatsami, V.**
"Seminar on Mixture Preparation and Wall Film Measurement".
UICEG Meeting, UMIST, June 1984.

33. **Finlay, I.C., McMillan, T. and Bannell, J.L.K.**
"Liquid Fuel Distribution in the Region of the Throttle Plate of an Air-Valve Carburettor".
Private Communications with Dr. I.C. Finlay, NEL.

34. **Hayashi, S. and Sawa, N.**
"A Study on the Transient Characteristics of Small SI Engines".
Bull. JSME Vol. 27, No. 224, 1984.

35. **Finlay, I.C., McMillan, T., Bannell, J.L.K. and Nightingale, C.J.E.**
"The Measurement of Droplet Sizes Leaving the Throttle Plate of an Air-Valve Carburettor".
NEL Report No. Y5/33, 1979.

36. **Nightingale, C.J.K. and Tsatsami, V.**
"Improved Mixture Preparation for Better Cold-Starting of SI Engines".
Automotive Engineer Vol. 9, No. 5, PP. 97-100, 1984.

37. **Phillips, N. P. and Ragner, P.**
"The Measurement of Fuel Droplet Distribution".
Final Year Reports, Mech. Eng. Dept., University of Aston, 1985.

38. **Yun, H.J., Lo, R.S. and Na, T.Y.**
"Theoretical Studies of Fuel Evaporation and Transportation in a Carburretor Venturi".
SAE Paper No. 760289.

39. **Lo, R.S. and Lalas, D.P.**
"Parametric Study of Fuel Droplet Flow in an Idealized Engine Induction System".
SAE Paper No. 770645.

40. **Picken, D.J., Soliman, H.A. and Fox, M.F.**
"Inlet Manifold Requirements For low Emissions".
Automotive Engineer, Vol 3, No. 4, PP. 59 -61, 1978.

41. **Finlay, I.C., Boam, D.J., and Bannell, J.L.K.**
"Computer Model of Fuel Evaporation in Air-Valve Carburettors".
Automotive Engineer, Vol 4, No. 6, PP. 51- 56, 1979.

42. **Boam, D.J. and Finlay, I.C.**
"A Computer Model of Fuel Evaporation in the Intake System of a Carburetted Petrol Engine".
I Mech E Conference on "The Fuel Economy and Emissions of Lean Burn Engines", Paper No. C89/79, June 1979.

43. **Low, S.C., Baruah, P.C. and Winterbone, D.E.**
"One-Dimensional Unsteady Air and Droplets Flow Model Which Includes Evaporation, Heat Transfer and Drag".
I Mech E Paper No. C65/81, 1981.

44. **Servati, H.B. and Yuen, W.W.**
"Deposition of Fuel Droplets in Horizontal Intake Manifolds and the Behaviour of Fuel Film Flow on Its Walls".
SAE Paper No. 840239.

45. **Burgoyne, J.H. and Cohen, L.**
"The Effect of Drop Size on Flame Propogation in Liquid Aerosols".
Proc. Roy. Soc. A225, No. 1162, 375, 1954.

46. **Sundukov, I.N. and Predvoditelev,**
"Flame Propogation in Two-Phase Mixtures".
7th Symp. (Int) on Combustion, PP. 352-57, 1958.

47. **Hayash, S. and Kumagai, S.**
"Flame Propogation in Fuel Droplet-Vapour Air Mixtures".
15th Symp. (Int). on Combustion, PP. 445 - 452, 1974.

48. **Mizutani, Y. and Nakajima, A.**
"Combustion of Fuel Vapour-Drop-Air Systems : Part I Open Burner Flames".
Comb. & Flame 20, PP. 343-50, 1973.

49. **Mizutani, Y. and Nakajima, A.**
"Combustion of Fuel Vapour-Droplet-Air Systems : Part II Spherical Flames in a Vessels".
Comb. & Flame 20, PP. 351-57, 1973.

50. **Ballal, D.R. and Lefebvre, A. H.**
"Flame Propagation in Heterogeneous Mixtures of Fuel Droplets, Fuel Vapour and Air".
18th Symp. (Int) on Combustion, PP. 321-28, 1981.

51. **Nizami, A.A. and Cernansky, N.P.**
"A Monodisperse Spray Combustion System and the Measurement of Oxides of Nitrogen".
Paper No. 78-37, Western States Section, The Comb. Inst., 1978.

52. **Nizami, A.A. and Cernansky, N.P.**
"NOx Formation in Monodisperse Fuel Spray Combustion".
17th Symp. (Int) on Combustion, PP. 475-83, 1979.

53. **Sarv, H., Nizami, A.A. and Cernansky, N.P.**
"Droplet Size Effects on NOx Formation in a One-Dimensional Monodisperse Spray Combustion System".
Trans. ASME, J. Engnr. Power, Vol. 105, 1983.

54. **Rao, K.V.L. and Lefebvre, A.H.**
"Minimum Ignition Energies in Flowing Kerosenes-Air Mixtures".
Comb. & Flame Vol. 27, PP. 155-68, 1979.

55. **Ballal, D.R. and Lefebuvre, A.H.**
"Igition and Flame Quenching of Flowing Hetrogeneous Fuel-Air Mixtures".
Comb. & Flame Vol. 35, PP. 155-68, 1979.

56. **Mansouri, S.H., Heywood, J.B. and Radhakrishnan, K.**
"Divided-Chamber Diesel Engine, Part I ; A Cycle-Simulation Which Predicts Performance and Emissions".
SAE Paper No. 820273.

57. **Hershey, R.L., Eberhardt, J.E. and Hottel, H.C.**
"Thermodynamic Properties of the Working Fluid in Internal Combustion Engines".
SAE J., Vol. 39, P. 409, 1936.

58. **Rabezzana, H., Kalmar, S. and Candelise, A.**
"An Analysis of Burning and Expansion in the Reaction Zone".
Automobile Engineer, PP. 347-53, Oct. 1939.

59. **Edson, M.H.**
" A Mathematical Model for Combustion in the Oto Cycle Engine".
Ind. & Eng. Chem., Vol. 52, No. 12, 1960.

60. **Patterson, D.J. and Wylen, G.V.**
"A digital Computer Simulation for Spark-Ignited Engine Cycle".
SAE Prog. Tech., Vol. 7, 1964.

61. **Semenov, N.N.**
"Thermal Theory of Combustion and Explosion, III. Theory of Normal Flame Propogration".
NACA T.M. NO. 1026, 1942.

62. **Eicheilberg, G.**
"Some New Investigations on old Combustion-Engine Problems".
Engineering Vol.148, PP.463-66, 547-50, 603-605, 1939.

63. **Strange, F.M.**
"An Analysis of the Ideal Otto Cycle, Including the Effects of Heat Transfer, Finite combustion Rates, Chemical Dissociation and Mechanical Losses".
SAE Prog. Tech., Vol 7, 1964.

64. **Phillipps, R.A. and Orman, P.L.**
"Simulation of Combustion in a Gasoline Engine Using a Digital Computer".
Advances in Automobile Engineering, Part IV, Pergammon Press, 1966.

65. **Mallard, E. and Le Chatelier H.**
Annales de Mines 4, pp. 274, 1883.

66. **Lucas, G.G. and James, E.H.**
"A Computer Simulation of a Spark Ignition Engine".
SAE Paper No. 730053.

67. **Benson, R.S., Annand, W.J.D. and Baruah, P.C.**
"A Simulation Model Including Intake and Exhaust Systems for a Single Cylinder, Four-Stroke Cycle Spark Ignition Engine".
Int. J. Mech. Sci., Vol. 17, PP. 97-124, Pergammon Press, 1975.

68. **Kuehl, D.K.**
"Laminar-Burning Velocities of Propane-Air Mixtures".
8th Symp. (Int) on Combustion, PP. 510-21, 1962.

69. **Hiroyasu, H. and Kadota, T.**
"Computer Simulation for Combustion and Exhaust Emissions in Spark Ignition Engine".
15th Symp. (Int) on Combustion, PP. 1213-222, 1974.

70. **Soliman, H.A.**
"The effects of Methane/Kerosene Mixtures as Spark Ignition Engine Fuels".
Ph.D. Thesis, School of Mech. and Prod. Eng. Leicester Polytechnic, 1978.

71. **Yuen, W.W. and Servati, H.**
"A Mathematical Engine Model Including the Effect of Engine Emissions".
SAE Paper No. 840036.

72. **Lichty, L.C.**
"Combustion Engine Processes".
McGraw Hill Book Co., 1967.

73. **Taylor, C.E.**
"The Internal Combustion Engines in Theory and Practice".
The MIT Press, 1976.

74. **Obert, E.F.**
"Internal Combustion Engines".
Intr. Textbook Co., 1968.

75. **Goodger, E.M.**
"Hydrocarbon Fuels".
The McMillan Press, 1975.

76. **Kraus, B.J. and Richard, G.P.**
"The Influence of Fuel Composition on Automotive Exhaust Emissions".
Inst. Mech. Eng. Symp. on "Air Polution Control in Transport Engines", 1971.

77. **Lane, W.R.**
"Shatter of Drops in Streams of Air".
Ind.& Eng. Chem., Vol.43, No. 6, PP.1312-17, 1951.

78. **Nukiyama, S. And Tanasawa, Y.**
"Experiments on the Atomisation of Liquids in Air Stream".
Reports Nos.1-6, Defence Res. Board, Dept. Nat. Defence, Ottawa (Canada), Mar. 18, 1950. (Translated by E. Hope Trans. from Trans. Soc. Mech. Eng. (Japan), vols. 4-6, 1938-1940.

79. **Ranz, W.E. and Marshall, W.R.**
"Evaporation From Drops".
Parts 1 & 2, Chem. Eng. Prog., Vol. 48, Nos. 3 and 4, 1952.

80. **Frieldlander, S.K. and Jonstone, H.F.**
"Deposition of Suspended Particles from Turbulent Gas Streams".
Ind. & Eng. Chem., Vol. 49, No. 7, PP. 1151-56, 1957.

81. **Rossini, F.D. et al**
"Selected Values of Properties of Hydrocarbons".
NBS, 1947.

82. **McCoy, D.D. and Hanratty, T.J.**
"Rate of Deposition of Droplets in Annular Two-Phase Flow".
Int. J. Multiphase Flow, Vol. 3, PP. 319-31, 1977.

83. **Andreussi, P. and Azzopardi, B.J.**
"Droplet Deposition and Intercharge in Annular Two-Phase Flow".
Int. J. Multiphase Flow, Vol. 9, No. 6, PP. 681-95, 1983.

84. **Sehmel, G.A.**
"Particle Eddy Diffusivities and Deposition Velocities for Isothermal Flow and Smooth Surfaces".
J. Aerosol Sci., Vol. 4, PP. 125-28, 1973.

85. **Hewitt, G.F. and Taylor, N.S.H.**
"Annular Two-Phase Flow".
Pergamon Press, 1970.

86. **Kataoka, I., Ishii, M. and Mishima, K.**
"Generation and Size Distribution of Droplets in Annular Two-Phase Flow".
Trans. ASME, Vol. 105, PP. 230-38, 1983.

87. **Reid, R.C., Prausnitz, J. M. and Sherwood, T.K.**
"The Properties of Gases and Liquids".
McGraw-Hill Co., 3rd Ed., 1977.

88. **Hewitt, G.F.**
"Liquid Mass Transfer in Annular Two-Phase Flow".
Technical Paper of 6th IHTC, 1978.

89. **Dallman, J.C. and Hanratty, T.J.**
"Interpretation of Entrainment Measurements in Annular Gas-Liquid Flows".
Technical Paper of 6th IHTC, 1978.

90. **Pletcher, R.H. and McManus, H.N.**
"An analytic Study of the Film Behaviour in Horizontal Annular Two-Phase Flow".
Interim Report ARO (D), Project No. 3199E, 1965.

91. **Azzopardi, B.J.**
"Drop Sizes in Annular Two-Phase Flow".
Experiments in Fluids, Vol. 3, PP. 53-59, 1985.

92. **Ingebo, R. D.**
"Atomization, Acceleration and Vaporization of Liquid Fuels".
4th Symp. (Int) on Combustion, PP. 684-701, 1953.

93. **James, R.**
"Metering of Steam-Water Two-Phase Flow by Sharp-Edged Orifices".
Proc. Inst. Mech. Eng., Vol. 180, Pt. 1, No. 23, 1965.

94. **Moody, L.F. and Princeton, N.J.**
"Friction Factors for Pipe Flow".
Trans. ASME, PP. 671-84, Nov. 1944.

95. **Slattery, J.C. and Bird, R.B.**
"Calculation of the Diffusion Coefficient of Dilute Gasses and of the Self-Diffusion Coefficient of Dense Gas".
A.I.Ch.E. Journal, Vol. 4, PP. 137-42, 1958.

96. **Kays, W.M. and Crawford, M.E.**
"Convective Heat and Mass Transfer".
McGraw-Hill, New York, 1980.

97. **Soltau, J.P.**
"Cylinder Pressure Variations in Petrol Engines".
Proc. Inst. Mech. Engrs., 2, P.99, 1960-61.

98. **Clarke, L.S.**
"Initiation and Some Controlling Parameters of Combustion in the Piston Engine".
Proc. Inst. Mech. Engrs., 5, P. 165, 1960-61.

99. **Curry, S.**
"A Three Dimensional Study of Flame Propogation in a Spark Ignition Engine".
SAE Trans., Vol. 71, PP. 628-50, 1963.

100. **Bailey, A.C.**
"Combustion Limitations of Gasses Fuels in Reciprocating Engines"
Ph.D. Thesis, University of Manchester, 1971.

101. **Rose, J.W. and Cooper, J.R.**
"Technical Data on Fuels".
BNCWEC, 17th Ed., 1977.

102. **Goldberg, S.A. and Pelevin, V.S.**
"Influence of Pressure on Rate of Flame Propagation in Turbulent Flow".
7th Symp. (Int) on Combustion, PP. 590-94, 1958.

103. **Agnew, J.T. and Graiff, L.B.**
"The Preesure Dependence of Laminal Burning Velocity by the Spherical Bomb Method".
Comb. & Flame, Vol. 5, PP. 209-19, 1961.

104. **Tanford, C. and Pease, R.N.**
"Theory of Burning Velocity II - The Square Root Law for Burning Velocity".
J. Chem. Phys., Vol. 15, No. 12, PP. 861-65, 1957.

105. **Manson, N.**
"Mechanisme de la Propogation des Deflagrations dans les Melanges Gaseux et Role de la Projection de Centres Actifs".
Revue de L'Institute Francais du Petrole et Annales des Combustibles Liquids, Vol. 4, No. 7, July 1949.

106. **Andrews, G.E. and Bradley, D.**
"The Burning Velocity of Methane Air Mixtures".
Comb. & Flame Vol. 19, PP. 275-88, 1972.

107. **Dugger, G. and Simon, D.**
"Prediction of Flame Velocities of Hydrocarbon Flames".
4th Symp. (Int) on Combustion, P. 336, 1952.

108. **Andrews, G.E. and Bradley, D.**
"Determination of Burning Velocities:A Critical Review".
Comb. & Flame, Vol. 18, PP. 133-53, 1972.

109. **Wanger, P., Dugger, G. and Gordon, L.**
"Flame Propogation V - Structural Influences on Burning Velocity. Comparison of Measured and Calculated Burning Velocity".
J. Am. Chem. Soc., Vol. 77, No. 1, PP. 227-31, 1955.

110. **Metghalchi, M. and Keck, J.C.**
"Laminar Burning Velocity of Propane Air Mixtures at High Temperature and Pressure".
Comb. & Flame Vol. 38, PP. 14-54, 1980.

111. **Sharma, S.P., Agrawal, D.D. and Gupta, C.P.**
"The Pressure and Temperature Dependence of Burning Velocity in A Spherical Combustion Bomb".
18th Symp. (Int) on Combustion, PP. 493-500, 1981.

112. **Metghalchi, M. and Keck, J.C.**
"Burning Velocities of Mixtures of Air with Methanol, Iso-octane, and Indolene at High Pressure and Temperature".
Comb. & Flame Vol. 48, PP. 191-210, 1982.

113. **Gerstein, M., Levine, O. and Worg, E.L.**
"Fundamental Flame Velocities of Pure Hydrocarbons".
J. Am. Chem. Soc., Vol. 73, No. 1, PP. 418-22, 1951.

114. **Yamazaki, K. and Hnuma, K.**
"Augmented Flames in an Engine Combustion Chamber".
6th Symp. (Int) on Combustion, PP. 914-18, 1958.

115. **De Soete, G.**
"A Survey of the Effects of Turbulence on Engine Combustion".
Adv.in Autom. Engineering, Pt. IV, Pergamon Press, 1966.

116. **Smith, J.R.**
"Turbulent Flame Structure in a Homogeneous Charge Engine".
SAE Paper No. 820043.

117. **Hodgetts, D.**
Discussion on Phillipps and Orman paper (64)

118. **Harrow, G.A. and Orman, P.L.**
"A Study of Flame Propogation and Cyclic Dispersion in a Spark-Ignition Engine".
Adv. in Autom. Engineering, Pt. IV, Pergamon Press, 1966.

119. **Beretta, G.P., Rashidi, M. and Keck, J.C.**
"Turbulent Flame Propogation and Combustion in Spark Ignition Engines".
Comb. & Flame, Vol. 52, PP. 217-45, 1983.

120. **Annand, W.J.D.**
"Geometry of Spherical Flame Propogation in a Disced-Shaped Combustion Chamber".
J. Mech. Engr. Sci., Vol. 12, No. 2, PP. 146-49, 1970.

121. **Rassweiler, G.M. and Withrow, L.**
"Motion Pictures of Engine Flames Correlated with Pressure Cards".
SAE Trans., Vol. 42, No. 5, PP. 185-205, 1938.

122. **Jones, A.L. and Evans, R.L.**
"Comparison of Burning Rate in a Natural Gas Fueled Spark Ignition Engine".
Trans. ASME, Vol. 107, PP. 908-13, 1985.

123. **Daniel, W.A.**
"Flame Quenching at the Walls of an Internal Combustion Engine".
6th Symp. (Int) on Combustion, PP. 886-94, 1956.

124. **Huls, T.A., Myers, P.S. and Uyehara, O.A.**
"Spark Ignition Engine Operation and Design for Minimum Exhaust Emissions"
SAE Trans., Vol. 75, 1967.

125. **Shinn, J.N. and Olson, D.R.**
"Some Factors Affecting Unburnt Hydrocarbons in Engine Combustion Products".
SAE Technical Prog. Series, Vol. 6, 1964.

126. **James, E.H.**
"Combustion Modelling in Spark Ignition Engines".
Automotive Engineer, Vol. 9, No. 3, PP. 29-33, 1984.

127. **Goolsby, A.D. and Haskell, W.W.**
"Flame-Quench Distance Measurement in A CFR Engine"
Comb. & Flame, Vol. 26, PP. 105-14, 1976.

128. **Dyer, T.M.**
"Sources of Unburned Hydrocarbon Emissions from Homogeneous-Charge Automotive Engines".
SANDIA Report No. SAND 83-8241, Sept. 1983.

129. **Friedman, R. and Johnston, W.C.**
"The Wall Quenching of Laminar Flames as a Function of Pressure, Temperature and Air/Fuel Ratio".
J. Applied Physics, Vol. 21, PP. 791-95, 1950.

130. **Gottenberg, W.G., Olson, D.R. and Best, H.W.**
"Flame Quenching During High Pressure, High Temperature Combustion".
Comb. & Flame, Vol. 7, PP. 9-16, 1963.

131. **Potter, A.E. and Berlad, A.L.**
"The Effect of Fuel Type and Pressure on Flame Quenching".
4th Symp. (Int) on Combustion, PP. 27-36, 1952.

132. **Dugger, G.L., Simon, D.M. and Gerstein, M.**
"Basic Considerations in the Combustion of Hydrocarbon Fuels in Air".
NACA Report No. 1300, 1957.

133. **Chueh, P.L. and Prausnitz, J.M.**
"Vapour Liquid Equilibria at High Pressures: Calculation of Partial Molar Volumes in Non Polar Liquid Mixtures".
A.I.Ch.E. Journal, Vol. 13, No. 6, PP. 1099-107, 1967.

134. **Chueh, P.L. and Prausnitz, J.M.**
"A Generalized Correlation for the Compressibilities of Normal Liquids."
A.I.Ch.E. Journal, Vol. 15, No. 3, PP. 471-72, 1969.

135. **Maly, R. and Ziegler, G.**
"Theoretical and Experimental Investigation of the Knocking Process".
International Symp. on "Knocking of Combustion Engines", held in Wolfsburg, Germany, on 26/27 Nov. 1981.

136. **By, A., Kempiniski, B. and Rife, J.M.**
"Knock in Spark Ignition Engines".
SAE Paper No. 810147.

137. **Natarajan, B. and Bracco, F.V.**
"On Multidimensional Modelling of Auto-Ignition in Spark-Ignition Engines".
Comb. & Flame, Vol. 57, PP. 179-97, 1984.

138. **Baum, M.M.**
"On Predicting Spontaneous Combustion".
Comb. & Flame, Vol. 41, PP. 187-200, 1981.

139. **Trumpy, D.**
"The Pre-Knock Kinetics of Ethane in a Spark Ignition Engine".
SAE Trans, Vol. 78, 1969.

140. **Burnwell, W.G. and Olson, D.R.**
"The Spontaneous Ignition of Iso-octane Air Mixture Under Steady Flow Conditions".
SAE Paper No. 650510.

141. **Rifkin, E.B. and Walcutt, C.**
"A Basis for Understanding Antiknock Action".
SAE Trans., Vol. 65, 1957.

142. **Kadota, T., Hiroyasu, H. and Oya, H.**
"Spontaneous Ignition Delay of a Fuel Droplet in High Pressure and High Temperature Gaseous Environment".
Bull. JSME, Vol. 19, No. 130, 1976.

143. **Eyzat, P. and Douaud, A.**
"D-3-L'ORDINATEUR ET L'OPTIMISATION DU SYSTEME MOTEUR-CARBURANT"
FISITA 15th Congress INTL BLLD No. 6844.48, Paris, 1974.

144. **Douaud, D.**
"Modelling the knocking Phenomenon in Engines-Applications to Identifying the Autoignition Delay of Fuels and to Optimizing the Engine-Fuel System".
Int. Symp. on "Knocking of Combustion Engines", held in Wolfsburg, Germany, on 26/27 Nov. 1981.

145. **Livengood, J.C. and Wu, P.C.**
"Correlation of Autoignition Phenomena in Internal Combustion Engines and Rapid Compression Machines".
5th Symp. (Int) on Combustion, P.347, 1954.

146. **Ames, W.F.**
"Non-Linear Ordinary Differential Equations in Transport Processes"
Academic Press, New York & London, 1968.

147. **Lanchester, F.W.**
"The Energy Balance Sheet of the Internal Combustion Engine".
Proc. Inst. Mec. Engrs., Vol. 141, PP. 289-327, 1939.

148. **Janeway, R.N.**
"Quantitative Analysis of Heat Transfer in Engines".
SAE Journal, Vol. 61, P. 371, 1938.

149. **Richardo, H.R.**
"The High Speed Internal Combustion Engines".
Blackie and Son Ltd., London, 1953.

150. **Pye, D.R.**
"The Internal Combustion Engine".
Vol. 1, 2nd Ed., Oxford University Press, 1937.

151. **David, W.T. and Leah, A.S.**
"Fuel Economy in Petrol Engines".
Proc. Inst. Mech. Engrs., Vol. 143, PP. 289-312, 1940.

152. **Alkidas, A.C.**
"Heat Transfer Characteristics of a Spark Ignition Engine".
Journal of Heat Transfer, Vol. 102, PP. 189-93, 1980.

153. **Alkidas, A.C. and Myers, J.P.**
"Transient Heat Flux Measurements in the Combustion Chamber of a Spark Ignition Engine".
Trans. ASME, Vol. 104, PP. 62-67, 1982.

154. **Overbye, B.D., Bennethum, J.E., Uyehara, O.A. and Myers, P.S.**
"Unsteady Heat Transfer in Engines".
SAE Trans., Vol. 69, PP. 461-94, 1961.

155. **Nusselt, W.**
"Die Warmeubergang in den Verbrennungs-Kraftmaschinen".
Z. Ver. dtsch. Ing. P.67, 692, and 708, 1923.

156. **Briling,**
Quoted in Ref. **(159)**.

157. **Elser, K.**
"Instationare Warmeubergang in Diesel-Motoren".
Mitt. Inst. Thermodyn. Zurich, No. 16, 1954.

158. **Oguri, T.**
"On the Coefficient of Heat Transfer Between Gases and Cylinder Walls of SIE".
Bull. JSME, Vol. 3, No. 11, PP. 363-69, 1960.

159. **Annand, W.J.D.**
"Heat Transfer in the Cylinders of Reciprocating Internal Combustion Engines".
Proc. Inst, Mech. Engrs, Vol. 177, No. 36, PP. 973-96,1963.

160. **Johnson, T.H., Myers, P.S. and Uyehara, O.A.**
"End Gas TEmperature, Pressure, Reaction Rate and Knock".
SAE Paper No. 650585.

161. **Advisory Group for Aerospace Research and Development**
"Properties of Air and Combustion Products with Kerosine and Hydrogen Fuels".
British Siddeley Engines Ltd., 1967.

162. **Kandiner, H.J. and Brinkley, S.R.**
" Calculation of Complex Equilibrium Relations".
Industrial Engineering Chemistry, Vol. 42, P. 850, 1950.

163. **Vickland, C.W.**
"A Consideration of the high temperature Thermodynamics of Internal Combustion Engines".
SAE Prog. Technical, Vol. 7, No. 1, 1964.

164. **Newhall, H.K.**
"Kinetics of Engine Generated Nitrogen Oxides and Carbon Monoxide".
12th Symp. (Int) on Combustion, PP. 603-13, 1969.

165. **Spadiccini, L.J. and Chinitz, W.**
"An Investigation of Nonequilibrium Effects in an Internal Combustion Engine".
ASME Paper No. 71-WA/FU2.

166. **Annand, W.J.D.**
"Effects of Simplifying Kinetic Assumptions in Calculating Nitric Oxide Formation in Spark Ignition Engines".
Proc. Inst. Mech. Engrs., Vol. 188, 41/74, 1974.

167. **Way, R.J.D.**
"Methods for Determination of Composition and Thermodynamic Properties of Combustion Products for Internal Combustion Engine Calculations".
Proc. Inst. Mech. Engrs., Vol. 190 60/76, 1977.

168. **Wimmer, D.B. and McReynolds, L.A.**
"Nitrogen Oxides and Engine Combustion".
Paper 380E, SAE Summer Meeting, St. Louis, Missouri, June 1961.

169. **Huls, T.A. and Nickol, H.A.**
"Influence of Engine Variables on Exhaust Oxides of Nitrogen Concentrations from a Multi-Cylinder Engine".
SAE Paper No. 670482.

170. **Benson, R.S. and Barauah, P.C.**
"Performance and Emission Predictions for a Multi-Cylinder Spark Ignition Engine".
Proc. Inst. Mech. Engrs., Vol. 191 32/77, PP. 339-54, 1977.

171. **Whitehouse, N.D., Stotter, A., Goudie, F.O. and Prentice B.W.**
"Method of Predicting some Aspects of Performance of Diesel Engine Using a Digital Computer".
Proc. Inst. Mech. Engrs., Vol. 176, No. 9, PP.195-17, 1962.

172. **Anderson, R.J. and Russell, T.W.F.**
"Film Formation in Two-Phase Annular Flow".
A.I.Ch.E Journal, Vol. 16, No. 4, PP. 626-33, 1970.

173. **Quandt, E.R.**
"Measurement of Some Basic Parameters in Two-Phase Annular Flow".
A.I.Ch.E Journal, Vol. 11, No. 2, PP. 311-18, 1965.

174. **Gill, L.E., Hewitt, G.F. and Lacey, P.M.C.**
"Data on the Upwards Annular Flow of Air-Water Mixtures".
Chem. Eng. Sci., 20, 71, 1965.

175. **Stull, D.R. and Prophet, H.**
"JANAF Thermodynamical Tables" NSRDS - NBS37, 1971.